The role of oncogenic KRAS in the immune evasion of non-small cell lung cancer

Edurne Mugarza Strobl

University College London

and

The Francis Crick Institute

PhD Supervisor: Professor Julian Downward

A thesis submitted for the degree of

Doctor of Philosophy

University College London

December 2020

Declaration

I, Edurne Mugarza Strobl, confirm that the work presented in this thesis is my own. Where information has been derived from other sources, I confirm that this has been indicated in the thesis.

Abstract

Lung cancer is a highly mutated tumour type in which, if effective, cancer immunotherapies have proven to be superior to other treatment modalities. However, tumours develop mechanisms by which they are able to evade the actions of the immune system, some of which may render them unresponsive to drugs aimed to boost antitumor immunity. KRAS is the most frequently mutated oncogene in cancer. Activating mutations in KRAS are found in up to a third of all lung cancer patients and have been previously shown to trigger immunosuppressive actions by tumour cells. Approximately a third of KRAS-mutant lung cancer patients harbour G12C mutations, which are amenable to therapeutic targeting thanks to the development of novel $KRAS^{G12C}$ inhibitors, which are currently being tested in clinical trials. In this study, we aim to unveil new immunosuppressive mechanisms triggered by oncogenic KRAS signalling *in vitro* and in clinically relevant mouse models. Additionally, we try to elucidate the effects of novel $KRAS^{G12C}$ inhibitors on the tumour microenvironment, with the ultimate goal of developing rational combination therapies. Using human cell lines, we have generated a gene expression dataset of KRAS-dependent genes. We have also developed a modified version of the murine lung cancer cell line 3LL to be able to perform experiments in an *in vivo* setting. Making use of these tools, we have established a link between KRAS signalling and the recruitment of immunosuppressive myeloid cells to the tumour microenvironment. Furthermore, the use of a therapeutic compound against $KRAS^{G12C}$ has shown profound changes in the tumour microenvironment, further underscoring the fact that KRAS signalling can be immunosuppressive. This study highlights the possibility of therapeutically targeting components of the tumour microenvironment in KRAS-mutant lung cancer, in combination with standard of care treatments or novel therapies such as $KRAS^{G12C}$ inhibitors.

Impact Statement

KRAS-mutant lung cancer affects approximately half a million people worldwide yearly, and lung cancer (of which 20% is KRAS-mutant lung cancer) constitutes the third most common cancer in the UK. Despite great advances in immune therapies and KRAS-targeted therapies in the clinic, a large number of patients will remain resistant to such individual treatments and it is highly likely combinatorial treatments will be needed to achieve long-term regressions. This work aims to unravel novel mechanisms of immune evasion in KRAS-mutant lung cancer and mechanistic insights into the action of novel KRAS inhibitors, to aim to understand mechanisms of resistance to immune therapies or KRAS-targeted agents, respectively. In addition, we develop and make use of novel clinically relevant mouse models that will aid in the investigation of new combinatorial approaches to KRAS-mutant lung cancer treatment.

Acknowledgement

Firstly, I would like to thank Julian for giving me the opportunity to carry out this research project in his lab, and for his guidance over the last four years. I have been incredibly lucky to have his excellent mentorship and he has set up an exceptional example of the type of scientist I one day would be honoured to become.

My work would not have been possible without the support of the people in the lab. I would firstly like to highlight Miriam, whose mentorship has been instrumental in this process. Thanks, Miriam, for all the advice, help, countless brainstorming sessions (often with a beer or two) and your patience with me. I am also grateful to Febe for our fruitful immunology discussions and outstanding collaborations. My deepest thanks also go to Chris and Sareena for their invaluable experimental help (thanks in particular to Sareena for making daily life in the lab so fun and full of laughter). I would also like to thank Jesse for being the best PhD buddy someone can ask for. Thank you to everyone in the Downward lab, both past and present, for all the advice, help, troubleshooting, conversations, jokes, trips to the bar and laughs over the years.

I am deeply thankful to my Thesis Committee, Prof. Sergio Quezada, Prof. Caetano Reis e Sousa and Dr. Erik Sahai for their feedback, advice and comments that have helped this project move forward. Thanks also to Dr. Andreas Wack for his kind advice on macrophages.

For this project, I have been lucky to make use of some of the outstanding facilities at the Crick. Firstly, I would like to acknowledge the incredible work of Miriam Llorian Sopena in the Bioinformatics facility, and thank her for her kindness and patience with my struggles understanding bioinformatics data. Huge thanks also go to everyone in the BRF, in Experimental 1 and mostly in the in vivo imaging unit (Caroline Zverev, Scott Lighterness, James Cormack, Alex Dobre, Anthony Horwood and many others). They have been incredibly helpful with animal experiments and have always done so with a kind smile on their faces. Thanks to

everyone at the Flow Cytometry Facility, Genomics Equipment Park, High Throughput, Advanced Sequencing and Experimental Histopathology for their support and help.

Finally, thanks to all the people who have been there all along. Thanks to my friends, in particular the Cuadrilla, for many years of constant support. Thanks to my family, Mami, Aita, Erik and Ele for always supporting and encouraging me. Last but not least, thanks to Davide for going on this journey with me from day one to the finish line and being with me in the good and the bad times.

Table of Contents

Table of figures

List of tables

Abbreviations

4-OHT: 4-hydroxytamoxifen

APOBEC: apolipoprotein B mRNA editing enzyme, catalytic polypeptide-like

AT2: alveolar type II pneumocytes

CCL2: CC-chemokine ligand 2

CCR2: CC-chemokine receptor 2

CT: computed tomography

CTLA-4: cytotoxic T-lymphocyte antigen 4

CX_3CR1: CX_3C-chemokine receptor 1

CXCL10: Chemokine (C-X-C motif) ligand 10

CXCL11: Chemokine (C-X-C motif) ligand 11

CXCL9: Chemokine (C-X-C motif) ligand 9

DC: dendritic cell

ER: estrogen receptor

FACS: fluorescence activated cell sorting

GM-CSF: granulocyte-macrophage colony-stimulating factor

GSEA: gene set enrichment analysis

ICB: immune checkpoint blockade

IFN: interferon

IFNα: interferon alpha

IFNβ: interferon beta

IFNγ: interferon gamma

ISG: interferon response genes

JAK: Janus kinase

KD: knock-down

KO: knock-out

KP: K-ras$^{LSL\text{-}G12D/+}$; p53$^{fl/fl}$

KRAS: Kirsten Rat Sarcoma

M-CSF: macrophage colony-stimulating factor

MDSC: myeloid-derived suppressor cells

NK cell: natural killer cell

NSCLC: non-small cell lung cancer

PD-1: programmed death – 1

PD-L1: anti-programmed death ligand

RNA-Seq: RNA sequencing

SCLC: small cell lung cancer

sgRNA: guide RNA

siRNA: small interfering RNA

STAT: signal transducer and activator of transcription

TAM: tumour-associated macrophage

TME: tumour microenvironment

Treg: regulatory T cell

WT: wild-type

Chapter 1. Introduction

1.1 Lung cancer

1.1.1 Introduction to the disease

Lung cancer is one of the most common cancer types, the third most prevalent in the UK, accounting 13% of new cancer cases (data from Cancer Research UK). Lung cancer is also the leading cause of cancer-related deaths in both men and women, making up almost 25% of all cancer deaths (data from the American Cancer Society). Despite all the efforts in clinical and preclinical research, survival rates in lung cancer have had little improvement since the 1970s, providing a highly unmet need in the clinic.

Lung cancer arises from malignant cell growth in the bronchi, bronchioles or alveoli. From the lungs, malignant cells can extend to neighbouring lymph nodes, from which they can then migrate to different organs and form distant site metastases. The most common organs where lung cancer cells metastasize include the brain, the bones and the liver. Around 70% of patients diagnosed with lung cancer present with advanced metastatic disease (Lemjabbar-Alaoui et al., 2015). The presence of metastasis is generally associated to poor prognosis, as most lung cancer-related deaths occur due to metastatic spread, rather than the primary tumour.

1.1.2 Lung cancer subtypes

Lung cancer is categorised in different subtypes, which differ in the cell of origin, location within the lung and underlying cause. The subtype of lung cancer with which a patient is diagnosed determines which treatment regime will be followed.

Small cell lung cancer (SCLC) accounts for 15-20% of all lung cancer cases in the UK (data from CRUK, last reviewed in January 2020) and is hence less common than its counterpart, non-small cell lung cancer (NSCLC). It is highly metastatic and the most aggressive form of lung cancer. SCLC arises from neuroendocrine cells in the central airways and infiltrates the bronchial airways (Dela Cruz et al., 2011).

Smoking constitutes one of the major causes of SCLC, and as such, tumours present highly complex genomic alterations as a consequence of carcinogen-induced mutagenesis (George et al., 2015). These tumours are generally driven by inactivating alterations in tumour suppressor genes p53 and Retinoblastoma 1 (Rb1) (George et al., 2015). Currently there is no established molecular-targeted therapy available for SCLC, but research is underway to elucidate targetable molecular alterations in this disease.

NSCLC, the main focus of this thesis, is the most prevalent type of lung cancer accounting for up to 80-85% of all lung cancer cases in the UK (data from CRUK, last reviewed in January 2020). NSCLC is a highly aggressive tumour type. In fact, patients with untreated metastatic NSCLC have an overall survival of 10% at one year (Roman et al., 2018). Patients with NSCLC can be further subdivided into three main subtypes, squamous cell carcinoma, large cell carcinoma and adenocarcinoma (see Figure 1).

Large cell carcinoma is the least frequent NSCLC tumour type that affects around 10% of all lung cancer patients (Data from US patients -SEER, NIH-, updated on April 2020). It consists of a diverse group of tumours with a high tendency to spread to lymph nodes and distant sites and is therefore associated with a poor prognosis.

Squamous cell carcinoma constitutes approximately 20% of all lung cancer, arising from basal cells in main bronchi in the lung (Data from US patients -SEER, NIH-, updated on April 2020). It is a highly mutated cancer type, where a vast number of molecular alterations have been described that could act as drivers, such as amplifications in the transcription factor SRY-box 2 (SOX2), amplifications and mutations in the kinase PIK3CA, amplifications in growth factor receptors such as the fibroblast growth factor receptor 1 (FGFR1) and the insulin-like growth factor 1 receptor (IGF1R), among others (Heist et al., 2012). Additionally, a number of molecular alterations have been described to occur in known tumour suppressor genes, such as over 80% of patients showing alterations in TP53, RB1 and PTEN (Cancer Genome Atlas Research, 2012).

Lung adenocarcinoma is the most common type of NSCLC, with about 50% of all lung cancer patients harbouring this disease. It arises in the peripheral bronchi and alveoli (Data from US patients -SEER, NIH-, updated on April 2020), where the cells of origin are type II pneumocytes and Clara cells (Pikor et al., 2013).

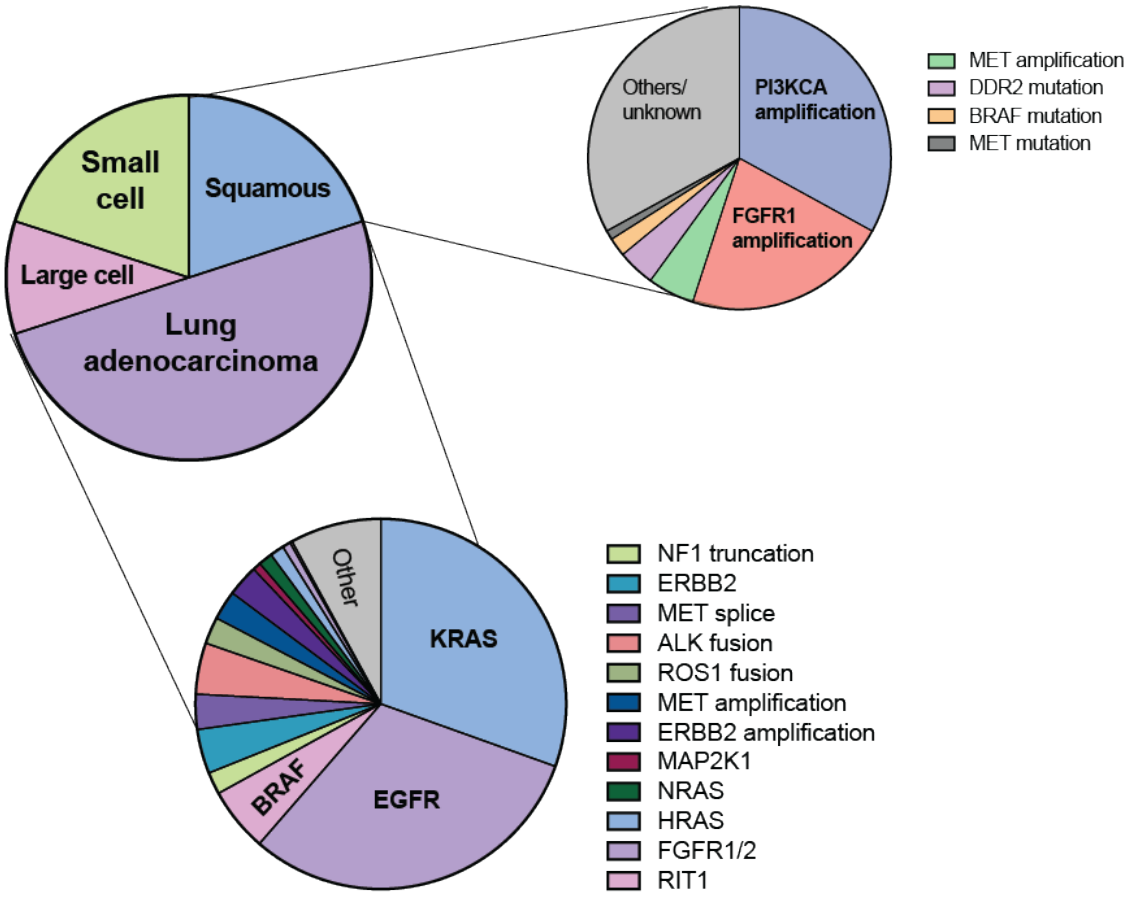

Figure 1. Summary of lung cancer subtypes and the most common molecular drivers.

Data of histological subtypes of lung cancer (top left) is based on a cohort of US patients, (data from SEER, NIH, updated April 2020). Data for squamous cell carcinoma drivers (top right, not including tumour suppressors) derived from (Heist et al., 2012). Data of driver genes of lung adenocarcinoma represents patients in a metastatic setting, derived from (Skoulidis et al., 2018) and excluding tumour suppressor genes.

NSCLC tumours are mostly caused by chronic exposure to carcinogens associated to tobacco smoking (Pikor et al., 2013) which lead to complex genomic alterations. Several tobacco agents play a role in NSCLC development, predominantly nicotine-derived nitrosamines. Nitrosamines such as 4-(methylnitrosamino)-1-(3-

pyridyl)-1-butanone (NNK) and N'-nitrosonornicotine (NNN) induce carcinogenesis by causing DNA adducts, which, if not correctly repaired result in the generation of DNA mutations (Hecht, 2003). If these mutations cause an activation of an oncogene or an inactivation of a tumour suppressor gene, they can prime the initiation of tumour growth.

Several molecular alterations have been found in lung adenocarcinoma. The data for LUAD patients depicted in Figure 1 represents molecular drivers commonly found in metastatic LUAD patients (Skoulidis et al., 2018). Mutations in the Kirsten Rat Sarcoma (KRAS) oncogene are the most common alterations in patients with smoking history, whereas epidermal growth factor receptor (EGFR) mutations are found mostly in non-smokers (Pikor et al., 2013). In addition to these drivers, they are commonly accompanied by alterations in tumour suppressor genes, most notably LKB1 (STK11) and TP53 (Skoulidis et al., 2018), further enhancing molecular and clinical heterogeneity in these tumours.

1.1.3 Treatment strategies for NSCLC

Treatment regimens for lung cancer patients in the clinical setting vary depending on the histology, stage and molecular status of the disease.

If the tumour is resectable patients are usually treated with a curative intent. They can undergo surgery, which can be followed with radiotherapy and/or platinum-based chemotherapy to augment the efficacy of the treatment (following NICE© guidelines, UK). More recently, emerging data has shown efficacy of adjuvant EGFR inhibitor osimertinib for patients with sensitizing EGFR mutations who have undergone resection (Wu et al., 2020). This has been FDA approved and is undergoing NICE© evaluation.

In the advanced setting, EGFR inhibitors are given as a first line treatment to patients that present with mutations in EGFR. First-line choices in the UK include the first and second-generation inhibitors erlotinib, gefitinib & afatinib or the more novel agent erolitinib, as per NICE© guidance. Patients who relapse on first or second-generation inhibitors may be given osimertinib in the second-line, should

they be T790M mutation positive. In the case of patients with ALK fusions or alterations in ROS1, they are treated with ALK and ROS1 inhibitors (following NICE© guidelines, UK). One common feature of targeted therapies, however, due to the inherent genetic instability of tumour cells, is the eventual recurrence of the disease. In these cases, recommended treatment strategies usually either consist of a second-line TKI, where available, or combination chemotherapy which may be combined with the anti-programmed death ligand 1 (PD-L1) antibody atezolizumab (following NICE© guidelines).

Most NSCLC patients, however, do not have available targeted therapies. Notably, KRAS-mutant patients, which account for 25% of all NSCLC patients in the UK, currently have no targeted therapy option available. This constitutes a major unmet need in the clinical practice of NSCLC, is extensively being addressed by the scientific community (and growingly by pharmaceutical companies) and will be the focus of this thesis.

For these advanced stage patients with no targetable alterations, the main alternative consists of the use of the newly developed immune modulatory antibodies. The current treatment guideline is based on expression of the immune checkpoint ligand PD-L1 by the tumour tissue. If the PD-L1 expression is lower than 50%, the patients are eligible for treatment with pembrolizumab combined with chemotherapy. In patients with a PD-L1 expression over 50%, pembrolizumab monotherapy or as a combination with chemotherapy are options (following NICE© guidelines). Upon relapse, patients are usually treated with chemotherapy alone (following NICE© guidelines).

Responses to immune checkpoint blockade have been widely reported to correlate with tumour mutation burden (Hellmann et al., 2018). This is likely due to the fact that mutations lead to the generation of neoantigens that are presented on the surface of the tumour cells and make them susceptible to immune cell attack. It is known that NSCLC constitutes a highly mutated tumour type (Alexandrov et al., 2013), second only to melanoma, the most mutated cancer type. Within NSCLC patients, smokers usually present with a highly mutated tumour phenotype and are

therefore predicted to have a better response to immunotherapeutic targeting (Govindan et al., 2012).

After their initial success in melanoma, immune checkpoint blockade agents have only recently been approved for clinical use in NSCLC. The anti-PD-1 antibody nivolumab was approved initially for the treatment of advanced squamous NSCLC in March of 2015 (Borghaei et al., 2015). This approval was granted following a phase 3 clinical study where overall survival for nivolumab was higher than with docetaxel, the standard regime of chemotherapy treatment for NSCLC. This was rapidly followed by the approval of nivolumab for non-squamous NSCLC in October of the same year. The alternative anti-PD-1 antibody pembrolizumab was also granted approval for treatment of advanced NSCLC expressing PD-L1 (Garon et al., 2015). Since then, checkpoint blockade agents have increasingly gained relevance in the clinical treatment of NSCLC and nowadays constitute the first line treatment in a large number of cases.

Clinical responses to checkpoint blockade agents have been extraordinary, providing a remarkable improvement in long-term responses of a subset of patients. However, there is an urgent need to better understand patterns of response and mechanisms of resistance to improve patient selection, prognosis, and aid in the design of rational combination therapy approaches.

1.2 The biology of RAS oncogenes

1.2.1 Early history of RAS research

RAS family members are widely known to be the most commonly mutated oncogenes across human cancer. Interestingly, RAS-related research originated from discoveries in the virology field. In 1964, Jennifer Harvey isolated a viral preparation from a rat that was able to induce sarcomas in rodents, termed as Harvey murine sarcoma virus (Ha-MSV) (Harvey, 1964). Additional viruses with oncogenic properties were subsequently identified, most notably the Kirsten murine sarcoma virus (Ki-MSV) (Kirsten and Mayer, 1967). Some years later, it was discovered that these viruses contained genomic sequences that they had acquired from the rat genome (genes such as Hras in Ha-MSV and Kras in KI-MSV, respectively) (Ellis et al., 1981).

In parallel, in the 70s, research was underway by several groups to discover new functions of genes by introducing exogenous DNA into mammalian cells. One of such techniques consisted of transfecting DNA from transformed cells into NIH 3T3 mouse fibroblasts. These cells retain normal growth capacities, and when transformed, undergo morphologic changes that can be visualised with ease (i.e. they can form foci when they lose contact-inhibition of growth). Using such techniques, several labs reported transforming abilities of DNA derived from cancerous cell lines (Perucho et al., 1981).

The key breakthrough that linked the known retroviral oncogenes and oncogenes present in tumour DNA was achieved by three studies published in 1982 ((Der et al., 1982) (Santos et al., 1982)) (Parada et al., 1982). One report shows that transformed DNA from NIH 3T3 cells hybridised with known retroviral oncogenes v-h-ras and v-k-ras (Der et al., 1982). Concomitantly, the two other studies also reported homologies between retroviral oncogenes and sequences obtained from transformed cells (Santos et al., 1982) (Parada et al., 1982). The third member of the RAS family, NRAS, not previously identified in virus studies, was discovered in 1983 in a neuroblastoma cell line (Hall et al., 1983).

Nowadays it is known that the human genome contains three different RAS genes, KRAS (in chromosome 12), NRAS (in chromosome 1) and HRAS (in chromosome 11), which encode for a total of four RAS proteins, since KRAS encodes for two isoforms that arise from alternative RNA splicing (KRAS4A and KRAS4B, the latter being the major isoform expressed in human cells) (Zhou et al., 2016).

During the 70s and the 80s, intense research was carried out leading to discoveries about biochemical and cellular properties of RAS family proteins. It was shown that RAS genes encoded for 21kDa proteins (Shih et al., 1979), that these proteins are associated to the plasma membrane (Willingham et al., 1980) and that they can bind guanine-diphosphate (GDP) and guanine-triphosphate (GTP) (Scolnick et al., 1979).

Concomitantly, molecular cloning of the HRAS gene allowed researchers to find that the oncogenic properties of RAS family members were due to a single point mutation in their genomic sequence (Tabin et al., 1982) (Taparowsky et al., 1982) (Reddy et al., 1982). Subsequently, the confirmation that all these findings were relevant for human cancer came with the discovery of mutated KRAS sequences in a patient tumour biopsy (Santos et al., 1984). Additional tumour types and mouse cancer models were then reported to have RAS mutations in their genome. Most notably, RAS mutations were found in colon (Bos et al., 1987) (Forrester et al., 1987), lung (Rodenhuis et al., 1987) and pancreatic cancer (Almoguera et al., 1988). These findings highlighted the breadth and importance of RAS family members as oncogenes in a variety of cancer types.

Additional studies, however, shed light on the insufficiency of a single oncogenic hit to give rise to a full transformation event. It was found that a concurrent activation of an additional oncogene (i.e. Myc or adenovirus E1A) or the inactivation of a tumour suppressor gene (i.e. p53) was required for transformation of cells *in vitro* by Ras (Land et al., 1983) (Ruley, 1983). This provided the basis for the current view that malignant transformation stems from the collaboration of distinct molecular alterations occurring in a cell.

1.2.2 Molecular mechanism and signalling of RAS

In 1984, several groups described that the function of RAS proteins was to act as GTPases, meaning that they were involved in the hydrolysis of GTP to GDP. It was also found that this intrinsic enzymatic activity was attenuated approximately 10-fold in oncogenic (mutant) versions of the proteins (Gibbs et al., 1984) (McGrath et al., 1984) (Sweet et al., 1984). These findings provided evidence that aberrant RAS function in tumours originates from an augmented GTP-binding of the protein. Thanks to the observation of structural homologies between RAS and the alpha subunit of G proteins, it was established that the function of RAS was to mediate signalling across the plasma membrane (Hurley et al., 1984). Such a function was confirmed by studies suggesting that GTP binding to RAS (and hence, its activation) could be induced by stimulation of cells with epidermal growth factor (EGF) (Kamata and Feramisco, 1984), which led to transformation and mitogenic activation of the cells. Furthermore, by the use of Ras neutralising antibodies, it was established that such neutralisation abrogated the transformative ability of cell surface tyrosine kinases, but not of cytoplasmic kinases (Smith et al., 1986). This provided the basis of the current knowledge that RAS bridges the communication from growth factor activated, plasma membrane-associated receptors and intracellular mediators of signalling to trigger cellular responses to extracellular stimuli.

Further research on the molecular function of RAS continued with the discovery of upstream regulators of RAS that were able to accelerate the release of GDP and binding of GTP to mediate the activation of RAS, known as guanine nucleotide-exchange factors (GEFs) (Wolfman and Macara, 1990) (Downward et al., 1990). On the contrary, Ras GTPase activating proteins (GAPs) were described to increase intrinsic GTPase activity of

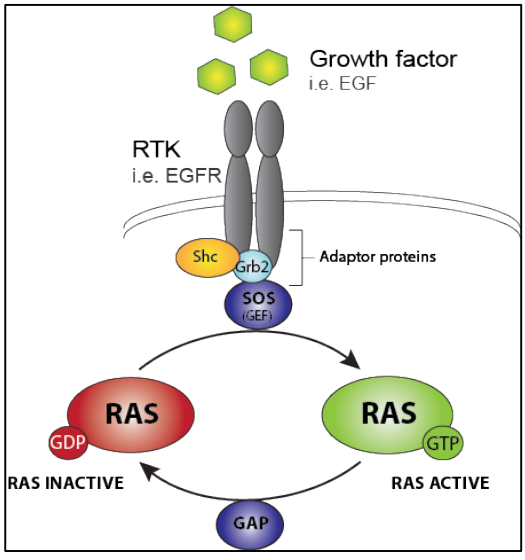

Figure 2. Schematic of RAS activation.

normal Ras proteins, but not mutant Ras proteins (Trahey and McCormick, 1987). A large number of RasGEFs and RasGAPs have since then been discovered through the years. Another piece of the puzzle solved soon thereafter was the elucidation of the mechanism by which RAS could receive signals from membrane receptors, by the discovery of adaptor molecules that could bind to both the activated receptors and to RasGEFs (McCormick, 1993). A simplified schematic of this process is illustrated in Figure 2.

In the late 80s, crystal structures of H-Ras became available (Tong et al., 1989). Structural studies determined the existence of two key regions in Ras proteins, namely switch I and switch II, of outmost importance in the interaction of Ras with its regulators and effectors, which changed conformation upon GTP hydrolysis. When GTP is bound to RAS, the γ-phosphate binds to switch I and switch II, in a compact conformation that permits the interaction with effector molecules (Milburn et al., 1990). When the γ-phosphate is hydrolysed, it causes a conformational change in these regions, forming an inactive state that is not able to bind effector proteins. These studies also allowed to elucidate the structural basis of the malfunction of RAS in the case of a mutation in codon 12 (mutations in RAS genes are explained in more detail in subsection 1.2.3). In fact, the glycine residue present in codon 12 (Gly12), is located in a GAP-binding region of RAS (see Figure 5A). As glycine is the only amino acid that does not contain a side chain, the substitution of glycine by any side chain-containing residue provides a steric hindrance in the transition state of the GTP hydrolysis reaction, rendering it insensitive to GAPs (Scheffzek et al., 1996) (Figure 5A). We now know that GEFs and GAPs are crucial for the tight regulation of the GTPase activity of RAS. Current knowledge has demonstrated that mutant RAS is not entirely insensitive to GAPs, and that even mutant RAS is able to cycle between a GTP- and a GDP-bound state, albeit with different kinetics than WT Ras (Patricelli et al., 2016) (Figure 5B).

Soon thereafter, research was focused on finding downstream signalling pathways activated by GTP-bound RAS. The first of such pathways to be discovered (which remains the main pathway known to be activated by RAS), was the MAPK cascade in 1993. This was prompted by the identification that the Raf serine/threonine kinase, a known retroviral oncogene, was found to preferentially bind to GTP-

bound RAS (Warne et al., 1993) (Moodie et al., 1993). This knowledge was crucial for the current vision of oncogenic signalling, which we know is initiated by extracellular factors, propagated in the cell by signalling molecules and finally reach the nucleus, where they are able to modulate gene expression to achieve specific functional outcomes. The next RAS effectors to be discovered were phosphoinositide 3-kinase (PI3K) (Rodriguez-Viciana et al., 1994) and Ral guanine nucleotide dissociation stimulator (RAL-GDS) (Hofer et al., 1994). Currently, a large number of RAS effector pathways are known and linked to diverse biological responses from cells. These cellular responses constitute mainly cell survival, migration, growth arrest, senescence, differentiation and apoptosis (see Figure 3). For instance, the PI3K and MAPK pathways are known to mediate protein translation and cell cycle progression. On the other hand, pathways mediated by RAC and RHO lead to gene expression changes that affect the cytoskeleton and thus, cell motility. Additionally, RAS-mediated activation of PLCε affects nuclear transport and Ca^{2+} signalling in the cell. Finally, RAL-GDS mediated signal transduction leads to changes in membrane trafficking and vesicle formation (Malumbres and Barbacid, 2003). These constitute examples of the pleiotropic effects of RAS activation, driven by different effector molecules activated in response to different stimuli.

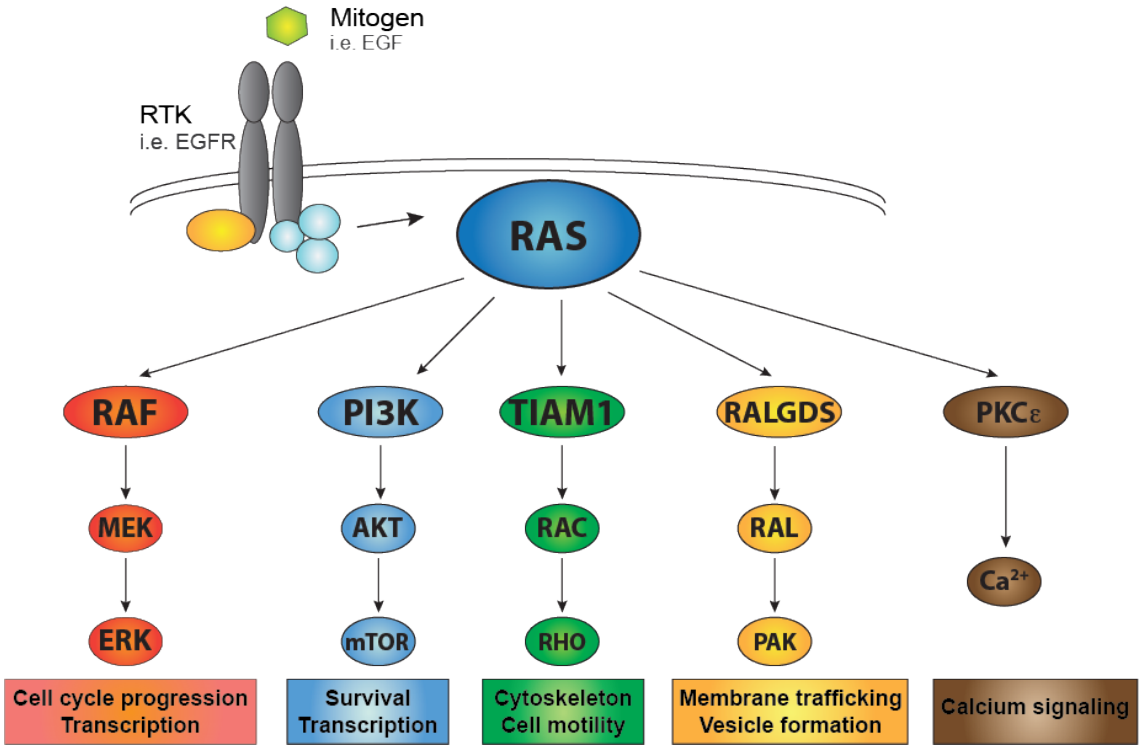

Figure 3. Summary of RAS effector pathways and their biological outcomes.

Although a lot is known about RAS effector pathways and their function, research is still underway to elucidate additional pathways and their biological outputs, including those pathways stemming from less well-characterised RAS family members such as RRAS, MRAS, RAP and RAL. Research is also underway to examine the role of RAS activated effector pathways in modulating non-cell intrinsic biological functions, that is, outputs beyond cell survival and proliferation. The elucidation of such mechanisms is the main aim of this thesis.

The ultimate function of such diversity in signalling pathways is for a cell to be able to adequately respond to a number of signals stemming from the exterior in a specific manner, with the ultimate goal of promoting cell survival. It is therefore logical that upon a constitutive activation of RAS molecules, which occurs by maintaining RAS in its GTP-bound state, an uncontrolled overgrowth of cells can ultimately result in a malignant transformation.

1.2.3 RAS mutations in cancer

RAS is the most frequently mutated oncogene in cancer, present in 27% of all human cancers (COSMIC v75). However, the type of mutation and the proportion of tumours that have KRAS mutations vary among cancer types. The first mutations discovered in RAS proteins were the mutations in codon 12, swiftly followed by the finding of mutations in codons 13 and 61. These three codons account for 97-99% of all the mutations found in RAS (Cox and Der, 2010). As mentioned in the previous subsection, alterations in codons 12 and 13 provide steric hindrances that impede the GTP hydrolysis of RAS, leading to a constitutive activation of the protein and its effector signalling pathways (Prior et al., 2012) (Figure 5A).

Even though RAS research has largely viewed all RAS family members as relatively equal, due to their large sequence similarity (82-90%), different isoforms differ in their mutation patterns (Hobbs et al., 2016). The reason for such variability is under continuous research. The effector binding regions of the proteins are virtually identical, but the differences arise at the hypervariable region at their C-terminus. This region is crucial for lipid modifications which determines their membrane binding kinetics and localisation at cellular membranes. This could allow for RAS engagement with different groups of activators and effectors, providing isoform specificity of signalling attributes (Zhou et al., 2016).

KRAS is the most frequently mutated isoform (85%) in human cancer, followed by NRAS (12%) and HRAS (4%) (Hobbs et al., 2016). Mutation frequencies vary largely across cancer types. For instance, of KRAS (codon 12 and 13) is mutated in approximately 95% of all pancreatic cancer patients and 45% of colorectal cancer patients (data from the RAS initiative). As mentioned in the previous section, KRAS mutations are also present in approximately 35% of all lung adenocarcinoma patients. In contrast, 15% of patients with acute myeloid leukemia and 15% of melanoma patients have mutations in NRAS, which is most frequently mutated in codon 61 (data from the RAS initiative and (Cox and Der, 2010)). Other tumour types such as bladder cancer and some types of head and neck squamous cell carcinoma (HNSCC) can be presented with mutations in HRAS in about 10% and

5% of the patients, respectively (data from the RAS initiative). HRAS can be mutated both in codons 12 and 61 (Prior et al., 2012). 43% of all mutations in KRAS are produced by G→A transitions at the second base of codons 12 or 13, which give rise to G12D or G13D mutations. The next common alterations are G→T transversions that make G12V mutations. However, in lung cancer, the predominant alterations are a G→T and G→C transversions, associated with smoking, that create G12C mutations. In fact, for lung cancer, the most frequent KRAS mutation is G12C, present in 41% of all KRAS-mutant NSCLC patients (Roman et al., 2018). It is likely that tissue-specific exposure to carcinogens accounts for the distinct frequencies, but it is still largely unknown whether the biological outputs of the mutations differ in any way (see Figure 4).

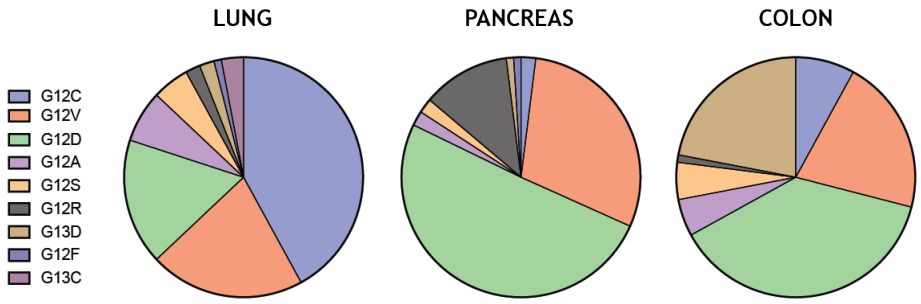

Figure 4. Summary of KRAS mutation frequencies across different cancer types.

1.3 KRAS^{G12C} inhibitors

1.3.1 Introduction to KRAS targeting approaches

Given the large prevalence of KRAS mutations in human cancer, intensive research efforts have been made to therapeutically target these tumours. Throughout the years a number of inhibitors have been developed that target proteins in the MAPK pathway, such as MEK, BRAF and EGFR. These have been clinically approved for a number of tumour types, but they are not necessarily effective in KRAS-mutant lung cancer. For instance, vemurafenib, the most common BRAF targeting drug, is mutation-specific and used in the clinical treatment of metastatic melanoma. EGFR-targeting drugs are only effective in EGFR-mutant tumours and are, actually, contraindicated for KRAS-mutant lung cancer patients (Gysin et al., 2011).

KRAS itself constitutes an excellent drug discovery target, due to its role in carcinogenesis and the fact that KRAS mutations are truncal events in tumour evolution. One report by McDonald et al. showed that knocking out the KRAS gene in KRAS-mutant cells affected their growth, while this did not occur with KRAS wild-type cells (McDonald et al., 2017), highlighting the KRAS dependency of KRAS-mutant cells. However, for decades, KRAS molecules were defined as ‘undruggable’. Despite these enormous efforts from the scientific community, researchers have struggled to find small molecule inhibitors that will effectively target KRAS. The surface of the protein is smooth and was thought to lack adequate pockets, and it has a picomolar affinity for the nucleotides GTP/GDP, making it very challenging to find adequate small molecules that will covalently bind to the protein and inhibit its function.

This view has changed dramatically over the last years, as new compounds have emerged which specifically target the cysteine mutant version of KRAS G12 (G12C). The ability to target the mutant form of KRAS selectively permits to circumvent toxicity concerns of targeting all RAS isoforms ubiquitously. As mentioned before, G12C is the predominant KRAS mutation found in lung cancer, making these inhibitors applicable to a large number of KRAS-mutant lung cancer

patients. This mutation, albeit present, is not so frequent in colon and pancreatic cancer patients (see Figure 4).

1.3.2 Molecular mechanism of KRAS^{G12C} inhibitors

Cysteines are attractive targets for drug discovery due to their inherent reactive nature, which can be exploited to generate covalent small molecule inhibitors. The mutant Cys 12 in KRAS, not present in wild-type KRAS, is located in close proximity to the nucleotide pocket and the switch regions of the protein which are involved in effector interactions (see 1.2.2). The switch II region of KRAS^{G12C}, when in its GDP-bound state, contains an allosteric binding pocket that allows the irreversible binding of compounds (as illustrated in Figure 5C).

While codon 12, 13 and 61 mutations in general have a diminished intrinsic GTPase activity compared to wild-type KRAS, KRAS^{G12C} has a GTPase activity that is similar to the wild-type counterpart (Hunter et al., 2015). In practical terms, this means that KRAS^{G12C} mutants spend an increased time of their cycle in a GDP-bound manner, compared to other mutants. The newly developed KRAS^{G12C} covalent inhibitors were developed taking advantage of the aforementioned feature and are able to bind KRAS^{G12C} in a GDP-bound state. They act by blocking KRAS in its inactive state and thereby impeding its association with downstream effectors (Ostrem et al., 2013) (Patricelli et al., 2016).

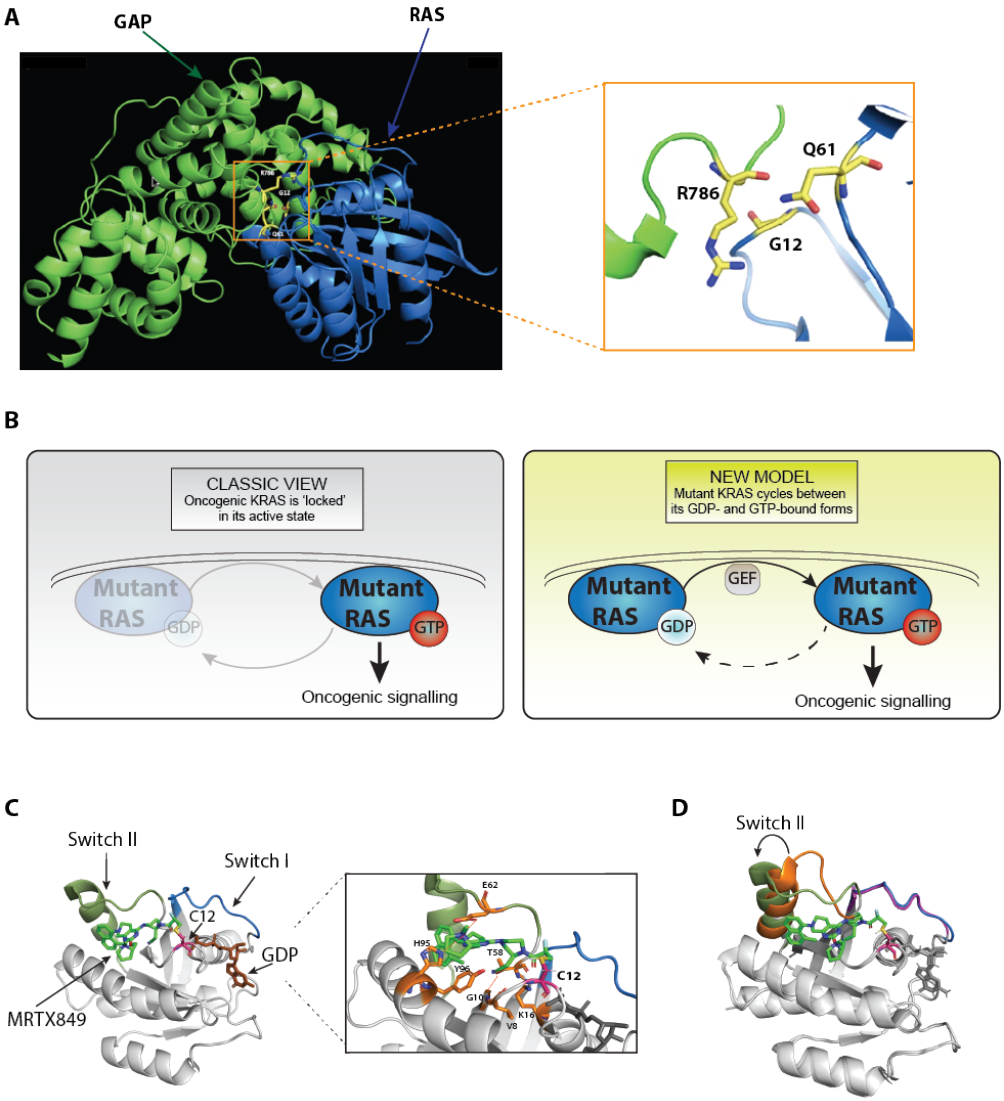

Figure 5. Structure of KRAS mutations and model of G12C inhibitors.

A) Structure of KRAS bound to a GAP, highlighting the localisation of frequently mutated residues in the GAP-binding pocket. Image (PDB: 1WQ1) based on (Scheffzek et al., 1997). B) Comparison of different models of mutant KRAS function, highlighting the current view that rather than remaining locked in the GTP-bound form, mutant KRAS exhibits a diminished GTP hydrolysis rate. C) Structural schematic of $KRAS^{G12C}$ bound to the MRTX849 inhibitor (based on PDB: 6UT0). This structure highlights the binding pocket underneath switch II where the inhibitor is able to access. D) Overlay of KRAS structure in presence (PDB: 6UT0) or absence (PDB: 4LDJ) of a $KRAS^{G12C}$ inhibitor, highlighting the shift in the switch II region that prevents GEF binding. Panels A, C and D have been generated with help from Soly Ismail and are reproduced with his permission.

1.3.3 Development of KRAS^{G12C} inhibitors

Shokat and colleagues were the first to describe, using crystallographic studies, the existence of the novel allosteric binding pocket behind the switch-II region in G12C mutant KRAS, which they called switch-II pocket (S-IIP) (Ostrem et al., 2013). They reported the development of small molecules (notably, compound 12) that could, for the first time, irreversibly and specifically bind to KRAS^{G12C} (Figure 5C). They reported that these molecules were able to disrupt both switch I and switch II (Figure 5D), promoting GDP-binding of KRAS and impeding RAF association in *in vitro* assays and in human G12C mutant lung cancer cell lines. They also provided first evidence that treatment of cells with these inhibitors decreased their viability and increased apoptosis *in vitro* (Ostrem et al., 2013), albeit at a very low potency.

Further optimisation of the structure of the newly developed KRAS^{G12C} inhibitors, led to the development of ARS-853 in 2016 (Patricelli et al., 2016). This compound, also targeting the S-IIP in KRAS^{G12C}, was able to effectively inhibit KRAS signalling (particularly the MAPK pathway, but also the PI3K pathway) in a number of KRAS-mutant cell lines, with a potency in the range of a drug candidate. They also showed effects of the drug on cell cycle proteins and apoptosis in *in vitro* cultured cells, as well as its ability to inhibit the growth of the human KRAS^{G12C} lung cancer cell line H358 in culture (Patricelli et al., 2016) (Lito et al., 2016).

The first *in vivo* data of KRAS^{G12C} inhibitors was reported in a paper by Janes et al in 2018 (Janes et al., 2018). Their drug candidate, ARS-1620 was shown to be more potent and with more rapid KRAS-GDP binding kinetics than its predecessors, compound 12 and ARS-853. Additionally, they were able to optimise its pharmacokinetic properties to be adequate to use *in vivo*. The rapid cycling of KRAS from its GDP- to its GTP-bound state and vice versa, provided an extra challenge to develop drugs that would achieve sufficient *in vivo* target occupancy. They showed KRAS pathway inhibition at a higher potency than ARS-853 in human cell lines, but, most importantly, they revealed for the first time the use of a KRAS^{G12C} inhibitor in mice, by using xenografts of human KRAS^{G12C} cancer cell lines. ARS-1620 was able to significantly inhibit tumour growth in this setting (Janes et al., 2018).

1.3.4 G12C inhibitors in the clinic

The *in vitro* and pre-clinical data of $KRAS^{G12C}$ inhibitors provided by the Shokat group revealed to be promising, so the evident next step was to develop, for the first time, $KRAS^{G12C}$- targeting drugs that could be used in clinical cancer patients.

One of the first reports from the use of such drugs in the clinic came from Mirati Therapeutics Inc. (Mirati). They developed a new G12C targeting drug called MRTX849 that showed marked tumour regression in 65% of tumour cell lines and patient-derived xenograft mouse models (Hallin et al., 2020). Moreover, they showed initial partial responses in two $KRAS^{G12C}$-positive lung and colon cancer patients who were refractory to multiple lines of therapy. These two patients were a part of a phase I/II clinical trial launched by Mirati (NCT03785249) where MRTX849 was administered orally once daily in a continuous regimen. In addition to reporting patient data, they also aimed to identify vulnerabilities and rational combination therapies of KRAS inhibition by performing a clustered regularly interspaced short palindromic repeats (CRISPR)-Cas9 screen in the presence or absence of MRTX849. Hits of this screen included proteins that regulate RAS-dependent signalling and cell cycle transition. In line with this information, they showed that blockade of EGFR-family members and inhibitors of the phosphatase Src homology region 2 domain-containing phosphatase-2 (SHP2) can increase the anti-tumour activity of $KRAS^{G12C}$ inhibitors. $KRAS^{G12C}$ inhibitors also showed synergistic effects when combined with mTOR inhibitors, due to a stronger inhibition of the pathway (Hallin et al., 2020). The identification of adequate combination strategies is of outmost importance given the discovery that G12C inhibitors, albeit leading to a marked reduction in tumour growth, do generally not achieve a complete regression of the tumour, suggesting that resistance mechanisms take place that allow for the tumour to grow despite the inhibition of KRAS.

Concomitantly, another report from the pharmaceutical company Amgen was released describing an alternative $KRAS^{G12C}$ inhibitor that they have developed for the use in cancer patients (Canon et al., 2019), AMG510. They were the first company to initiate a phase I/II clinical trial with a $KRAS^{G12C}$ inhibitor

(NCT03600883) in G12C mutant cancer patients, the response of two of which was reported in this paper. The clinical results in this report were equivalently encouraging as the results from Mirati. Two patients exhibited objective partial responses and other two showed stable disease. All patients had progressed on previous lines of therapy.

Importantly, this report is the first one to show efficacy of $KRAS^{G12C}$ inhibitors in an immune competent murine cancer model, namely the colon cancer cell line CT26, modified to express a G12C mutation in KRAS. Using this model, they reported a complete regression of a subset of tumours after KRAS inhibition, which they suggested was due to an immune rejection of the malignant cells. These effects had never been observed before, because previous studies had utilised human cell lines implanted into immunodeficient mice. In line with this observation, they observed an astonishing synergy between AMG510 (now known as Sotorasib) and the immune therapeutic agent anti-PD-1. Immune profiling of the tumour suggested that KRAS inhibition was accompanied by changes in the tumour microenvironment, such as an increase in cytotoxic T cells. These changes could explain the T cell-dependent rejection of some tumours and the synergism with immune modulatory antibodies (Canon et al., 2019).

Great improvement has been made in the field of KRAS therapeutics, with the advent of $KRAS^{G12C}$ inhibitors, which have generated great excitement in the KRAS research field and in the clinical setting. Additional $KRAS^{G12C}$ inhibitors and other KRAS targeting strategies are currently under development. For a summary of these, refer to Table 1. Current and future research efforts will be aimed at elucidating resistance mechanisms of these inhibitors to develop rational combination strategies to target KRAS-mutant cancers.

Table 1. Summary of current KRAS-targeting approaches.

Adapted from (Mullard, 2019). N/A: non-applicable

Drug name	Company	Drug type	Clinical status
Sotorasib (AMG 510)	Amgen	$KRAS^{G12C}$ inhibitor	Phase I/II Monotherapy and with anti-PD-1
MRTX 849	Mirati Therapeutics	$KRAS^{G12C}$ inhibitor	Phase I/II
JNJ-74699157/ ARS-3248	J&J and Wellspring Biosciences	$KRAS^{G12C}$ inhibitor	Phase I
LY3499446	Eli Lilly	$KRAS^{G12C}$ inhibitor	Phase I/II
BI 1701963	Boehringer Ingelheim	KRAS-SOS1 inhibitor	Phase I Monotherapy and with MEK inhibitor
mRNA-5671	Moderna Therapeutics	Cancer vaccine for G12C, G12D, G13D and G12V	Phase I Monotherapy and with anti-PD1
G12D inhibitor	Mirati Therapeutics	$KRAS^{G12D}$ inhibitor	IND-enabling studies
RAS(ON) inhibitors	Revolution Medicines	Tri-complex inhibitors of mutated GTP-bound KRAS	Preclinical
N/A	Bayer	KRAS-SOS1 inhibitor	Preclinical
N/A	Sanofi/X-Chem	$KRAS^{G12C}$ inhibitor	Preclinical
N/A	X-Chem	$KRAS^{G12C}$ inhibitor (for active and inactive KRAS)	Preclinical
BBP-454	BridgeBio Pharma	Pan-KRAS inhibitors	Preclinical

Additionally, the study by Amgen (Canon et al., 2019) opened a new perspective that targeting KRAS could result in profound changes in the tumour microenvironment, beyond its tumour-cell intrinsic effects. Understanding such changes will be of outmost importance to develop combination strategies with immune therapies and to be able to stratify patients and predict responses according to their immune profile. In order to do so, it is crucial that adequate mouse models are developed that will display the heterogeneity in immune profiles found in human patients. Developing such mouse models and looking at tumour microenvironment changes upon KRAS inhibition are two of the main goals of this thesis.

1.4 Tumour microenvironment

1.4.1 Introduction to the tumour microenvironment

Previous sections have focused on tumour biology viewed from a tumour cell-intrinsic perspective. In fact, in the last decades, the focus of cancer research has been on the malignant cancer cell, aiming to elucidate the contributions of oncogenes and tumour suppressor genes and their role in carcinogenesis. With the advent of new techniques and data, our knowledge on oncogenic pathways and tumour cell signalling has been extraordinarily enriched and this has led to the development of new and effective cancer therapies.

However, more recently, the view of tumour biology has been expanded with the growing understanding that tumours are not solely comprised by malignant cells, but are rather a combination of different cell types that together form a heterotypic microenvironment. These additional cell types consist of resident and recruited cells that are able to communicate with each other and with the neoplastic cells, mainly through secreted soluble factors. Some aspects of the tumour microenvironment, such as the contributions of tumour angiogenesis and the extracellular matrix, have been known and studied for long time (Hanahan and Coussens, 2012). However, growing evidence suggests that diverse cell types present in the tumour microenvironment (TME) play a crucial role in tumour growth and metastasis.

1.4.2 Components of the non-immune TME

As mentioned, the TME is comprised of a large variety of cell types that interact with each other and with the cancer cells. Endothelial cells form the vasculature associated to the tumour, which is crucial for tumour growth, as it provides the nutrients and oxygen necessary for the malignant cells to survive. In fact, the induction of angiogenesis is a known factor to increase the rates of malignant cell proliferation (Hanahan and Folkman, 1996). This has led to the development of antiangiogenic molecules and drugs that aim to reduce nutrient availability in tumours to induce their death (Bergers and Hanahan, 2008). In addition, endothelial cells are known to secrete an array of soluble factors that are able to

recruit additional cell types or promote tumour growth directly (Hanahan and Coussens, 2012).

Cancer associated fibroblasts (CAFs) are an abundant group of fibroblastic cells that are recruited and/or activated in response to a tumour, possibly reflecting a defective wound healing response that has been initiated by the malignant cells. CAFs participate in extracellular matrix (ECM) remodelling and contribute to cancer cell proliferation and aggressiveness by secreting signalling proteins, but their relevance and abundance in the tumour microenvironment depends highly on the tumour type (Hanahan and Coussens, 2012). For instance, pancreatic cancers are characterised by a desmoplastic reaction and are mostly comprised of stromal cells. The role of CAFs in lung cancer is less studied, but they are known to contribute to tumour formation in the lung (Mahale et al., 2016). Their origin and prognostic value has been under controversy, but it is accepted that there is a variety of CAF subtypes that may differ in their role and origin (Cirri and Chiarugi, 2011).

Notably, tumours are infiltrated by diverse populations of leukocytes, including myeloid- and lymphoid- lineage cells, which are of outmost importance in tumour progression and that will be discussed in further depth in subsections 1.4.3 and 1.4.4.

1.4.3 T cells in the TME, cancer immunoediting

The role of the immune system is to detect and eradicate harmful invaders, such as bacterial and viral pathogens. The immune system consists of an innate arm, which is the first-line of defence, and recognises such pathogens in an unspecific manner, generating an inflammatory environment; and the adaptive arm, which requires a longer time to develop but recognises the pathogens specifically by their expression of ‘foreign’ molecules or antigens.

At the beginning of the 20th century, Paul Ehrlich was perhaps the first person to hypothesise that the immune system continuously detects and kills aberrantly growing malignant cells. In fact, he reasoned that if it were not for the presence of

an immune system, formation of tumours would be a much more frequent event (Schreiber et al., 2011). William Coley's experiments inducing tumour regression after injection of bacteria in patients provided early evidence in support of this hypothesis (Schreiber et al., 2011). This concept resurfaced half a century later, when Burnet and Thomas formed their 'cancer immunosurveillance' hypothesis, based on their discoveries of tumour antigens, mostly of viral origin, which suggested that tumours could indeed be seen by the host's immune system (Burnet, 1957). The idea of cancer immunosurveillance remained controversial for a number of years, until the 1990s, where mouse models of immunodeficiency were largely improved (Schreiber et al., 2011). Schreiber's group underscored the importance of an intact interferon-γ (IFN-γ) (a cytokine known to be secreted by cytotoxic T cells) response in rejecting transplanted tumour cells (Dighe et al., 1994). Furthermore, mice lacking IFN-γ responsiveness or adaptive immunity ($Rag1/2^{-/-}$ mice, which lack T and B cells) were more susceptible to carcinogen-induced and spontaneous primary tumour formation (Kaplan et al., 1998) (Shankaran et al., 2001). These reports and others, demonstrated that the immune system can exert tumour inhibiting functions, and that cytotoxic T cells were able to specifically recognise and eliminate tumour cells.

The current view, pivotal for the studies of tumour immunology, is that tumours express antigens on their surface that can be recognised by the host's immune system. Tumour-associated antigens (TAAs) can be of different types. For instance, in those tumours associated with viral infections, such as human papillomavirus (HPV)-induced cervical cancer, the proteins from the virus are foreign to the host and thus act as antigens (Schreiber et al., 2011). Alternatively, tumours are able to overexpress cellular antigens or cancer/testis antigens that are not expressed in normal tissues and can be detected by the immune system (Schumacher and Schreiber, 2015). However, it is widely accepted now that the most common type of antigen arises from mutations in the genomic sequence of tumour cells as a consequence of the inherent genomic instability of transformed cells. These mutated sequences, which differ from proteins expressed on normal cells, can be presented as peptides on the surface of the tumour cells, in association with major histocompatibility complexes (MHC), making them visible to cells in the immune system (Schumacher and Schreiber, 2015). Different tumour

types differ in the number of mutations present in their genome, leading to the current view that their immunogenicity, or ability to be recognised by the adaptive arm of the immune system, is inherently different (Alexandrov et al., 2013). The logical conclusion of such observations is that the mutational burden of a tumour will determine the responsiveness to immunotherapy approaches such as checkpoint blockade (Rizvi et al., 2015). This is a very simplistic view, as the process of responsiveness to immune therapy is much more complex. Enormous efforts from the research community are aiming to understand patterns of responsiveness and resistance to immune checkpoint blockade.

For an effective immune response to occur, T cells must encounter a tumour-associated antigen in the context of professional antigen presenting cells (APC) such as macrophages and dendritic cells. Antigen presenting cells are able to phagocytose material from tumour cells, process it and present it on their surface bound to MHC II. A specific subset of dendritic cells are able to, via a process termed cross-presentation, present these antigens bound to MHC I and thereby trigger *de novo* activation of CD8+ T cells (Bottcher and Reis e Sousa, 2018). The process of T cell activation requires not only the binding between MHC on APCs and the adequate TCR on T cells, but also co-stimulatory molecule binding and the release of cytokines (Medler et al., 2015). After adequate activation, antigen specific T cells are clonally expanded in response to IL-2. Activated CD8+ T cells acquire cytotoxic properties. When they encounter their specific antigen presented by a tumour cell, they are able to selectively exert their cytotoxicity and eliminate that tumour cell. The role of CD4+ T cells, activated via MHC II binding, is to assist CD8+ T cells, mostly via the secretion of cytokines, and they are also known as T helper cells. A schematic of this process is represented in Figure 6.

However, not all T cells are able to (directly or indirectly) exert anti-tumorigenic functions (Medler et al., 2015). A subset of CD4+ T cells, characterised by their expression of the transcription factor Foxp3 is known to exert regulatory function and is known as ‘regulatory T cells’ or Tregs. These cells are able to inhibit anti-tumour immune responses and in physiological conditions, provide means to prevent exacerbated immune responses, but tumours are able to recruit Tregs to promote immunosuppression (Sharma and Allison, 2015).

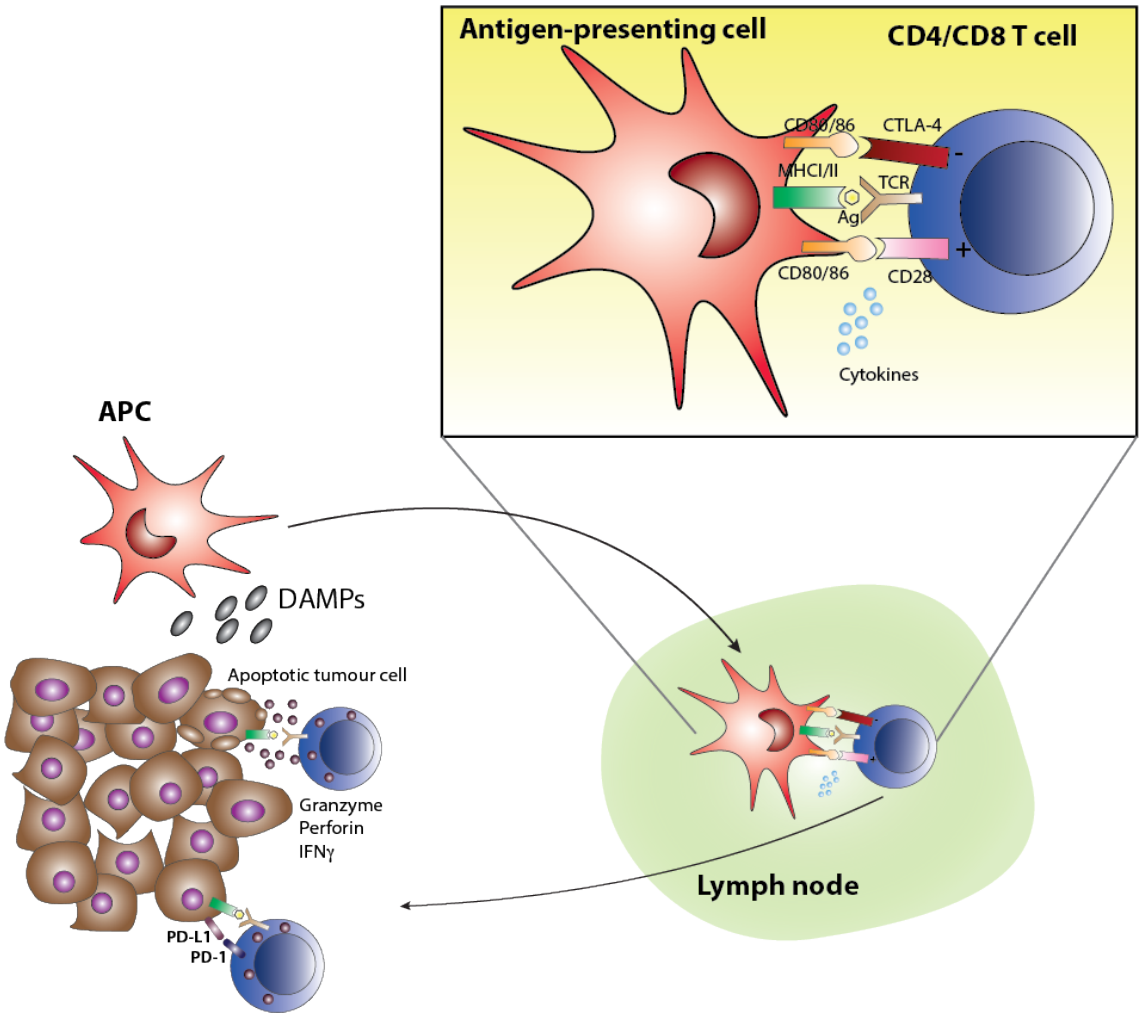

Figure 6. Schematic of an anti-tumour response.

This figure illustrates the steps of an anti-tumour response. APCs engulf antigen from dying tumour cells and migrate to the lymph node, where they activate T cells. Activated T cells then migrate back to the tumour, where they can selectively eliminate antigen-expressing tumour cells. The mechanisms of the inhibitory receptors CTLA-4 and PD-1 are also illustrated. APC: antigen presenting cell, Ag: antigen, DAMPs: danger associated molecular patterns. Figure adapted from (Medler et al., 2015).

Even though the adaptive immune system, mainly driven by T cells, has the ability to inhibit tumour growth, the cancer immunoediting hypothesis suggests that tumours find mechanisms by which they evade the actions of the immune system (such as the recruitment of Tregs mentioned above). In this context, the immune system would exert tumour-promoting actions by providing a selection force on tumour cells that will allow the most aggressive clones to grow (Rosenthal et al., 2019). Examples of such mechanisms, intrinsic to the tumour cell, include the loss

of expression of clonal neoantigens (Rosenthal et al., 2019) or MHC molecules (McGranahan et al., 2017) that will allow the tumour cell to hide from the immune system.

The most commonly known mechanism by which tumours evade the actions of cellular immune responses is by providing the signals to lead to T cell anergy or exhaustion. This immune escape mechanism has gained relevance with the advent of therapies that aim to reverse the action of these molecules and re-activate T cell responses, namely immune checkpoint blockade molecules (Sharma and Allison, 2015). Of these, CTLA-4 and PD-1 targeting compounds are the clinically most advanced therapeutic antibodies. These two molecules, however, differ in their precise mechanism and time of upregulation. CTLA-4 plays a role in dampening T cell activation, by competing with T cell antigen CD28 for binding with CD80/86 to provide adequate co-stimulation. In addition, CTLA-4 has been reported to be highly expressed by Tregs and the mechanism of anti-CTLA-4 antibodies has been shown to be, at least partially, through their ability to specifically deplete Tregs from the TME (Quezada et al., 2006) (Arce Vargas et al., 2018). In contrast, PD-1 is upregulated on antigen-experienced T cells as a negative regulation mechanism. Upon binding its ligands, PD-1 attenuates T cell activity by directly supressing signalling through the TCR receptor (Yokosuka et al., 2012). These ligands are often expressed in non-lymphoid tissues and this pathway therefore plays a critical role in limiting T cell activity in peripheral tissues (Keir et al., 2006).

One major defining characteristic of adaptive immune responses is their memory, meaning that once T cells are effectively activated to recognise an antigen, this recognition lasts for a lifetime. This constitutes the reason why, if effective, immune therapies such as immune checkpoint blockade. lead to long term responses in patients, reflective of a successful immune response.

As it will be discussed in the next section, other mechanisms that promote tumour growth by evading adaptive immune responses are based on the recruitment of additional immune cell types that are ‘corrupted’ by the tumour milieu and acquire tumour-promoting properties.

1.4.4 Beyond T cells: additional components of the immune TME

T cell responses to cancer have been widely studied as they are considered the most critical arm of the anti-tumour immune response, due to their direct cytotoxic capabilities. Nevertheless, a vast array of different immune cells are recruited in response to a growing tumour.

One other component of the adaptive arm of the immune system is the B cell. B cells can be highly abundant, constituting up to 25% of all cell in some tumours (Coronella-Wood and Hersh, 2003). B cells are thought to play immunomodulatory roles and they are thought to also constitute targets of immune checkpoint blockade antibodies (Postow et al., 2015). B cells can make antibodies, which, in theory, could opsonise tumour cells for antigen presentation, activate the complement cascade or contribute to NK cell mediated killing via antibody-dependent cell cytotoxicity (ADCC). In contrast, some immune-suppressive functions have been attributed to tumour infiltrating B cells. B cells are known to secrete a number of factors that induce angiogenesis (Folkman, 1971). A subset of B cells, called regulatory B cells (Bregs) secrete immunoregulatory cytokines that suppress effector cells, such as interleukin 10 (IL-10) or transforming growth factor beta (TGFβ) (Lund, 2008). All in all, B cells constitute a possibly understudied cell type with controversial roles in anti-tumour immunity.

Besides T cells, NK cells are the other cell type which is also able to exert direct cytotoxic actions on tumour cells, despite being part of the innate arm of immunity. Rather than recognising specific antigens, NK cells recognise their targets based on a lack of MHC molecules on their surface, and their function is tightly regulated by a combination of activatory and inhibitory receptors (Lanier, 2008). In this manner, NK cells are able to recognise and kill ‘stressed’ cells, like virus-infected or tumour cells, in a faster fashion than adaptive cells such as T cells. Currently, research is underway aiming to therapeutically harness NK cell activity to target cancer, either by targeting checkpoint molecules on NK cells or by adoptive transfer strategies, among others (Morvan and Lanier, 2016).

1.4.5 Myeloid cells in the TME

Myeloid cells are a diverse population of immune cells that are able to sense and respond to tissue injuries by clearing harmed cells and regulating immune responses (Lavin and Merad, 2013). There are three groups of terminally differentiated myeloid cells: macrophages (and their immature version, monocytes), dendritic cells (DCs) and granulocytes or neutrophils, that are highly abundant in the TME and play important roles in tumour progression. Myeloid cells can arise from multipotent haematopoietic stem cells (HSC) in the bone marrow and can be found in circulation before homing to tissues/tumours in response to attracting stimuli, such as specific chemokines (Gabrilovich et al., 2012). Additionally, different organs contain tissue-specific myeloid cells of embryonic origin, such as Langerhans cells (DCs) in the skin or the microglia (macrophages) in the brain. In inflammatory conditions, such as tumours, the phenotypic and functional properties of myeloid cells are generally altered and differ from those cells found in homeostatic conditions (Bowman et al., 2016).

DCs are myeloid cells that, when activated and matured, specialise in antigen processing and presentation to effector cells. They are key in connecting innate and adaptive immunity, and absolutely crucial to mount an effective immune response. Consistently, DCs have been described to exist in tertiary lymphoid structures and in proximity to T cells in human lung tumours, suggesting a role in T cell activation, at least in early stages of lung cancer (Lavin et al., 2017). However, it is known that often tumour-associated DCs re not able to generate an adequate immune response, due to the actions of many tumour-derived soluble factors that lead to an abnormal DC differentiation (Gabrilovich, 2004). These abnormal DCs may actively suppress T cell function, thereby promoting immune tolerance (Lin et al., 2010). This has been clinically confirmed by the finding of defective DCs in cancer patients, including in NSCLC patients (Perrot et al., 2007).

As previously mentioned, this thesis focuses on lung cancer. As an organ, the lung is largely specialised to perform gas exchange, which occurs in the alveoli. As a consequence, the lung is in constant contact with exogenous particles and potential pathogens which need to be adequately dealt with to avoid tissue damage and

infection. Myeloid cells, in particular macrophages, play a crucial role in the lung to this end. Alveolar macrophages are present in the lumen of the alveoli in the lung and play an important role in lung development, surfactant homeostasis, pathogen clearance and immune regulation (Guilliams et al., 2013). They are phenotypically dissectible thanks to their expression of integrin CD11c and lack of expression of the phagocytic receptor CD11b (Misharin et al., 2013). Similar to other tissue-resident macrophage populations in different organs, such as the microglia in the brain or Kupffer cells in the liver, alveolar macrophages derive from fetal yolk sac macrophages that seed the lung during embryonic development (Guilliams et al., 2013). These macrophages constitute a long-lived cell population with self-renewing capabilities (Guilliams et al., 2013) (Hashimoto et al., 2013). In contrast, interstitial macrophages are defined as CD11b+CD11c-F4/80+, are of monocytic origin, and are present in lower proportions than the alveolar counterpart in healthy lung (Guilliams et al., 2013) (Loyher et al., 2018). They are usually located in the pleura, along blood vessels and in proximity to large airways of the lungs (Rodero et al., 2015).

However, inflammatory tissue environments, such as those arising from the growth of a tumour, significantly alter the composition found in homeostasis. For instance, while the tissue-resident microglia is the only macrophage population present in normal brain, brain tumours display an infiltration of both microglia and monocyte-derived macrophage populations, which exhibit different transcriptional profiles, as evidenced by lineage tracing experiments (Bowman et al., 2016). Similarly, pancreatic ductal adenocarcinoma (PDAC), a prominently KRAS-driven tumour type, exhibits abundant macrophage infiltration in a cohort of patients (Zhu et al., 2017). Both bone marrow derived, inflammatory monocytes and tissue-resident macrophages have been shown to act as sources for TAMs in a mouse model of PDAC and harbour distinctive roles in tumour progression (Zhu et al., 2017). In this report, they made use of a widely utilised method to discern the origin of tissue-macrophages by making use of $CCR2^{-/-}$ mice. CCR2 is critical for monocytes to egress from the bone marrow (Serbina and Pamer, 2006) and therefore $CCR2^{-/-}$ mice allow for the investigation of the contribution of circulating monocytes to the macrophage pool in a tissue. Interestingly, in their model of PDAC, Zhu et al. showed that loss of monocyte-derived macrophages by $CCR2^{-/-}$ had no effects on

tumour progression while depletion of tissue-resident macrophages significantly improved survival (Zhu et al., 2017). Thus, it is of outmost importance to examine the functional roles and phenotypes of immune populations in the TME as they may provide therapeutic targets.

The advent of novel single cell analysis techniques has allowed the identification and dissection of novel immune cell subsets present in an array of contexts, including human lung cancer (Lavin et al., 2017). TAMs have been shown to exhibit a distinct transcriptional signature compared to healthy lung tissue macrophages, which correlates with poor survival in a TCGA cohort of lung adenocarcinoma patients (Lavin et al., 2017). Extensive knowledge is available which demonstrates that TAMs, recruited to inflammatory sites such as tumours in response to chemoattractant molecules such as CC-chemokine ligand 2 (CCL2) (Lavin et al., 2017), are corrupted during malignancy to promote tumour progression. In their report, Lavin et al. observed that the TME exhibits tumour-promoting characteristics in a cohort of Early Lung Adenocarcinoma patients which have not previously undergone treatment. This data suggests that cues from tumour cells themselves play a strong role in forming the immune TME (see examples of this in 1.5). TAM functions include the promotion of angiogenesis (Lin et al., 2006), aiding tumour cell extravasation and metastatic cell seeding and protection of tumour cells against chemotherapy-induced apoptosis (Qian and Pollard, 2010). TAMs, via immunosuppressive cytokine secretion, are also able to suppress anti-tumour immunity by dampening T cell activation and often, in a tumour context, they are unable to effectively present antigen (DeNardo et al., 2009). In a flow cytometric analysis of a transplantable model of murine lung cancer, a CD64+ macrophage population expanded and accumulated in the tumour parenchyma, originating from an Ly6C+ monocyte population, whereas the number of alveolar macrophages was strongly reduced with tumour growth and limited to the healthy alveolar space (Loyher et al., 2018). Both subsets also displayed differential transcriptional and cytokine profiles, suggesting that both populations contribute differently to the TME. Interestingly, making use of $CCR2^{-/-}$ mice, they identified an additional subset of macrophages that seemed to arise from a CCR2-independent accumulation of resident IMs. In addition, they observed that the location of the tumour in the lung affected the macrophage composition, with monocyte-derived macrophages being

more predominant in tumours developing close to the pleura as compared with nodules located in the alveoli, adding an extra layer of complexity in the landscape of TAM infiltration in lung cancer. Deep phenotypic and functional analyses of macrophage subsets in lung cancer are therefore of utmost importance as it may provide novel therapeutic targets.

Monocytes constitute the immature form of myeloid cells, and are usually found in circulation. In physiological conditions, monocytes are recruited to inflammatory site and differentiated into macrophages. However, signals in the TME, which can be released by tumour cells, can block monocytes in their immature form, and hence immature monocytes can be found in tumour tissues. Tumours are also able to corrupt monocytes to make them tumour-promoting and highly immune suppressive (more so than their mature counterparts). Due to their origin and function, these cells have been termed myeloid-derived suppressor cells, which (Gabrilovich et al., 2012). There are defined by their expression of CD11b and Gr1, but their phenotype in cancer is more diverse, as they can express other markers such as low levels of F4/80, CD115 (or CSF-1R) and CCR2 (Youn et al., 2008). Their main role is to suppress T cell responses through the production of reactive nitrogen species (Youn et al., 2008). The frequency of MDSCs in the blood constitutes a poor prognosis factor, in a number of tumour types and in response to therapies (Diaz-Montero et al., 2009).

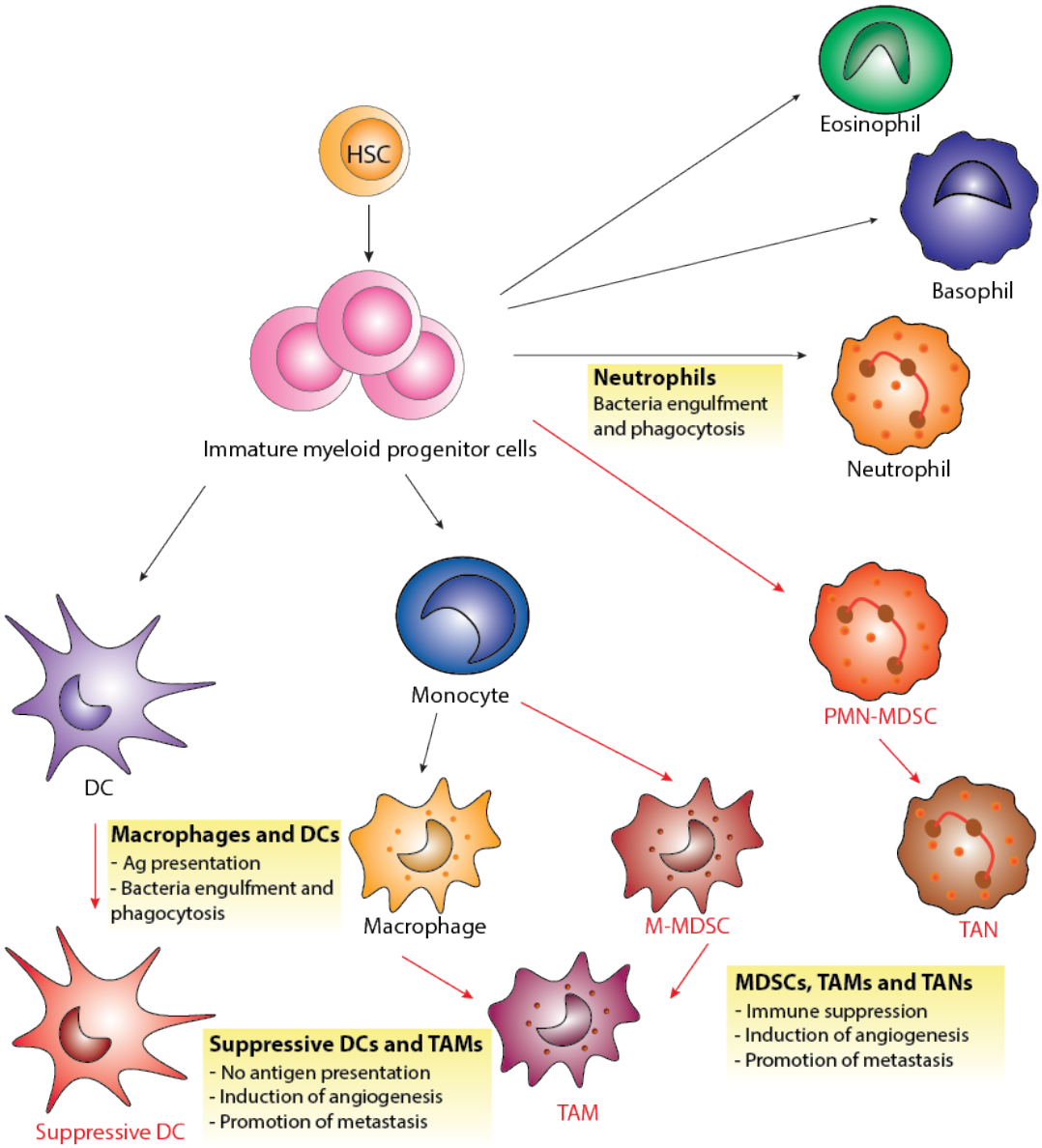

Figure 7. Aberrant differentiation of bone marrow derived myeloid cells in the TME.

Schematic illustration of myeloid populations and their aberrant differentiation status in the TME (adapted from (Gabrilovich et al., 2012)). Red arrows and labels represent populations present in the TME, black arrows indicate physiological differentiation pathways. Ag: antigen, HSC: haematopoietic stem cell, PMN-MDSC: polymorphonuclear-myeloid derived suppressor cell, M-MDSC: monocytic-myeloid derived suppressor cell, TAN: tumour-associated neutrophil, TAM: tumour-associated macrophage, DC: dendritic cell

Neutrophils, or polymorphonuclear leukocytes, also known as granulocytic myeloid-derived suppressor cells (gMDSC), comprise another subset of myeloid cells characterised by their specific nuclear morphology and that they contain granules in their cytoplasm. The physiological role of neutrophils is to engulf and destroy pathogens such as bacteria. Neutrophils are usually present in circulation in their mature form, although certain inflammatory stimuli such as signals arising from the tumour may cause their immature form to be released from the bone marrow (Summers et al., 2010). Tumour-associated neutrophils are known to exert pro-tumorigenic actions such as promoting tumour angiogenesis and metastasis, with a crucial role in forming pre-metastatic niches (Gabrilovich et al., 2012). Neutrophils are recruited to tumour sites in response to CXC-chemokines released by stromal cells or by tumour cells. A schematic of all bone marrow-derived myeloid cells and their aberrant differentiation in tumour sites is illustrated in Figure 7.

With the increasing knowledge about the composition and the functions of the cells present in the TME, it is now clear that limiting the immunosuppressive and pro-tumorigenic functions of myeloid cells constitutes a valid therapeutic strategy in cancer. The elucidation of the molecular mechanisms responsible for myeloid cell-driven immunosuppression and angiogenesis has initiated efforts to inhibit such pathways, such as the use of nitroaspirin to block reactive nitrogen species (De Santo et al., 2005) or anti-VEGF antibodies to inhibit angiogenesis. Another strategy is to inhibit myeloid cell accumulation in circulation and in tumour sites, by blocking myeloid chemoattractants like CCL2 (Qian et al., 2011) or chemokine receptors such as CXCR2 (Yang et al., 2008). Other ideas in development includes aiming to repolarise macrophages into a pro-inflammatory phenotype and to restore antigen-presenting capabilities of DCs and macrophages (Gabrilovich et al., 2012).

1.4.6 Types of immune TMEs

Previous subsections have aimed to explain the different cells that can be present in the TME. However, it is important to note, that the cell composition of the TME can vary greatly between tumour entities. As mentioned previously, for instance, pancreatic cancer is widely desmoplastic and characterised by a high infiltration of

fibroblasts, more so than other tumour types. Additionally, tumours, even those from the same origin, are known to generate unique TMEs depending on the tissue they arise in. In this manner, the TME of a breast tumour growing in breast tissue is distinct from the TME generated by the same tumour cells that have metastasised to the brain or the bone, for example (Soukup and Joyce, 2018). This suggests that the TME is driven by characteristics of the tumour but it is also shaped by signals coming from the tissue itself. Factors that determine the given TME of a tumour are largely unknown, but it has been suggested that tumour genetics, together with characteristics of the host such as age, microbiome and germline genetics may contribute to the composition of the TME. TMEs can also look different in different tumours from the same patient and even in different regions of the same tumour, possibly as a reflection of the tumour heterogeneity and subclonality (Rosenthal et al., 2019).

Efforts have been made to attempt to classify different TME types into a distinct number of phenotypes. Such a classification, as the one described below suggested by D. Chen and I. Mellman, is probably an oversimplification of the wide continuum when it comes to TME compositions, but it is a useful way to distinguish TMEs of different tumours and their potential clinical meaning (Chen and Mellman, 2017).

The first TME type is the ‘immune-inflamed’ phenotype. This phenotype is characterised by a high infiltration of immune cells, including CD4 and CD8 T cells and myeloid cells. The immune cells in this instance can be found infiltrating the tumour (Chen and Mellman, 2017). These tumours express many proinflammatory and effector cytokines, such as IFNγ and T cell recruitment chemokines CXCL9 and CXCL10, and may exhibit PD-L1 staining (Herbst et al., 2014). Presence of this type of TME suggests that an effective immune response occurred in the past, but it was overcome by the tumour by driving immune suppressive mechanisms, such as T cell exhaustion. The patients harbouring such a TME are the most likely to respond to immune checkpoint blockade approaches, although responses do not occur in all of the patients (Herbst et al., 2014). In fact, PD-L1 staining is currently the most used biomarker of response to immune checkpoint blockade (Herbst et al., 2014).

The second type is the ‘immune-excluded’ phenotype, which also shows highly abundant immune infiltration. However, in this case, immune cells, rather than infiltrating the tumour, are retained in the stroma surrounding the tumour (Joyce and Fearon, 2015). These tumours have likely experienced an antitumour response, but have been able to evade it by effectively impeding immune cell infiltration. In these cases, treatment with checkpoint blockade antibodies may lead to activation of those T cells observed in the periphery, but because they are unable to form direct interactions with tumour cells, clinical responses to immune therapies are rarely seen (Chen and Mellman, 2017).

The third profile is the ‘immune-desert’ phenotype, characterised by a lack of T cells anywhere in the proximity of the tumour, although myeloid cells may be present (Chen and Mellman, 2017). These tumours can express cytokines and cell populations associated with immune suppression or tolerance, such as regulatory T cells (Tregs) MDSCs and TAMs. In these tumours, no effective anti-tumour immunity was probably mounted, so these patients very rarely respond to immune checkpoint blockade agents (Herbst et al., 2014).

In conclusion, the TME is composed of cell types that are attracted to tumour sites due to their inflammatory characteristics, but once there, signals from the tumour convert them into functionally distinct populations that play different roles in tumour progression. The elucidation of mechanisms driving this infiltration and polarisation of TME cells is of outmost importance in order to develop novel anti-tumoural therapeutic strategies.

1.5 Oncogenes and the TME

1.5.1 Introduction

Previous sections have focused on the role of oncogenic pathways in tumour progression, and the role of the TME in this process as a separate concept. Nevertheless, these two components are highly intertwined. In fact, one of the major factors in determining the landscape of the TME, as previously mentioned, is the genomic composition of the tumour. Correlations of RNA-based metrics of immune activity with genetic data stemming from the Cancer Genome Atlas (TCGA) dataset, revealed that there was indeed an association between genomic drivers in the tumours (such as PIK3CA, MET or TP53) and immune cell activation or infiltration of certain immunosuppressive populations, such as macrophages (Rooney et al., 2015). This suggests that aberrant signalling pathways in the tumour, which can be activated through gain-of-function alterations in oncogenes or loss-of-function alterations in tumour suppressor genes, not only have tumour cell-intrinsic biological outputs, but are also able to signal to the exterior and shape the immune TME, in order to avoid anti-tumour immune responses and promote tumour progression (Spranger and Gajewski, 2018). Elucidating the molecular mechanisms by which tumour cell signalling drives immune evasion will be critical to reveal resistance mechanisms to immune therapies such as checkpoint blockade, and will provide means to predict responses to such therapies. Additionally, understanding the mechanisms of immune evasion, and therefore, resistance to checkpoint blockade, will aid in the design of rational and personalised anti-cancer treatment combinations and result in an increase the number of patients that respond to checkpoint blockade therapies.

Immune evasion mechanisms triggered by tumour-intrinsic pathways include mechanisms leading to defective T cell activity, such as impeding T cell priming or promoting T cell exhaustion. Other mechanisms aim to hide tumour-associated antigens from the immune system, by downregulating such antigens or components of the antigen presentation machinery. Another way of driving immune evasion is the recruitment of immune inhibitory cell populations. Examples of some

known tumour suppressor genes and oncogenes and how they mediate immune evasion are listed below (and summarised in Figure 8).

1.5.2 Immune evasive properties of tumour suppressor genes

Liver kinase B1 (LKB1) is a tumour suppressor gene that is mutated in approximately 30% of patients with NSCLC, often found together with mutations in KRAS, and is associated with a bad prognosis (Ji et al., 2007). As mentioned in section 1.1.2, NSCLC is a highly mutated cancer type, and is therefore predicted to harbour a large number of neoantigens, so it should be susceptible to an anti-tumour immune response (Alexandrov et al., 2013) (Rizvi et al., 2015). However, Lkb1 deletion in mouse models has been associated with an increase in neutrophil infiltration, along with a decrease in T cells (Koyama et al., 2016). Additionally, T cells in this model exhibited an exhausted phenotype, characterised by a reduced cytokine production and an increased expression of PD-1, T cell immunoglobulin and mucin domain-containing protein 3 (TIM3) and lymphocyte activation gene 3 (LAG3). Gene expression profiling revealed that loss of Lkb1 led to higher levels of interleukin-33 (IL-33), CXCL7 and IL-6. In fact, neutrophil depletion or IL-6 blockade were able to reverse this phenotype and render Lkb1-deficient tumours sensitive to anti-PD-1 therapy (Koyama et al., 2016) (Skoulidis et al., 2018).

In melanoma, another highly mutated tumour type that should be able to generate effective anti-tumour responses, inactivation of the tumour suppressor gene phosphatase and tensin homolog (PTEN) has been associated with a defective T cell-mediated tumour killing and decreased T cell recruitment into tumours (Peng et al., 2016). In a similar manner to LKB1, PTEN loss in tumour cells also increased the expression of immunosuppressive cytokines, such as CCL2 and VEGF. Moreover, treatment with a specific PI3Kβ inhibitor improved the efficacy of immune checkpoint blockade treatment.

p53 is the most frequently altered tumour suppressor gene in cancer. In consequence, the effects of p53 loss on immune evasion have been widely studied. p53 loss has been widely linked to the expression of an array of cytokines

(Spranger and Gajewski, 2018) and more recently, mouse models of breast cancer have unveiled a mechanism by which p53 loss leads to an accumulation of tumour-promoting neutrophils in a Wnt –dependent manner (Wellenstein et al., 2019).

1.5.3 Immune evasive properties of oncogenes

The Wnt-beta-catenin pathway is frequently altered in melanoma, and has been associated with a non-T cell inflamed phenotype (Spranger et al., 2015). The use of a BRAF-mutant, Pten floxed mouse melanoma model confirmed that β-catenin positive tumours indeed displayed reduced T cell infiltration and were resistant to checkpoint blockade (Spranger et al., 2015). β-catenin positive tumours had a decreased production of CCL4 and other chemokines with caused a reduced recruitment of DCs, followed by defective T cell priming. T cell trafficking was also affected by increased β-catenin signalling, due to a decrease in T cell chemoattractant CXCL9 and CXCL10 (Spranger et al., 2015). Adoptive transfer of mature DCs was able to restore treatment sensitivity in β-catenin positive tumours.

MYC is a transcription factor that, when overexpressed, acts as an oncogene in a high number of human cancers, by regulating cell proliferation, differentiation and survival (Dang, 2012). Evidence suggests that the activation of an effective immune response, by activation of CD4 T cells and a decrease of macrophages and neutrophils underpins the successful tumour cell elimination upon Myc inactivation (Rakhra et al., 2010) (Sodir et al., 2011). Further research discovered that transcription of the checkpoint ligand PD-L1 and the antigen presenting cell inhibitor CD47 were controlled directly by MYC (Casey et al., 2016). Other effects of Myc activation include an increase in the macrophage chemoattractant CCL9 and IL-23, which orchestrates the exclusion of effector cells such as T and NK cells (Kortlever et al., 2017), promoting an immunosuppressive TME.

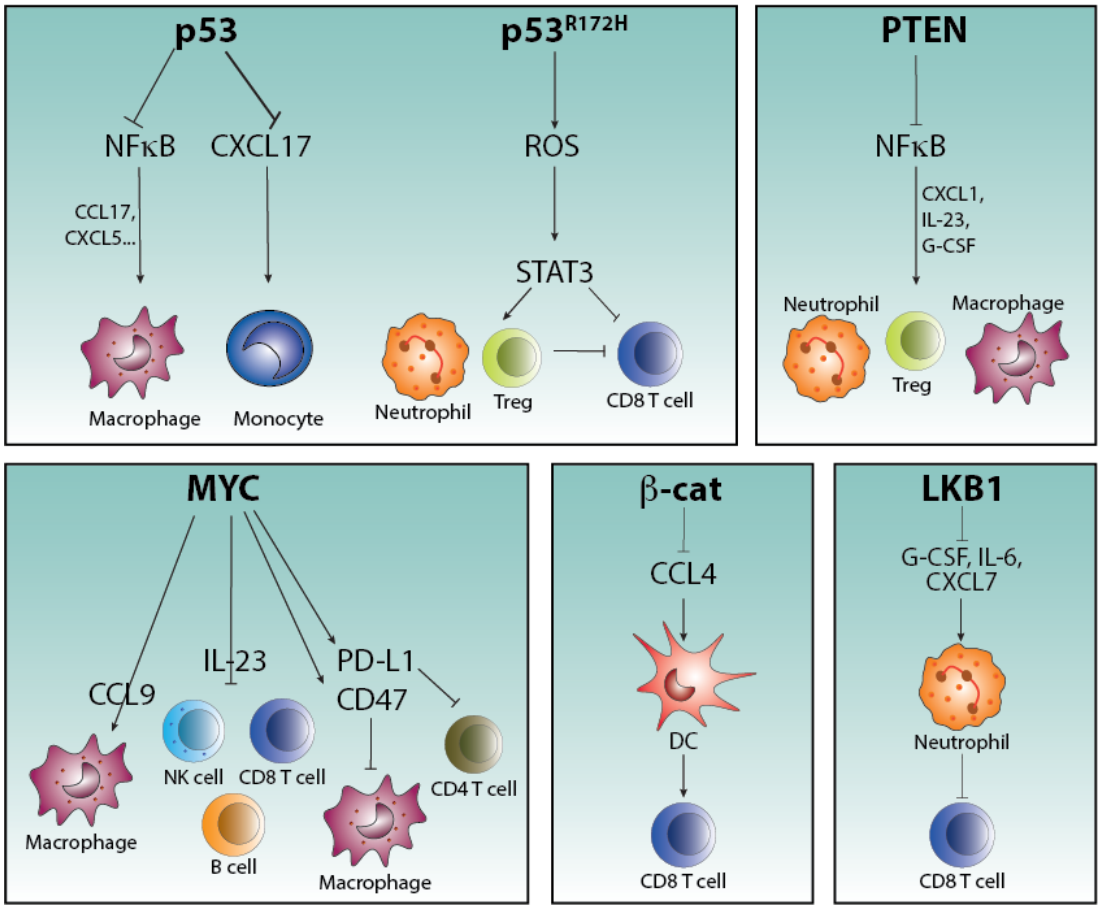

Figure 8. Summary of known immune evasive mechanisms of oncogenes/tumour suppressor genes.

Adapted from (Wellenstein and de Visser, 2018). Treg: regulatory T cell, DC: dendritic cell, NK: natural killer.

1.5.4 KRAS and the TME

As mentioned before, the focus of this thesis is KRAS-mutant lung cancer. We aim to elucidate mechanisms by which oncogenic signalling by KRAS affects the TME and drives immune evasion and resistance to immune therapies. Some research has been done in the past looking at the effects of KRAS signalling on the TME, especially on cytokine secretion, some of which is summarised below.

Some examples of non-tumour cell-autonomous effects of KRAS signalling have been known for some time. For example, it has been shown to activate matrix metalloproteinases to degrade components of the basement membrane to promote invasion and metastasis (Ballin et al., 1988). Moreover, Ras signalling is known to

transcriptionally upregulate VEGF and repress thrombospondin-1 (TSP-1), thereby promoting tumour angiogenesis (Okada et al., 1998) (Watnick et al., 2003).

However, reports about how KRAS influences the immune microenvironment have only started to arise more recently. One of such first reports described a mechanistic link between KRAS signalling and CXCL8/IL-8 secretion. This human chemokine, which does not have a homolog in mice, is known to bind to receptors on target cells, such as neutrophils, to attract them to inflammatory sites. This discovery was made using an $HRas^{G12V}$ activated transgene on human cells, whose expression increased CXCL8 transcription. CXCL8 activation proved to be pro-tumorigenic and was suggested to exert its actions in a non-cell-autonomous manner by affecting tumour vascularisation (Sparmann and Bar-Sagi, 2004). However, as they had to utilise nude mice to implant the human cells, experiments were performed in the absence of an adaptive immune system, so effects of KRAS signalling on immune responses could not be examined.

Using a similar system, where a mutant form of Ras was induced exogenously on human kidney cells, another report described the link between Ras signalling and IL-6 secretion (Ancrile et al., 2007). IL-6 was also pro-tumorigenic and acted in a paracrine manner, probably by promoting tumour vascularisation. Tumours in this report were also implanted in immunodeficient mice so no conclusions could be drawn about the role of tumour-derived IL-6 on the adaptive immune system.

A report from the K.K. Wong lab in 2006 looked at the effects of $KRAS^{G12D}$ activation in Clara cells in the lung of wild-type mice (Ji et al., 2006). This activation led to a dramatically shortened life span of the mice, which exhibited hyperplasia of lung bronchiolar cells followed by adenoma (and in some instances, adenocarcinoma) formation. The main feature of these lungs was their pronounced inflammation, characterised by the infiltration of macrophages and neutrophils. The authors linked this to an increase in the neutrophil chemokines CXCL2/MIP-2 and CXCL1/KC (orthologues of human CXCL8) and the macrophage chemoattractants CCL2/MCP-1 and CCL3/MIP-1α (Ji et al., 2006). They suggested that expression of these cytokines was driven by oncogenic KRAS signalling. This report showed that mutant KRAS signalling in the lung promotes inflammation, but failed to

describe a mechanistic link between KRAS signalling in tumour cells and the secretion of immunosuppressive chemokines.

In a genetically engineered mouse model (GEMM) of KRAS-mutant pancreatic cancer, they established a link between mutant KRAS and the secretion of the granulocyte monocyte-colony stimulating factor (GM-CSF), which could be inhibited by the abrogation of downstream pathways of KRAS (Pylayeva-Gupta et al., 2012). They showed that this chemokine plays a role in the proliferation and differentiation of myeloid cells. Knock down of GM-CSF confirmed its role in the accumulation of myeloid cells in the tumour site and impeded tumour growth in the pancreas of the mice. The immunosuppressive role of GM-CSF was confirmed by an increase in CD8 T cells observed in the tumours upon GM-CSF knockdown (KD), and depletion of CD8 T cells restored tumour growth capacity of GM-CSF KD tumours. They hereby showed a mechanism by which oncogenic KRAS signalling in pancreatic cancer is able to evade an immune response via the recruitment of immunosuppressive myeloid cells (Pylayeva-Gupta et al., 2012).

Research in our lab has aimed to find mechanisms of immune evasion triggered by oncogenic KRAS signalling in mouse models of lung cancer. Work by Matt Coelho and others in the lab showed an elegant mechanism by which oncogenic KRAS signalling led to a stabilisation of the 3'UTR of the mRNA for PD-L1 (Coelho et al., 2017). This complex mechanism involves the activity of tristetraprolin (TTP), which stabilises the PD-L1 mRNA and is blocked by ERK signalling. They showed that restoring tumour cell TTP in immunocompetent mouse models abrogated tumour growth in an immune-dependent manner, as this effect could not be observed when tumours were implanted in immunodeficient mice (Coelho et al., 2017). This work provided irrefutable evidence for a role of oncogenic KRAS signalling in mediating the escape from an anti-tumour immune response in lung cancer and provided a target (TTP) that can be used to enhance the immunogenicity of such tumours.

1.6 Thesis objectives

The advent of new immunotherapies has revolutionised the field of cancer treatment and generated excitement in the cancer immunology field (Sharma and Allison, 2015). Particularly in highly mutated cancer types, such as NSCLC, which is highly prevalent and aggressive, immunotherapies such as checkpoint blockade have proven superior to other treatment modalities, but only a subset of patients respond (Rizvi et al., 2015). It is now known that oncogene-driven signalling is able to shape the composition of the TME, thereby promoting immunosuppression and evading anti-tumour immune responses. In this work, we aim to elucidate such immunosuppressive roles mediated by the oncogene KRAS in the context of NSCLC. Understanding how KRAS signalling promotes immune evasion will provide insight into potential resistance mechanisms to immune checkpoint blockade, in addition to providing mechanistic rationales for combination therapies.

Research efforts in the last decades have yielded the discovery of specific $KRAS^{G12C}$ inhibitors that are now entering the clinic and appear to be highly effective in NSCLC treatment (Canon et al., 2019) (Hallin et al., 2020). However, it seems like inevitably tumours will acquire mechanisms of resistance and progress, and research suggests that long-term responses to such drugs is achieved when an effective anti-tumour immune response is generated (Canon et al., 2019). The second aim of this project is to investigate the changes in the TME that occur in response to such drugs, with the overall aim of finding novel treatment combinations that will result in a long-lasting tumour regression. Additionally, the use of such drugs, which are able to inhibit KRAS signalling specifically in tumour cells, has proven to be an excellent tool to investigate KRAS signalling-driven immune suppressive mechanisms in *in vitro* and *in vivo* models of KRAS-mutant lung cancer.

In order to be able to translate our findings to the clinical setting, it is necessary to use adequate mouse models. Currently there is limited mouse models of NSCLC that are immune-proficient and have a genomic complexity comparable to human NSCLC. Additionally, in the literature presented in previous sections and to the best of my knowledge, no immune-competent mouse lung cancer models have been

used to assess the immune-related effects of $KRAS^{G12C}$ inhibitors. Thereby. an important objective of this thesis is to develop novel mouse models of NSCLC that closely recapitulate the human disease and that can be used to examine molecular mechanisms of KRAS-mutant lung cancer and KRAS-targeting approaches in a pre-clinical setting.

I hope that this work, by unravelling new mechanisms of immunosuppression in KRAS-mutant lung cancer, will provide the basis for new therapeutic options and combination treatment strategies for patients harbouring this devastating disease, for which current therapeutic interventions are limited.

Chapter 2. Materials & Methods

2.1 Cell culture

Cell lines used in this thesis are listed in Table 2. Cells were grown in RPMI or DMEM medium supplemented with 10% fetal calf serum, 4mM glutamine (Sigma), 100units/ml penicillin and 100mg/ml streptomycin (Sigma). Cells were sub-cultured by removing the media, washing with PBS and adding an appropriate volume of Trypsin (Sigma) to de-attach the cells from the flask. Cells were then re-seeded in a fresh container in an appropriate dilution. Cells were allowed to grow for not more than 20 sub-culture passages.

Table 2. Cell lines used in this thesis.

Cell line	Growth Medium	Source
NCI-H23	RPMI	The Francis Crick Institute
NCI-H358	RPMI	The Francis Crick Institute
Type II pneumocytes	RPMI	Olivier Pardo, Michael Seckl (Imperial College, London) and (Molina-Arcas et al., 2013)
3LL (LL/2)	RPMI	The Francis Crick Institute
MC38	RPMI	The Francis Crick Institute
CT26	RPMI	The Francis Crick Institute
ChA9.6	RPMI	Mariano Barbacid
KPAR1.3	DMEM	Downward lab, established by Jesse Boumelha
CT26-KRAS^{G12C}	RPMI	Mirati Therapeutics
KPB6-KRAS^{G12C}	DMEM	Sergio Quezada, CRISPR-edited by Pablo Romero Clavijo (Downward lab)
3LL	RPMI	ATCC (CRL-1642^{TM})

2.1.1 *In vitro* drug treatments

Cells were plated at an appropriate density and left to grow for at least 24h before drug treatment. Drugs were administered in fresh medium (Table 3) and allowed to act for different time points before downstream analysis.

Table 3. *In vitro* and *in vivo* drugs.

Drug	Concentration	Source
ARS-1620	2μM	Wellspring Biosciences
4-OHT	500nM	Sigma-Aldrich
Decitabine	250nM	Selleckchem
Trametinib	10nM	Selleckchem
GDC0941	500nM	Selleckchem
sc-514	25μM	Selleckchem
CAY10576	10μM	Selleckchem
Everolimus	100nM	Selleckchem
MRTX1257	50-100nM	Mirati Therapeutics
Ruxolitinib	500nM	Selleckchem
Tamoxifen (*in vivo*)	150mg/kg	Sigma-Aldrich
MRTX1257 (*in vivo*)	50mg/kg	Mirati Therapeutics
Anti-PD-L1 (*in vivo*)	10mg/kg	BioXcell
Anti-CTLA-4 (*in vivo*)	5mg/kg	BioXcell

2.2 *In vitro* viability assays and incucyte

For viability assays, the CellTiter-Blue assay (Promega) was used. Cells were grown in 96-well plates and treated appropriately for 72 hours. At the end of the experiment, 5μl of the CellTiter-Blue reagent was added to each well and the reaction was incubated for 90 minutes in the incubator at 37°C. Fluorescence was subsequently measured using and EnVision plate reader (Perkin Elmer) with excitation/emission wavelengths of 560/590nm. For data analysis, medium containing wells were used as a background and subtracted from the values of the cell-containing wells.
For incucyte experiments, cells were plated in 96-well well at low density and growth was monitored for 4-5 days using an Incucyte® ZOOM system (SARTORIUS, Essen Bioscience).

2.3 Immunoblotting

Cells were cultured in multiwell-plates and received appropriate treatments prior to protein isolation. At the end of the experiment, plates were placed on ice, medium was removed and cells were washed with ice cold PBS. Lysis buffer was prepared using 10X Cell Lysis Buffer (Cell Signaling Technologies), supplemented with EDTA-free protease inhibitor cocktail tablets (Roche), 1mM PMSF and 25mM NaF. Cells were de-attached using a rubber scraper and collected in tubes which were left on ice for approximately 10 minutes for lysis. Tubes were then centrifuged at 4°C for 15 minutes at 14,000rpm, after which the pellet was discarded and the supernatant was transferred to a new tube.
Protein abundance was measured using the Lowry-based DC Protein Assay (BioRad) using bovine serum albumin as a standard. Equal amounts of protein were taken for each sample and NuPAGE LDS Sample Buffer (4X, Thermo Fisher) was added. Samples were incubated at 95°C for 5 minutes for protein denaturation and either stored at -20°C or loaded (20-30mg per sample) onto NuPAGE 4-12% Bis-Tris protein gels (Thermo Fisher). Protein transfer to PVDF membranes was performed using the Trans-Blot Turbo Transfer System (BioRad) or standard manual transferring techniques. For antibody detection, horseradish peroxidase-

conjugated antibodies were used (GE Healthcare) and data was developed using an Amersham Imager 600 (GE Healthcare) or standard film techniques. Immunoblot quantification was performed using ImageJ software (NIH). Primary antibodies used are listed in Table 4.

Table 4. List of western blot antibodies.

Target	Source	Identifier
pERK1/2 (T202/Y204)	Cell Signalling Technology	9101
ERK	Cell Signalling Technology	9107
pAKT (S473)	Cell Signalling Technology	4060
AKT	Cell Signalling Technology	2920
pS6 (S235/S236)	Cell Signalling Technology	2211
S6	Cell Signalling Technology	2317
Vinculin (hVIN-1)	Sigma-Aldrich	V9131
NRAS	Santa Cruz Biotechnology	sc-31
panRAS (RAS10)	Merck Millipore	MABS195
pSTAT1 (T701)	Cell Signalling Technology	9167
STAT1	Cell Signalling Technology	9172
STAT2	Cell Signalling Technology	4594
c-MYC	Abcam	ab39688

2.4 Ras pull down assay

Active Ras was measured using the Ras Activation Assay Kit from Millipore following manufacturer's instructions. Cells were lysed in Mg2+ Lysis Buffer (MLB, 5% NP40, 750mM NaCl, 125mM Hepes, 50mM MgCl2, 5mM EDTA, 10% Glycerol) containing protease inhibitors (see Immunoblotting). Briefly, 500μg of protein (see section Immunoblotting for details on protein quantification) were incubated with

RAF-RBD containing agarose beads and rotated for 75 min at 4°C. Following incubation, samples were washed three times with MLB buffer and resuspended in 4X NuPAGE™ LDS Sample Buffer (ThermoFisher). Pulled down protein was then analysed by Immunoblotting, using 20μg of non-bead incubated protein to normalise for total Ras levels.

2.5 Molecular cloning

Guide RNA sequences for the CRISPR-Cas9-mediated knockout of murine NRAS and CCL2 were designed as follows:

- NRAS 56 (5'-gRNA-'3): GCCTGCTGGACATACTGGAC. PAM: TGG.
- NRAS 63 (3'-gRNA-'5): GTCCAGTATTGTCCAGCAGGC. PAM: AGG.
- CCL2 51 (3'-gRNA-'5): ACACGTGGATGTCTCCAGCCG. PAM: CAG
- CCL2 64 (5'-gRNA-'3): GCAAGATGATCCCAATGAGT. PAM: GAG

Forward and reverse oligonucleotide guide RNAs were phosphorylated and annealed using 10 units of T4 polynucleotide kinase (New England Biolabs, following manufacturer's instructions) and incubated at 37°C for 30min followed by an incubation at 95°C and a gradual cooling at 5°C/min to 25°C.
Annealed sgRNAs were subsequently cloned into 100ng of target vector px458-pSpCas9(BB)-2A-GFP (Addgene #48138, see vector map below in Figure 9) using a single step digestion-ligation reaction with 10 units of BbsI (also known as BpiI) enzyme (ThermoFisher) for digestion and 1500 units of T7 DNA ligase (New England Biolabs) for ligation, in a reaction containing 1mM DTTand 1mM ATP. The reaction was incubated in cycles of 37°C for 5 min and 23°C for 5 min for a total of 6 cycles. Following digestion-ligation, unwanted recombination products were removed by incubating the reaction products with 10 units of PlasmidSafe™ exonuclease (Plasmid-Safe™ ATP-dependent DNase, Lucigen) at 37°C for 30min. Cloned plasmids were then transformed into STBL1.3 competent bacteria (ThermoFisher) and cultured in ampicillin-containing agar plates. Single colonies were isolated and expanded before DNA isolation using a commercial Maxiprep kit

(QIAGEN). Plasmids were Sanger Sequenced by the Genomics Equipment Park at the Crick using a U6 promoter-targeting primer.

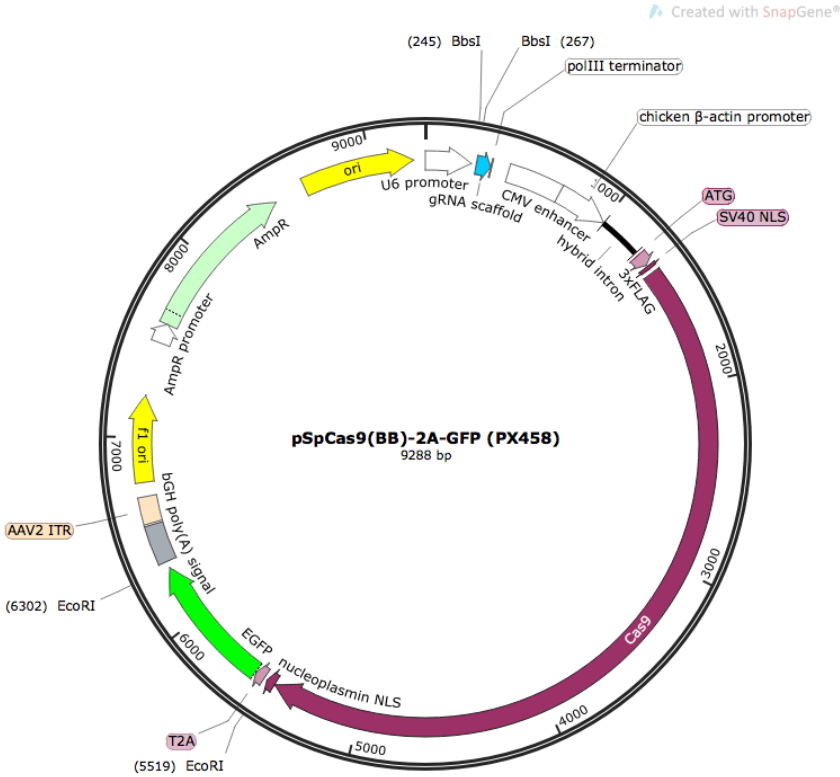

Figure 9. Map of px458-GFP vector.
Generated using SnapGene® (GSL Biotech LLC) software.

2.5.1 RAS isoform sequencing

For sequencing of RAS mutations, DNA was extracted from cells using the QuickExtract™ DNA Extraction Solution (Lucigen). Briefly, cells were pelleted and 500μl of the QuickExtract™ solution was added before incubation at 65°C for 15 minutes.
The PCR reaction of a total of 34 cycles was performed using 200ng of genomic DNA using the PrimeSTAR® HS DNA Polymerase (Takara) for 1min per 1kb. Annealing temperature was set at 56°C for all reactions. See below the primers used for amplification:

- KRAS G12 (forward): GTGTTGATGAGAAAGTTGTAAGTGAC
- KRAS G12 (reverse): CTTGCACCTATGGTTCCCTAACAC

- NRAS Q61 (forward): CACCACCACCTCCTCACTCTTTC
- NRAS Q61 (reverse): AAGTTGTATGTTTCCTAAGTCCATATA

Sanger Sequencing was performed using the forward primer for each gene. Sequencing was carried out by the Genomics Equipment Park at the Crick.

2.6 CRISPR/Cas9

3LL cells were transiently transfected with the cloned vector described in the section 'Molecular cloning' using Lipofectamine 3000 Transfection Reagent (ThermoFisher) following manufacturer's instructions. Briefly, 5μl of Lipofectamine were mixed with 140μl OptiMEM (Gibco) medium. Concomitantly, 3μg of plasmid DNA were diluted in 150μl OptiMEM medium and 6μl of P3000 reagent (ThermoFisher) was added. After 5-10min of incubation, both components were mixed in a 1:1 ratio, incubated for 20-30min and 250μl of the final solution were added dropwise to previously seeded cells.
GFP-positive cells were sorted 48h after transfection using a MoFlo XDP sorter (Beckman) and single cell cloned manually by plating the cells at a density of 1 cell/well in a 96-well plate. Clones were left to grow for 2 weeks before expanding to 24-well and subsequently 6-well plates, at which stage cells were plated for protein extraction. Protein levels for NRAS and CCL2 were checked by western blot (see 'Immunoblotting') and ELISA assays (see 'ELISA') respectively.

2.7 siRNA experiments

siGENOME siRNAs against mouse Stat 1(Dharmacon) were dissolved in siRNA resuspension buffer (Dharmacon) and stored at -20°C. On the day of use, siRNAs were thawed on ice and diluted in HBSS (ThermoFisher) to reach a concentration of 250nM (10μl of siRNA per well). This solution was mixed with 10μl HBSS (Gibco) containing 0.1μl DharmaFECT 4 transfection reagent (Dharmacon) per well. The transfection complex was incubated for 20-40 minutes before adding dropwise (200μl per well) to freshly seeded cells (not more than 10 minute prior to

transfection). As a control, cells were either Mock-transfected (no siRNA) or transfected with a siGENOME RISC-free control (Dharmacon).

2.8 Quantitative PCR (qPCR)

RNA was extracted using commercial column-based techniques, RNeasy Mini Kit (QIAGEN) or RNeasy Micro Kit (QIAGEN) following manufacturer's instructions, and eluted in 30-40μl RNase-free water. For *in vivo* tumour samples, tumours were individually isolated from the lungs, lysed and homogenised using the QIAshredder (QIAGEN) following manufacturer's instructions prior to RNA extraction using the commercial kits described above. SuperScript II Reverse Transcriptase (Thermo Fisher) was then used to generate cDNA, starting from 250-500ng of RNA using a two-step protocol. Briefly, 3μl of RNA were incubated with1μl of 50μM Random Hexamers and 0.5μl of 10mM pre-mixed dNTPs at 65°C for 5 min. Subsequently, the reaction was incubated with 1μl of 0.1M DTT (ThermoFisher), 2μl of 5x First Stand Buffer (ThermoFisher) and 0.5μl (20 units) of the RNase inhibitor RNaseOUT™ (ThermoFisher) at 25°C for 10min and 42°C for 50min before reaction inactivation by incubating at 70°C for 15 min. Obtained cDNA was then diluted to a final concentration of 1.25ng/μl.
qPCR was performed using SYBR Green FAST Master Mix (Applied Biosystems). 5ng of cDNA (in 4μl), 1ml of 2μM primers (see Table 5) and 5μl of the Master Mix were used per reaction. qPCR reactions were carried out in a 96-well 7500 Fast Real-time or a 384-well QuantStudio system (both from Applied Biosystems).
For a list of primers used see Table 5. Gene expression changes relative to the housekeeping genes were calculated using the ΔΔCT method.

Table 5. Table of qPCR primers.

Hs=Human, Mm=Mouse. Primers from QIAGEN have unknown sequence.

Gene	Species	Sequence	Source	Catalog number
DUSP6	Hs	NA	QIAGEN	QT00209986
CD274	Hs	NA	QIAGEN	QT00082775
GAPDH	Hs	NA	QIAGEN	QT00079247

PVR	Mm	AAAAACTAGAAAAAGTAAAA (Fw) AAAAACTAGAAAAAGTAAAA (Rev)		
F2rl1	Mm	TGCTGGGAGGTATCACCCTT (Fw) CAGAGGGCCATGCCATTACT (Rev)		
Cd44	Mm	CTTGGCCACCAGAGATCGAG (Fw) CAGATTCCGGGTCTCGTCAG (Rev)		
Areg	Mm	TGCCTTCTGGCAGTGAACTC (Fw) CCTTGTCATCCTCGCTGTGA (Rev)		
Ereg	Mm	CAGATGGAAGACGATCCCCG (Fw) CCAGGCACACTGTGAATCCT (Rev)		
Spp1	Mm	CCTTGCTTGGGTTTGCAGTC (Fw) ACAGGGATGACATCGAGGGA (Rev)		
Gapdh	Mm	CAAGCTCATTTCCTGGTATGACA (Fw) GGATAGGGCCTCTCTTGCTC (Rev)		
Ccl2	Mm	CACTCACCTGCTGCTACTCA (Fw) GCTTGGTGACAAAAACTACAGC (Rev)		
Cxcl1	Mm	ACTCAAGAATGGTCGCGAGG (Fw) GTGCCATCAGAGCAGTCTGT (Rev)		
Cxcl2	Mm	AGGGCGGTCAAAAAGTTTGC (Fw) CAGGTACGATCCAGGCTTCC (Rev)		
Csf1	Mm	GGGGCCTCCTGTTCTACAAG (Fw) TCTGTCCTCATCCTGGGTCA (Rev)		
Csf2	Mm	NA	QIAGEN	QT01164324
Ifngr1	Mm	TGCCTGGGCCAGAGTTAAAG (Fw) TACGAGGACGGAGAGCTGTT (Rev)		
Ifngr2	Mm	TCACCTTCCAGCAATGACCC (Fw) ACCTATGCCAAGAGCCATCG (Rev)		
Stat1	Mm	AAGTCTGGCAGCTGAGTTCC (Fw) TCTTCGGTGACAATGAGAGGC (Rev)		
Stat2	Mm	CCCTGGTCGACCTATTGCTG (Fw) CAAGAACTTTGCTCCAGCCG (Rev)		
Stat3	Mm	ACGAAAGTCAGGTTGCTGGT (Fw) TGTGTTCGTGCCCAGAATGT (Rev)		
Irf1	Mm	GACCCTGGCTAGAGATGCAG (Fw) CTCCGGAACAGACAGGCATC (Rev)		
Irf2	Mm	AATTCCAATACGATACCAGGGCT (Fw) GAGCGGAGCATCCTTTTCCA (Rev)		
Irf7	Mm	GCGTACCCTGGAAGCATTTC (Fw) GCACAGCGGAAGTTGGTCT (Rev)		
Irf9	Mm	GCCGAGTGGTGGGTAAGAC (Fw) GCAAAGGCGCTGAACAAAGAG (Rev)		
Cxcl9	Mm	CCAAGCCCCAATTGCAACAAA (Fw) GTCCGGATCTAGGCAGGTTT (Rev)		

Cxcl10	Mm	AATGAGGGCCATAGGGAAGC (Fw) AGCCATCCACTGGGTAAAGG (Rev)		
Cxcl11	Mm	GAAGGTCACAGCCATAGCCC (Fw) CTCTGCCATTTTGACGGCTT (Rev)		
H2-D1	Mm	NA	QIAGEN	QT01657761
H2-K1	Mm	GACCGTTGCTGTTCTGGTTG (Fw) TCACGCTAGAGAATGAGGGTCA (Rev)		
Ciita	Mm	CAAGGATCTTCCTGCCATCCG (Fw) CCAGGTGTTGCAGAGAAGAGA (Rev)		
B2m	Mm	TCTCACTGACCGGCCTGTAT (Fw) ATTTCAATGTGAGGCGGGTG (Rev)		
Cd274	Mm	CGCCACAGCGAATGATGTTT (Fw) AGGATGTGTTGCAGGCAGTT (Rev)		
STAT1	Hs	GGAAGGGGCCATCACATTCA (Fw) GTAGGGTTCAACCGCATGGA (Rev)		
STAT2	Hs	ACCATTCTGGACATGGCTGG (Fw) CTCCGACTCACAAAGCCCAT (Rev)		
IRF1	Hs	CCAAATCCCGGGGCTCATC (Fw) CTGCTTTGTATCGGCCTGTG (Rev)		
IRF7	Hs	TGTGCTGGCGAGAAGGC (Fw) TGGAGTCCAGCATGTGTGTG (Rev)		
IRF9	Hs	TCCTCCAGAGCCAGACTACT (Fw) CAATCCAGGCTTTGCACCTG (Rev)		
CXCL9	Hs	GGTGTTCTTTTCCTCTTGGGC (Fw) AACAGCGACCCTTTCTCACT (Rev)		
CXCL10	Hs	AAGTGGCATTCAAGGAGTACCT (Fw) ACACGTGGACAAAATTGGCT (Rev)		
B2M	Hs	CGTGGCCTTAGCTGTGC (Fw) AATGTCGGATGGATGAAACC (Rev)		
SOCS1	Hs	NA	QIAGEN	QT00202475
TAP1	Hs	GTGGCCTATGCAGTCAACTC (Fw) TGCCCACCAATGTAGAGGAT (Rev)		
TAP2	Hs	ATGCCCTTCACAATAGCAGC (Fw) ATCCTGGATCTCCCGAAGCA (Rev)		
ATF4	Hs	TCCAACAACAGCAAGGAGGAT (Fw) TCCAACGTGGTCAGAAGGTC (Rev)		
MYC	Hs	TACAACACCCGAGCAAGGAC (Fw) TTCTCCTCCTCGTCGCAGTA (Rev)		
Hsp90	Mm	AGATTCCACTAACCGACGCC (Fw) TGCTCTTTGCTCTCACCAGT (Rev)		
Sdha	Mm	TCGACAGGGGAATGGTTTGG (Fw) TCATACTCATCGACCCGCAC (Rev)		

HSP90	Hs	AGATTCCACTAACCGACGCC (Fw) TGCTCTTTGCTCTCACCAGT (Rev)		
ACTB	Hs	NA	QIAGEN	QT00095431

2.9 RNA sequencing and bioinformatics analysis

RNA was extracted using the RNeasy Mini Kit (QIAGEN) from three independent experiments. RNA quality was measured using the 2100 Bioanalyzer (Agilent). Libraries were prepared using the KAPA Hyper Prep kit (Roche) and sequenced (sequencing read length, 75bp) in an Illumina HiSeq 4000 system by the Advanced Sequencing Facility at the Francis Crick Institute. Bioinformatic analysis was performed by the bioinformatics facility at the Francis Crick Institute. Briefly, reads were aligned using to relevant reference genome (mouse Ensembl GRCm38 - release 89 for 3LL and human Ensembl GRCh38 – release 38 for human cell lines). For data analysis, the R package DESeq2 was used and Gene Set Enrichment analysis was performed following gene sets available from MSigDB (Broad Institute).

2.10 Whole exome sequencing

DNA was extracted from cells using the QuickExtract DNA Extraction Solution (Lucigen) and submitted to the Advanced Sequencing Facility at the Francis Crick Institute. Genomic DNA sequencing was performed with 110x coverage using 100 base pair paired end read lengths. DNA library prep was performed using aSureSelectXT reagent kit (Agilent) and gDNA was sequenced using an Illumina HiSeq system.

Data analysis was performed by the bioinformatics facility at the Francis Crick Institute. Sequencing reads were aligned to the Mus musculus reference genome (mouse Ensembl GRCm38 - release 89). For mutation calling, DNA from wild-type C57Bl/6 mice was taken as a reference and analysed using the Mutect algorithm developed by the Broad Institute.

2.11 Neoantigen prediction

Whole exome sequencing data of non-synonymous SNP-containing genes (in .vcf format) was combined with RNA sequencing data of expressed genes (TPM >0). Peptide sequences for obtained variants were converted using the SeqTailor tool from Rockefeller University (http://shiva.rockefeller.edu/SeqTailor/), by selecting the Mouse reference genome and a window size of 12aa on both sides of the variant. MHC binding prediction was performed using the IEDB 2.22 prediction method (http://tools.iedb.org/mhci/). Analysis was performed by the bioinformatics facility at the Francis Crick Institute.

2.12 *Ex vivo* immune cell culture

Mice were sacrificed using a schedule 1 method. Femurs and tibias from the mice were dissected and collected in ice cold PBS. Bones were flushed using ice cold PBS using 21g needles. Flushed cells were centrifuged, filtered through a 45μM mesh and monocytes were magnetically isolated using the Monocyte Isolation Kit (BM, mouse) from Miltenyi as per manufacturer's instructions. Isolated cells were cultured in RPMI medium with 100ng/ml carrier-free mouse recombinant M-CSF (Biolegend) overnight before changing the medium to appropriate treatment (conditioned medium or control RPMI). Cells were left to grow for 5-6 days before harvesting for downstream assay.

2.12.1 Transwell assay

Cell migration was quantitated in duplicate using 24 well Transwell inserts (6.5 mm) with polycarbonate filters (5 μm pore size) (Corning Costar, Acton, MA). Monocytes (0.5×10^6 in 100μl of RPMI) were added to the upper chamber of the insert. The lower chamber contained 600μl of RPMI 1640 medium or filtered conditioned medium from tumour cells. The plates were incubated at 37°C in 5% CO_2 for 1.5 h and cells that had migrated into the lower chamber were harvested and counted using flow cytometry.

2.13 Immunohistochemistry

Animals were culled using a Schedule 1 method, and fixed in 10% neutral buffered formalin for 24-48 hours, after which they were conserved in 70% ethanol until further use by the Experimental Histopathology department at the Francis Crick Institute. Briefly, tissues to be examined were paraffin-embedded and microtome-cut in 4μm sections. Automatic haematoxylin and eosin (H&E) staining was performed using a Tissue-Tek Prisma 6132 device (Sakura). For immunohistochemistry, firstly antigen retrieval was performed by citrate buffer (pH 6.0) microwaving or trypsin treatment. Slides were subsequently incubated in primary antibodies (CD3 –Abcam ab134096-, CD8 –ThermoFisher Scientific 14-0808-82-, F4/80 –ThermoFisher Scientific 14-4801-). Slides were stained using biotinylated secondary antibodies and signal was detected using HRP/DAB. Images were retrieved using a Leica Zeiss AxioScan.Z1 slide scanner and analysis was done using the ZEN 2 (Blue Edition) software (Zeiss).

2.14 Flow cytometry

2.14.1 In vivo flow cytometry

Mice were culled using schedule 1 methods and lungs dissected (a spleen was also dissected to use as single stain control). Tumours were dissected from the lungs and cut into small pieces before incubating in digestion solution (1mg/ml collagenase type I –Thermofisher-, 50u/ml DNase –Life Technologies - in HBSS buffer –Life Technologies-) at 37°C for 30min. Samples were homogenised by passing through a needle and re-incubated at 37°C for 20min. Samples were filtered through a 70μM cell strainer (Falcon), erythrocytes were shocked using ACK lysing buffer (Life Technologies) and samples were re-filtered through 70μM cell strainers. After washes in PBS, samples were stained with fixable viability dye eFluor780 (BD Horizon™) for 30min at 4°C. Samples were washed three times in FACS buffer (2mM EDTA, 0.5% BSA in PBS pH7.2) and stained using appropriate antibody mixes (see Figure 27) or single stain controls. Single stained OneComp eBeads™ (ThermoFisher) were also used as additional single stain controls. After

staining, samples were fixed in fix/lyse solution (Thermofisher) or FixPerm solution (Thermofisher) if intracellular staining was needed, and stored overnight at 4°C. The following day, samples were either stained with an intracellular antibody or washed and analysed using a FACSymphony™ analyser (BD). Data was analysed using FlowJo software v10 (LLC).
For a list of antibodies used, see Table 6.

2.14.2 *In vitro* flow cytometry

For FACS analysis *in vitro*, cells were harvested with trypsin, filtered and washed in FACS buffer before appropriate antibody treatment. If samples were to be fixed, a fixable viability dye (Fixable Viability Stain 780, BD Horizon™) was used to stain for viability prior to surface antibody staining. For intracellular staining, cells were treated with 1μl Brefeldin A (BD GolgiPlug™) 6h before harvesting. Cells were permeabilised using the FixPerm (ThermoFisher) solution prior to staining.
After antibody staining, cells were washed and, if not previously stained with a fixable viability dye, DAPI (final concentration 1mg/ml) was added shortly before data acquisition. Samples were run in a LSRII or LSRFortessa (BD) and FlowJo software v10 (LLC) was used to analyse the data.
For a list of antibodies used in this thesis, see Table 6.

Table 6. List of flow cytometry antibodies.
All antibodies target mouse proteins.

Target	Fluorophore	Clone	Source	Catalog number
H-2L^{d}/H-2D^{b}	PE	28-14-8	Biolegend®	114507
H2-Kb	AF647	AF6-88.5	Biolegend®	116512
CD45	PerCP	30-F11	Biolegend®	103130
CD3	FITC	17A2	Biolegend®	100204
gdTCR	BV605	GL3	Biolegend®	118129
CD4	BUV737	GK1.5	BD Biosciences	564298
CD8	BUV395	53-6.7	BD Biosciences	563786

Foxp3	eFluor660	FJK-16s	eBioscience	50-5773-82
CD44	BV421	IM7	Biolegend®	103039
CD62L	BV711	MEL-14	Biolegend®	104445
CD69	BV605	JES5-16E3	Biolegend®	104530
PD-1	BV785	29F.1A12	Biolegend®	135225
LAG3	PE-Cy7	eBioC9B7W	eBioscience	25-2231-82
NKp46	BV421	29A1.4	Biolegend®	137612
CD49b	AF488	DX5	Biolegend®	108913
CD19	PE	6D5	Biolegend®	115507
B220/CD45R	BV605	RA3-6B2	Biolegend®	103244
CD11c	BUV395	HL3	BD Biosciences	564080
CD11b	BUV737	M1/70	BD Biosciences	564443
Ly6G	BV711	1A8	Biolegend®	127643
Ly6C	BV785	HK1.4	Biolegend®	128041
PD-L1	PE	MIH5	eBioscience	12-5982-81
F4/80	BV785	EMR1	Biolegend®	123141
CD24	BV605	M1/69	Biolegend®	101827
CD103	BV421	M290	BD Biosciences	562771
CD64	PE-Cy7	X54-5/7.1	Biolegend®	139314
CD206	BV711	C068C2	Biolegend®	141727
TIM3	PE	RMT3-23	Biolegend®	119703
CD86	BV785	GL-1	Biolegend®	105043
MHCII	FITC	M5/114.15.2	Biolegend®	107605
CXCL9	PE	MIG-2F5.5	Biolegend®	515603

2.15 Cytokine assays

2.15.1 ELISA

Cells were cultured and subjected to treatment as appropriate. Medium was harvested and used in ELISA protocols or frozen at -20°C for later use. For detection of CCL2 and CXCL9, Human CCL2/MCP-1 DuoSet ELISA, Mouse CCL2/JE/MCP-1 DuoSet ELISA and Mouse CXCL9/MIG DuoSet ELISA kits (from R&D Systems) were used, following manufacturer's instructions. Briefly, 96-well polystyrene plates for ELISA (R&D) were coated overnight with the coating antibody provided by the Kit, diluted in 0.1M $NaHCO_3$ buffer. The following day, plates were washed using a solution of 0.01% Tween (Sigma) in PBS. Plates were then blocked with a solution of 10% fetal calf serum (Sigma) in PBS for 1h. After washes as before, experimental samples and recombinant cytokines to be used as standards were added to the plate and incubated for 2h. Plates were then washed and a biotinylated detection antibody, diluted in blocking buffer, was added at the concentration instructed by the Kit and incubated for 2h. After washing, plates were incubated with a solution Streptavidin-HRP for 20min before addition of a chemoluminescent substrate supplied by the Kit. After incubating for 10-20min (depending on signal intensity), absorbance at 450nm was measured using a Tecan microplate reader.

2.15.2 Cytokine array

Cells were cultured and subjected to treatment as appropriate. Medium from cells was harvested and used in the Human Cytokine Array Kit or the Proteome Profiler Mouse Cytokine Array Kit, Panel A (both from R&D Systems), as per manufacturer's instructions. Briefly, pre-coated array membranes were blocked using 2ml of Array Buffer 6 rocking for 1h before addition of a pre-mixed solution containing a maximum of 1ml of each sample and 15μl of the detection antibody cocktail supplied by the reagent kit. Samples and antibodies were incubated overnight at 4°C on a rocking platform shaker. On the following day, membranes were washed using the Wash Buffer supplied by the kit before developing using a

Streptavidin-HRP method. After adding the chemiluminescent substrate provided in the kit, membranes were developed using standard film techniques.

2.16 *In vivo* studies

All studies were performed under a UK Home Office approved project license and in accordance with institutional welfare guidelines.

2.16.1 Cell line transplantation

Cells were harvested using trypsin and re-suspended in PBS at an appropriate concentration for injection. For subcutaneous injection, cells were mixed 1:1 with Geltrex^{TM} matrix (ThermoFisher) and 400.000 3LLΔNRAS cells were injected in a total volume of 100μl subcutaneously in either flank of the mice. Tumour growth was followed twice a week by caliper measurements and tumours were left to grow not larger than 1.2cm in diameter following a UK Home Office approved project license.
For orthotopic growth, cells were harvested as before and 1 million 3LLΔNRAS cells were injected in PBS in a total volume of 100μl in the tail vein of the mice (pre-heated at no warmer than 40°C). Mouse weight was monitored regularly as a measure of tumour growth and mice were sacrificed if weight loss was over 10% as per the UK Home Office approved project license. Tumour burden was also assessed by regular Computed Tomography (CT) scanning of the lungs, see 'Computed Tomography'.

2.16.2 GEMM experiments

The source of all genetically engineered mice, all of C57Bl/6 origin, used in the thesis are listed in Table 7. Tumour growth was assessed by computed tomography (2.16.3) and regular weight monitoring. Mice were euthanised at end of experiment or when displaying signs of ill health, including weight loss.
For carcinogen administration, urethane (Carbamic acid ethyl ester, Sigma-Aldrich) was administered at a dose of 1mg/kg dissolved in PBS (pH 7.4) intraperitoneally,

in three doses (every 48h). Mice were kept in a heating chamber (37°C) with access to water and food until recovery.

Tamoxifen (Sigma-Aldrich) was dissolved in ethanol at 55°C at 300mg/ml, aliquoted and store at -80°C until further use. Prior to use, aliquots were dissolved 1:10 in sunflower oil and shaken at 55°C until complete homogenisation of the solution. Mice were treated with 150mg/kg tamoxifen by oral gavage.

Table 7. Summary of mouse strains

Strain	Source	Identifier
C57Bl/6J WT	The Francis Crick Institute	
C57Bl/6J Rag1$^{-/-}$	The Francis Crick Institute	Rag1^{tm1Mom}
C57Bl/6J Rag2$^{-/-}$	The Francis Crick Institute	Rag2^{tm1Fwa}
C57Bl/6J IL2r$\gamma^{-/-}$	The Francis Crick Institute	Il2rg^{tm1Wjl}
C57Bl6 Ccr2$^{-/-}$	The Francis Crick Institute (Andreas Wack)	Ccr2^{tm1Mae}
R26-LSL-hAPOBEC3B	The Francis Crick Institute (Charles Swanton)	Gt(ROSA)26Sor$^{tm1(Apobec3B)Harr}$
Trp53$^{fl/fl}$	The Francis Crick Institute (Julian Downward)	Trp53^{tm1Brn}
Sftpc-CreERT2	The Francis Crick Institute (Julian Downward)	Sftpc$^{tm1(cre/ERT2)/Blh}$
R26-mTmG	The Francis Crick Institute	Gt(ROSA)26Sor$^{tm4(ACTB-tdTomato,-EGFP)Luo}$
KRAS$^{G12D-LSL}$	The Francis Crick Institute	Kras^{tm4Tyj}
KRAS^{FSF}	The Francis Crick Institute (Julian Downward)	Kras^{tm5Tyj}
KRAS^{lox}	Mariano Barbacid	Kras^{tm2Bbd}
Trp53^{frt}	The Francis Crick Institute (Julian Downward)	Trp53$^{tm1.1Dgk}$

2.16.3 Computed Tomography

Mice were anesthetised by inhalation of isoflurane (Abbott Labs) and CT scanned using the Quantum GX2 micro-CT imaging system (Perkin Elmer). Breathing rate and body temperature were measured throughout the scan using in-built physiological monitoring devices.
Scanning parameters were as follows: copper & aluminium filter 0.06 + 0.5mm respectively, 1 degree's rotation step over 360 degrees, source current 40μA, source voltage 90kV, image isotropic pixel size 50μm. Scan mode at High Speed & Gating 4min. Gating technique set at Respiratory Gating. Lung images were grouped into bins based on the respiratory cycle and images reconstructed using the Quantum GX2 program with parameters set at Acquisition FOV 36mm & Recon FOV 25mm.
Estimations of lung tumour volumes were generated by highlighting 3D regions of interest in imaging program Analyze from AnalyzeDirect.

2.16.4 Therapeutic drug treatments

Mice were treated with 50mg/kg MRTX1257 (Mirati Therapeutics) or 10% Captisol® (Ligand) in 10mmol/L citrate buffer (pH 5.0) as vehicle control daily via oral gavage. For short-term experiments, mice were sacrificed 28h or 8 days after treatment initiation for downstream analysis.
For immunotherapy treatments, mice were administered 10mg/kg anti-PD-L1 (BioXCell) and 5mg/kg anti-CTLA-4 (BioXCell) or isotype control (10mg/kg IgG2b and 5mg/kg syrian hamster IgG2) dissolved in PBS at a dose of 4μl/g mouse intraperitoneally twice a week for a total of four doses.

2.17 Statistical analysis

For most experiments, data were compared using unpaired or paired two-tailed Student's t-tests. In mouse tumour analysis, the Mann-Whitney u-test was used for volume comparison. To compare read counts of individual genes in mRNA-seq datasets of two groups, Wald test was used with a Benjamini and Hochberg

correction with an FDR Q value of 5% to obtain adjusted p values. Guide for p value representation:

Symbol	Meaning
*	$p \leq 0.05$
**	$p \leq 0.01$
***	$p \leq 0.001$
****	$p \leq 0.0001$

To compare two survival curves, the Mantel-Cox log-rank test was used (Statistical analysis was performed by Crick Bioinformatics Facility). Statistical analyses were performed in Prism 7 (GraphPad Software) or in RStudio.

Chapter 3. Results 1: Oncogenic KRAS regulates immune-related genes in human cell lines

3.1 Introduction

The main objective of this thesis is to elucidate molecular mechanisms by which oncogenic signalling triggered by KRAS is able to evade immune responses in the context of NSCLC. As discussed in the introduction, examples of such mechanisms elicited by other oncogenes are known, and for KRAS in particular, a number of mechanisms have been elucidated *in vitro* (Sparmann and Bar-Sagi, 2004) (Ancrile et al., 2007), in oncogene-driven lung inflammation (Ji et al., 2006) and in mouse models of pancreatic cancer (Pylayeva-Gupta et al., 2012). However, in NSCLC such mechanisms are largely unknown, and are now beginning to be unravelled in part by work from our lab (Coelho et al., 2017).

In order to begin addressing our question, we set out to perform a gene expression analysis of KRAS-dependent genes in human lung cancer cells. In this chapter, and throughout the thesis, we have used cell lines and chemical and genetic tools with which we can specifically inhibit or trigger oncogenic KRAS signalling (Figure 10). Using *in silico* tools, we aimed to examine whether immune-related genes could be a part of the KRAS-dependent gene signature. The ability to specifically activate or inhibit oncogenic KRAS signalling will allow us to unveil KRAS-regulated genes and pathways that play a role in the immune evasion of NSCLC.

3.2 Validation of *in vitro* systems of KRAS activation/inhibition

To assess gene expression changes in response to KRAS signalling, we need tools to be able to specifically modulate KRAS activity. The newly available $KRAS^{G12C}$ inhibitors (1.3) comprise an excellent tool to efficiently suppress KRAS signalling in these cells. In this case, we have used the human NCI-H358 (H358) and NCI-H23 (H23) human lung cancer cell lines, known to be sensitive to the action of $KRAS^{G12C}$ inhibitors, such as ARS-1620 (Ostrem et al., 2013) (Janes et al., 2018). As a negative control to account for off-target effects of ARS-1620, or the solvent DMSO, we made use of an additional lung cancer cell line that instead harbours a $KRAS^{G12S}$ mutation, A549. In these $KRAS^{G12S}$ cells, the specificity of the $KRAS^{G12C}$ inhibitor ARS-1620 should prevent any effect of the drug on the downstream signalling of the oncogene (Ostrem et al., 2013).

In addition, we made use of a cell line originated from primary human alveolar type II pneumocytes (AT2), which has been transformed *in vitro* (Kemp et al., 2008). Type II pneumocytes are considered to be the cell of origin of lung adenocarcinoma (Xu et al., 2012) (Mainardi et al., 2014). In our lab, these cells were engineered to express an inducible oncogenic KRAS, by the introduction of a $KRAS^{G12V}$-ER expressing vector (Molina-Arcas et al., 2013) (Coelho et al., 2017). In this manner, 4-hydroxytamoxifen (4-OHT) treatment of the cells leads to the stabilisation of the $KRAS^{G12V}$-ER fusion protein, thereby initiating an oncogenic cascade of signalling. As a control for off-target effects of 4-OHT administration, we made use of the AT2 parental cell line that does not contain this plasmid.

These three human cell lines, H358, H23 and AT2-$KRAS^{G12V}$-ER, were used to specifically block or activate KRAS activity to address downstream effects of its signalling (Figure 10) on gene expression patterns. The $KRAS^{G12S}$-containing cell line A549 and the parental AT2 cells were used as negative controls.

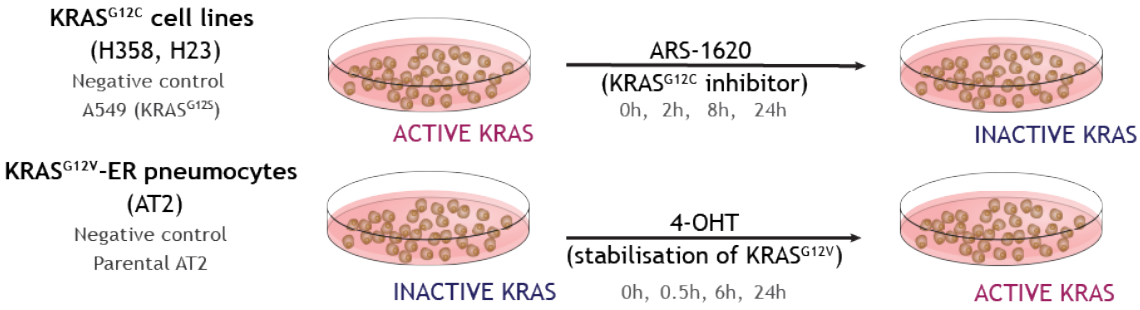

Figure 10. Summary of *in vitro* models of specific KRAS activation/inhibition.

To validate these *in vitro* systems, we sought to confirm that ARS-1620 and 4-OHT treatments affected KRAS activity by inhibiting or increasing KRAS-GTP binding, respectively. For this purpose, we made use of a protein pulldown assay based on beads conjugated to the Ras-binding domain (RBD) of the downstream effector RAF. These beads can pull down RAS in its GTP-bound form and are thereby used as a measurement of RAS activity. As shown in Figure 11A and B, treatment with 2μM ARS-1620 was able to significantly reduce KRAS-GTP levels in the KRAS^{G12C} lung cancer cell lines H358 and H23, and even though there was a slight trend of reduced RAS-GTP in the KRAS^{G12S} A549 cell line, this was not significant. Additionally, 4-OHT treatment of the AT2 (KRAS^{G12V}-ER) cell line led to an increase in the GTP-bound fraction of RAS, as a readout of the stabilisation of the oncogenic KRAS protein (Figure 11C and D). In the negative control, virtually no active RAS was detected, which is not unexpected given that these cells do not possess an oncogenic RAS protein. These results validate the systems and corroborate that the treatments are able to effectively modulate KRAS activity.

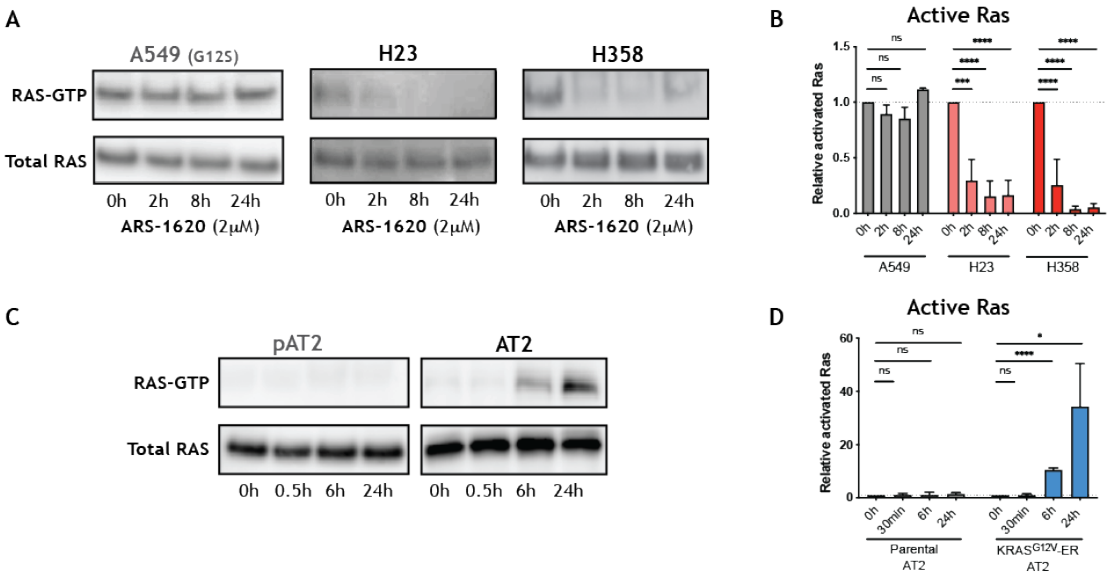

Figure 11. RAS-GTP loading is effectively affected in all conditions.

A) Representative blots for cell lines H358, H23 and A549 at different time points after 2μM ARS-1620 treatment. B) Quantification of active Ras (RAS-GTP) in all cell lines (n=3, Mean+SD, Student's T test). Results are normalised to 0h condition for all cell lines. C) Representative blots for $KRAS^{G12V}$-ER type II pneumocytes (AT2) and parental pneumocytes (pAT2) at different time points after 500nM 4-hydroxytamoxifen (4-OHT) treatment. D) Quantification of active Ras (RAS-GTP) in all cell lines (n=3, Mean+SD, Student's T test). Results are normalised to 0h condition for all cell lines.

Furthermore, we wanted to confirm that this alteration of KRAS activity was indeed leading to changes in its downstream signalling. With this aim, we examined the phosphorylation status of the most prominent downstream effectors of RAS, namely ERK and AKT, upon different treatments.

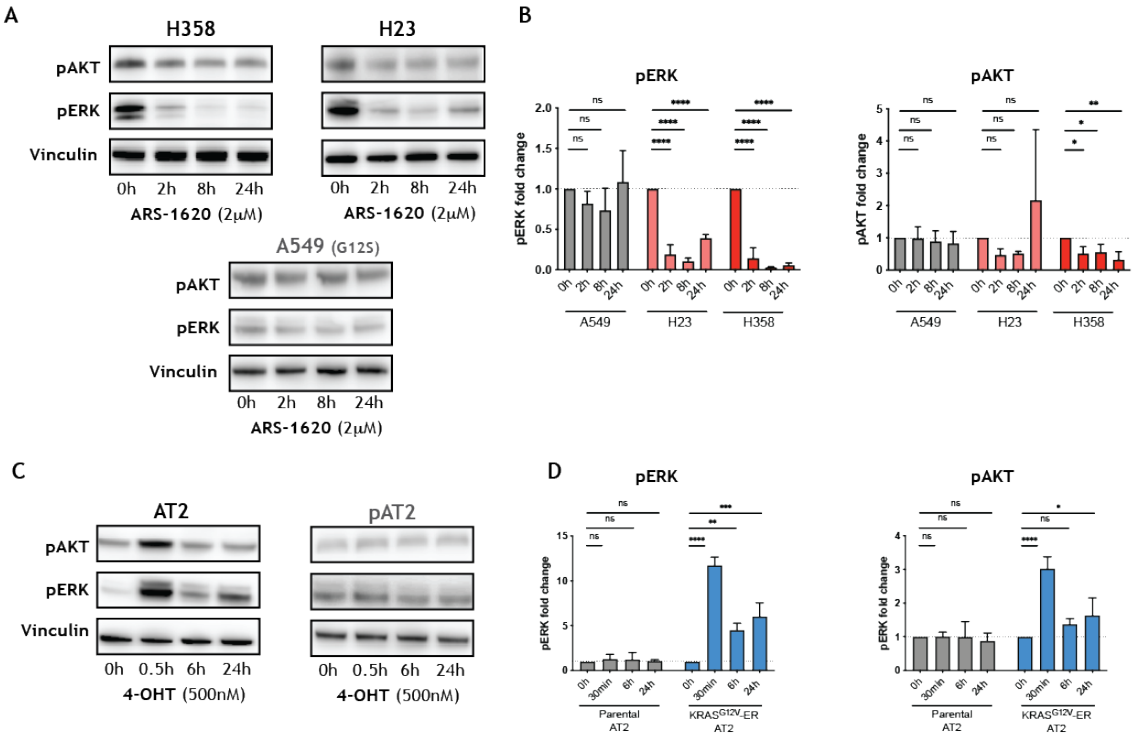

Figure 12. Effective RAS pathway inhibition/activation is achieved in all conditions.

A) Representative blots for cell lines H358, H23 and A549 at different time points after 2μM ARS-1620 treatment. pAKT=phospho-AKT, pERK=phospho-ERK. Quantification of pERK in all cell lines (n=3, Mean+SD, Student's T test). Results are normalised to 0h condition for all cell lines. C) Representative blots for $KRAS^{G12V\text{-}ER}$ type II pneumocytes (AT2) and parental pneumocytes (pAT2) at different time points after 500nM 4-hydroxytamoxifen (4-OHT) treatment. D) Quantification of pERK in all cell lines (n=3, Mean+SD, Student's T test). Results are normalised to 0h condition for all cell lines.

As displayed in Figure 12A and B, downstream effector phosphorylation was inhibited by ARS-1620 treatment in $KRAS^{G12C}$ cell lines, but not in the $KRAS^{G12S}$ cell line. As in the previous figure, there is a slight non-significant reduction of pERK, but not pAKT, in the negative control cell line in the first two time points. As the effect does not seem to increase with time, we excluded the possibility that this could be due to on-target effects of the inhibitor and concluded it is probably a reflection of intrinsic variabilities in the experiment. Figure 12C and D show that stabilisation of $KRAS^{G12V}$ by 4-OHT led to downstream activation of effector pathways in AT2 cells (but not in the parental cell line control). These results show

that we are able to effectively modulate KRAS-mediated signalling in our *in vitro* systems.

The main goal of this section was to unveil KRAS-regulated genes and pathways by RNA sequencing (RNA-Seq), to elucidate whether immune-related genes could be regulated by KRAS-signalling. In order to validate the quality of the RNA and confirm that we were able to affect KRAS pathway in a transcriptional manner, we assessed gene expression changes of some known KRAS-regulated genes. Dual specificity phosphatase 6 (DUSP6) is a phosphatase that acts as a negative regulator of the MAPK pathway, whose expression is known to be upregulated by oncogenic KRAS. In addition, research from our lab has shown that PD-L1 mRNA stability is directly affected by KRAS signalling (Coelho et al., 2017). We used DUSP6 and PD-L1 as a transcriptional readout of KRAS pathway activation in our cell line systems.

Figure 13A and B show the downregulation and upregulation of DUSP6 in the human $KRAS^{G12C}$ cell lines and in the AT2 cell line, respectively. Figure 13C and D show the same trend for the gene CD274, which encodes the checkpoint ligand PD-L1. No significant changes were observed when the negative controls, A549 and the parental AT2 cell lines, were subjected to the same treatment. In the A549 cell line, a non-significant increase of both DUSP6 and PD-L1 was observed at the earliest time point. Again, this may reflect intrinsic variabilities of the experiment, or it could be a consequence of the medium change performed to administer the treatment. Overall, this data confirmed that we were able to detect gene expression changes upon interference with KRAS signalling. We were thus confident that these *in vitro* systems were performing adequately and followed up by performing an RNA-Seq analysis of these samples.

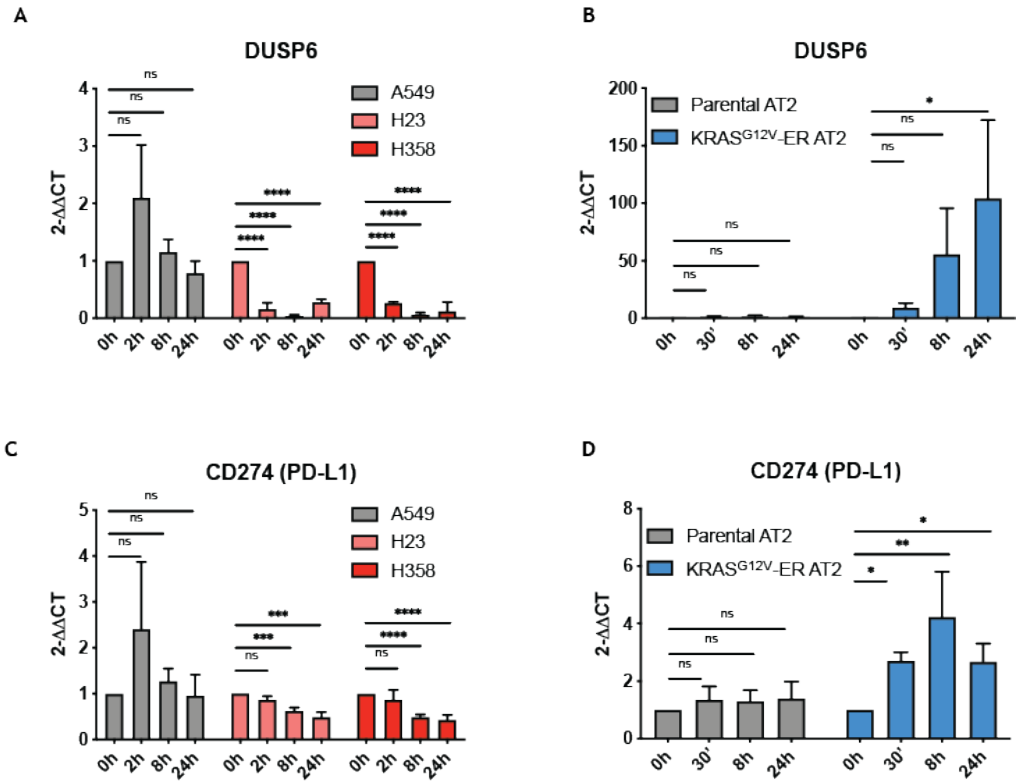

Figure 13. Known RAS-responsive genes are regulated in all conditions.

A) Gene expression values for DUSP6 in human G12C cell lines and the negative control A549. B) Gene expression values for DUSP6 in human KRAS^{G12V}-ER pneumocytes and the negative control parental pneumocytes. C) Gene expression values for CD274 in human G12C cell lines and the negative control A549. D) Gene expression values for DUSP6 in human KRAS^{G12V}-ER pneumocytes and the negative control parental pneumocytes. Values calculated using $2^{-\Delta\Delta Ct}$ method using at least two housekeeping genes, all conditions are normalised to non-treatment control value (n=3, Mean±SD).

3.3 Gene expression analysis of KRAS-regulated genes

Using the *in vitro* systems described and validated in subsection 3.2, we aimed to perform RNA sequencing (RNA-Seq) analysis to obtain a KRAS-regulated gene dataset. For robustness, we used three biological replicates of RNA for each condition. We examined a total 3 human lung cancer cell lines (two experimental and one control) treated with ARS-1620 for KRAS inhibition at 2 hours, 8 hours and 24 hours post-treatment (Figure 10). We also submitted 2 pneumocyte cell lines (parental and engineered) treated with 4-OHT for KRAS activation 0.5 hours, 6 hours and 24 hours post-treatment (Figure 10). These samples were sent to the Advanced Sequencing Facility at the Crick, where they performed DNA library preparation and sequencing of the RNA provided. The data generated was analysed by Miriam Llorian Sopena at the Bioinformatics Facility at the Crick.
The first analysis after the appropriate quality control steps of the sequencing consisted of performing a principal component analysis of the gene expression patterns of our samples. In the ARS-1620 treated conditions, the samples clustered largely based on the cell line, suggesting that the cell type, rather than the treatment, was causing most of the differences in gene expression, and no distinctions were observed across replicates (Figure 14A). The result was slightly different for the pneumocyte samples, where a large separation was seen in the AT2 condition across treatments (Figure 14A). This indicates two things: firstly, that the two pneumocyte cell lines do not differ significantly in terms of their gene expression, which is not surprising, given that the AT2-KRAS^{G12V} is a single cell clone derivative of the parental AT2 cell line. In addition, the differences across treatment time points suggests that oncogenic KRAS activation in this cell line leads to profound changes in gene expression, mostly at the 6h and 24h time points. No significant changes were observed between the untreated and 0.5h time point, nor across replicates. Together, these results highlight the robustness of the biological replicates used for the assay.

We followed by performing an unsupervised clustering analysis of the differentially expressed genes (compared to the untreated control) in all conditions. Once more, the genes clustered largely based on cell type. However, for the H23 and H358 conditions, the 8h and 24h time points tended to cluster separately from the 0h and

2h treatment conditions, indicating gene expression changes upon KRAS inhibition by ARS-1620 treatment occurred rather late after administration of the drug. On the contrary, no such clustering was observed in the A549 negative control samples (Figure 14B). We observed a similar pattern in the AT2 samples, were the 6h and 24h time points clustered separately from the untreated and 0.5h treatment condition, which clustered with the parental AT2 genes, suggesting that gene expression changes upon KRAS activation were occurring at least 6h after 4-OHT administration (Figure 14B).

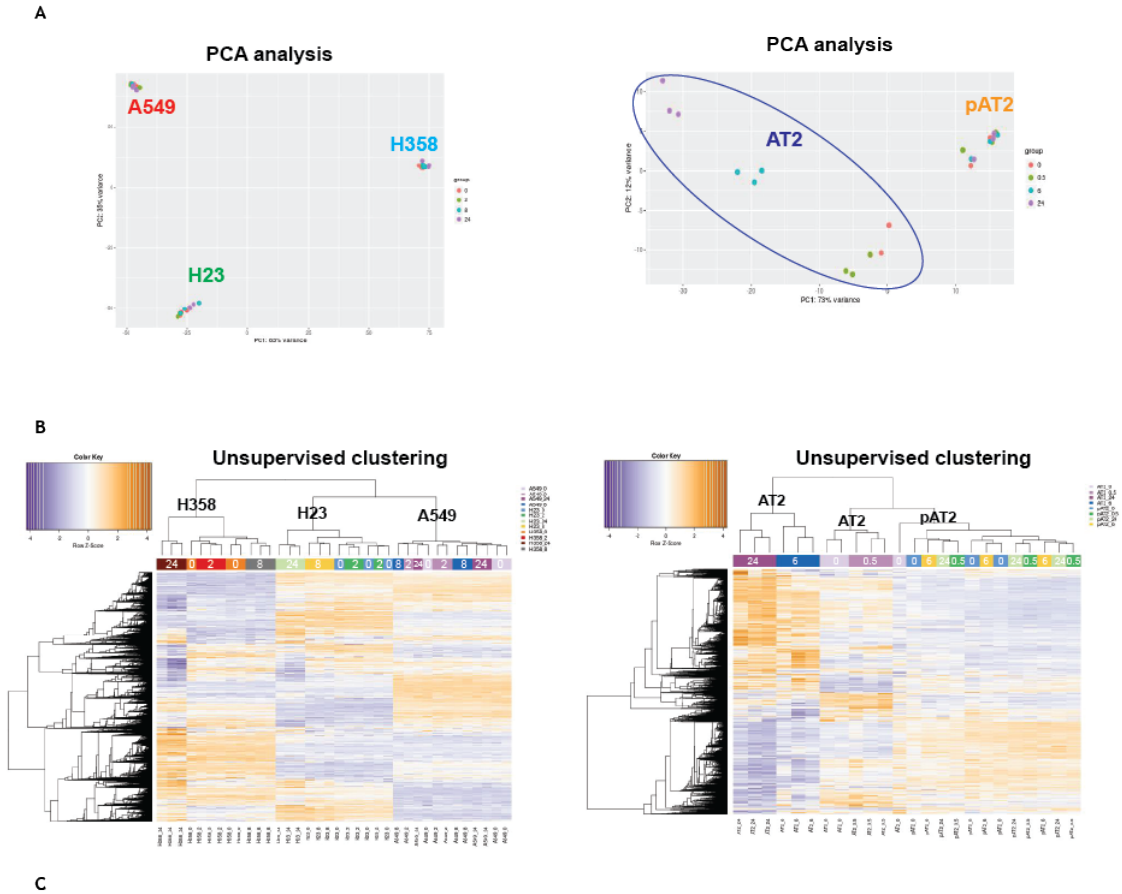

C

Differentially expressed genes

	H23	H358	A549
2h vs 0h	3	685	983
8h vs 0h	3497	2542	170
24h vs 0h	8883	10236	27

Differentially expressed genes

	AT2	pAT2
0.5h vs 0h	270	2
6h vs 0h	4488	1
24h vs 0h	6863	1

Figure 14. RNA-Seq analysis shows differentially expressed genes across conditions

RNA-Seq analysis. Data generated by the bioinformatics facility at the Francis Crick Institute. A) Principal Component analysis of G12C cell lines (left) and pneumocytes (right) B) Unsupervised clustering of all differentially expressed

genes. C) Summary of all significant (padj<0.05) differentially expressed gene numbers in all conditions.

Figure 14C shows a quantification of all the significant differentially expressed genes in all conditions. A large number of genes were differentially expressed at the 2h time point in the negative control, A549. This is likely due to the fact that genes in these table have been filtered according to their significance, but not the degree of the change in gene expression, so these changes, although significant represent genes whose expression changes minimally. However, the earliest treatment time point for all other cell lines showed the least gene expression changes, and gene number subsequently increased with time, reflective of changes due to increasing times of KRAS inhibition, which did not occur in the A549 or pAT2 (negative control) cell lines. These results confirm that modulation of KRAS activity leads to profound changes in gene expression in cells, but different cell lines displayed large differences in their gene expression patterns.

Subsequent analysis focused on finding common KRAS-regulated genes and pathways across cell lines. We sought to understand which pathways were regulated by KRAS signalling and whether there were commonalities in such pathways across cell types. To do so, we performed a gene set enrichment analysis (GSEA) of the different genes in the $KRAS^{G12C}$ and the AT2 cell lines at 8h (6h for AT2) and 24h post-treatment (Figure 15). The early time points were discarded from analysis due to insufficient differentially expressed genes. Differentially expressed pathways were relatively consistent across cell types. The highest ranking KRAS-induced pathways included Myc targets, cell cycle genes, E2F targets and mTOR signalling, which are known processes regulated by KRAS. Reassuringly, the pathway ‘KRAS SIGNALING UP’ was upregulated with KRAS activation and downregulated with KRAS inhibition in all conditions.

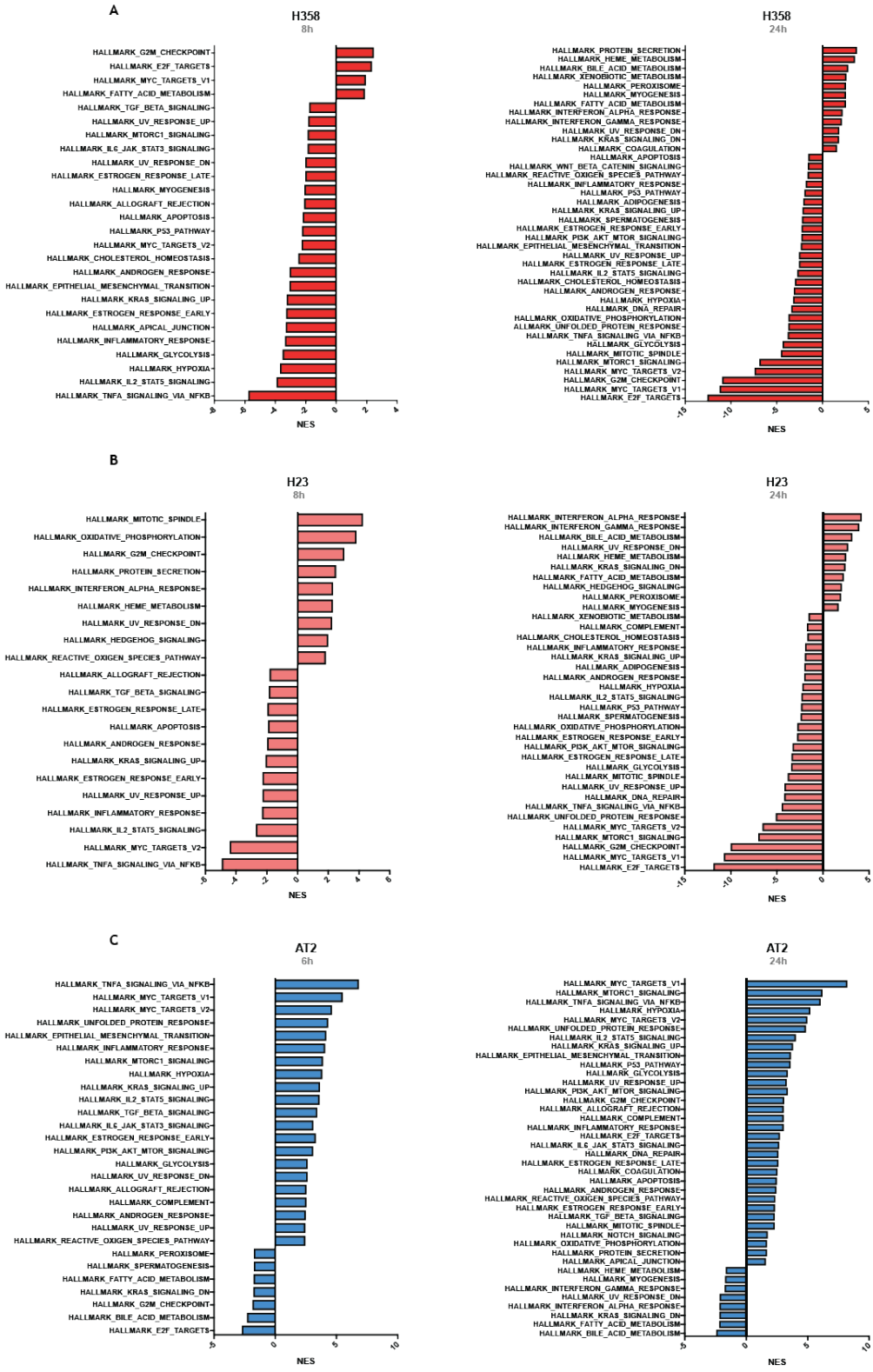

Figure 15. Gene set enrichment analysis of the RNA-Seq (FDR q value >0.05).

GSEA was performed using the MSigDB analysis 'Hallmarks'. Genes with a false discovery rate (FDR) q value of over 0.05 were considered for the analysis. NES= normalised enrichment score.

Some significantly enriched pathways included immune-related pathways, which confirmed our hypothesis that KRAS signalling is able to modulate immune-related genes (Figure 16). Immune-related gene sets significantly upregulated by KRAS included ‘INFLAMMATORY RESPONSE’. ‘IL2-STAT5 SIGNALING’ AND ‘TNFa SIGNALING VIA NFkB’. On the contrary, some immune-related pathways were downregulated by KRAS activity, such as ‘INTERFERON ALPHA RESPONSE’ and ‘INTERFERON GAMMA RESPONSE’, suggesting that KRAS signalling negatively regulates these pathways.

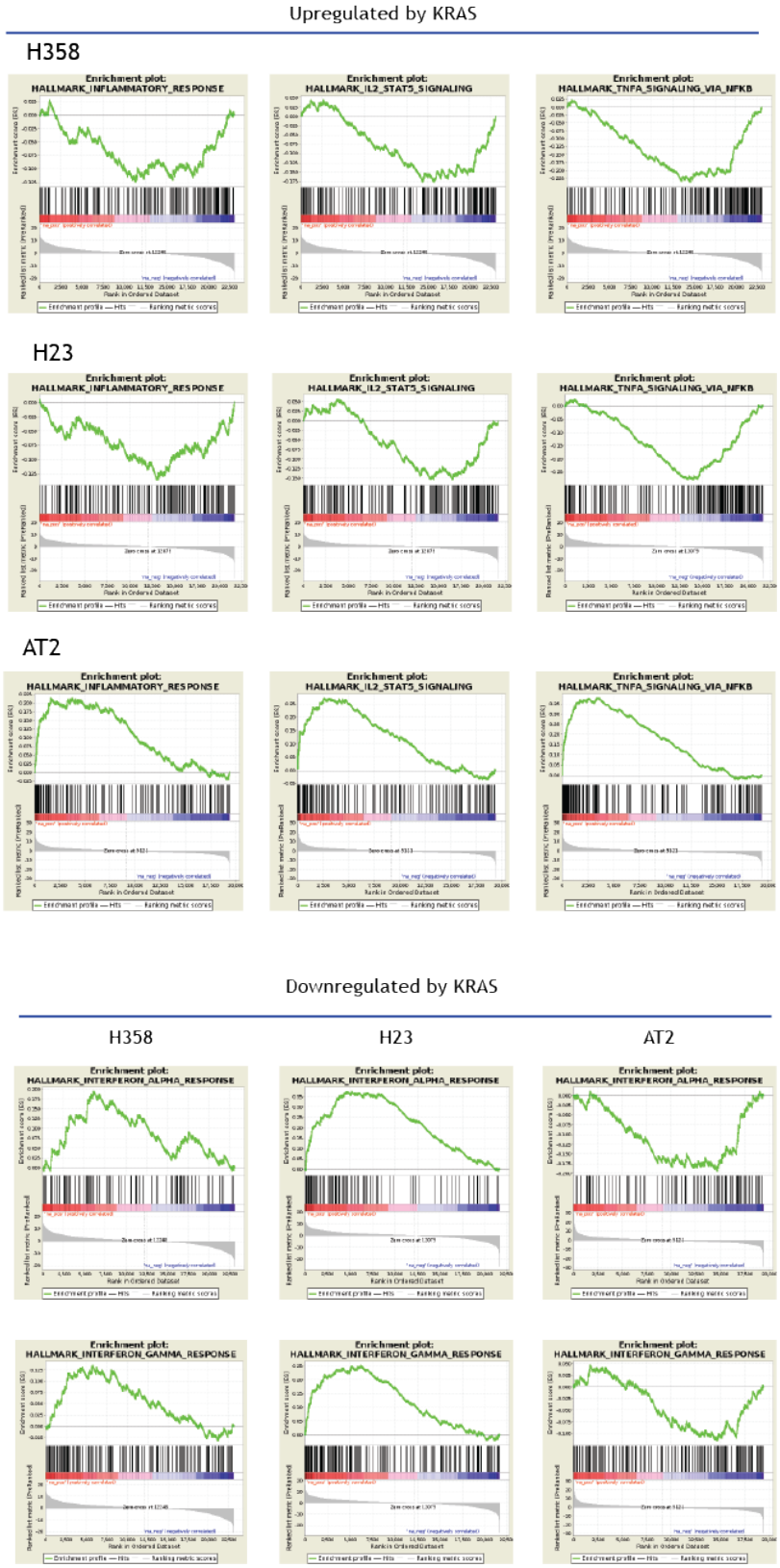

Figure 16. Gene set enrichment analysis of immune-related pathways.

GSEA plots of immune related genes. Plots shown belong to gene set 'Hallmarks' available on MSigDB.

Some examples of genes belonging to these pathways are plotted in Figure 17. Most of these genes are regulated by KRAS in all cell lines tested, suggesting that they comprise common mechanisms of KRAS-mediated signalling. All of these genes have described roles on the regulation of immune responses and can act in a variety of ways, such as by being secreted (like LIF, IL1B and CLCF1), by regulating extracellular nucleotide levels (such as NT5E) or by mediating antiviral interferon signalling (like STAT2, STAT3 and IRF9). Together, these results indicate that KRAS signalling can regulate the expression of immune mediator genes in a tumour-cell intrinsic manner and that such changes are robust across cell lines, indicating the universality of these findings.

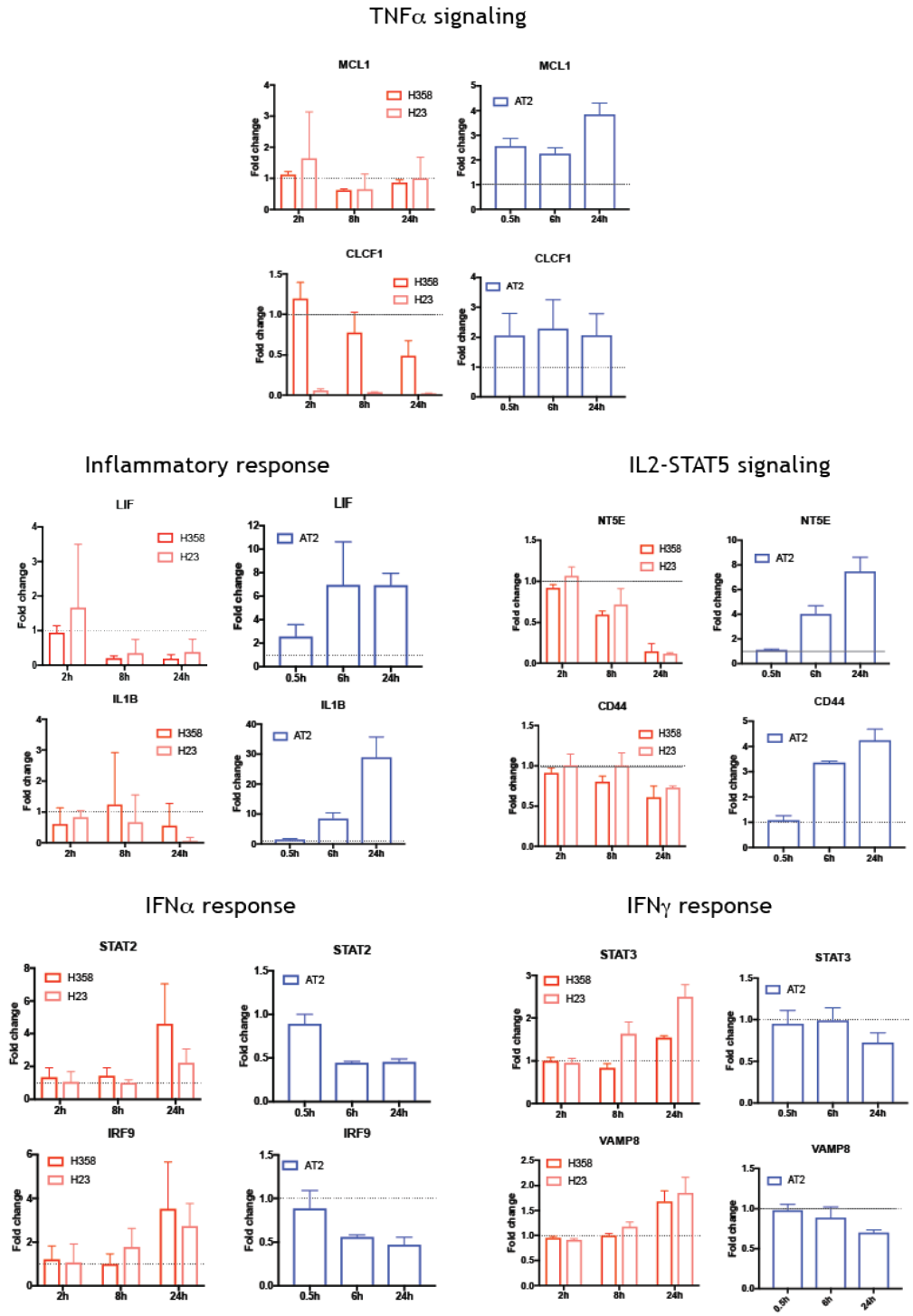

Figure 17. Examples of genes differentially regulated in RNA-Seq.

Representative genes of each pathway in Figure 16. Graphs represent fold change of RNA-Seq reads upon KRAS activation/inhibition. Mean + SD (n=3).

Finally, we sought to generate a list of genes that are positively regulated by KRAS and belong to immune-related gene set enrichment pathways. For this purpose, we only considered genes significantly changing in the 24h of KRAS-modulating treatment across all three cell lines tested (Figure 18A). The final list of genes obtained consisted of 84 genes of a variety of functions (Figure 18B). The list includes known KRAS-regulated genes such as DUSP6. It also features genes that have not been reported to be KRAS-dependent before. They include known immune regulators such as leukemia-inhibitory factor (LIF), associated with immune tolerance at the maternal-fetal interface (Ander et al., 2019). Polyoma virus receptor (PVR) is a known ligand for TIGIT (T cell immunoreceptor with Ig and ITIM domain), a known inhibitory molecule on T cells (Kucan Brlic et al., 2019). We have therefore unveiled new KRAS-dependent genes with known roles in the regulation of immune responses, strengthening our hypothesis that oncogenic KRAS signalling may play an immune modulatory role in lung cancer. This list of KRAS-dependent genes has been used in an *in vivo* CRISPR-Cas9 screen (work from Jesse Boumelha in the lab). The aim of this screen is to describe new mediators of immune evasion in an immunogenic mouse model of KRAS-mutant lung cancer.

A

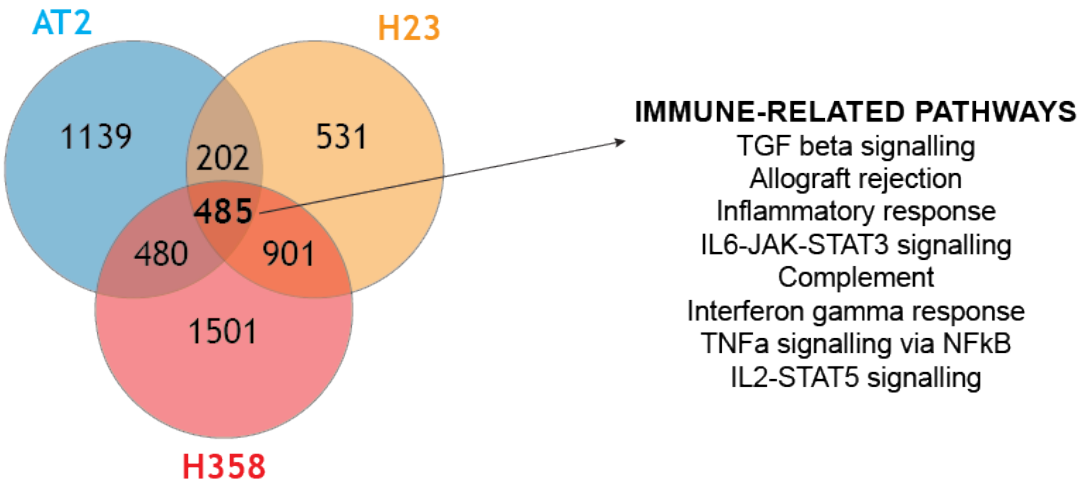

B

TNFRSF12A	BHLHE40	UPP1	SPP1	YRDC	CLCF1
PLAUR	NT5E	MAFF	PLAU	MMP1	PFN1
WWTR1	MYC	SPRY4	PDCD2L	PNP	PFKB3
PRKCH	IER3	LPAR1	GFPT2	NME1	EREG
MAP2K3	BCAR3	SPRED2	EIF5A	ETV4	DUSP4
IL4R	DUSP5	CD44	SLC7A1	SPHK1	ADORA2B
RAPGEF3	PHLDA1	RNF4	UCK2	PUS1	TFPI2
CCNE1	DUSP6	MTHFD2	ZEB1	NOP2	PRNP
SERPINE1	MCL1	ISOC1	BTG3	CCND3	PTPRE
AREG	SLC20A1	PFKP	SGMS2	ODC1	EGR1
CCND1	OSMR	ATP2B1	ANXA5	FOSL1	FOS
SH2B3	IFNGR2	PVR	ABCE1	FJX1	PLAT
VEGFA	ITGA2	CXCL2	GEM	PHLDA2	LRRC8C
HBEGF	F2RL1	CDC6	ACOX2	LIF	LDLR

Figure 18. KRAS-dependent, immune-related genes.

A) Venn diagram showing the number of significantly ($p<0.05$) regulated genes (up in AT2, down in H23 and H358) (left). Only the genes common to all three cell lines were analysed, and filtered according to their presence in one of the selected immune-related pathways (right). B) Final list of 84 KRAS-regulated, immune-related genes.

3.4 Protein validation of KRAS-regulated cytokines

RNA expression data can be very useful to understand changes in gene expression pathways and processes and to obtain datasets for further examination. Thereby, as a validation, we sought to understand whether protein expression of known immunomodulatory cytokines could be altered by modulation of oncogenic KRAS activity *in vitro*. We did this by performing cytokine release assays that can measure proteins in the medium of cultured cells. We used AT2 cells in the presence or absence of 4-OHT and H358 control and ARS-1620 treated cells. Figure 19A shows the results for AT2. In the absence of oncogenic KRAS, the only cytokine that could be detected in the medium, even at high exposures, was Serpin Family E Member 1 (SERPINE1), also known as Plasminogen Activator Inhibitor Type 1 (PAI-1), a cytokine that plays a role in inhibition of fibrinolysis known to be secreted by alveolar cells. Activation of KRAS in these cells led to the secretion of a number of cytokines and chemokines, all of which were observed in the RNA-Seq analysis, pointing out to a transcriptional regulation of these genes. In contrast, H358 cells exhibited a secretion of a large number of cytokines in basal conditions (Figure 19B), consistent with tumour cells' ability to recruit and modulate cells in the TME. KRAS inhibition by ARS-1620 administration resulted in the decrease of secretion of a number of cytokines. The cytokines are displayed in order of release quantity (Figure 19B, left), indicating that neutrophil chemoattractant IL-8 was the highest secreted cytokine. KRAS-regulated cytokines coincided with those found in AT2 cells, with the exception of macrophage inhibitory factor (MIF), which did not show KRAS-dependent regulation in these cells and CCL2 which was not secreted by H358 cells. CXCL1 and IL-8 are neutrophil chemoattractants, while GM-CSF, MIF and CCL2 play a role in the macrophage differentiation, regulation of macrophage function, and monocyte recruitment, respectively. This data suggests that KRAS signalling could play an important role in the shaping of the myeloid compartment of the TME.

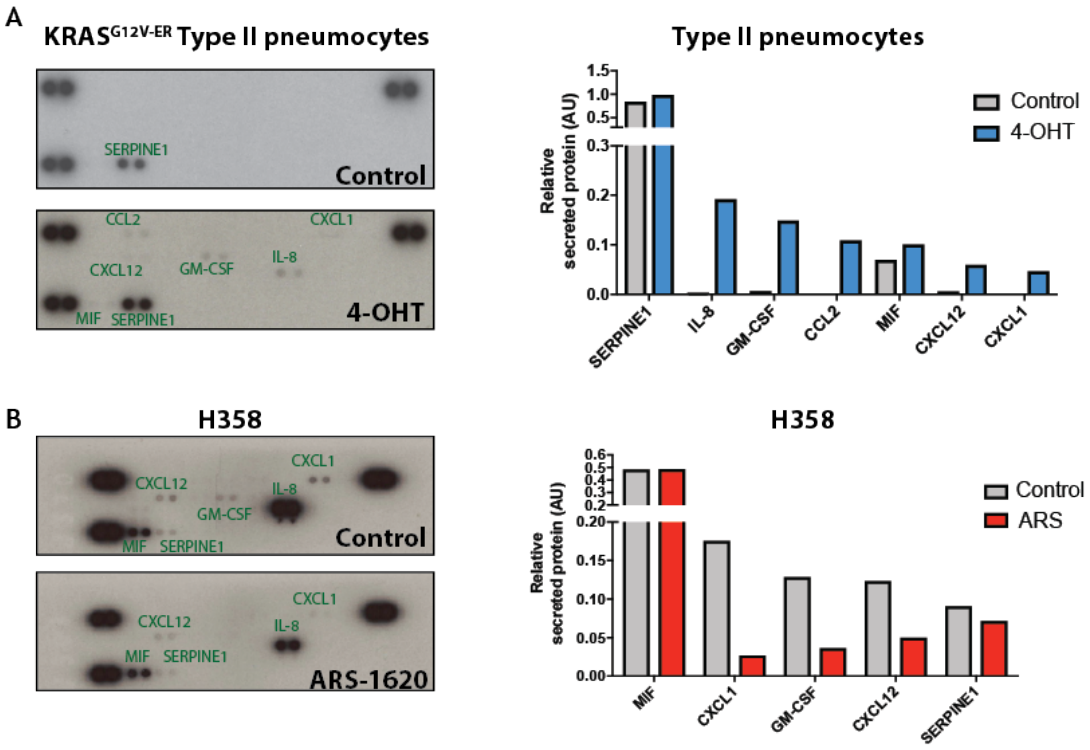

Figure 19. Secretion of cytokines can be KRAS-dependent.

A) AT2 cells were treated with 500nM 4-OHT for 24h before medium was harvested for cytokine array. Cytokine array is shown on the left and quantification of cytokines in both conditions on the right. Cytokines are displayed in order of intensity. B) H358 cells were treated with 2μM of ARS-1620 for 24h. Cytokine array is shown on the left and quantification of both conditions on the right. Cytokines are displayed in order of intensity.

3.5 Conclusions and future directions

In this chapter, we assessed changes in gene expression triggered by oncogenic KRAS. By making use of both KRAS activating and inhibiting approaches, we have aimed to exclude viability-related effects of $KRAS^{G12C}$ inhibitors. At the time that this experiment was carried out, it constituted one of the first gene expression analyses making use of $KRAS^{G12C}$ inhibitors and was therefore a useful tool to several projects in the lab investigating the effects of such inhibitors on different biological pathways. We made use of two different human $KRAS^{G12C}$ mutant cell lines for robustness, and excluded KRAS inhibitor driven gene expression changes that occurred in one cell line only. We hypothesised that the differences in the cell lines were due to additional alterations that differed between them. Both cell lines are models of KRAS mutant, p53 mutated/deleted lung cancer, but their exact genomic composition is likely different. However, we focused on common changes occurring on both cell lines in our quest for universal KRAS-driven gene expression changes.

As perhaps expected, the gene expression changes resulting from an activation or inhibition of oncogenic KRAS were very vast and it was a challenge to dissect out the genes that may play a role in shaping anti-tumour immune responses *in vivo*. We therefore took a perhaps biased approach of investigating those genes that belonged to immune-related pathways, potentially neglecting genes with an unknown immune regulatory function. Similarly, we narrowed down our genes of interest by examining only those genes that were upregulated by KRAS activation (or downregulated by KRAS inhibition), again possibly neglecting KRAS-inhibited pathways, such as interferon responses. In our work using clinical $KRAS^{G12C}$ inhibitors we further explored the link between KRAS signalling and interferon responses in a pre-clinical setting, work that was based on data stemming from the RNA-Seq presented in this chapter (5.4). By making use of the list of KRAS-dependent genes described in Figure 18, an *in vivo* CRISPR-Cas9 screen was carried out and a number of the genes were discovered to play a role in KRAS-mutant murine lung tumour growth in an immune-competent setting but not in immune-deficient mice (work carried out by other people in the lab and therefore out of the scope of this thesis).

This data served as an original confirmation of our hypothesis that tumour cell-intrinsic oncogenic KRAS signalling can regulate pathways that may lead to the evasion of anti-tumour immune responses. We also discovered new KRAS dependent genes and validated the KRAS-dependent secretion of cytokines that may play a role in such processes, underscoring the need of further examination of these mechanisms, which are largely unknown.

In order to further validate the KRAS-dependent genes, pathways and cytokines unveiled in this chapter by the use of human cell lines, we needed to shift to a model where we could examine the interaction between tumour cells and the immune system *in vivo*. Our aim moving forward was therefore to develop and characterise adequate mouse models of KRAS-mutant lung cancer in which we can examine the interplay between oncogenic KRAS signalling in tumour cells and the tumour microenvironment.

Chapter 4. Results 2: Development and characterisation of a KRAS^{G12C}-mutant mouse lung cancer model and investigation of CCL2 as a KRAS-regulated cytokine

4.1 Introduction

In our aim to elucidate the role of KRAS signalling on immune evasion in NSCLC, we have examined the transcriptional output of KRAS signalling and performed *in silico* analyses of KRAS-regulated genes that could play a role in the tumour-immune crosstalk. As a way forward, we sought to further investigate the role of these genes and other KRAS-dependent mechanisms.

The advent of the newly developed KRAS^{G12C} inhibitors has proven extremely useful in the previous chapter. We would like to be able to use such inhibitors *in vivo*, for two main reasons. The first reason is that we would like to be able to validate and further examine the role of the genes described in the previous chapter, and identify and characterise additional tumour cell-intrinsic mechanisms by which KRAS signalling affects the TME. Additionally, as these inhibitors are yielding promising results in clinical trials, we would like to investigate the effect of these drugs on the composition of TME and shaping of the immune responses to NSCLC (see Chapter 5).

To this end, the use of immunocompetent mouse models is crucial. The most commonly used KRAS-mutant lung cancer mouse models include the KRAS$^{G12D\text{-}LSL}$-p53$^{fl/fl}$ (or 'KP', (DuPage et al., 2009)) model which harbours a KRAS^{G12D} mutation and urethane induced tumours which generate KRAS^{Q61R} mutations (Westcott et al., 2015), rendering them unsuitable for KRAS^{G12C} inhibitor studies. This chapter focuses on the establishment of a murine KRAS^{G12C}-mutant transplantable lung cancer model, which is susceptible to KRAS^{G12C} inhibition. We have also assessed its immunogenicity and characterised its TME composition *in vivo*. We have then sought to elucidate mechanisms by which KRAS-mediated signalling contributes to the establishment of the TME of these tumours.

The 3LL cell line (also known as Lewis lung carcinoma, LL/2 or LLC) is a murine lung cancer cell line that is widely used in lung cancer research. This cell line, developed by Dr. Margaret R Lewis at the Wistar Institute in the 1950s, originated from a spontaneously developed carcinoma found in the lung of a C57Bl/6 mouse (Mayo, 1972). It is widely used as a syngeneic model for lung cancer and can be grown as a subcutaneous and orthotopic tumour (Kellar et al., 2015). Unpublished characterisation (unpublished, work performed in our lab) of this cell line as a murine model has established that after intravenous administration of one million cells, approximately 3-5 tumours form in the lung (per mouse) and can be detected by microCT scanning 2-3 weeks after injection. If left untreated, mice succumb to lung tumours approximately 4 weeks after injection, highlighting the fast growth and aggressiveness of this model. Interestingly, these tumours tend to grow as a protrusion from the lung rather than within the lung tissue, which contrasts with other lung tumour models such as the 'KP' model. For example images of 3LL lung tumours acquired by imaging mass cytometry, please refer to (van Maldegem et al., 2021).

4.2 Knock-out of NRAS makes the 3LL cell line sensitive to KRAS inhibition

The 3LL cell line has been reported to be driven by a $KRAS^{G12C}$ mutation (Marazioti et al., 2018) and an NRAS mutation (Giannou et al., 2017). We Sanger sequenced the KRAS and NRAS locus of the 3LL cell line and indeed were able to detect a homozygous $KRAS^{G12C}$ and a homozygous $NRAS^{Q61H}$ mutation (Figure 20A). We were particularly interested in the $KRAS^{G12C}$ mutation, as it potentially made this cell line suitable for $KRAS^{G12C}$ inhibitor studies. Thus, we administered ARS-1620 to this cell line and examined its effects in terms of cell viability and downstream signalling. However, as illustrated in Figure 20B, the viability of the cells remained unaffected by administration of the KRAS inhibitor. In line with this result, downstream signalling of KRAS was only mildly inhibited by a 24h treatment with the drug (Figure 20C, also in (Molina-Arcas et al., 2019)). We therefore concluded that this model was not adequate to use for KRAS inhibitor studies due to its lack of susceptibility to these drugs.

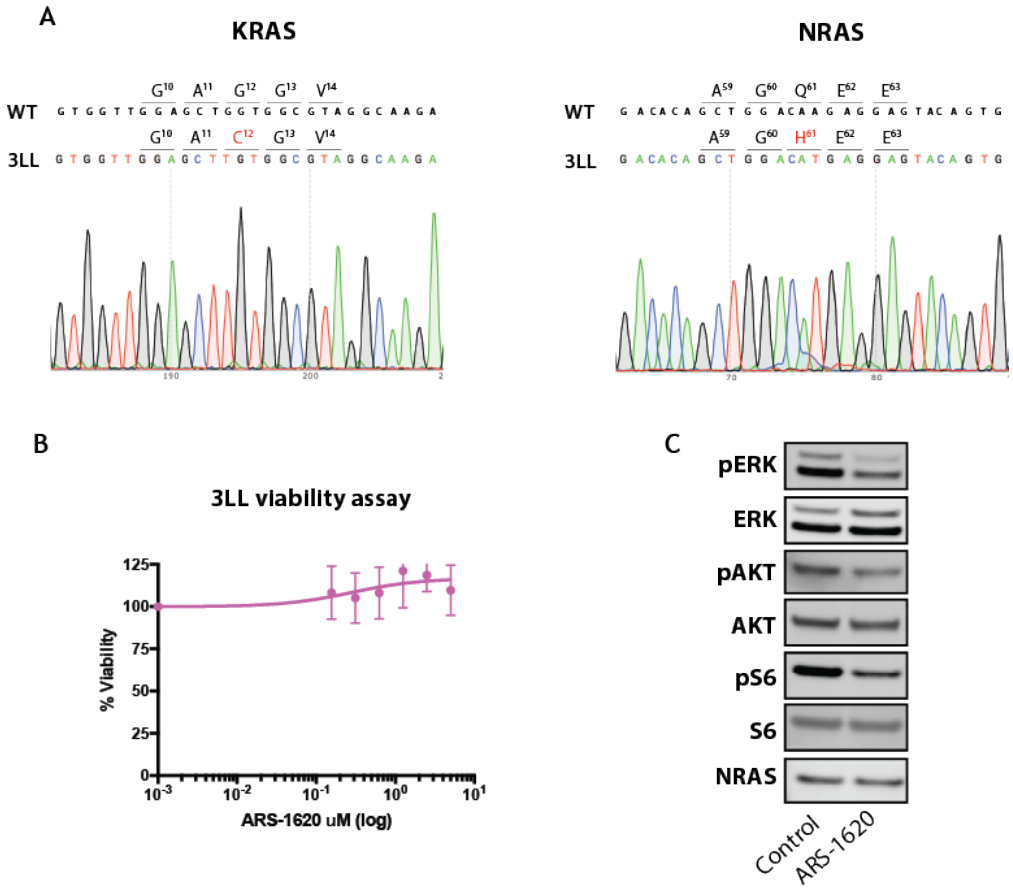

Figure 20. 3LL cells have a KRAS^{G12C} and an NRAS^{Q61H} mutation and are resistant to KRAS^{G12C} inhibition.

A) Sanger sequencing for KRAS and NRAS genes in 3LL cells, mutated codons are highlighted in red. WT = wild type reference sequence for KRAS (Gene ID: 16653) and NRAS (Gene ID: 18176) sequence. B) Cell viability quantification upon administration of serial dilutions of ARS-1620. Cell viability was measured after 3 days of treatment. Mean±SEM of three technical replicates (one representative experiment out of three is shown). C) Western blot of downstream signalling upon 24h of 2μM ARS-1620 treatment. Experiment performed by Sareena Rana (Molina-Arcas et al., 2019).

We suspected that the mutated NRAS protein had the ability to compensate for the lack of oncogenic KRAS upon administration of a KRAS inhibitor. We therefore hypothesised that removing the NRAS gene could make these cells susceptible to KRAS inhibition. To test this, we decided to make an NRAS knock-out (KO) derivative of this cell line using CRISPR-Cas9 technology. We designed two different guide RNAs (sgRNA) targeting exon 2 of the NRAS gene, where the mutation is located (Figure 21A). The pipeline of the KO generation is illustrated in Figure 21B. We cloned the sgRNAs separately into a mammalian vector expressing the enzyme Cas9 and GFP as a selection marker. We transfected the cells with either of both vectors and sorted the GFP+ cells using fluorescence-activated cell sorting (FACS). After allowing for the recovery of the sorted cells, they underwent single cell cloning. Screening for NRAS deleted cells, obtained using both sgRNAs for robustness, was done in two steps. Firstly, DNA of the growing clones was sequenced in their NRAS locus and those cells that were wild-type (WT) were discarded. After letting single cell clones grow, we extracted protein from them and blotted for the NRAS protein, which was absent in a subset of clones. An example of four clones is displayed in Figure 21C. NRAS KO clones #63 and #86 were used for subsequent examination.

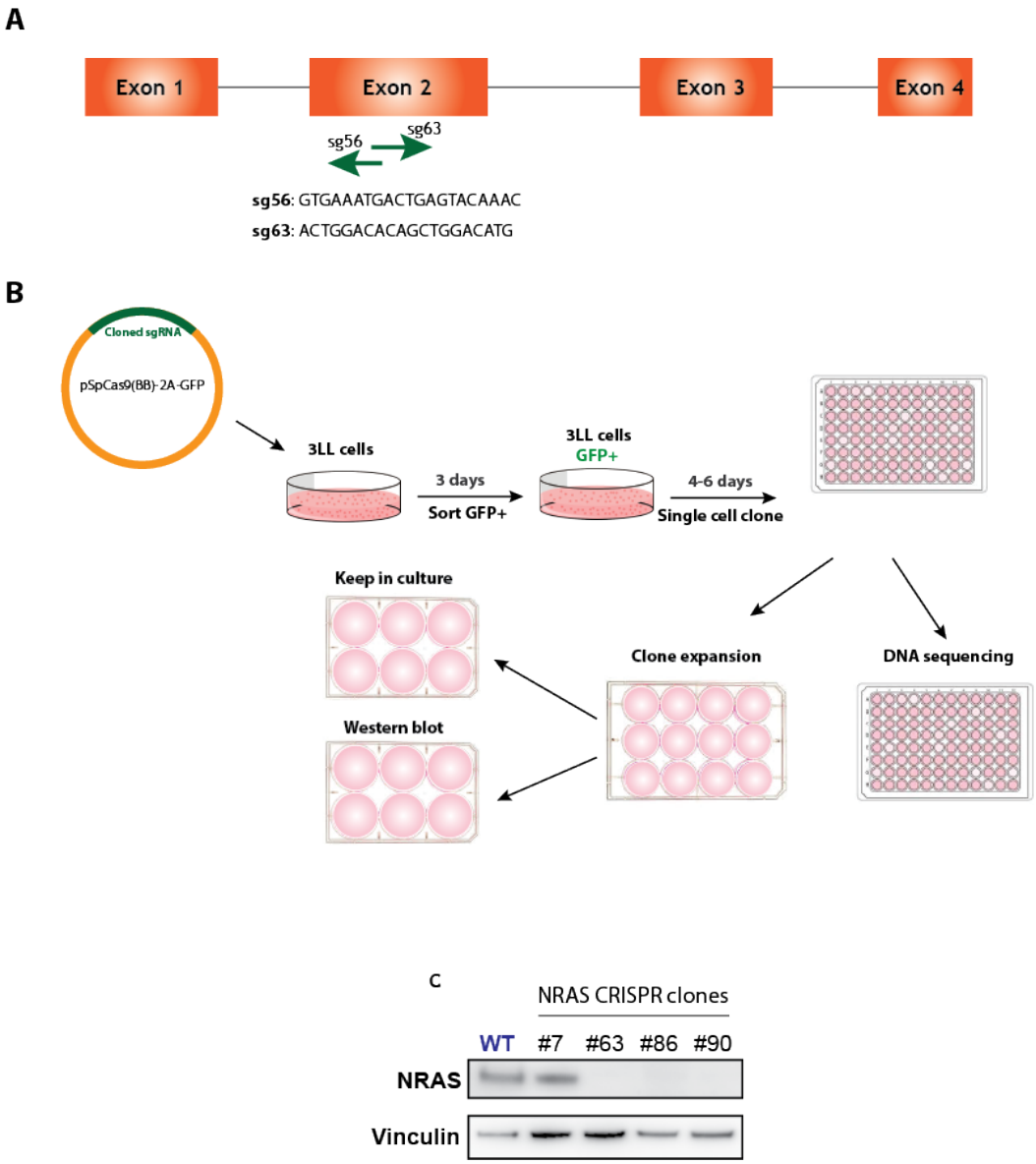

Figure 21. NRAS CRISPR-Cas9 KO pipeline schematic.

A) Schematic of the NRAS gene and the location of the guide RNAs designed. B) Illustration of the pipeline followed for CRISPR-Cas9 knockout generation. C) Representative western blot of four CRISPR-Cas9 single cell clones, blotted for NRAS.

The NRAS KO derivatives of the 3LL cell line were then treated with the KRAS inhibitor. The viability of 3LL NRAS KO #63 and 3LL NRAS KO #86 was reduced to approximately 50% upon ARS-1620 administration, in contrast to the parental 3LL WT cell line (Figure 22A). In addition, downstream signalling in both ERK and AKT pathways was significantly reduced by KRAS inhibition (Figure 22, also in (Molina-Arcas et al., 2019)). Further characterisation of these cells has been reported by

our lab in (Molina-Arcas et al., 2019). For all further experiments, we made use of 3LL NRAS KO clone #86 unless otherwise specified, and we termed it 3LL ΔNRAS.

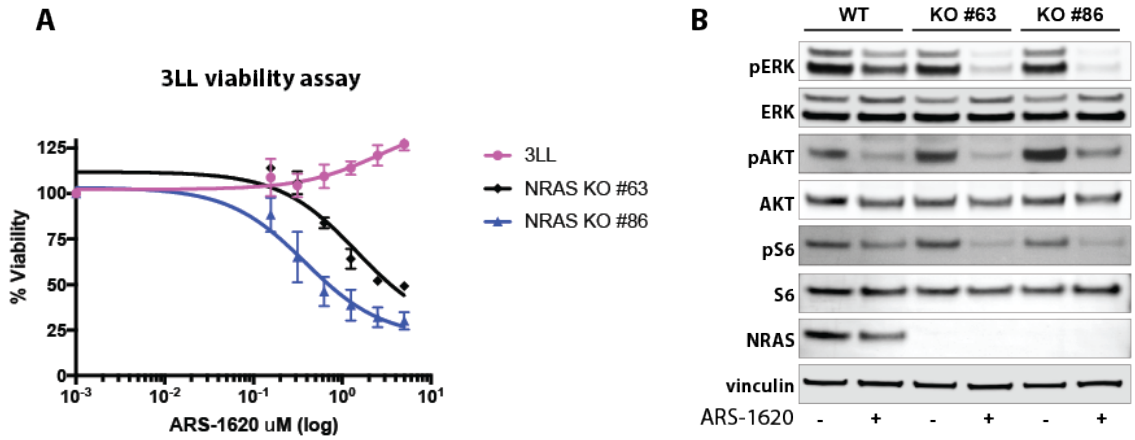

Figure 22. CRISPR KO of NRAS renders 3LL cells sensitive to KRAS^{G12C} inhibition.

A) Cell titer blue-based cell viability quantification upon administration of serial dilutions of ARS-1620. Cell viability was measured after 5 days of treatment. Mean ± SEM of three technical replicates (one representative experiment out of three is shown). B) Western blot of downstream signalling upon 24h of 2μM ARS-1620 treatment. Experiment performed by Sareena Rana (Molina-Arcas et al., 2019).

To effectively assess whether NRAS deletion increases susceptibility to KRAS inhibition, we sought to validate some of our hit genes from the RNA-Seq described in 3.3. We administered ARS-1620 to both the 3LL WT and the ΔNRAS derivative *in vitro*. Treatment with ARS-1620 had little or no effect on most of the genes tested on the parental 3LL cell line (Figure 23), in line with our previous findings that these cells are partially resistant to KRAS inhibition. However, ARS-1620 was able to reduce the expression of all genes tested in the 3LL ΔNRAS cells (Figure 23). These findings, on one hand, confirmed that NRAS deletion renders the 3LL cell line increasingly susceptible to the action of KRAS^{G12C} inhibitors. On the other hand, it served as a validation of the KRAS-regulation of the genes described in the previous chapter in an independent model.

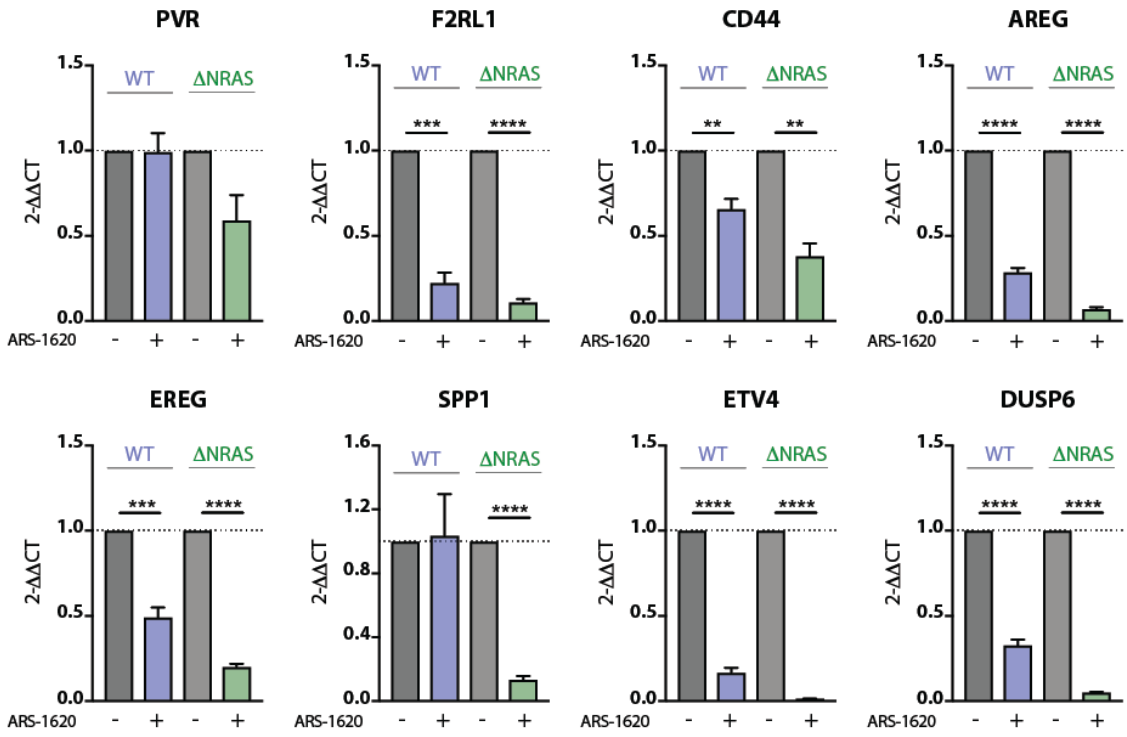

Figure 23. Validation of RNA-Seq hits in 3LL WT and ΔNRAS cell lines.

Genes represent selected KRAS-target genes from the RNA-Seq analysis. Cells were treated *in vitro* with 2μm of ARS-1620 for 24h. Gene expression data was calculated and plotted using the $2^{-\Delta\Delta CT}$ method using at least two housekeeping genes and normalised to the untreated control sample for each cell line.

We have therefore established, by CRISPR-Cas9 gene editing, a murine lung cancer cell line sensitive to the actions of $KRAS^{G12C}$ inhibitors. This cell line can be used *in vivo* as a model for lung cancer and we aimed to use it for our studies of the immune TME in KRAS-mutant NSCLC. For this purpose, we firstly needed to characterise the degree of immunogenicity of this model.

4.3 3LL ΔNRAS is a highly mutated cell line with a large number of predicted neoantigens

It is widely accepted, albeit with some degree of controversy, that the degree of immunogenicity of a tumour correlates largely with its somatic mutation burden (Hellmann et al., 2018). It is reasoned that these mutations will give rise to neoantigens that can be recognised by the host's adaptive immune system (1.4.3). Thereby, we sought to elucidate the mutation burden of the 3LL ΔNRAS cell line, to be able to somewhat predict its degree of immunogenicity. Even though a large number of somatic mutations merely augments the probability of having neoantigens, it does not necessarily mean the cell line is immunogenic. However, if no or low numbers of mutations were to be found in this cell line, it would serve us to exclude the possibility that this cell line is able to elicit any anti-tumour immune response *in vivo*.

For this purpose, we performed a whole exome sequencing analysis of the two NRAS KO clones (#63 and #86). After DNA extraction and sequencing by the Advanced Sequencing Facility at the Crick, single nucleotide variant (SNV) analysis was done by Phil East at the bioinformatics facility. The adequate control for such an experiment would consist of somatic DNA from the same mouse the tumour was developed from. However, as stated previously, this cell line was developed in the 1950s, so this was not feasible. We therefore used DNA obtained from a pool of tails originating from the C57Bl/6 mouse colony that we commonly utilise for our experiments. Variant calling analyses revealed an astonishingly high number of nucleotide variations present in both cell lines (Figure 24A), with over 2000 nonsynonymous single point mutations predicted per cell line. Most of the SNVs were present in an allelic frequency of 1 (homozygous) or 0.5 (heterozygous), with relatively few mutations found at a lower frequency, consistent with the fact that these cell lines are single cell clones (Figure 24B). According to these predictions, the 3LL ΔNRAS cell lines harbour a large number of mutations which should in theory be recognised by the host's immune system.

A

	Total	Synonymous	Nonsynonymous	Nonsense
3LL NRAS KO #63	3396	1236	2073	88
3LL NRAS KO #86	3422	1225	2110	88

B

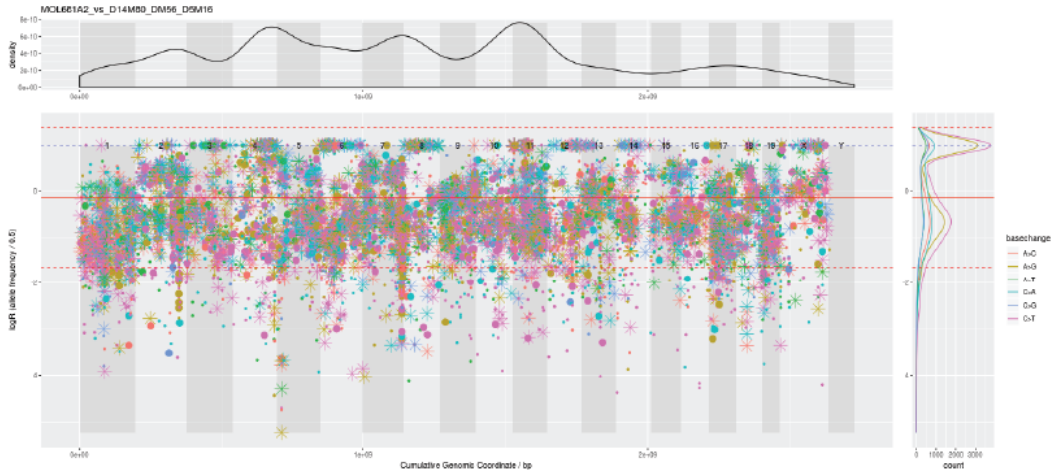

Figure 24. Whole exome sequencing of 3LL NRAS KO clones.

Data analysed by the Bioinformatics facility of The Francis Crick Institute. A) Summary table of final number of SNVs in reference to wild-type C57Bl/6 DNA. B) LogR plot of SNVs for 3LL NRAS KO #86. The x axis represents the genomic distribution, while the y axis shows the allelic frequency. Mutation types are coded by colours.

Additionally, we performed *in silico* analysis to predict whether any of these mutations could lead to the synthesis of peptides that could be presented by major histocompatibility complexes (MHC). We combined the previously described whole exome sequencing data with gene expression data obtained from an RNA-Seq experiment that will be presented later (5.3). This analysis allowed us to establish which of the mutated genes were expressed by the cell line. Subsequently, we obtained peptide sequences containing the mutated residues and performed a neoantigen prediction analysis based on the predicted affinities of the peptides to the MHC molecules (Figure 25A, analysis performed by Miriam Llorian Sopena). Since C57Bl/6 mice are known to contain H2-Db and H2-Kb alleles, we used these to perform the analysis. The pipeline predicted that there are tens of high affinity peptides with high affinity for either H2-Db and H2-Kb present in the cells, and this number was even higher for medium affinity peptides (Figure 25B). We therefore

concluded that these cells harboured a sufficient amount of putative neoantigens to be able to be detected by the immune system.

However, for these antigens to be recognised by immune cells, they need to be presented by MHC molecules. We therefore wanted to investigate whether these cells had any of these molecules present in their surface. To our surprise, both the parental and the NRAS KO clones, despite being positive for the MHC molecule H2-Db, did not express any H2-Kb molecules (Figure 25C). Even when stimulated with IFNγ, a known inducer of MHC expression (Zhou, 2009), they remained negative for H2-Kb (Figure 25C). We hypothesised that there might exist an epigenetic silencing mechanism for this gene in these cells, as the gene was found intact in the whole exome sequencing data, but no mRNA transcripts for it were detected in the RNA-Seq analysis.

A

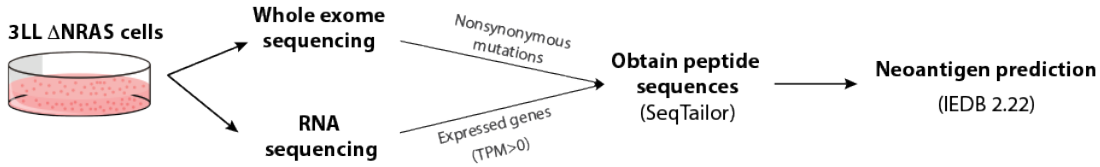

B

	High affinity (ic50>50nM)	Medium affinity (ic50: 50-500nM)
H2Db (9mer)	11	27
H2Db (10mer)	10	31
H2kB (8mer)	35	108
H2kB (9mer)	24	187

C

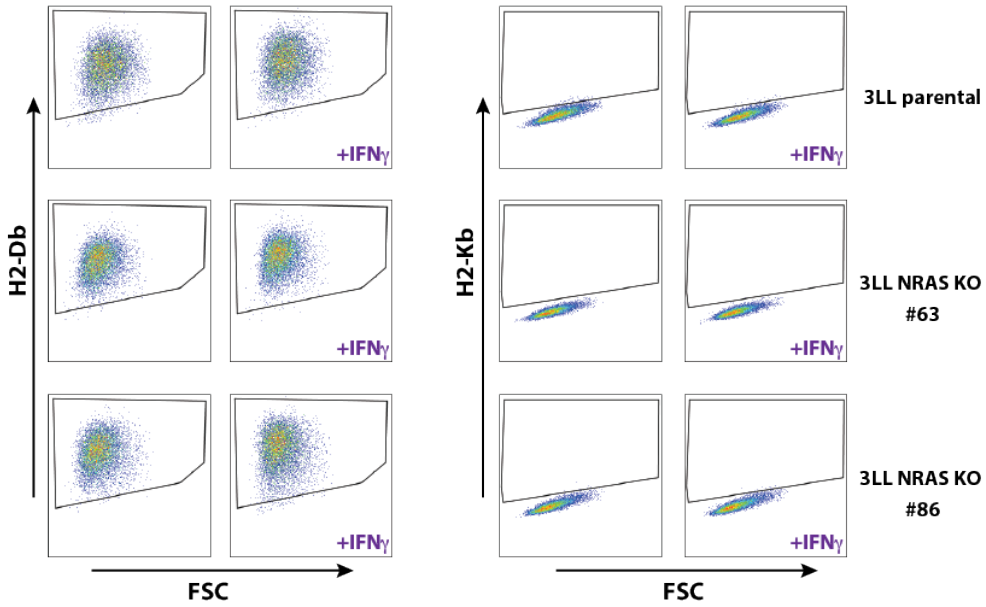

D

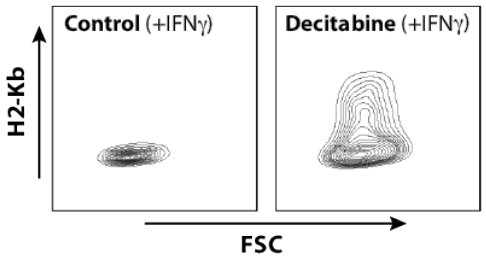

Figure 25. 3LL cells have a large number of predicted neoantigens.

A) Pipeline followed for neoantigen prediction analysis. Analysis performed by the bioinformatics facility at the Francis Crick Institute. TPM=transcripts per megabase. B) Summary of peptides predicted to have high or medium affinities to relevant MHC molecules. C) FACS analysis for H2-Db and H2-Kb expression *in vitro*, either untreated or treated with 100ng/ml mouse recombinant IFNγ (x axis represents forward scatter, pre-gated on live cells). D) 3LL NRAS KO #86 cells were treated

with either IFNγ as above or with IFNγ with Decitabine (250nM) for 24h before surface H2-Kb expression analysis.

Consequently, due to the absence of one MHC allele, not all putative neoantigens described in Figure 25B would be presented to the immune system. However, even just the predicted H2-Db binders should be of sufficient number to elicit a T cell response. Interestingly, a larger number of predicted neoantigens was obtained for H2-Kb binders (Figure 25B), suggesting that the cells might have undergone a negative selection for H2-Db binding epitopes *in vivo*. This further suggests that these peptides are likely to be able to be detected and eliminated by the host's immune system. We therefore conclude that the 3LL ΔNRAS cell line harbours sufficient neoantigens to be detected by the adaptive immune system of the host, making it a suitable model to study anti-tumour immune responses.

Additionally, we were able to partially restore surface H2-Kb expression on 3LL cells by treatment with the DNA methylation inhibitor Decitabine (Figure 25D). We therefore hypothesised that these cells have previously undergone epigenetic remodelling, probably in response to selective pressures *in vivo*, which has resulted in the loss of one allele of MHC. We thus postulated that this cell line, after undergoing immune editing *in vivo*, will constitute a model of immune evasive KRAS-mutant lung cancer. In order to validate this hypothesis, we carried out several experiments to assess the immunogenicity of our transplantable lung cancer cell line, which will be described in the following sections.

4.4 3LL ΔNRAS tumours are not susceptible to anti-tumour immune responses and display a largely immunosuppressive TME

A widely used manner of establishing whether a tumour can be recognised by the adaptive immune system is to assess its growth in immunocompetent and immunodeficient mice. If the tumour is able to develop more rapidly in immunodeficient conditions, it indicates that the presence of T and B cells is able to inhibit, at least partially, the growth of the tumour (Schreiber et al., 2011).

We therefore implanted 3LL ΔNRAS cells in either $Rag^{-/-}$ (mice unable to perform V(D)J recombination and thus lacking mature B and T cells) or $Rag^{+/-}$ or wild-type mice as a control. When implanted subcutaneously, no growth difference was observed when the tumours were grown in immunocompetent or immunodeficient animals. Additionally, knockout of the common gamma chain of the interleukin 2 (IL-2) receptor (IL-2rγ) leads to a deficiency in NK cells, which is useful to assess NK sensitivity of tumours (Zhao et al., 2019). A slight increase in tumour growth was seen when tumours were grown in a $Rag^{-/-}$ $Il2R\gamma^{-/-}$ background, suggesting that these tumours were susceptible to NK cell attack (Figure 26A). In a similar manner, when tumours were implanted orthotopically, by intravenous injection and metastasised to the lungs, no survival difference was observed in WT versus $Rag^{-/-}$ mice (Figure 26B). Together, these results suggest that 3LL ΔNRAS tumours do not elicit adaptive anti-tumour immune responses, despite displaying a large mutation burden that should make them susceptible to the actions of adaptive immunity. We hypothesised that these cells have developed mechanisms that allows them to evade the actions of anti-tumour immunity.

We went on to perform a deep analysis of the TME established by these tumours. We decided to do so in an orthotopic setting where tumours grow in the lungs of the mice after intravenous injection, as it would comprise a more clinically relevant setting. Immunoprofiling was done by flow cytometric analysis of the tumours, making use of three different antibody panels established in our group that cover most of the cells commonly present in the TME (Figure 27).

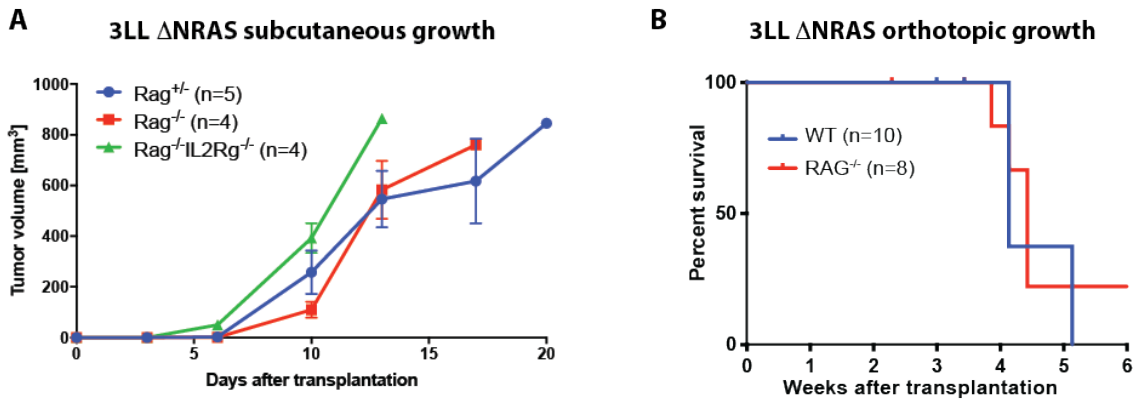

Figure 26. 3LL ΔNRAS tumours do not elicit an anti-tumour immune response. A) 400.000 3LL ΔNRAS #86 cells were injected into the flanks of either $Rag^{+/-}$, $Rag^{-/-}$ or $Rag^{-/-}IL2R\gamma^{-/-}$ mice and tumour growth was measured regularly. Mean±SEM of each measurement is shown. B) $1x10^6$ 3LL ΔNRAS #86 cells were injected intravenously and mouse weight was measured as a surrogate for tumour burden.

The first antibody panel focuses on T cells, with markers to detect different populations (CD3, γδTCR, CD8, CD4, Foxp3) and their activation status (CD69, CD44, CD62L and PD-1). Using CD44 and CD62L we are able to distinguish naïve and antigen-experienced (effector and memory) T cells. Using PD-1 and LAG3, we are able to distinguish antigen-experienced and exhausted T cells. The second panel allows for the detection of NK cells (CD49b+ NKp46+), B cells (B220+ CD19+), neutrophils (Ly6G+Ly6C+), monocytes (Ly6C+Ly6G-) and macrophages (F4/80). In this panel we are able to distinguish CD11b+ and CD11c+ macrophages, which constitute two different macrophage populations in our model, with CD11b+ macrophages being much more prominent. According to Misharin et al (Misharin et al., 2013), CD11c+ macrophages comprise tissue-resident alveolar macrophages, whereas CD11b+ macrophages are interstitial macrophages derived from bone marrow-derived monocytes. However, this classification is based on healthy lung tissue and may not accurately reflect the macrophage heterogeneity present in a growing tumour, such as our 3LL model. Our third panel combines markers of dendritic cells (CD24, CD103) and macrophages (CD64) and their activation status. It includes markers of professional antigen presentation and co-stimulation, MHCII and CD86, to examine the antigen presentation capabilities of macrophages and DCs. The gating strategy followed to obtain all the populations is presented in Figure 28.

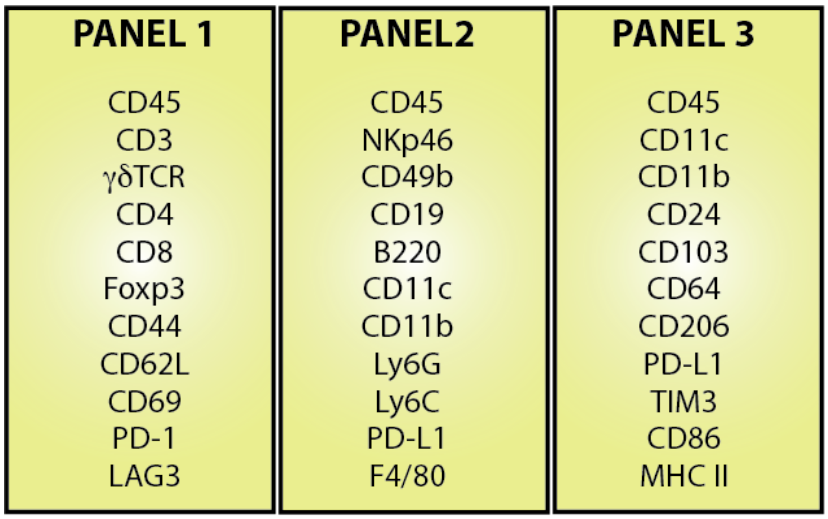

Figure 27. Flow cytometry immunophenotyping panels.

By making use of these flow cytometry panels, we isolated and immunophenotyped pooled 3LL ΔNRAS lung tumours from different mice and compared them to the immune landscape of healthy lungs from non-tumour bearing mice (Figure 29A). The overall immune landscape was completely altered in tumours, as compared with healthy lung, as illustrated in Figure 29E.

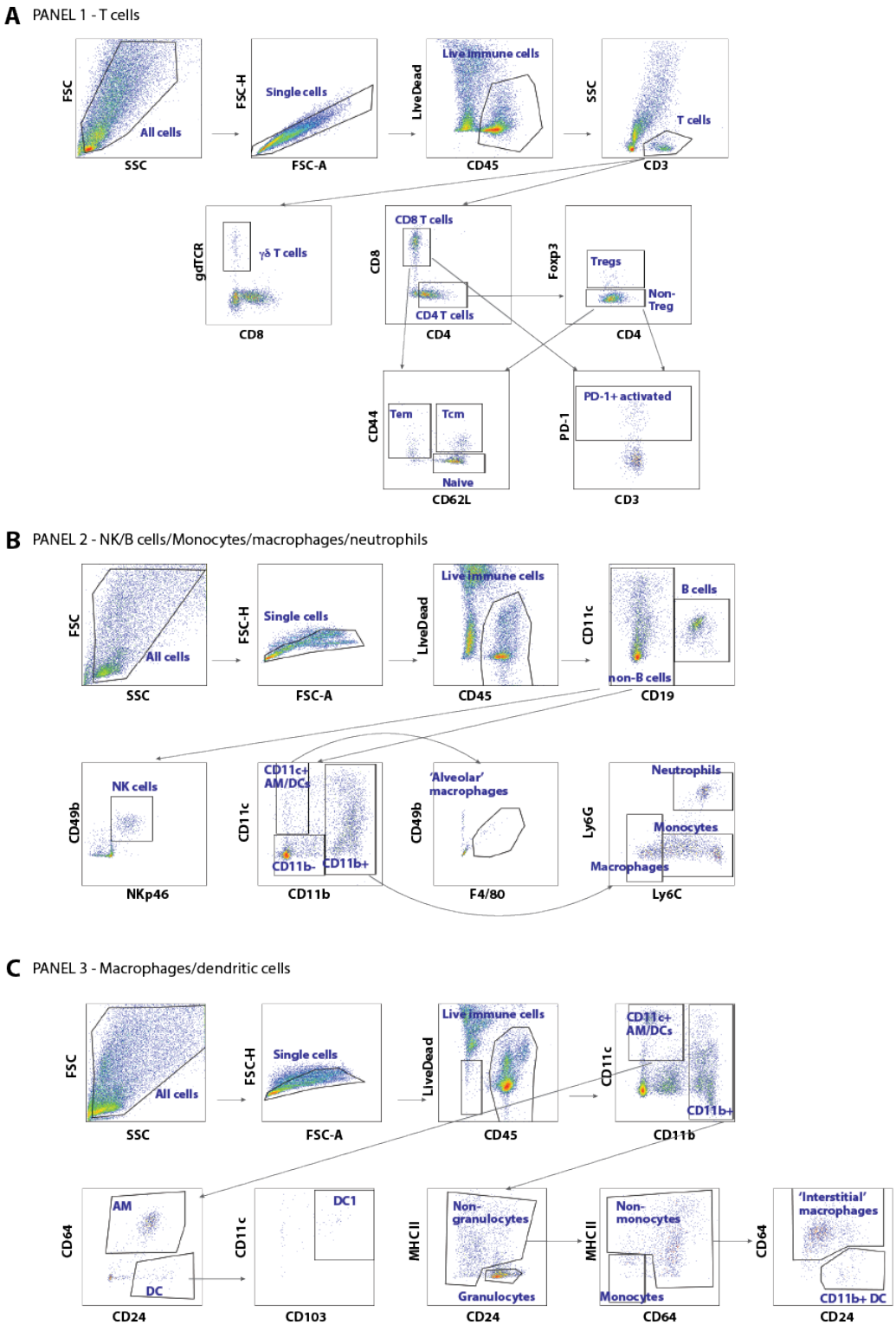

Figure 28. Flow cytometry immunophenotyping gating strategy.

Flowjo gating strategy for immunophenotyping of antibody panel 1 (A), panel 2 (B) and panel 3 (C), based on the strategy followed in (Misharin et al., 2013). Tregs=regulatory T cells, Tem=T effector memory, Tcm= T central memory, NK=natural killer, AM=alveolar macrophages, DC=dendritic cells.

The overall T cell composition and the presence of different T cell subsets was not significantly changed in tumours compared to normal lung (Figure 29B). When examining T cell phenotype, tumour T cells displayed markers of activation, such as CD69. In addition, there were less naïve T cells than in the healthy lung, potentially suggesting an increase in antigen exposure in this setting (Figure 29B). There was also an increase in PD-1+ CD8 T cells, further confirming our hypothesis that T cells have become activated in a tumour setting (Figure 29B). This data suggests that at least a proportion of T cells have become activated, likely in response to tumour antigens.

Regarding other cell types, additional cytotoxic cells such as NK cells seemed to be decreased in the tumours (Figure 29C), consistent with the previous finding that these tumours are susceptible to cytotoxic actions exerted by NK cells, which may indicate that the tumour might be excluding these cells. B cells were also slightly reduced in the tumour (Figure 29C), suggesting that they might be playing an anti-tumorigenic role in this context. cDC1 (conventional Dendritic Cell 1) is the subset of dendritic cells that are able to cross-present engulfed antigens by MHC class I, thereby leading to *de novo* activation of CD8+ T cells (Bottcher and Reis e Sousa, 2018). In our FACS panel, we were able to recognise these cells via their expression of CD103 and found that they were slightly decreased in the TME of 3LL ΔNRAS tumours (Figure 29C).

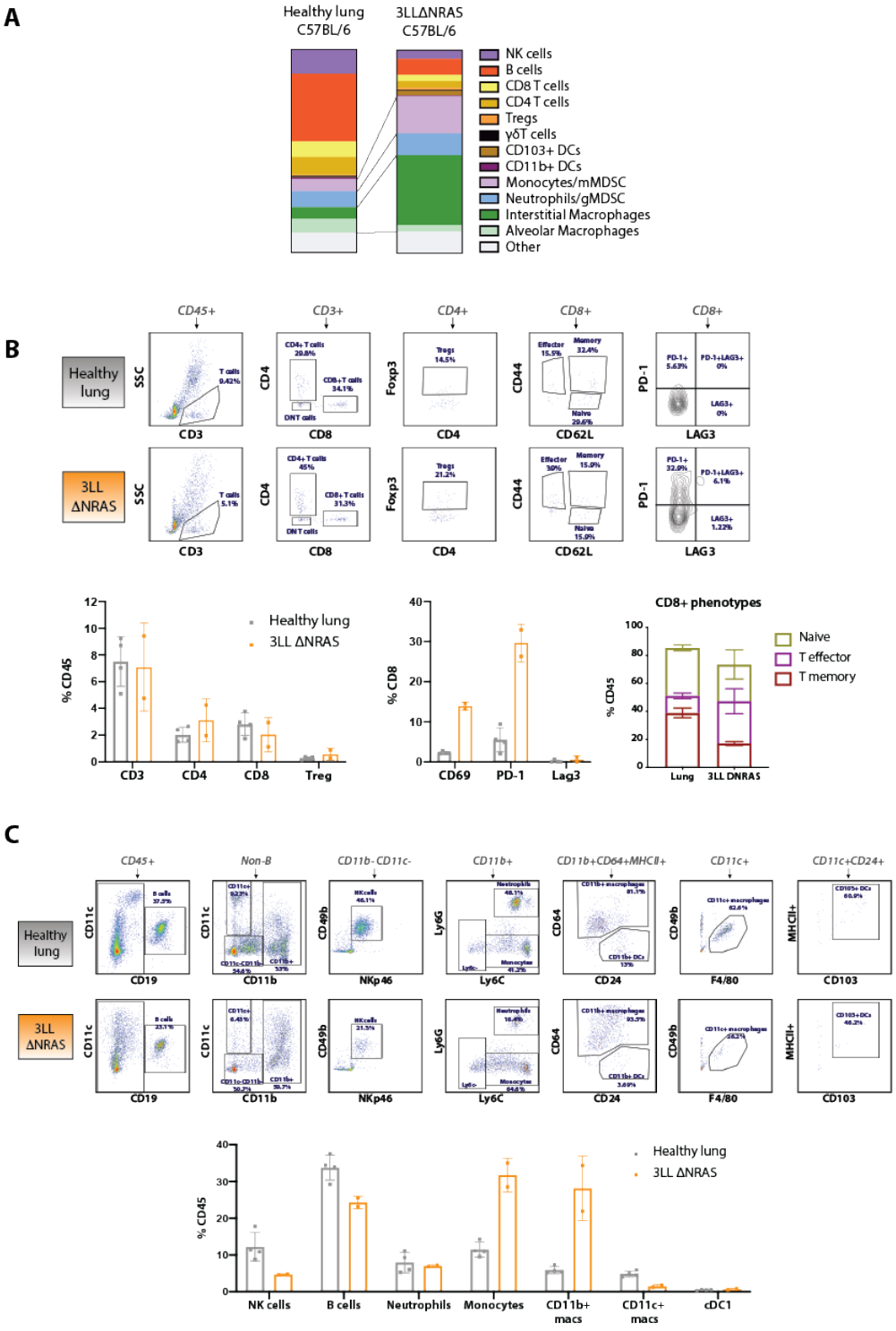

Figure 29. Immunophenotyping of 3LL ΔNRAS tumours.

Immunophenotyping of 3LL ΔNRAS lung tumours. A) Summary of all immune populations assessed. B) Representative plots of T cell populations (above). Detailed plots of each immune population (below, mean±SD). Each dot represents one mouse. B) Representative plots of non-T cell populations (above). Detailed plots of each immune population (below, mean±SD). Each dot represents one mouse.

The myeloid compartment was also found to be re-structured in the tumour setting. Neutrophil infiltration was not altered in this mouse model (Figure 29C). However, the monocyte/macrophage compartment was completely different from the normal lung landscape, with a marked increase in both monocytes and CD11b+ 'interstitial' macrophages (IM) (Figure 29C). These increases were accompanied by a decrease in CD11c+ 'alveolar' macrophages (AM, Figure 29C). As a result, approximately 50% of all leukocytic infiltration in the tumour was comprised of monocytes and macrophages. As a clarification, the definition of 'interstitial' and 'alveolar' populations is based on markers expressed in macrophage populations in healthy lungs (CD11b for 'interstitial' and CD11c for alveolar macrophages, respectively (Misharin et al., 2013)). We are aware that tumour-associated macrophages might be phenotypically and functionally distinct to these populations so this nomenclature might not be ideal. This just comprises a manner to differentiate CD11b+ from CD11c+ macrophages.

We characterised the immune landscape of 3LL DNRAS tumours by immunohistochemistry staining. CD3+ T cells were largely excluded from a large tumour found in a lung of a tumour-bearing mouse (Figure 30A). A smaller tumour found in another mouse did show a small presence of CD8+ T cells, albeit mostly found at the edges of the tumour, suggesting some form of exclusion (Figure 30B). More detailed analysis of this phenomenon was performed by other people in the lab by imaging mass cytometry, please refer to (van Maldegem et al., 2021) for details and quantification. Finally, F4/80 staining of macrophages could be seen in all areas of all tumours examined (Figure 30C, see light brown staining in between tumour cells, data confirmed by imaging mass cytometry in (van Maldegem et al., 2021)).

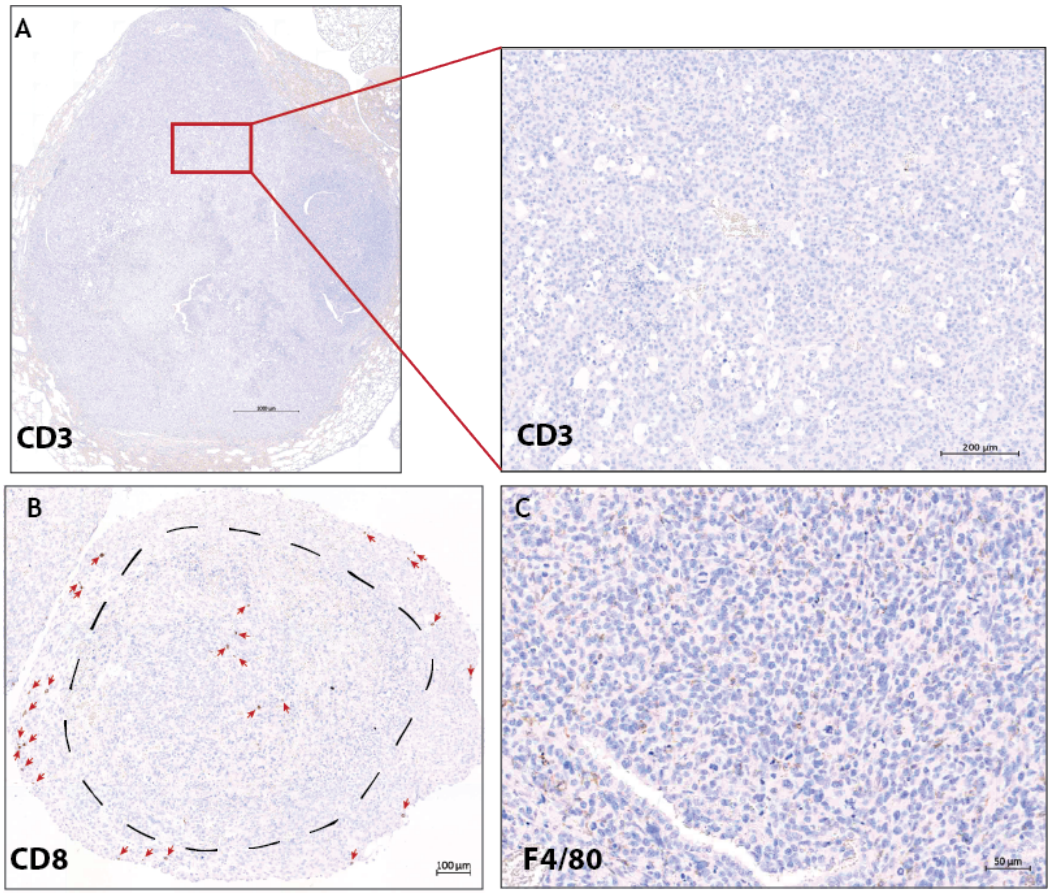

Figure 30. Immune infiltration in situ (IHC) of 3LL ΔNRAS tumours.

Immunohistochemistry analysis of 3LL ΔNRAS lung tumours. Lung tumour staining with anti-CD3 (A, whole tumour on the left and higher magnification on the right), B) Whole tumour histological image with anti-CD8 staining. Dashed line represents the border between tumour and normal tissue and red arrows point towards single CD8+ cells. C) High magnification image of F4/80 staining in the tumour.

Together, these results point towards the 3LL ΔNRAS being an immune evasive lung tumour model that is likely able to evade anti-tumour immune responses by recruiting a large number of tumour-promoting/immunosuppressive cell types, mostly monocytes and macrophages, into its TME. We hypothesise that these immunosuppressive myeloid cells are able to exclude (van Maldegem et al., 2021) and promote the exhaustion of T cells that have become activated in response to tumour antigens.

4.5 3LL ΔNRAS cells secrete factors that promote *ex vivo* macrophage growth

We next wondered what was the role of tumour-secreted factors in shaping the TME of 3LL ΔNRAS tumours, as we were interested in cancer cell-intrinsic mechanisms by which tumours are able to evade immune responses. As the main component of the TME of these tumours was found to be macrophages, we aimed to examine whether tumour-derived factors directly played a role in promoting macrophage growth.

To do so, we used an *ex vivo* setting by which we obtained monocytes extracted from bone marrow of mice. We cultured these monocytes with either control medium or conditioned medium obtained from *in vitro* cultured 3LL ΔNRAS cells (Figure 31A). Bone marrow-derived cell growth (Figure 31B) and viability (Figure 31C) was significantly improved when the cells were cultured under 3LL conditioned medium. We then wanted to confirm that these cells were indeed macrophage populations, by staining them for known macrophage markers F4/80 and CD64. Whereas only a minor proportion of cells were macrophages in the control medium-cultured setting, a vast majority of monocytes were able to differentiate to macrophages in the 3LL conditioned medium cultured samples (Figure 31D). In fact, more macrophage differentiation was observed in these samples than in monocytes cultured with the known macrophage differentiation factor M-CSF.

Our data strongly suggests that tumour-derived factors are able to promote macrophage growth and differentiation from monocytes. We believe that these tumours, probably via secretion of soluble factors, are able to recruit and promote the differentiation of monocyte-derived macrophages *in vivo* in order to promote immune evasion. We therefore wondered whether oncogenic KRAS signalling played a role in the secretion of such factors.

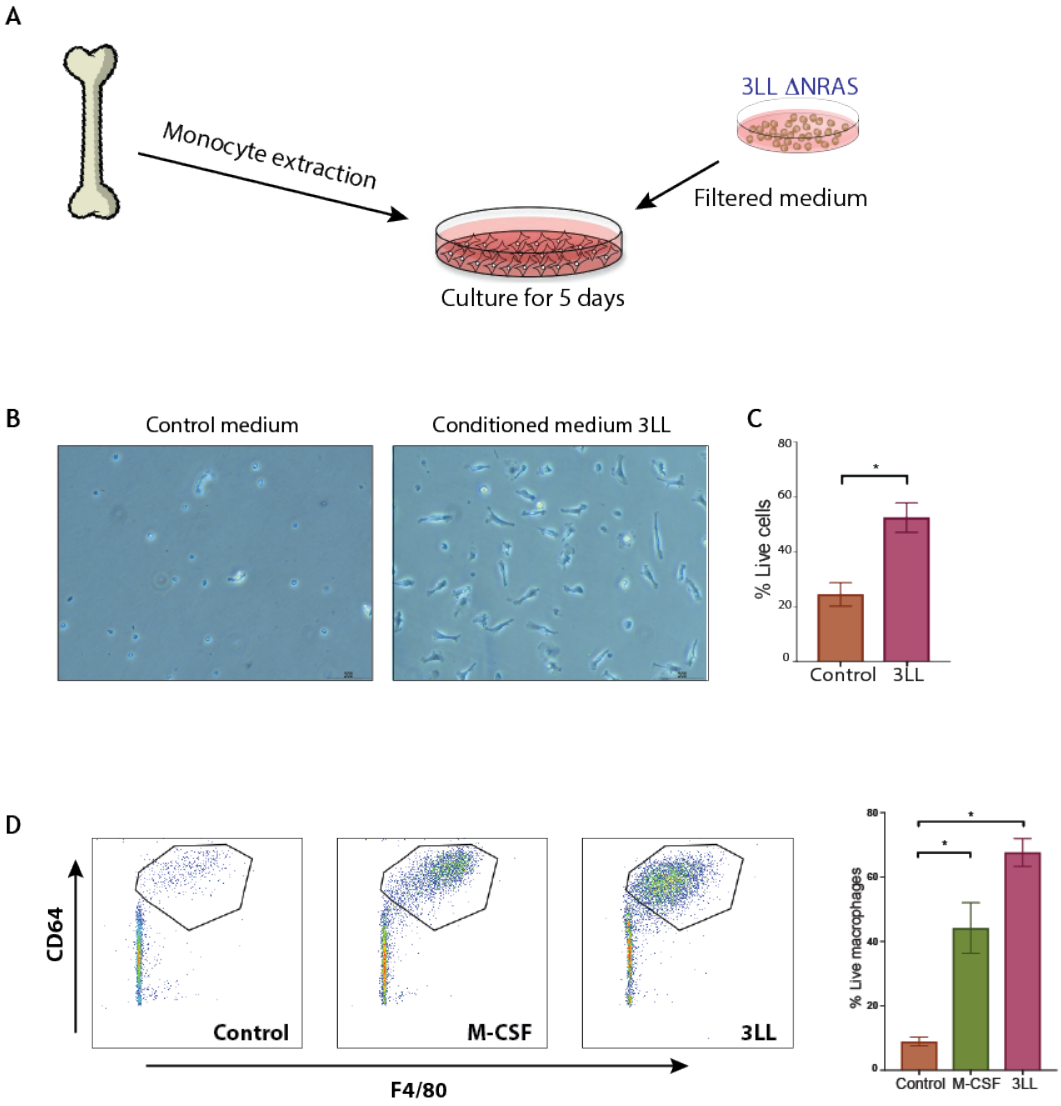

Figure 31. *Ex vivo* culture of bone marrow-derived macrophages.

A) Schematic of conditioned medium experiments. B) Microscopy images of monocyte-derived cells in culture, under control RPMI medium (left) or conditioned medium from 3LL ΔNRAS cells (right). C) Quantification of viability (DAPI) of cultured cells (Mean±SD, student's t test, data from 3 independent experiments). D) FACS analysis of macrophages post-culture. FACS plots are shown on the left, quantification on the right (One representative experiment is shown, error bars represent technical replicates -n=2-, student's t test).

4.6 The secretion of a number of cytokines, most notably CCL2, by 3LL ΔNRAS is KRAS-dependent

In order to better understand which factors secreted by the 3LL ΔNRAS cells could contribute to the shaping of their TME, we performed a cytokine array using medium from 3LL ΔNRAS cells cultured *in vitro*. A number of cytokines were found to be secreted by 3LL ΔNRAS cells in steady-state conditions (Figure 32A), most notably the monocyte chemoattractant chemokine (C-C motif) ligand 2 CCL2, also known as monocyte chemoattractant protein 1 (MCP-1) and the TIMP matrix metalloproteinase inhibitor-1 TIMP-1.

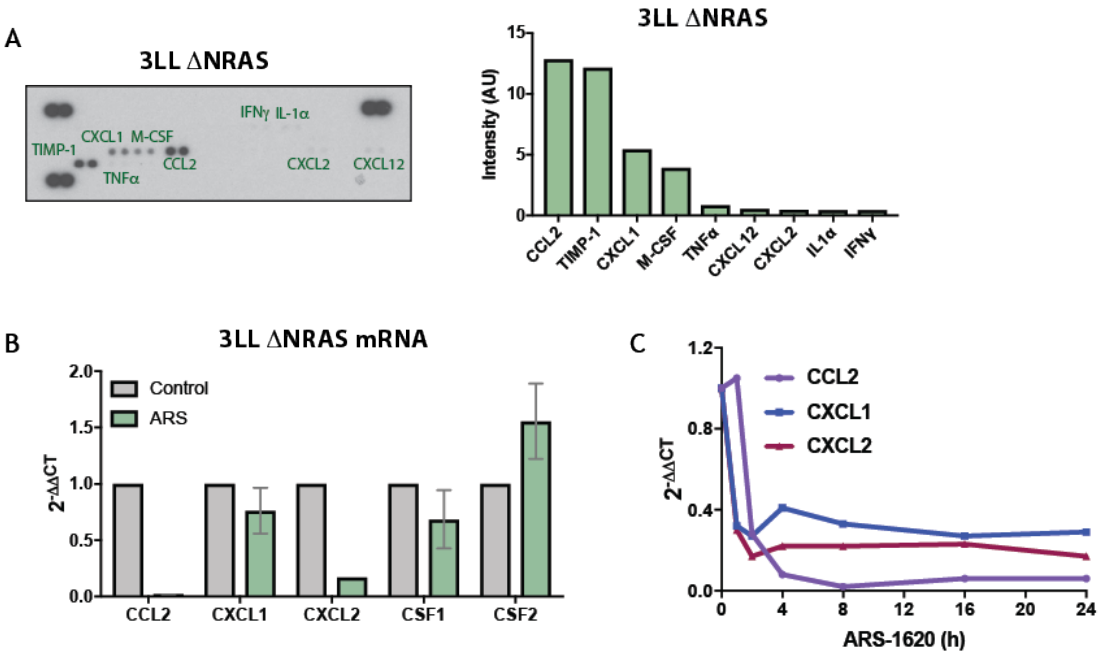

Figure 32. KRAS-dependent cytokines in 3LL ΔNRAS.

A) Medium from 3LL ΔNRAS cells *in vitro* was harvested for a cytokine array (left), quantification is shown on the right (intensity values normalised to control array spots represented in arbitrary units). B) qPCR analysis of cytokines in presence or absence of 2μM ARS-1620 (24h treatment, mean±SD, n=3). Control data for all cytokines was normalised to a value of 1. C) Time course RNA analysis of KRAS-dependent cytokines (2μM ARS-1620). Control data for all cytokines was normalised to a value of 1.

As we were aware that the TME of 3LL ΔNRAS tumours consisted mainly of myeloid cells (Figure 29), we investigated the KRAS-dependency of the myeloid

chemoattractants by determining their susceptibility to KRAS inhibition. We found that the expression of monocyte chemoattractant CCL2, the most highly secreted cytokine, and the neutrophil chemoattractants CXCL1 and CXCL2 was decreased by treatment with ARS-1620 (Figure 32B). We also found that this decrease occurred early after KRAS inhibition (Figure 32C). In contrast, the macrophage differentiation factor M-CSF (gene name CSF1) did not significantly change its expression after KRAS inhibition (Figure 32B). GM-CSF (gene name CSF2), a previously reported KRAS-dependent cytokine (Pylayeva-Gupta et al., 2012) that was also found to be KRAS-dependent in Chapter 3, was not secreted by these cells (Figure 32A) nor did its mRNA expression differ by KRAS inhibition (Figure 32B). This suggests that some KRAS-dependent mechanisms can be cell line-specific.

We decided to focus our studies on the monocyte chemoattractant CCL2, for a number of reasons. Firstly, it revealed to be the most prominent cytokine secreted by 3LL ΔNRAS cells, suggesting that this cytokine is likely important for tumour growth *in vivo*. CCL2 is a cytokine known to be responsible for the recruitment of CCR2-expressing myeloid cells from the bone marrow to inflammatory sites and tumours (Yoshimura, 2018). This correlated with the TME found *in vivo*, as 3LL ΔNRAS tumours had a high capacity to recruit monocytes and macrophages. Additionally, the expression of the CCL2 gene was abrogated by treatment with ARS-1620, suggesting that expression of this gene is oncogenic KRAS-dependent, as previously reported by Ji et al. in healthy lung (Ji et al., 2006) and Agalioti et al. in the context of malignant pleural effusion (Agalioti et al., 2017) .

We therefore started by validating the KRAS-regulation of this gene at the protein level, by examining CCL2 secretion by 3LL ΔNRAS cells in presence or absence of ARS-1620. Consistent with the mRNA data, CCL2 secretion was significantly reduced upon KRAS inhibition at different time points (Figure 33A). We then confirmed CCL2 as a KRAS-dependent gene in the human type II pneumocytes that harbour an inducible oncogenic KRAS protein (3.1), where 4-OHT administration resulted in a significant increase in CCL2 secretion to the medium (Figure 33B). In order to narrow down the mechanism of CCL2 regulation by

mutant KRAS, we treated 3LL ΔNRAS cells with inhibitors targeting different KRAS downstream pathways. Only treatment with the MEK inhibitor trametinib led to a decrease in both CCL2 gene expression (Figure 33C) and secretion of the cytokine (Figure 14D), suggesting that CCL2 is regulated in a KRAS-MEK-ERK dependent manner.

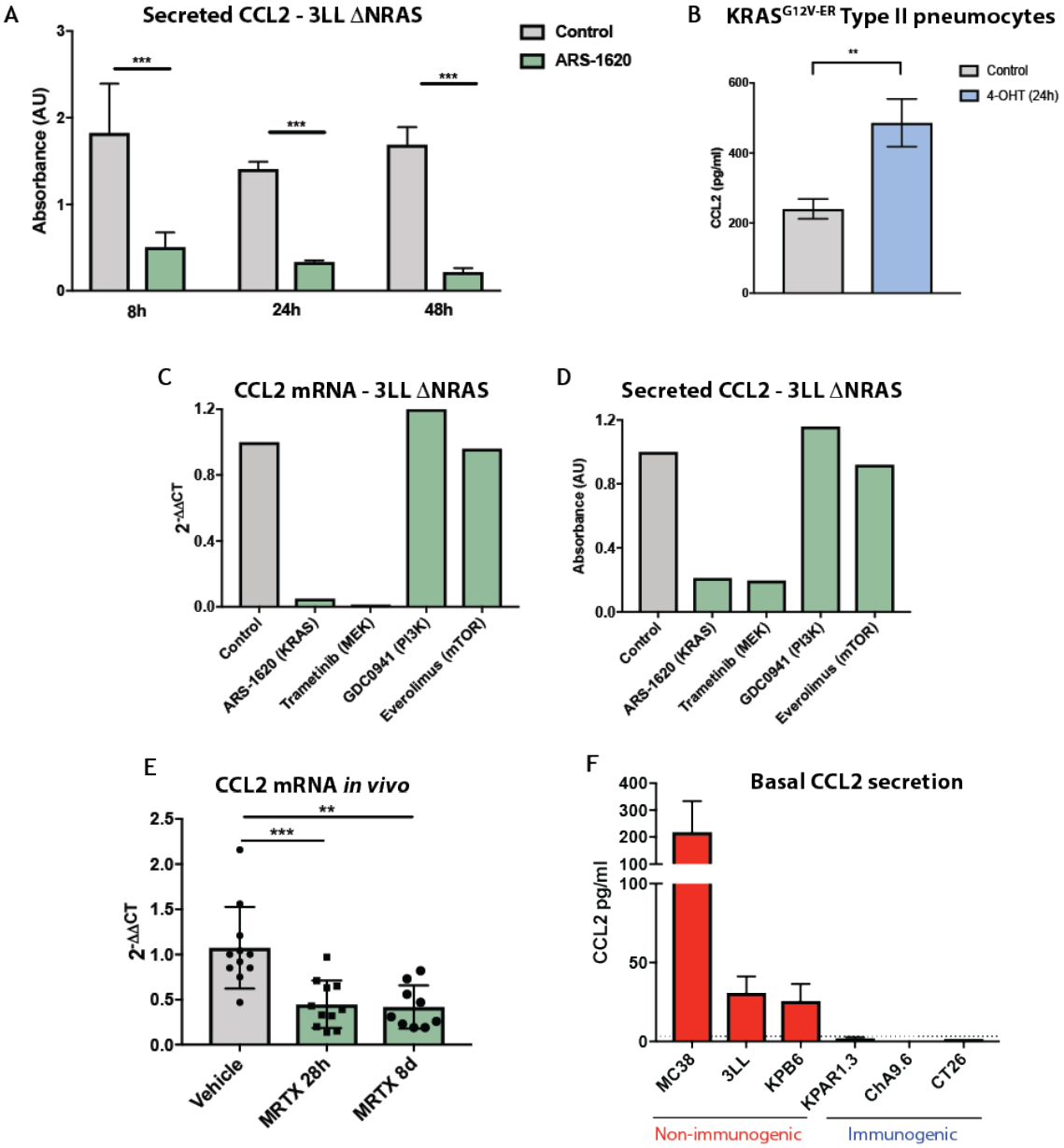

Figure 33. CCL2 is a KRAS-dependent cytokine, regulated via MEK signalling.

A) Secretion of CCL2 was measured by ELISA 8h, 24h and 48h after 2μM ARS-1620 treatment. (n=3, mean+SD, Student's T test). B) Secretion of CCL2 in AT2 cells after 24h of 500nM 4-OHT treatment (n=3, mean±SD, Student's T test). Absolute values were calculated using standard curve method. C) CCL2 mRNA

analysis after 24h treatment of 3LL ΔNRAS cells with different inhibitors. D) CCL2 secretion analysis after 24h treatment of 3LL ΔNRAS cells with different inhibitors (2μM ARS-1620, Trametinib 10nM, GDC0941 500nM, Everolimus 100nM). E) C57Bl/6 mice bearing orthotopic 3LL ΔNRAS tumours were treated with vehicle (n=11) or 50mg/kg MRTX1257 daily for 28h (n=11) or 8 days (8d, n=9). qPCR analysis shown was performed using the $2^{-\Delta\Delta CT}$ method, by normalising to one of the control conditions. Each dot represents one tumour (mean±SD, student's t test, each dot represents a tumour). F) Basal CCL2 secretion of different cell lines tested by ELISA (mean+SD of three independent samples, dashed line depicts limit of detection).

Additionally, we investigated whether the KRAS-mediated regulation of CCL2 was relevant in the *in vivo* setting. ARS-1620 only shows modest effects *in vivo* (Janes et al., 2018), so we decided to use the more potent clinical inhibitor MRTX1257 for our studies in mice (Hallin et al., 2020). We performed an experiment where after intravenous administration of 3LL ΔNRAS cells, lung tumour-bearing mice were treated with daily doses of MRTX1257 for either 28h or 8 days, after which tumours were extracted for RNA analysis (5.3). Gene expression of CCL2 was significantly reduced after MRTX1257 treatment at both time points examined (Figure 33E), suggesting that CCL2 expression *in vivo* was largely tumour-derived and dependent on oncogenic KRAS.

We also compared CCL2 secretion levels across a number of mouse tumour cell lines whose immunogenicity is known (Figure 33F). Non-immunogenic models included the KRAS mutant colon cancer cell line MC38 and the lung cancer cell line established from non-immunogenic $KRAS^{G12D\text{-}LSL}$, $p53^{fl/fl}$ (KP) model, KPB6, which, together with the 3LL ΔNRAS cell line, secreted detectable levels of CCL2 to the medium. On the other hand, the APOBEC-expressing immunogenic cell line KPAR1.3 established in our lab, another KRAS-mutant lung cancer cell line known to respond to immunotherapy, ChA9.6, and the known KRAS-mutant colon cancer cell line CT26, known to harbour a strong immunogenic antigen, were not able to secrete CCL2. This suggests that not all KRAS-mutant cell lines secrete CCL2, but its secretion could be associated with their immunogenicity *in vivo.* CCL2 secretion could serve one of the mechanism by which KRAS mutant tumours are able to generate an immunosuppressive TME.

4.7 Tumour-derived CCL2 is important for tumour growth and shaping of the TME

4.7.1 Generation and in vitro characterisation of CCL2 KO cells

We have demonstrated that CCL2 is a KRAS-regulated cytokine in 3LL ΔNRAS cells. We next sought to elucidate the role of tumour-derived CCL2 in regulating monocyte migration *in vitro* and in shaping the TME and tumour growth *in vivo*. To that end, we generated CCL2 knockout derivatives of the 3LL ΔNRAS cell line using CRISPR-Cas9 technology. We designed two different sgRNAs targeting different regions of the CCL2 gene (Figure 34A). The cloning and KO generation pipeline were identical to Figure 21, also illustrated in Figure 34B. For the clone screening strategy, however, we took advantage of the fact that CCL2 is a secreted protein, and used ELISA to screen for CCL2 secretion from single cell clones transfected with either of the sgRNAs (Figure 34B). A large number of clones were negative for CCL2 secretion, as shown in Figure 34C. We also tested the growth of the KO clones obtained *in vitro* by placing them in an Incucyte machine and following their growth kinetics, and observed no significant difference in their intrinsic growth *in vitro* (Figure 34D).

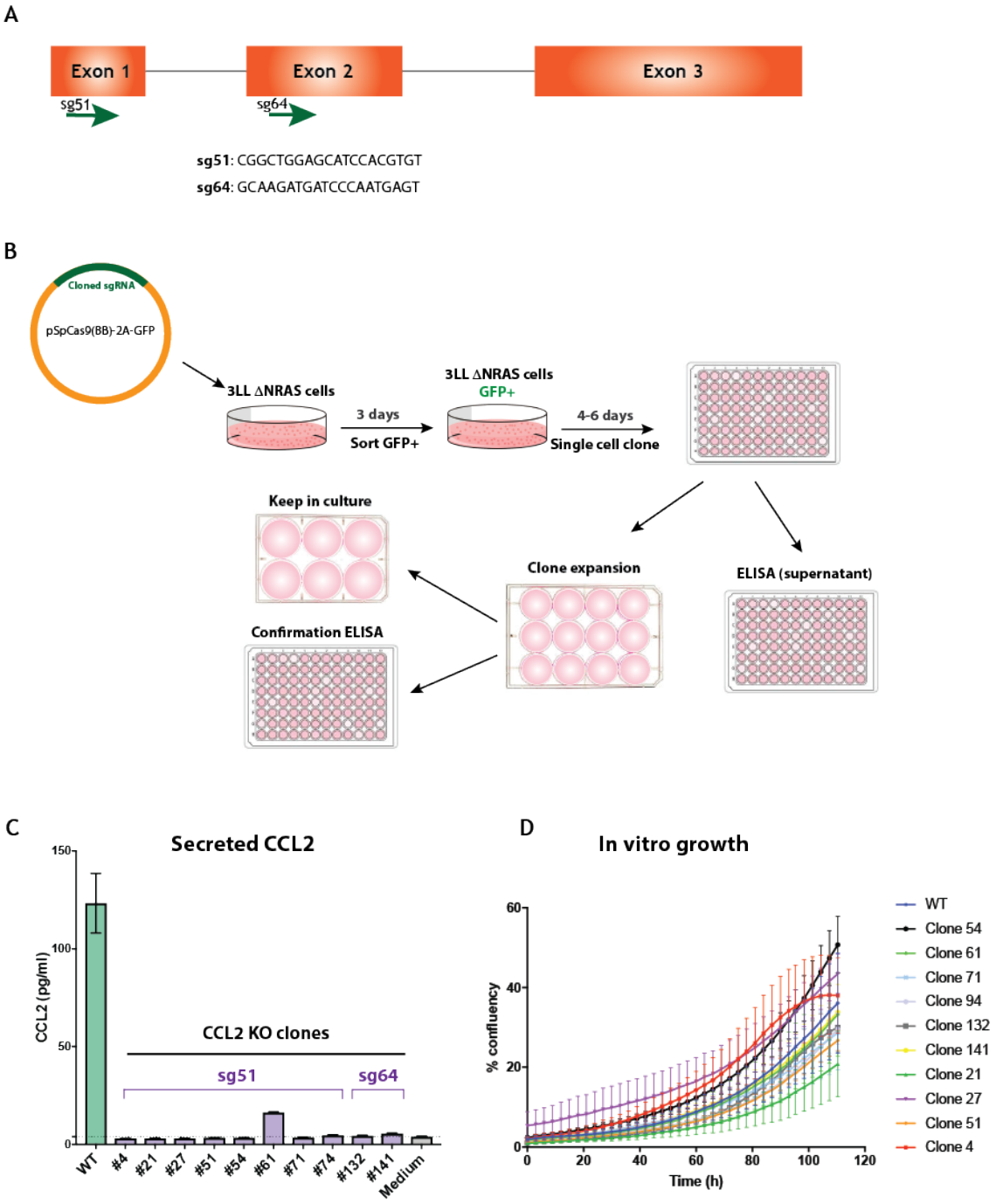

Figure 34. Generation of CCL2 KO cells by CRISPR-Cas9 technology.

A) Schematic of the CCL2 gene and location and sequence information on the sgRNAs designed. B) KO generation pipeline. C) Confirmation ELISA analysis of secreted CCL2, using WT cells as control. A standard curve generated using recombinant murine CCL2 was used to obtain absolute CCL2 concentrations (Mean+SD, 3 technical replicates). D) Cell growth assessed by a 5-day incucyte assay (mean±SD of three wells per clone).

Making use of the newly generated CCL2 KO clones of the 3LL ΔNRAS cell line, we sought to confirm the chemoattractant role of CCL2. To this end, we used the well-established transwell assay. We isolated monocytes from murine bone marrow, and placed the obtained cells in the upper chamber of a well containing a porous membrane (Figure 35A). We filled the lower chamber with either control medium or conditioned medium obtained from wild-type or CCL2 KO 3LL ΔNRAS cells. In addition, we treated 3LL ΔNRAS cells with a $KRAS^{G12C}$ inhibitor and collected conditioned medium to assess the role of oncogenic KRAS on *ex vivo* monocyte migration. We incubated the cells for 3h before harvesting and counting the monocytes that had migrated to the lower chamber.

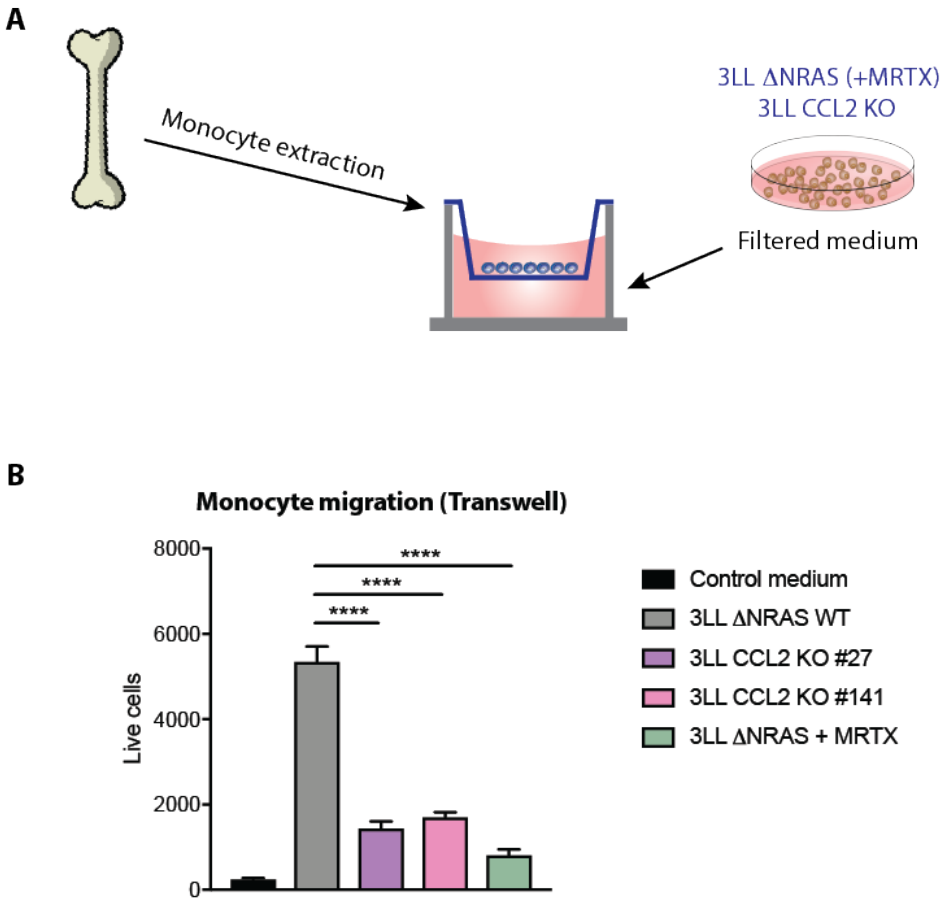

Figure 35. Tumour-derived CCL2 plays a role in monocyte migration *in vitro*.

A) Schematic of *ex vivo* BMDM transwell assays. B) Transwell bottom chamber cell count as measured by FACS (pre-gated on DAPI- cells). Mean+SD of three technical replicates is shown (Student's T test). One representative experiment out of three is displayed.

As shown in Figure 35B, monocytes were prone to migrate to the lower chamber of the transwell when in presence of 3LL conditioned medium (grey bar). This finding may explain the high degree of monocyte infiltration that 3LL ΔNRAS tumours display in vivo (Figure 29). Consistent with the monocyte chemoattractant role of chemokine CCL2, CCL2 KO-derived conditioned medium significantly abrogated monocyte migration in this experiment (purple and pink bars). In addition, consistent with the KRAS-dependent regulation of CCL2, conditioned medium from $KRAS^{G12C}$ inhibitor-treated cells also inhibited monocyte migration (green bar). We therefore confirmed that tumour cell derived, KRAS-dependent CCL2 plays a role in monocyte chemoattraction, which may explain the high degree of monocyte infiltration observed in this lung tumour model.

4.7.2 Tumour growth assessment of CCL2/CCR2 KO mice

Next, we sought to investigate the growth and phenotype of CCL2 KO tumours *in vivo*, in comparison to 3LL ΔNRAS WT tumours. We wanted to know whether tumour-derived CCL2 played a role in the shaping of the TME, as CCL2 is known to also be secreted by other cells, most notably macrophages (Yoshimura, 2018). If additional sources of CCL2 were to compensate for the lack of tumour derived CCL2, no difference would be seen between the WT and the CCL2 KO tumours.

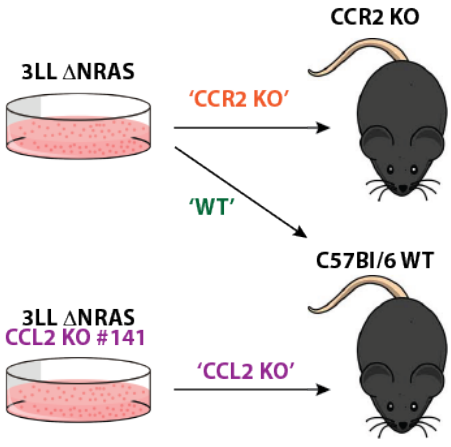

Figure 36. Schematic of CCL2-CCR2 KO experiments.

As discussed before, the role of the chemokine CCL2 is to recruit bone marrow-derived myeloid cells, like monocytes, by binding to its receptor CCR2 on their surface (Yoshimura, 2018). Hence, if the main source of CCL2 were the tumour cells, we would expect that deletion of tumour-derived CCL2 would have similar effects to systemic deletion of CCR2+ cells. We therefore obtained CCR2 KO mice (kindly provided by Dr. Andreas Wack at the Francis Crick Institute) which we also injected with 3LL ΔNRAS cells. We injected and compared tumour growth of 3LL ΔNRAS tumours grown in WT C57Bl/6 mice, 3LL ΔNRAS tumours grown in CCR2 KO mice (of C57Bl/6 background), and 3LL ΔNRAS CCL2 KO cells (single cell clone #141) grown in wild-type C57Bl/6 mice (as illustrated in Figure 36).

We firstly investigated the consequences of CCL2 deletion in tumour cells on their growth *in vivo*. We administered CCL2 KO cells (clone #141) subcutaneously in the flank of mice, and compared its growth to 3LL ΔNRAS WT tumours (Figure 37A). No difference could be observed in subcutaneous growth of these tumours. We then wondered whether KO of CCL2 could have effects on the metastatic seeding capability of these cells and performed intravenous injections followed by computed tomography (CT) scan assessment of tumour growth. At 3 weeks post-injection, the number of tumours found was decreased in CCL2 KO tumours as compared to 3LL ΔNRAS WT tumours (Figure 37B). However, there was no difference in the size of the tumours found (Figure 37C). This suggested that in the lungs, tumour initiation could be dampened by the lack of tumour-derived CCL2 but tumour growth itself was not affected.

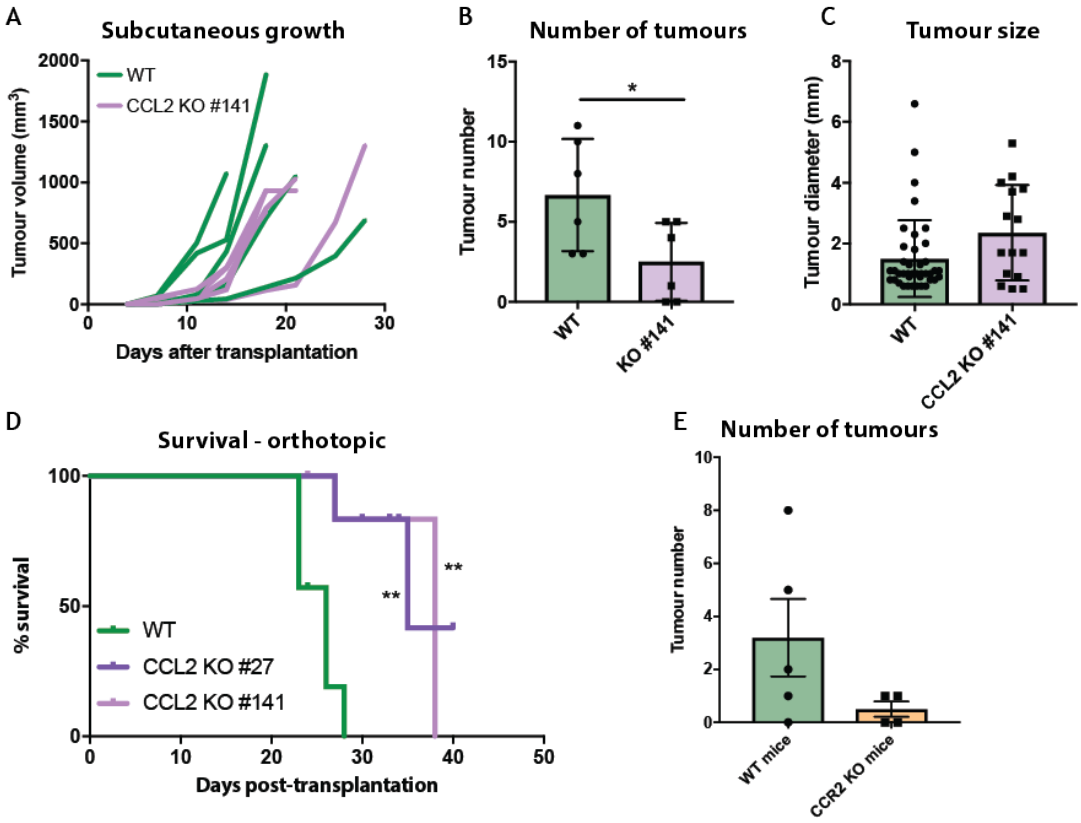

Figure 37. In vivo growth of CCL2/CCR2 KO mice.

A) Subcutaneous administration of 400.000 cells (WT or CCL2 KO clone #141) into the flank of C57Bl/6 mice. Tumour growth was monitored by calliper measurements. B) Number of tumours after intravenous injection as measured by CT scans 3 weeks post-injection, comparing WT (n=6), KO #141 (n=6) tumours. (Mean±SD, Mann-Whitney test). Data obtained and analysed by Chris Moore. C) Tumour diameter after intravenous injection as measured by CT scans. Each dot represents a tumour. WT (n=40) and KO #141 (n=15). Mean±SD. Data obtained and analysed by Chris Moore. D) Survival curve of mice after 10^6 cells were injected intravenously (WT or CCL2 KO clones). Significance was assessed using the Log-rank (Mantel-Cox) method. E) Growth of 3LL ΔNRAS cells in CCR2 KO mice. Graph shows tumour number per mouse, each dot represents a mouse (Mean±SD). Data obtained and analysed by Chris Moore.

We wanted to avoid the potential bias of examining the effects a single cell clone of CCL2 KO. Therefore, we decided to carry out a survival experiment using four different clones for which different sgRNAs had been used to KO the CCL2 gene. We injected these clones and compared the survival of the mice, by using weight loss as a surrogate. The mice bearing CCL2 KO tumours had a significant extension of survival, as displayed in Figure 37D, suggesting that the role of CCL2 in this setting *in vivo* is pro-tumorigenic.

We were able to observe a similar trend by utilising CCR2 KO animals, in which the recruitment of monocytes from the bone marrow into inflammatory sites is impaired. In these mice, 3LL ΔNRAS tumour number was reduced 3 weeks post-injection (Figure 37E). Two of the four CCR2 KO mice injected harboured tumours that were large but their size could not be quantified due to their complex location in the lung cavity, suggesting that, as is the case with the CCL2 KO tumours, once the tumours are established tumour growth is not affected.

4.7.3 Immune characterisation of CCL2/CCR2 deficient tumours

We carried out flow cytometry analysis to immuno-phenotype and compare the immune infiltration of 3LL ΔNRAS tumours grown in WT C57Bl/6 mice, 3LL ΔNRAS tumours grown in CCR2 KO mice and 3LL ΔNRAS CCL2 KO cells grown in wild-type C57Bl/6 mice (Figure 36). In this manner, we were able to assess the contribution of tumour-derived CCL2 in shaping the TME of 3LL ΔNRAS lung tumours. In addition, the use of CCR2 KO mice would allow us to examine the relevance of bone marrow recruited monocytes in the TAM population of these tumours. For this experiment, we used a flow cytometry antibody panel similar to panel 2 described in Figure 27, but slightly modified to include additional information on monocyte and macrophage populations in the tumour, as these were the populations that we were most interested in examining.

The immunophenotyping was performed 4 weeks after injection. At this time point, fewer tumours were obtained from CCL2 KO tumours and CCR2 KO mice than WT mice/tumours. In addition, less mice in the KO settings displayed lung tumours, hence why there were less data points analysed for these conditions (Figure 38). However, the tumours examined were roughly of the same size (consistent with the fact that tumour growth itself is not affected in these settings) so we are fairly confident that the tumours were at a similar stage of development at the time of analysis and that differential tumour growth did not affect the analysis. For flow cytometry analysis, we pooled tumours from the same mouse, yielding one sample per mouse. However, from the microCT scan data and physical examination of the tumours at the time of acquisition, there were no obvious differences in size that could mask the overall effects of the genotypes.

The first finding of the FACS analysis was that despite total CD45+ immune cell number was unaltered in CCL2 KO tumours, there was a decrease in total immune cell infiltration in CCR2 KO, indicating that immune infiltration was severely disrupted in this setting (Figure 38A). The infiltration of B cells and cytotoxic cells like T cells and NK cells was significantly increased in CCL2 KO tumours, with a similar trend in CCR2 KO mice. This would indicate that in the adaptive and NK cell compartment, CCL2 KO in tumours or systemic CCR2 deletion have similar positive effects.

For the CCR2 KO data, it is important to raise a technical point. All population frequencies were calculated as a percentage of CD45+ immune cells. As will be subsequently discussed, profound changes in the monocyte/macrophage compartment were observed, which could alter total population frequencies, leading to a relative increase in other populations. Hence, the increase in B, T and NK populations observed in the CCR2 KO mice could just reflect a depletion in other populations.

CCL2 KO tumours had no changes (or even a slight decrease) of neutrophil infiltration (Figure 38B), while CCR2 KO mice had a significant increase in neutrophils, potentially due to the technical caveat discussed before. This contradictory data between CCL2 KO and CCR2 KO raises the possibility that tumour derived CCL2 could play a role in neutrophil recruitment in a CCR2-independent manner. However, the decrease in neutrophils in CCL2 KO tumours is not significant and additional experiments would have to be performed to validate this finding.

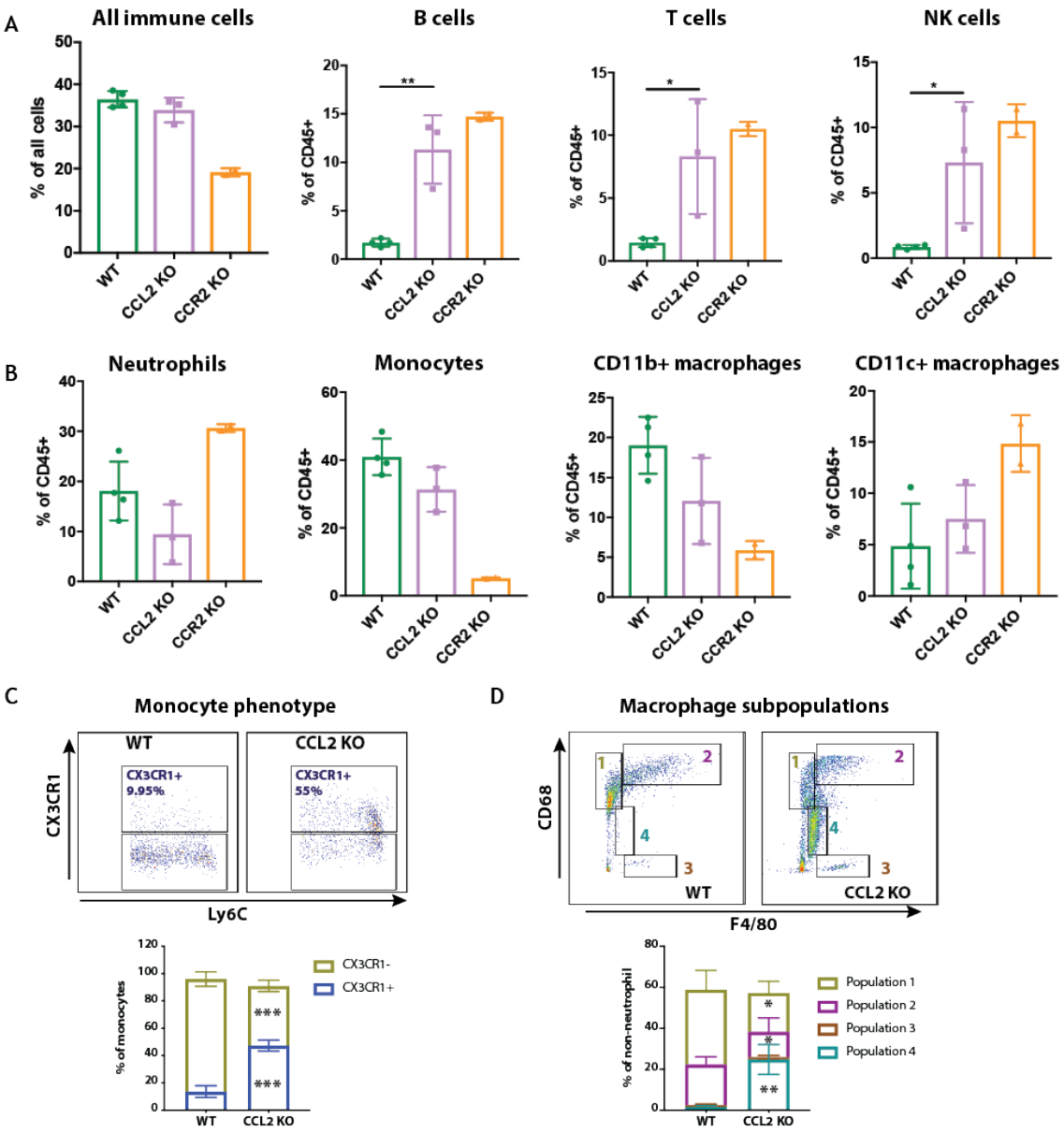

Figure 38. Analysis of CCL2 KO tumours and tumours in CCR2 KO mice.

Immunophenotyping of 3LL (WT or CCL2 KO #141) tumours 3 weeks after intravenous injection into WT or CCR2 KO mice. A) Changes in all immune cells, lymphocytes and NK cells (each dot represents one mouse, mean±SD, student's T test). B) Changes in myeloid cells (each dot represents one mouse, mean±SD, student's T test). C) Changes in monocyte phenotype based on CX_3CR1+ expression (pre-gated on live, CD45+, CD11b+ Ly6C+ cells). Each dot represents one mouse, mean±SD, T test). D) Changes in macrophage subpopulations based on F4/80 and CD68 expression (pre-gated on CD45+, live, Ly6C- cells). Quantification is shown below (mean±SD, student's T test).

As expected, monocyte recruitment (Figure 38B) was virtually abrogated in CCR2 KO mice, but, perhaps surprisingly, remained unaltered in the CCL2 KO tumours. When examining monocyte phenotypes further (Figure 38C), we discovered a change in the type of monocytes found in the tumour. In WT tumours, a large proportion consisted of CX_3CR1- monocytes. However, in CCL2 KO tumours, approximately half of monocytes were CX_3CR1+ monocytes. We therefore hypothesise that CX_3CR1+monocytes are recruited in a CCL2-independent, yet CCR2-dependent manner. This is particularly interesting and potentially relevant therapeutically because CX_3CR1+ or 'patrolling' monocytes have been reported to play an anti-metastatic role in lung tumours (Hanna et al., 2015).

Regarding macrophages (Figure 38B), CCR2 KO mice displayed a significant decrease in 'interstitial' (CD11b+) macrophages, while having an increased 'alveolar' macrophage (CD11c+) compartment. The same trend, although less prominent, was observed in CCL2 KO tumours, suggesting a potential role for tumour-derived CCL2 in the recruitment of monocytes that give rise to 'interstitial' macrophages. We hypothesised that these 'alveolar' macrophages might consist of a lung tissue-resident population that remains unchanged upon inhibition of the CCL2-CCR2 axis, as suggested in (Misharin et al., 2013). When examining macrophage populations further (Figure 38D), we encountered a differential expression of macrophage markers F4/80 and CD68, which are generally used to define macrophages broadly, across experimental groups. No distinction between CD11b+ and CD11c+ populations was made to generate this plot and samples were only pre-gated based on expression of CD45+ and lack of the monocyte/neutrophil marker Ly6C. A new population with intermediate expression of both CD68 and F4/80 ('population 4') was found in CCL2 KO tumours, that was virtually non-existent in WT tumours. We suggest that this population potentially constitutes a macrophage subtype derived from CX_3CR1+ monocytes. Nevertheless, lineage tracing studies would be required to confirm this hypothesis. It would also be interesting to be able to examine whether these macrophage populations differ in their function, by perhaps sorting out the different populations and performing RNA and functional analyses.

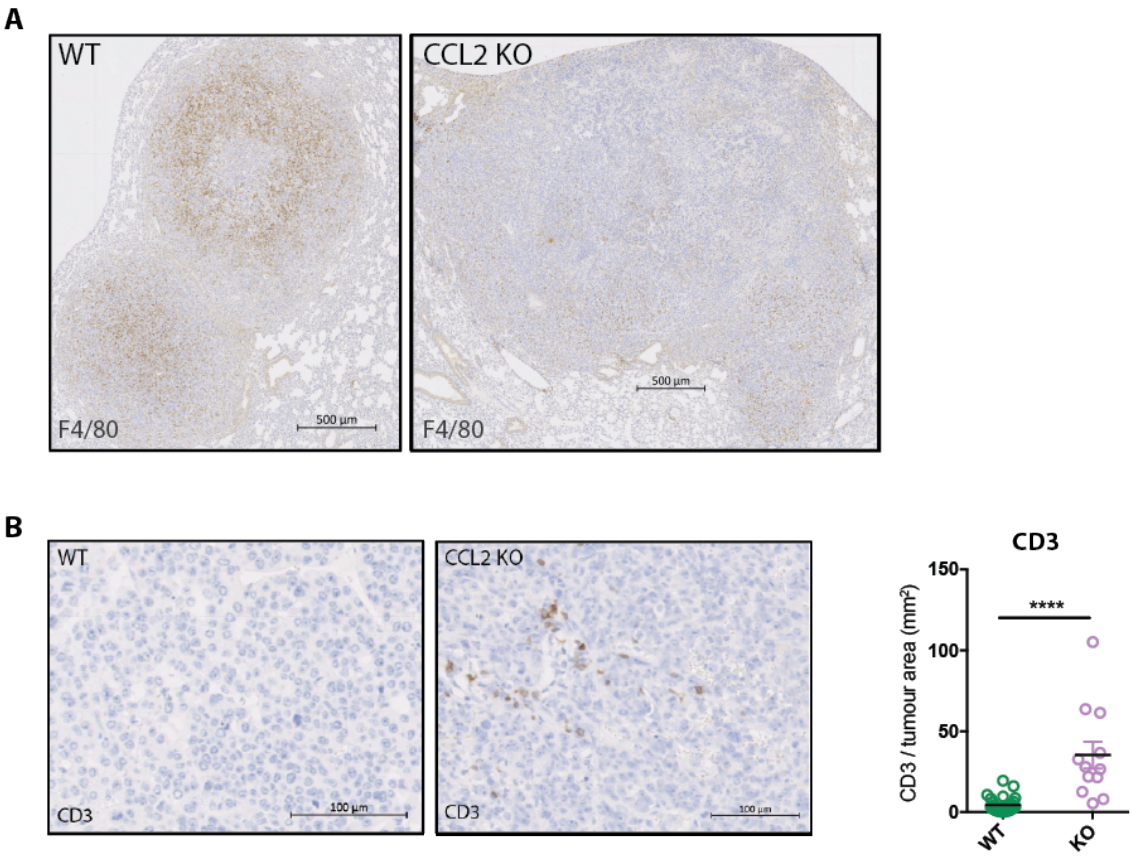

Figure 39. Immunohistochemistry of CCL2 KO tumours.

A) F4/80 staining of whole 3LL ΔNRAS WT or CCL2 KO (clone #141) tumours. One representative tumour per group is shown, 28 WT and 12 KO tumours were examined. B) Examples of CD3 staining on tumour regions of 3LL ΔNRAS WT or CCL2 KO (different clones pooled) tumours (left). Right: quantification of CD3 staining was performed by assessing the number of CD3+ cells per mm^2 of tumour. Each dot represents a tumour (Mean±SEM, Student's T test).

We have also confirmed the decrease in tumour-infiltrating macrophages by F4/80 immunohistochemistry staining (Figure 39A). Whereas 3LL ΔNRAS WT tumours are heavily infiltrated by F4/80+ macrophages, particularly in the tumour core, CCL2 KO tumours show much lower F4/80 expression, with most of it expressed at the tumour rim. Additionally, we performed CD3 staining on tumours to examine the spatial location of CD3+ T cells. WT tumours were largely devoid of T cells in the tumour core, while some CD3+ cells were observed in CCL2 KO tumours (Figure 39B, left). A quantification of tumour-infiltrating CD3+ T cells is displayed showing a significant increase in CD3+ cells in CCL2 KO tumours in Figure 39B. This data not only confirms the previously described FACS data, but also shows that whereas

3LL WT tumours are filled with macrophages and are devoid of T cells in the tumour bed, CCL2 KO tumours display less macrophage infiltration and allow for T cell infiltration into the tumour.

In general, we have observed profound changes in the TME of CCL2 KO tumours, which suggests an important role of tumour-derived CCL2 in the shaping of the TME of 3LL ΔNRAS tumours. We have shown that inhibiting tumour-derived CCL2 has distinct effects from CCR2 deletion, for instance, monocyte recruitment and macrophage infiltration was largely abrogated in CCR2 KO mice, but not in CCL2 KO tumours. This suggests that either there are alternative sources of CCL2 or that CCL2 can use CCR2-independent pathways to recruit alternative monocytes and macrophages to the TME. The further examination of these mechanisms will provide insight into the biological role of CCL2 in the TME and determine whether CCL2 (or CCR2) comprise a suitable therapeutic target in KRAS-mutant lung tumours. The increase in cytotoxic populations and ‘non-classical’ monocytes, together with the reduced tumour cell seeding in the lung, suggest that the effects of blocking CCL2-CCR2 could have an anti-tumoural effect.

4.8 Conclusions

In this chapter, we report the establishment of a murine lung cancer cell line susceptible to $KRAS^{G12C}$ inhibition that can be used *in vivo*. This cell line has been very useful throughout the entire thesis to assess the effects of KRAS signalling on the shaping of the TME and modulation of immune responses, as well as the elucidation of the effects of the use of $KRAS^{G12C}$ inhibitors on the remodelling of the TME (Chapter 5).

We have immunologically characterised this model and concluded that it is a highly mutated cell line with a large number of putative neoantigens, despite it has lost one MHC allele. It has an immune evasive TME largely comprised of immunosuppressive cell types. We have not made direct comparison between the TME of this model and other KRAS-mutant murine lung cancer models in this work, but we suggest that this model has a predominant monocyte/macrophage infiltration in contrast to other, urethane-driven models (see 6.3.2). This model, despite being highly mutated, has been reported to be resistant to immune checkpoint targeting agents (Li et al., 2017). This is in line with a large proportion of KRAS-mutant NSCLC patients, whose tumours have a high mutation burden, yet are resistant to ICB treatments. We therefore argue that it comprises an excellent model to elucidate mechanisms of immune evasion in KRAS-mutant lung cancer and to investigate combination treatments that could make these tumours sensitive to immune-targeting agents. However, it is a transplantable model that has potentially previously undergone *in vivo* selection and is therefore highly aggressive, thus not fully recapitulating multistage tumour evolution. In contrast, human tumours evolve much more slowly, with selective pressure from the host's anti-tumour immune response occurring gradually, which is not reflected by a fast-growing transplantable tumour such as the 3LL model.

By making use of this model, we have unveiled the monocyte chemoattractant CCL2 as being a KRAS-regulated factor. Its gene expression and protein secretion are dependent on oncogenic KRAS signalling via MEK. See Figure 40 for a schematic illustration of our findings. *In vivo*, we observed that absence of tumour-specific CCL2 promoted survival of tumour-bearing mice by reducing the number of

tumours seeding in the lung after intravenous injection. We have shown that absence of tumour-specific CCL2 leads to a remodelling of the TME, with a transformation in the myeloid compartment and increased presence of cytotoxic cells. It is important to note that due to the lower metastatic seeding observed in CCL2 KO tumours and CCR2 KO mice, the number of tumours analysed in our immunophenotyping analysis was rather low and perhaps insufficient to infer conclusions without being repeated in higher numbers. In line with our findings, lung tumours in CCR2$^{-/-}$ mice were smaller in (Loyher et al., 2018), and in that report, they suggested a role for monocyte-derived macrophages in tumour cell dissemination rather than tumour growth, similar to our finding in CCL2 KO tumours and thus strengthening our findings. However, both our findings and those in (Loyher et al., 2018) suggest that even in the absence of monocyte-derived cells, tumours are able to grow, hence also highlighting a role for tissue-resident macrophages in supporting tumour expansion.

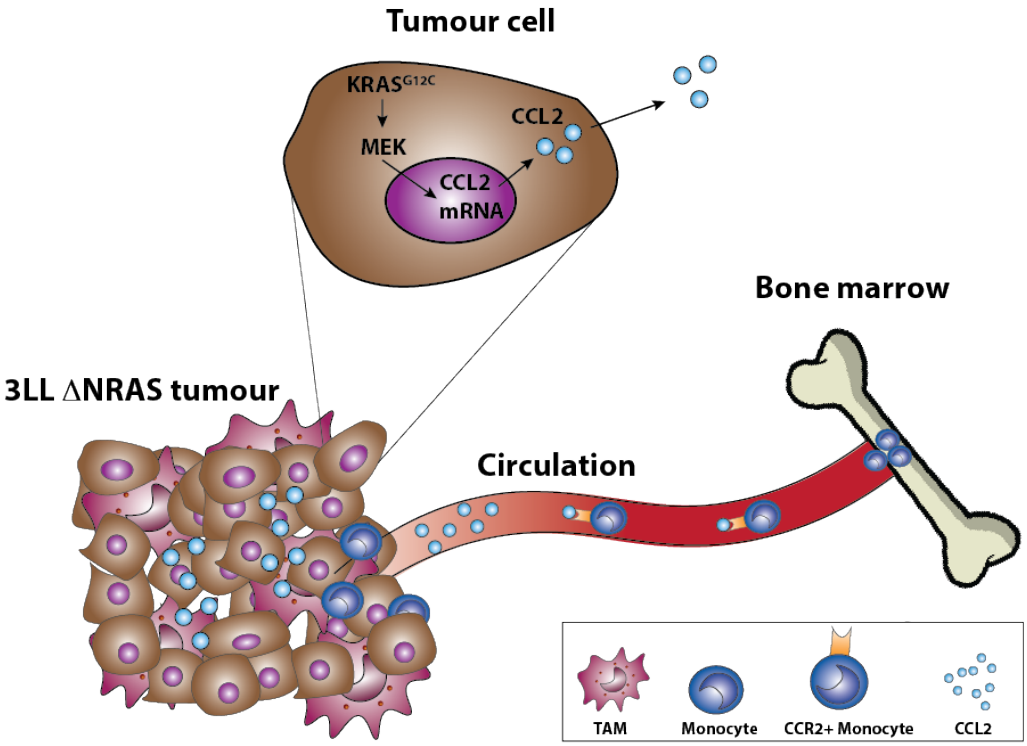

Figure 40. Illustration of KRAS-dependent regulation of CCL2 and recruitment of bone marrow-derived CCR2+ monocytes.

TAM=tumour-associated macrophage.

These results open new questions around the suitability of targeting the CCL2-CCR2 axis therapeutically. It would also be interesting to examine the role of this axis in other KRAS-driven lung cancer models, given the KRAS-dependent regulation of the CCL2 gene. Follow-up experiments will include tumour-specific CCL2 deletion after tumour initiation, by generation of an inducible-Cas9 version of the 3LL ΔNRAS cell line expressing sgRNAs targeting CCL2. This will serve to assess whether CCL2 is indeed a valid therapeutic target, or its role consists exclusively of dampening tumour seeding in the lung. Additionally, we will examine whether administration of CCR2 inhibitors, which are approved for clinical use in a number of conditions and are currently being tested as treatment options for patients with solid tumours, could provide a therapeutic benefit in this and other KRAS-mutant lung cancer models.

Chapter 5. Results 3: Investigation of the effects of $KRAS^{G12C}$ inhibitors on the TME of NSCLC and establishment of the link between KRAS and the IFN pathway

5.1 Introduction

In previous chapters, we have shown that oncogenic KRAS signalling is able to exert immunosuppressive actions, for instance by the transcriptional upregulation of myeloid chemoattractant cytokines. We have therefore demonstrated that oncogenic KRAS-mediated signalling can have effects that go beyond tumour cell-intrinsic features.

As mentioned in the introduction (1.3), over the past decades, a vast amount of research has been made in an aim to therapeutically target oncogenic KRAS, leading to the discovery of direct covalent $KRAS^{G12C}$ inhibitors. These inhibitors are now paving their way into clinical practice and have shown promising early signs of clinical activity, especially in patients with KRAS-mutant NSCLC (Canon et al., 2019) (Hallin et al., 2020) (Hong et al., 2020). Nevertheless, a known caveat of targeted therapies is their lack of long-term efficacy. This is largely due to the ability of tumour cells to develop resistance mechanisms that enable cell survival and ultimately lead to clinical relapses. Therefore, the development of rational combination therapies, particularly those leading to a tumour cell rejection by the immune system, known to be long-lasting, is of outmost importance.

In this chapter, we aim to understand the changes in immune infiltration and TME composition upon $KRAS^{G12C}$ inhibition in our 3LL ΔNRAS mouse model of lung cancer. We hypothesised that, due to the immunosuppressive action of KRAS signalling, its tumour cell-specific inhibition could have an impact on the anti-tumour immune response. This knowledge could be used to rationally design combination strategies aiming to harness the immune system that would lead to long-term responses in $KRAS^{G12C}$ -mutant lung cancer. Additionally, this setting could serve to identify novel mechanisms of immune evasion driven by oncogenic KRAS.

5.2 KRAS^{G12C} inhibition profoundly alters the TME of 3LL ΔNRAS tumours

We made use of our KRAS^{G12C}-mutant mouse model of lung cancer, 3LL ΔNRAS, (Chapter 4) for our KRAS^{G12C} inhibitor studies *in vivo*. As described before (4.2), this is a C57Bl/6-background murine cell line, which can be transplanted into immunocompetent mice, making it suitable for studies of the tumour immune response. For our experiments, we injected 3LL ΔNRAS cells intravenously into C57Bl/6 mice and allowed approximately 3 weeks for tumours to form in the lung. At that stage, we started daily treatment with the KRAS^{G12C} inhibitor MRTX1257 (kindly provided by Mirati Therapeutics Inc., from now on referred to as MRTX) or vehicle as a control (Figure 41A). For the *in vivo* experiments described in this section, we made use of the KRAS^{G12C} inhibitor from Mirati Therapeutics, as it has a higher potency than the previously used drug, ARS-1620. One week of treatment with MRTX led to a halt in tumour growth, as could be detected by microCT scanning of the mice (Figure 41B, shown as percentage of tumour volume relative to the pre-treatment scan for each individual tumour), consistent with the clinical and preclinical data available for these inhibitors (Hallin et al., 2020) (Canon et al., 2019).

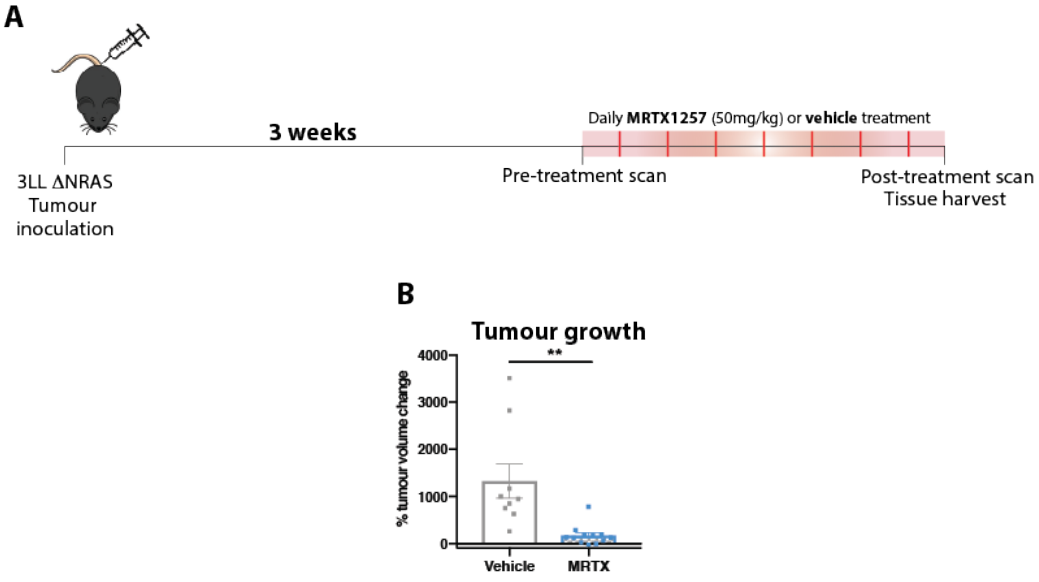

Figure 41. MRTX1257 experiment schematics.

A) Schematic of 3LL ΔNRAS *in vivo* experiments with MRTX1257. For all experiments, 1x10^6 cells were injected into the tail vein of C57Bl/6J mice. Tumours grew for 3 weeks before treatment (daily oral gavage of 50mg/kg MRTX1257 drug

or vehicle). B) Variation in tumour volume after 7 days of vehicle or 50mg/kg MRTX1257 treatment (daily). Y axis shows volume variation relative to the pre-treatment scan for each tumour (mean±SEM, Mann-Whitney, each dot represents a tumour, vehicle n=9, MRTX n=12). CT scan data obtained and analysed by Chris Moore.

Initially, we were interested in examining the composition of the immune TME after one week of MRTX treatment. Therefore, we used our immunophenotyping flow cytometry panel and gating strategy (Figure 27) to examine the immune infiltration of lung 3LL ΔNRAS tumours after seven days of vehicle or MRTX treatment. Figure 42 shows, firstly, that the overall infiltration of immune cells remains unaltered after treatment, thereby allowing to compare infiltration of other cell types as a proportion of total CD45+ cells. We found no significant change in T cell populations in the tumours, although there was a tendency towards increased Tregs and CD8+ T cell infiltration after treatment (Figure 42A and B). In addition, our FACS antibody panel allowed us to investigate the activation status of these T cells and found significant differences. CD8+ T cells expressing the early activation marker CD69 were significantly increased after treatment (Figure 42B). T cells expressing activation/exhaustion markers PD-1 and Lag3 were also significantly increased after KRAS inhibition (Figure 42B). Consistent with these findings, the effector compartment in CD8+ T cells was significantly expanded, with a relative decrease in the naïve T cell repertoire (Figure 42C). All this data suggests that the pool of antigen-experienced T cells has been expanded after MRTX treatment, suggesting a wave of T cell activation triggered by tumour cell-specific KRAS inhibition.

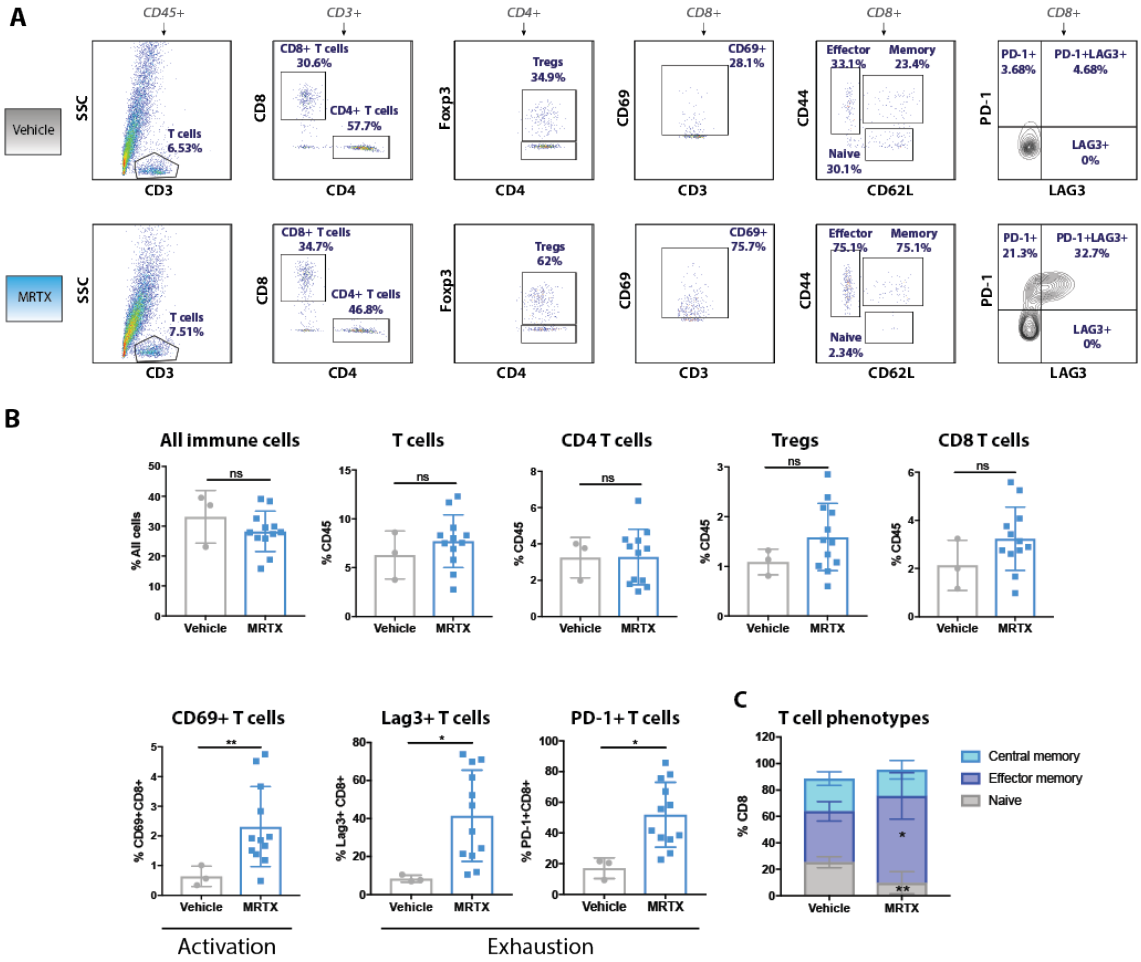

Figure 42. MRTX treatment increases T cell activation.

A) Representative plots of examined T cell populations. B) Quantification of T cell populations and phenotypes. Each dot represents a tumour (mean+/-SD, student's T test). Pre-gated on CD8 T cells. C) Stacked bar graph of T cell phenotypes (mean+/-SD, student's T test). Pre-gated on CD8 T cells.

Regarding additional immune cell types, we observed a mild decrease in B cell infiltration in response to KRAS inhibition (Figure 43A). We also found a significant decrease in neutrophil and monocyte infiltration (Figure 43A). This is consistent with the results of the previous chapter, where oncogenic KRAS signalling promoted the expression of monocyte and neutrophil chemoattractant molecules (Figure 32) and possibly reflects an inhibition of the release of such cytokines *in vivo*. cDC1 infiltration, although not significant, showed an upward trend (Figure 43A). In the macrophage compartment, we observed no significant difference in the proportion of infiltrating CD11c+ 'alveolar' macrophages (Figure 43A). However, we observed a large increase in CD11b+ 'interstitial' macrophages (Figure 43A). We

were quite surprised to observe this as we hypothesised that the decrease in monocytes would result in a decrease in macrophages. However, we cannot exclude that an influx of macrophages could result in response to tumour cell death triggered by treatment with the KRAS^{G12C}-targeting drug. In contrast, we observed a profound change in macrophage phenotype, with a significant increase in MHCII-expressing macrophages and a trend towards decreased in PD-L1 expressing macrophages (Figure 43B). We therefore hypothesise that there is a repolarisation of the macrophages rather than a change in their infiltration, but functional analyses would need to be performed to confirm this assumption.

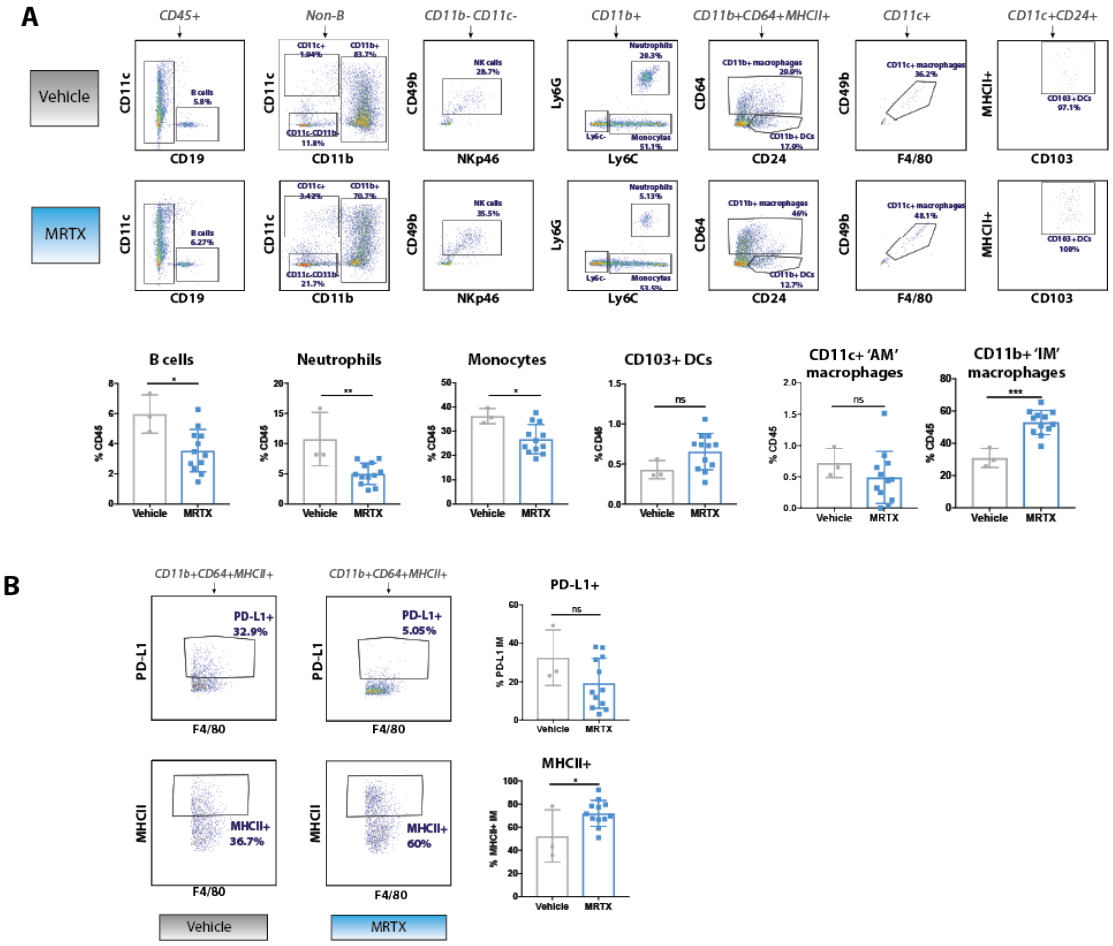

Figure 43. MRTX treatment alters myeloid cell composition.

A) Representative plots of non-T cell populations (above) and quantification of cell population, below. Each dot represents a tumour (mean±SD, student's T test). B) Representative plots (left) and quantification (right) of interstitial macrophage phenotypes. Each dot represents a tumour (mean±SD, student's T test). Pre-gated on CD11b+ macrophages.

These changes suggest that KRAS inhibition increases the presence of myeloid cells with pro-inflammatory and antigen presenting capabilities, potentially leading to a less immunosuppressive TME. The increase in antigen-presenting MHCII+ macrophages and the trend towards an increased number of dendritic cells could also explain the increase in T cell activation observed in Figure 42. In summary, the FACS data shows that tumour-specific $KRAS^{G12C}$ inhibition profoundly alters the TME, by increasing pro-inflammatory innate immune cell presence, reducing immunosuppressive populations and ultimately leading to an increased cytotoxic T cell activation.

5.3 Transcriptional changes upon KRAS^{G12C} inhibition *in vivo*

In order to understand the changes in immune-related gene expression pathways triggered by KRAS^{G12C} inhibition, we performed RNA sequencing experiments using 3LL ΔNRAS lung tumours treated with either vehicle or MRTX (Figure 44A). We sought to discover transcriptional changes triggered by oncogenic KRAS inhibition by looking at an early time point (28h) after treatment initiation. On the other hand, we wanted to assess transcriptional changes related to the immune infiltration remodelling found in the previous section, for which we examined tumour samples after 8 days of daily treatment with MRTX (with the last dose administered 4 hours before sacrifice). We used 3 mice per condition, with two tumours analysed per mouse, leading to a total of six samples sequenced per condition.

Additionally, in order to dissect tumour cell-intrinsic effects of MRTX treatment, we also sequenced RNA from 3LL ΔNRAS cells treated with MRTX *in vitro* for a 'short' time point (8h) and a 'long' time point (28h, consistent with the early time point *in vivo*) (Figure 44B). We sequenced three biological replicates of the *in vitro* samples per condition.

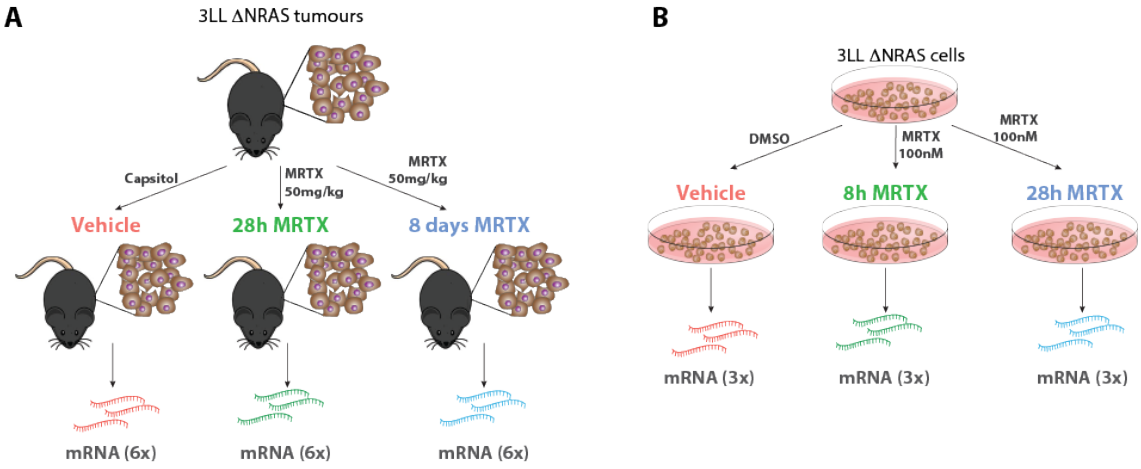

Figure 44. Schematic for RNA-Seq sample preparation.

A) In vivo, tumour-bearing mice were treated with vehicle or MRTX1257 for 8h or 8 days (seeFigure 41) before tissue harvesting and RNA extraction. 6 tumours, two tumours each from 3 mice, were taken from each condition for RNA-Seq analysis. B) *In vitro*, 3LL ΔNRAS cells were plated and treated 8h or 28h with MRTX1257 (or 28h DMSO control) before RNA extraction. Experiment was performed three times for three biological replicates.

5.3.1 RNA-Seq basic parameter analysis

The RNA samples were submitted to the Advanced Sequencing Facility at the Crick for RNA sequencing and data was analysed by Miriam Llorian Sopena at the Bioinformatics facility. First, we wanted to assess the quality of the biological replicates analysed by performing a PCA plot of the sequencing results for each sample. As shown in Figure 45A (left), the *in vivo* samples were largely grouped based on their treatment time point, with vehicle treatment and 8-day treatment samples showing the maximum separation trend and the 28h treatment showing an intermediate position, as expected. For the *in vitro* samples (Figure 45A, right), it is noteworthy to mention that one of the triplicates clustered differently from the other two, possibly reflecting a difference in the preparation of these samples. Nevertheless, all three replicates showed a good separation between treatments, indicating that the differences in gene expression found (as in the *in vivo* samples) were due largely to the type and duration of treatment received.

We also performed an unsupervised clustering of the differentially expressed (DE) genes in all conditions (Figure 45B). In the *in vivo* samples (left), with the exception of two 8-day treated samples, the vehicle samples tended to cluster together, and so did the treated ones. This variability is expected for *in vivo* data and we were glad to obtain a clustering result that was based mainly on treatment type. The clustering for the *in vitro* genes (right) was cleaner, with the vehicle, 8h and 28h samples clustering separately, suggesting that despite the suboptimal triplicates described in Figure 45A, the data was still robust.

Finally, we quantified the number of significantly DE genes, both up- and downregulated, in the MRTX-treated samples relative to the control samples (Figure 45C). The total number of DE genes increased with treatment duration for both *in vivo* and *in vitro* samples. A larger number of DE genes was obtained for the *in vitro* samples, possibly reflecting the increased robustness of a transcriptional analysis of a cell line *in vitro*, which yields more significant data compared to a complex *in vivo* system which tends to show larger data variability.

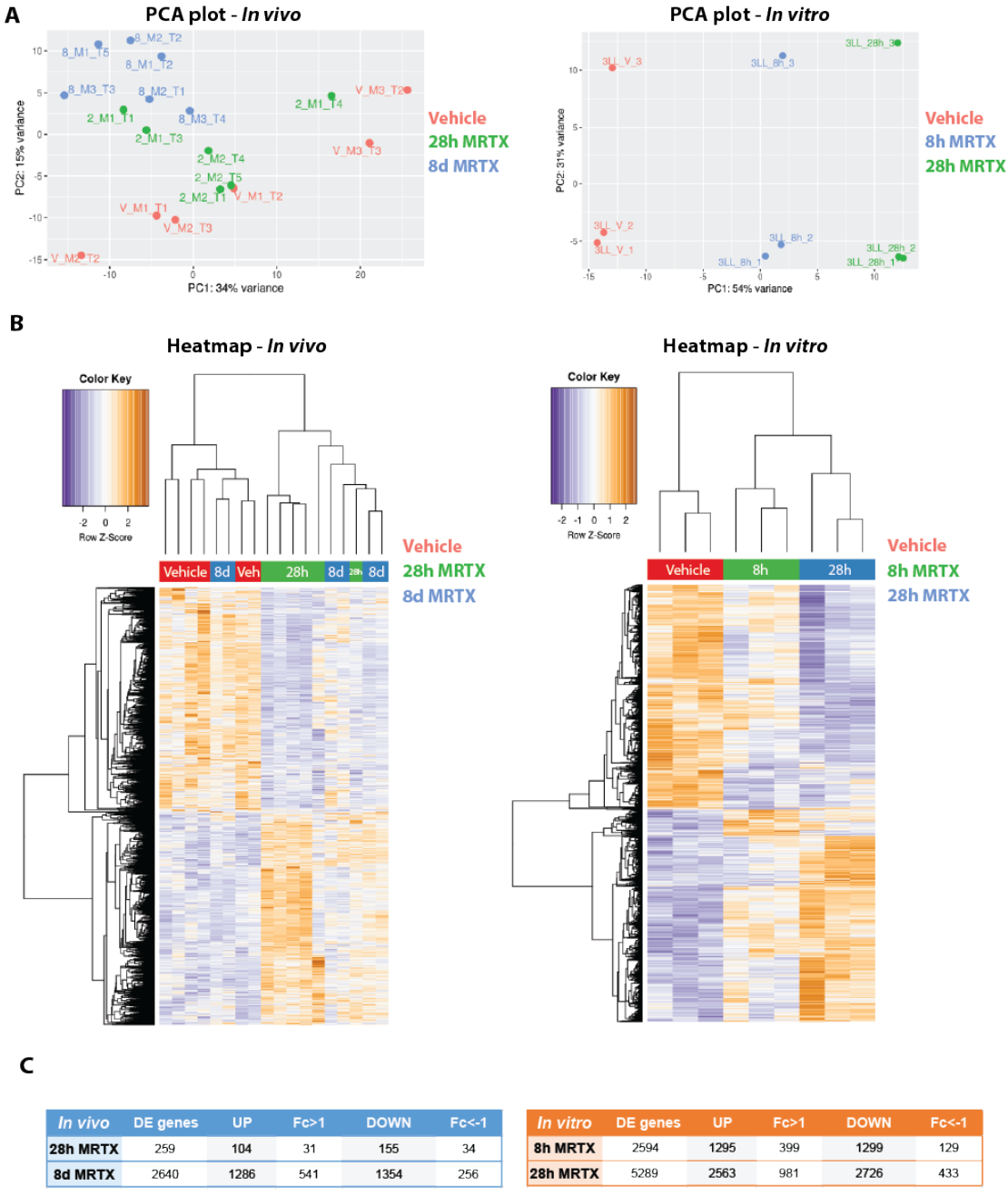

C

In vivo	DE genes	UP	Fc>1	DOWN	Fc<-1
28h MRTX	259	104	31	155	34
8d MRTX	2640	1286	541	1354	256

In vitro	DE genes	UP	Fc>1	DOWN	Fc<-1
8h MRTX	2594	1295	399	1299	129
28h MRTX	5289	2563	981	2726	433

Figure 45. RNA-Seq basic analysis.

A) Principal component analysis (PCA) plots for *in vivo* (left) and *in vitro* (right) gene expression data. B) Unsupervised clustering heatmap for *in vivo* (left) and *in vitro* (right) samples using all significant (padj<0.05) differentially expressed genes. C) Summary of significantly (padj<0.05) differentially expressed (DE) genes using vehicle control as a reference for *in vivo* (left) and *in vitro* (right) samples. DE=differentially expressed, Fc=fold change. Plots generated by Miriam Llorian Sopena.

5.3.2 *In vivo* RNA-Seq analysis

In order to gain confidence in the *in vivo* RNA-Seq data, we examined which genes were differentially expressed upon MRTX treatment. As shown in Figure 46, we found known KRAS-regulated genes, like MAPK signalling inhibitors as Sprouty RTK Signaling Antagonist 4 (Spry4) and Dusp genes (Dusp6 and Dusp7), to be significantly downregulated upon KRAS^{G12C} inhibition *in vivo*. This suggests that we were able to adequately observe the effects of KRAS inhibition despite the transcriptional noise and data variability of a complex multicellular *in vivo* system such as our 3LL ΔNRAS tumour model.

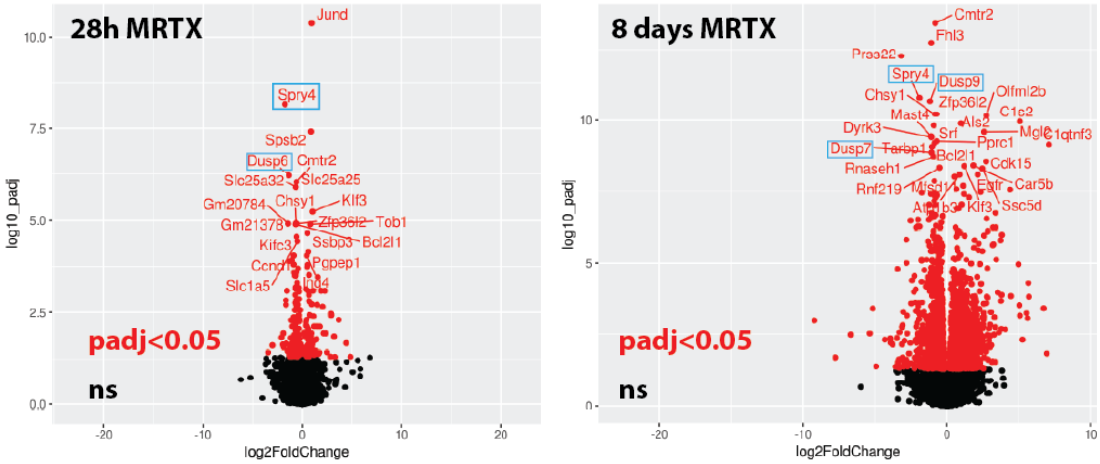

Figure 46. Differentially expressed genes *in vivo* include known KRAS-regulated genes.

Volcano plot of all differentially expressed genes *in vivo*, after 28h (left) and 8d (right) of MRTX treatment. Known KRAS-regulated genes are highlighted in blue. X axis displays log_2fold change and y axis shows the log_{10} of the p adjusted value. Plots generated by Miriam Llorian Sopena.

We analysed the gene expression data by performing pathway analyses using gene set enrichment analysis (GSEA) algorithms. In particular, we made use of the 'hallmarks' gene expression signature obtained from MSigDB. We were interested in which gene expression pathways were up- and downregulated after KRAS^{G12C} inhibition (28h and 8 days) *in vivo*. Consistent with the higher number of DE genes found at the 8-day time point, the amount of pathways differentially up- and downregulated was also higher at the later time point. Downregulated pathways mostly included cell cycle-related pathways, protein translation pathways and Myc

related pathways (which is often associated to KRAS signalling), as expected from the cytostatic effects of the KRAS inhibitor (Figure 47A). We could also observe, at the 8-day time point, an upregulation of the pathway 'KRAS signalling down', also serving as a positive control for the data.

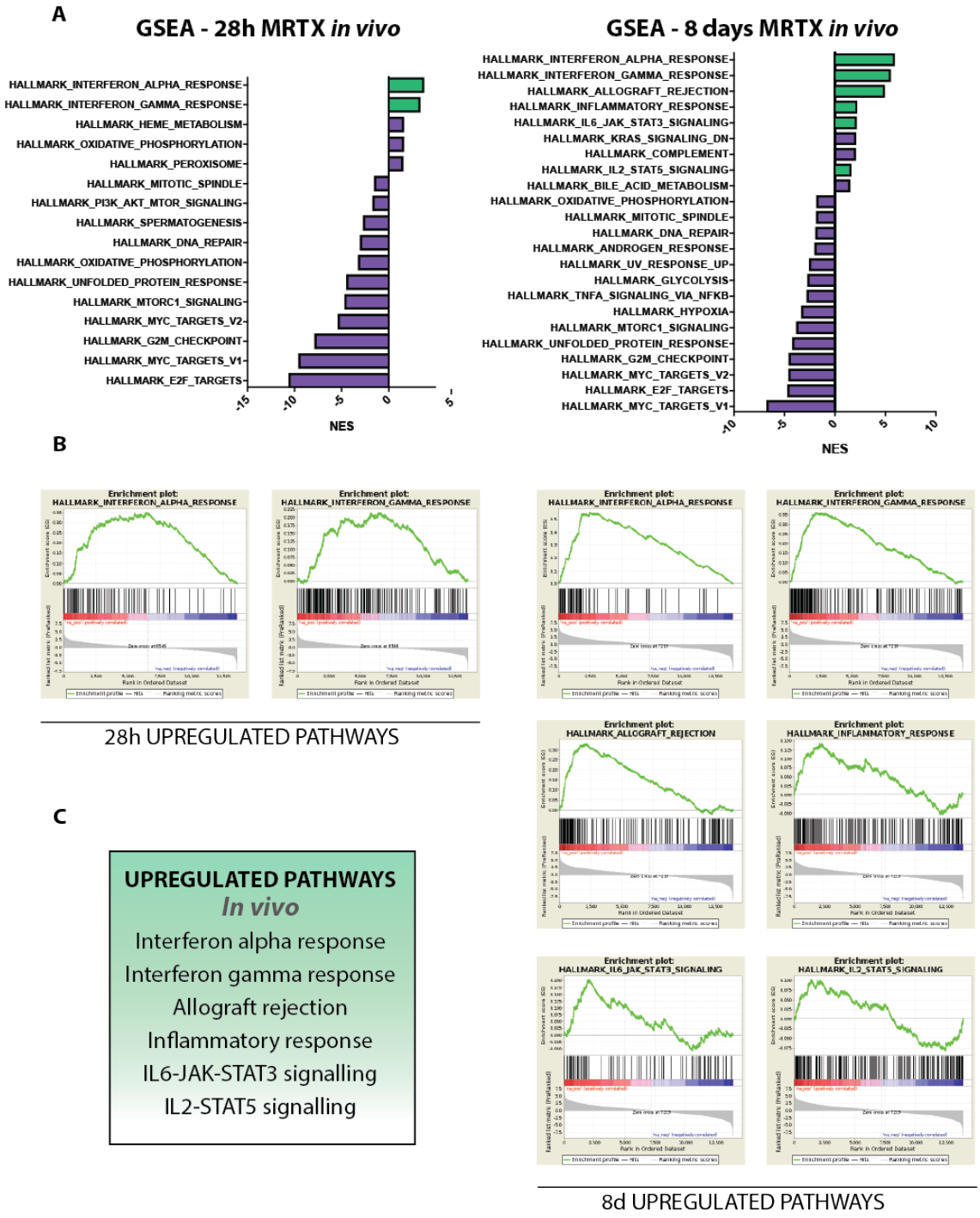

Figure 47. KRAS inhibition *in vivo* increases immunological gene expression pathways.

A) Summary of all pathways with a false discovery rate (q) < 0.05. Analysis was performed using 'hallmarks' collection from MSigDB. NES=normalised enrichment score. Green bars represent immune-related pathways. B) Individual gene set enrichment analysis plots for immune-related pathways. C) Summary of all immune-related upregulated pathways upon $KRAS^{G12C}$ inhibition.

We were mostly interested in those pathways related to the immune system in order to assess the changes occurring in the TME as a consequence of the treatment. We could observe that at the 8-day time point, most of the significantly upregulated pathways were related to immune responses, such as interferon alpha and gamma responses, allograft rejection, inflammatory response, complement and signalling pathways for inflammatory cytokines IL-6 and IL-2 (Figure 47B and C). This data suggests that the most prominent changes occurring due to the KRAS inhibition are associated to the remodelling of the immune microenvironment and potentially the generation of a strong inflammatory response. These changes could be observed at the 8-day time point only, suggesting that the immune system, in this model, requires several days to mount a response. However, the interferon gamma and alpha response increase could be observed at the earlier time point, hinting towards a tumour cell-intrinsic effect of these pathways rather than an upregulation of these responses mediated by immune cells. A more detailed analysis of this phenomenon will be described later in this chapter (5.4).

With the gene expression data, we were able to observe immunological features that we could not obtain from FACS data, such as additional markers of T cell activation (Figure 48A). Cytotoxic molecules such as granzymes were upregulated at 8-days post-treatment, and so were the IL-2 receptor subunit CD25 (possibly also reflecting an increase in Tregs), the T cell co-stimulatory molecules CD27 and OX40 (Figure 48A) and PD-1. In line with this data, mRNA levels of T cell exhaustion markers were also upregulated (Figure 48B). Consistent with the FACS data, we could see an increase in transcripts encoding for Lag3. Additionally, other exhaustion markers like Icos, Ctla4, Vista and Tim3 also tended to be increased at the 8-day time point. Together, this data suggests that a potent activation of T cells has occurred following KRAS inhibition.

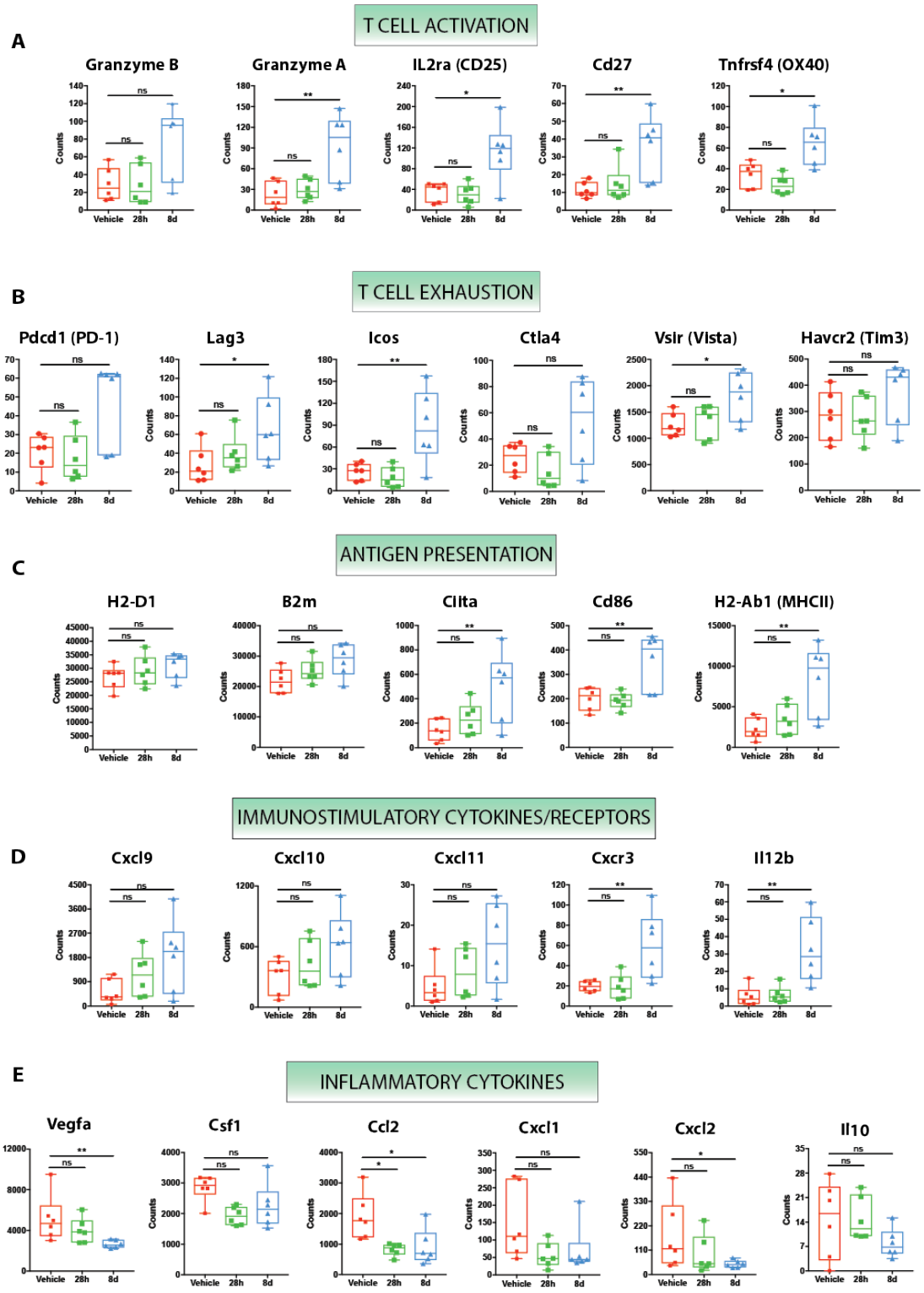

Figure 48. KRAS inhibition increases pro-immunogenic gene expression.

Examples of up-/downregulated genes by MRTX treatment *in vivo*. y axes show normalised counts from RNA-Seq analysis (Mean±quartiles, adjusted p values are plotted, n=6 in all groups, each dot represents a tumour sample).

We also gained insight on other immunological processes such as antigen presentation (Figure 48C). We could observe a trend towards increased genes encoding for components of MHC class I (H2-D1, B2m) and MHC class II (H2-Ab1, Ciita, Cd86) complexes. This increase in antigen presentation capability (in line with our observations by FACS) could explain the increase in T cell activation observed by both RNA and FACS analysis.

The RNA data also allowed us to examine the cytokines expressed in the TME (Figure 48D and E). Interestingly, T cell chemoattractant cytokines Cxcl9, Cxcl10 and Cxcl11 showed a trend towards a higher expression after $KRAS^{G12C}$ inhibition (Figure 48D). In line with this observation, the receptor for these cytokines (Cxcr3) expressed on T cells, was also upregulated following 8 days of MRTX treatment. Another known pro-inflammatory gene, IL12b, a Th1 response inducer, was upregulated after KRAS inhibition. In contrast with this, cytokines with a potential pro-tumorigenic, inflammatory function tended to be downregulated in our data (Figure 48E). Angiogenesis stimulatory factor Vegfa was significantly decreased after 8 days of MRTX treatment. In the myeloid compartment, cytokines responsible for monocyte (Ccl2) and neutrophil (Cxcl1, Cxcl2) recruitment, and macrophage polarisation (Csf1) all showed a downward trend following KRAS inhibition. This data is in line with the observations *in vitro* presented in the previous chapter (Figure 32). Finally, a cytokine known to exert an array of immunosuppressive actions, Il10, also showed a downward trend in its mRNA expression 8 days after treatment. The cytokine data indicates that there is an increase in the inflammatory cells recruited to the TME, while the recruitment of immunosuppressive cells is inhibited following tumour cell-specific KRAS inhibition.

Together, the RNA analysis performed on 3LL ΔNRAS tumours after MRTX treatment, suggests a profound remodelling of the immunosuppressive TME of these tumours as a consequence of tumour cell-specific $KRAS^{G12C}$ inhibition, in line with the FACS data discussed above. We concluded that all these changes converged in the generation of a more immune permissive environment and the generation of a potent immune and inflammatory response, potentially due to the abrogation of the immunosuppressive signalling effects triggered by oncogenic KRAS.

5.3.3 *In vitro* RNA-Seq analysis

In order to address molecular mechanisms by which KRAS inhibition *in vivo* led to profound changes in the TME and triggered immune responses, we sought to assess tumour cell-specific changes occurring after KRAS inhibition *in vitro*, in cultured 3LL ΔNRAS cells (Figure 44B).

We performed GSEA analysis in the same manner as the analysis performed for the *in vivo* data. As expected, the major immune-related pathways upregulated after KRAS inhibition *in vivo* (Figure 47) were not observed in the *in vitro* data, confirming that the *in vivo* data largely reflects a change in the TME occurring in response to the treatment. However, the downregulated pathways observed *in vitro* mirrored those observed *in vivo*, reflecting the direct effects of KRAS inhibition on the viability and signalling of the tumour cells (Figure 49). We could also observe an upregulation of the pathway 'KRAS signalling down' at both time points after KRAS inhibition *in vitro*.

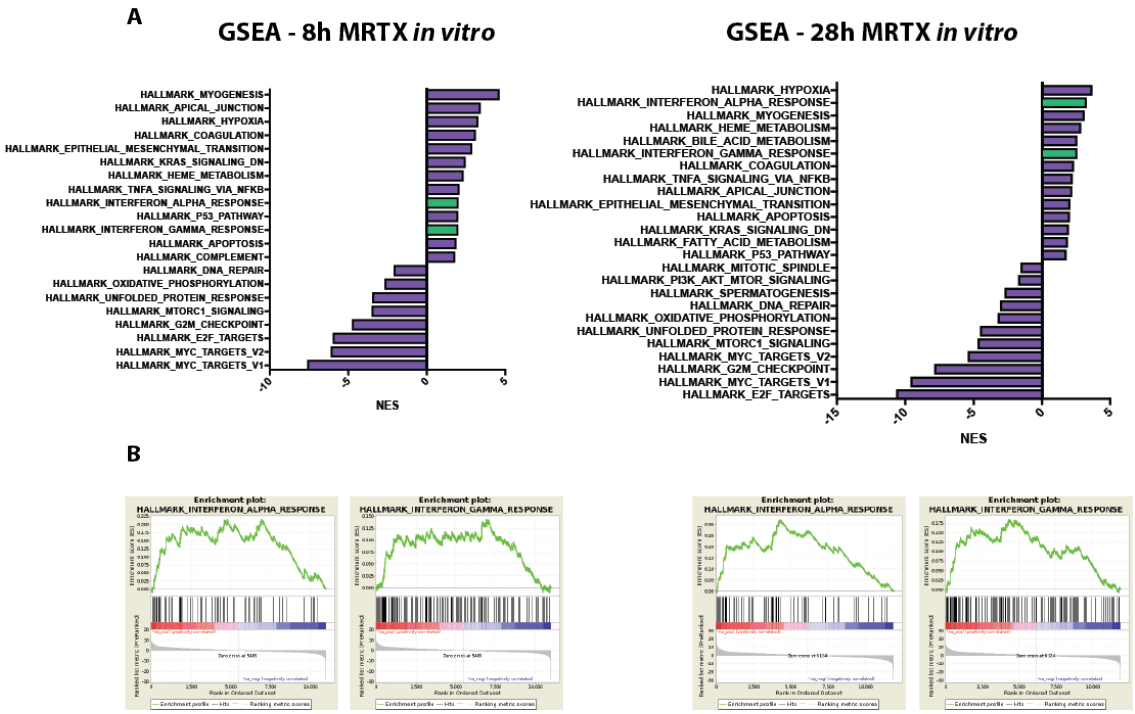

Figure 49. KRAS-dependent regulation of the IFN response is a tumour cell-intrinsic trait.

A) Summary of all pathways with a false discovery rate (q) < 0.05. Analysis was performed using 'hallmarks' gene set collection from MSigDB. NES=normalised

enrichment score. Green bars indicate immune-related pathways. B) Individual gene set enrichment analysis plot for interferon response pathways.

However, two of the immune-related pathways, interferon (IFN) alpha and interferon gamma responses, were significantly upregulated following KRAS inhibition *in vitro* at both time points analysed. This suggests that the increase in interferon-related genes is a tumour cell-intrinsic characteristic rather than a reflection of the changes in immune cell composition. It also indicates that oncogenic KRAS signalling has the ability to, in some manner, dampen IFN responses. These responses are crucial for mounting an immune response following a viral infection, or in this case, an anti-tumour immune response. These pathways were likewise significantly increased after KRAS inhibition in the human $KRAS^{G12C}$ cell line data presented in Chapter 3, in our *in vivo* data (Figure 47), and in the data using the $CT26^{KRASG12C}$ model presented in Canon et al. (Canon et al., 2019), where they observed an increase in the IFN score obtained by NanoString analysis following KRAS inhibition *in vivo*. This indicates that the ability of KRAS inhibition to increase IFN-related genes is a feature that can be observed in a number of *in vitro* and *in vivo* models, underscoring its relevance and potentially comprising a new mechanism by which oncogenic KRAS is able to evade anti-tumour immune responses.

5.4 Oncogenic KRAS signalling inhibition augments IFN responses *in vitro*

The RNA-Seq data of 3LL ΔNRAS cells treated with MRTX suggested that KRAS inhibition was able to transcriptionally increase genes in the IFN alpha and IFN gamma pathways. Interferon α/β (type I IFN) are known antiviral molecules released by normal cells in response to cytosolic DNA presence (Borden et al., 2007). In contrast, IFN gamma (type II IFN) is released by cytotoxic immune cells and is known to play antiviral, anti-tumour and immunomodulatory roles (Borden et al., 2007). Both molecules act in a similar manner, by engaging their receptors on the cell membrane and triggering a cascade of intracellular signalling, mediated by the JAK-STAT pathway (Figure 50A). IFN gamma stimulation leads to phosphorylated homodimers of STAT1, which are able to translocate to the nucleus and initiate transcription of interferon-response genes (ISGs). In contrast, type I IFNs lead to the heterodimerisation of STAT1 and STAT2, which, when bound to IRF9, translocate to the nucleus and lead to the transcription of ISGs. ISGs consist of genes that encode for proteins of the IFN pathway itself (such as STATs and IRFs) and pro-immunogenic genes (such as T cell chemoattractants CXCL9/10 and MHC related genes) (Borden et al., 2007).

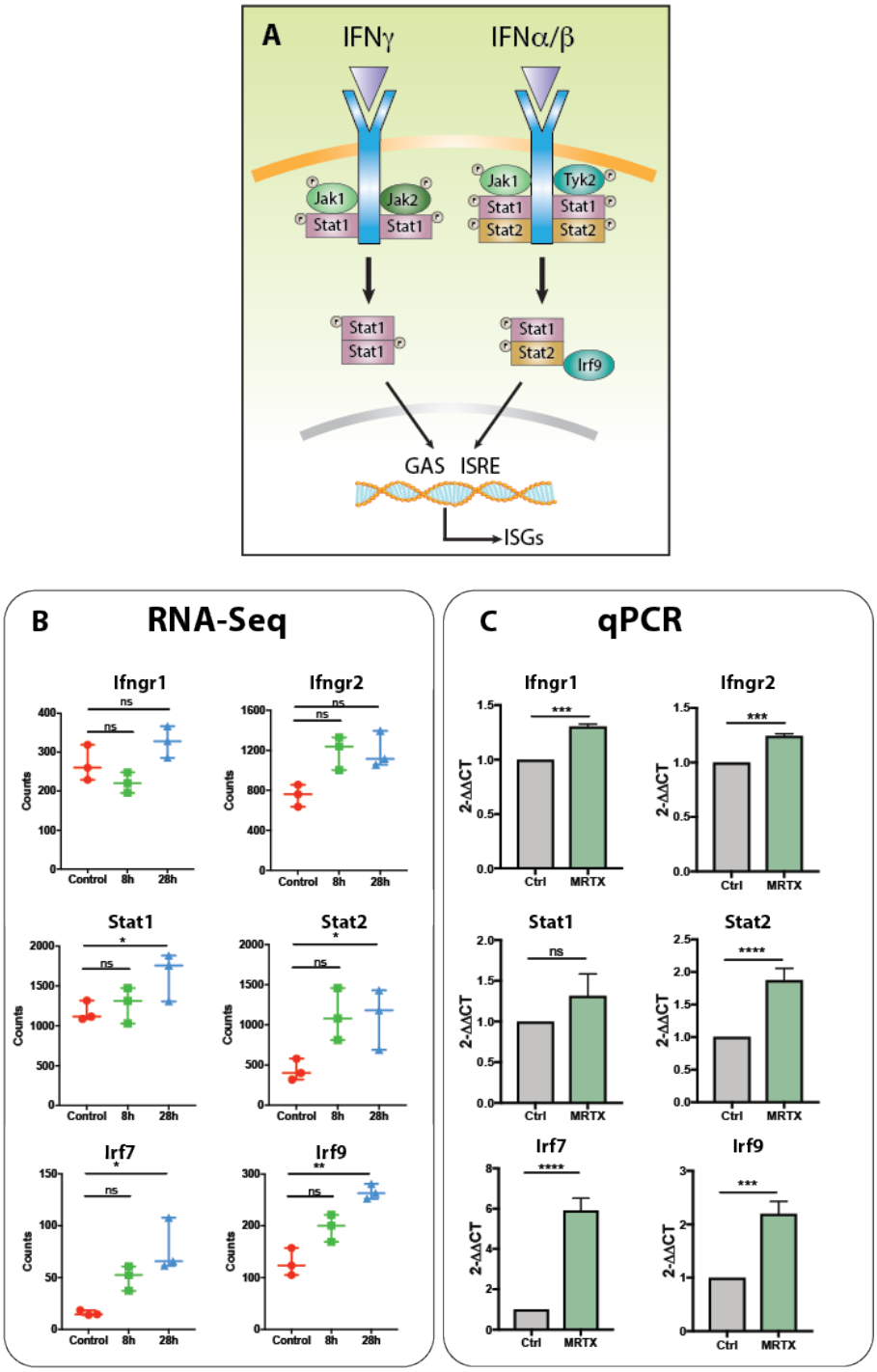

Figure 50. MRTX treatment leads to the upregulation of genes involved in the IFN response pathway

A) IFN pathway schematic. GAS=gamma interferon-activated site, ISRE=interferon-stimulated response element, ISG=interferon-stimulated genes. B) RNA-Seq data of IFN pathway genes (control, 8h MRTX, 28h MRTX, each dot represents one biological replicate, mean±min/max, p adjusted value is represented). C) qPCR data of IFN pathway genes upon MRTX treatment of 3LL ΔNRAS cells (50nM, 24h). $2^{-\Delta\Delta CT}$ method was used for the analysis, using at least

two different housekeeping genes (normalised to control, Mean+SEM of 4 biological replicates).

Firstly, we examined individual genes of the IFN pathway in the RNA-Seq data from Figure 49 and found that indeed, a number of genes encoding for components of the IFN pathway, such as the IFN gamma receptor, both STATs and a number of IRFs were upregulated upon MRTX treatment *in vitro* (Figure 50B). We were also able to confirm this upregulation in another set of samples using qPCR (Figure 50C).

Since we were able to observe a transcriptional upregulation of the interferon gamma and alpha response pathways also in human cell lines treated with a $KRAS^{G12C}$ inhibitor (see Chapter 3), we hypothesised that this was a widespread phenomenon. To confirm this in murine cell lines, we treated a number of $KRAS^{G12C}$ cell lines available in the lab with MRTX for 24h and assessed the expression of genes of the IFN pathway. Firstly, we made use of an unmodified version of the 3LL cell line (3LL). This cell line, where $NRAS^{Q61}$ has not been knocked out, is less sensitive to the actions of $KRAS^{G12C}$ inhibitors, and thus is a good model to distinguish the direct effects of cell signalling and drug-induced cell death. In addition, we obtained the $KRAS^{G12C}$ version of the colon cancer cell line CT26 (kindly provided by Mirati Therapeutics). Furthermore, using CRISPR knock-in methods, members of our lab were able to genetically edit the $KRAS^{G12D}$-p53 deleted mouse lung cancer cell line KPB6 (Coelho et al., 2017) to harbour a $KRAS^{G12C}$ mutation. We made use of two single cell clones that resulted from such editing for robustness.

Even though different genes were regulated at differing levels in all the cell lines, we observed a consistent trend of upregulation of IFN pathway genes upon MRTX treatment in all models (Figure 51). Differences in degrees of upregulation could reflect different sensitivities of the cell lines to $KRAS^{G12C}$ inhibition. This data indicates that KRAS-dependent regulation of IFN response genes is a widespread phenomenon that occurs across different models.

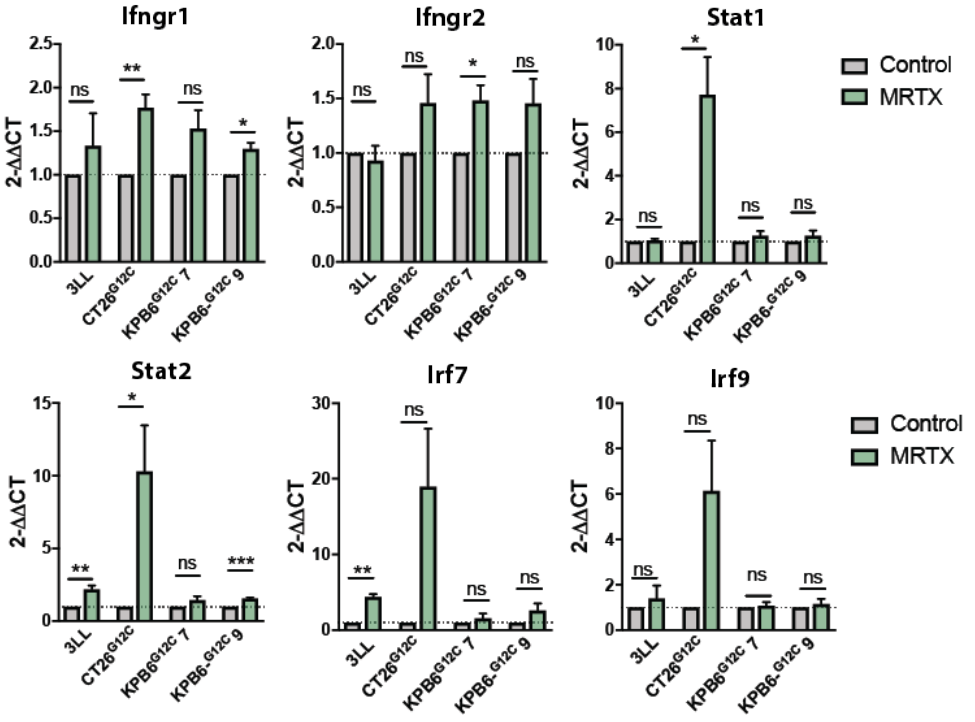

Figure 51. IFN pathway gene upregulation validation in murine KRAS^{G12C} models. qPCR data of IFN pathway genes upon MRTX treatment (50nM, 24h) in 4 mouse KRAS^{G12C} cell lines. $2^{-\Delta\Delta CT}$ method was used for the analysis, using at least two different housekeeping genes (normalised to control for each cell line, mean+SEM of 3 biological replicates, Student's T test).

The observation that KRAS inhibition is able to transcriptionally upregulate components of the IFN pathway led us to wonder whether KRAS inhibition could affect responses to IFN itself. We hypothesised that *in vivo*, presence of activated immune cells could lead to the secretion of IFNγ, thereby initiating an interferon response by the tumour cells. We sought to mimic this phenomenon *in vitro*, by treatment of 3LL ΔNRAS cells with recombinant IFNγ, in presence or absence of the KRAS^{G12C} inhibitor.

As displayed in Figure 52A, treatment of the cells with IFNγ led to an upregulation of known IFN response pathway components such as Irf7 and Stat2, but also downstream pro-immunogenic molecules such as Cxcl11. In addition, in a very striking manner, concomitant KRAS^{G12C} inhibition was able to enhance the transcriptional upregulation of these genes by IFNγ. Figure 52B shows a summary of all genes that we analysed, divided into their different functions. Interestingly, we found, that despite not all genes were statistically significant, the expression of all

of them was increased in IFNγ/MRTX treated conditions compared to IFNγ alone. This suggests that KRAS inhibition is able to enhance the pro-immunogenic effects of IFNγ in the 3LL ΔNRAS cell line.

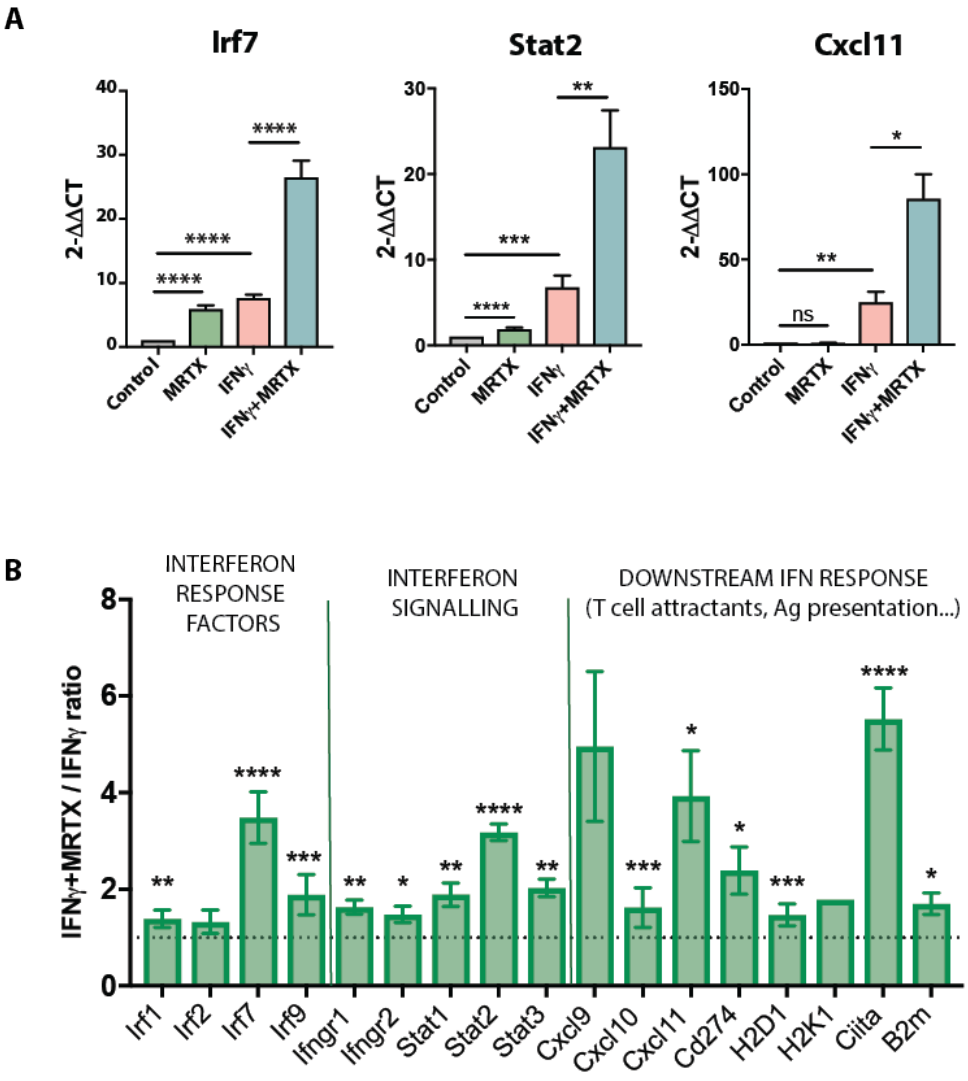

Figure 52. MRTX treatment augments the effects of IFNγ in 3LL ΔNRAS cells.

A) 3LL ΔNRAS cells were treated with MRTX (50nM), recombinant mouse IFNγ (100ng/ml) or both for 24h *in vitro*. Graphs show qPCR data for all conditions, analysed using the $2^{-\Delta\Delta Ct}$ method (using at least two housekeeping genes), relative to the control sample for each gene (mean+SEM of 4 independent experiments, student's t test). B) qPCR data ratios of IFNγ+MRTX/IFNγ conditions. Data was analysed as in A (Mean±SEM).

We then examined whether this augmentation of the IFN response also occurred in alternative models other than 3LL ΔNRAS. Figure 53A shows that the expression of

genes of the IFN pathway (i.e. Stat2) and downstream molecules (i.e. Cxcl11), triggered by IFNγ treatment, was additionally increased by treatment with MRTX, validating the observations made in the 3LL ΔNRAS cell line (Figure 53A). Figure 53B shows a summary of all genes examined in the form of heatmaps, where the colour intensity reflects the degrees of upregulation of each gene. Despite differences across cell lines, the general trend across all genes suggested a synergy between IFNγ and MRTX treatment, enhancing the robustness of our data showing a crosstalk between the KRAS and the IFN response. Interestingly, the analysis of this data highlighted the different degrees of response to MRTX and IFNγ of the different cell lines. For instance, treatment of MRTX alone had more striking effects in the $CT26^{G12C}$ cell line, suggesting a higher sensitivity of this model to $KRAS^{G12C}$ inhibition. On the contrary, both single cell clones of the $KPB6^{G12C}$ cell line showed different sensitivities to IFN treatment, with clone 7 appearing to be more sensitive to IFN. These observations may reflect different capabilities of the different models to mount an IFN response. However, the enhancement of the effects of IFNγ treatment by KRAS inhibition was a commonly observed pattern across all cell lines.

Finally, because we had focused on the transcriptional effects of IFN and MRTX administration, we wondered whether protein levels of these molecules were likewise affected by these treatments. Firstly, we examined surface levels of PD-L1, a known IFN response gene, on the 3LL ΔNRAS cell line by FACS. We were able to confirm that treatment with MRTX was able to enhance the upregulation of surface PD-L1 levels by IFNγ (Figure 53C). Additionally, we performed intracellular FACS staining to examine CXCL9 protein abundance in 3LL ΔNRAS cells. We were able to confirm that in addition to the mRNA upregulation, intracellular levels of T cell chemoattractant CXCL9 were enhanced upon KRAS inhibition compared to IFNγ treatment alone (Figure 53D). Furthermore, we assessed whether this led to an increased secretion of CXCL9 to the extracellular medium in a number of murine $KRAS^{G12C}$ mutant cell lines. We found that even though the secretion of CXCL9 was not significantly increased by IFNγ treatment in all models, concomitant KRAS inhibition was able to increase the amount of Cxcl9 detected in the medium of 3LL ΔNRAS, $CT26^{G12C}$ and $KPB6^{G12C}$ (9) cells (Figure 53E). This data suggests

that the transcriptional upregulation of IFN genes upon KRAS inhibition is able to influence protein levels and cytokine secretion by KRAS^{G12C} mutant tumour cells, likely accounting for changes in the TME *in vivo*.

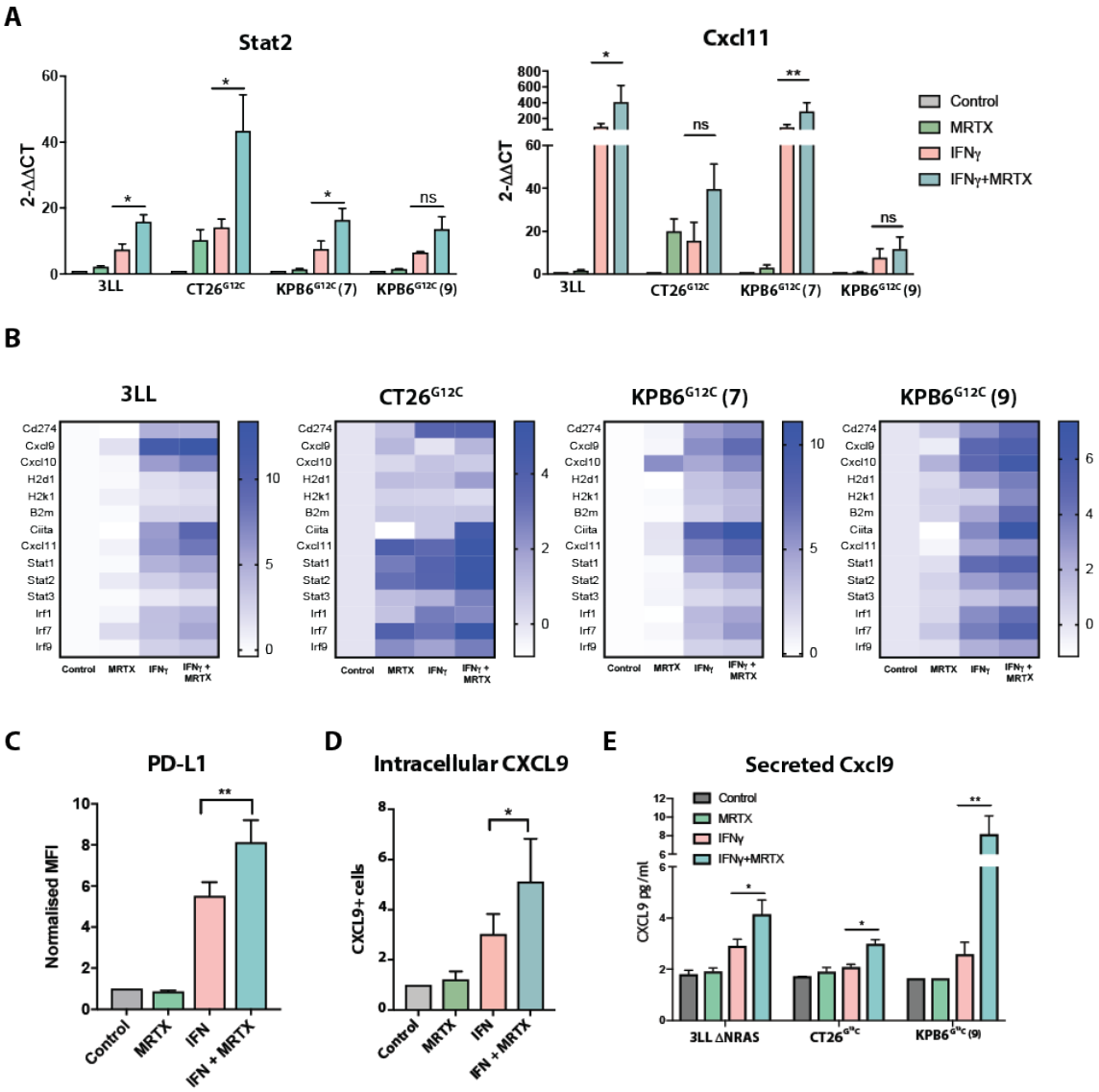

Figure 53. MRTX-driven augmentation of IFN response genes in additional cell lines.

A) KRAS^{G12C} cells were treated with MRTX (50nM), recombinant IFNγ (100ng/ml) or both for 24h *in vitro*. Graphs show qPCR data for all conditions, analysed using the $2^{-\Delta\Delta Ct}$ method (using at least two housekeeping genes), relative to the control sample for each gene in each cell line (mean+SEM of 4 independent experiments, student's t test). B) Heatmap summary of all qPCR data for all cell lines. Analysis was performed as in (A) and results are presented in $\log_2$ scale. C) 3LL ΔNRAS cells were treated as in (A) for 24h prior to FACS analysis of surface PD-L1

expression. Cells were pre-gated as live (DAPI-) cells. MFI of PD-L1 was normalised to control sample for each replicate (Mean+SEM of three independent experiments, paired ratio T test). D) Cells were treated as in (A) for 24h prior to FACS analysis of intracellular CXCL9 in permeabilised cells (Mean+SEM of three independent experiments, paired ratio T test). E) Cells were treated as in (A) and medium was harvested 24h after treatment. ELISA was performed to measure secreted CXCL9. Analysis was performed normalising to a standard curve of recombinant mouse CXCL9 (Mean+SEM of three independent experiments, paired ratio T test).

All the data shown to this point in this section indicates the ability of pharmacological $KRAS^{G12C}$ inhibition to augment responses to IFNγ by transcriptionally increasing components of the IFN pathway. The data hints towards a crosstalk between oncogenic KRAS and IFN pathways. However, the possibility still remains that the data shown above constitutes a reflection of the effects of such inhibitors on cell viability, rather than an effect of KRAS signalling itself. In order to exclude this possibility, we made use of the inducible $KRAS^{G12V}$ pneumocyte cell line ($KRAS^{G12V\text{-}ER}$ pneumocytes) described in Chapter 3. In this system, 4-OHT treatment *in vitro* leads to the stabilisation of a mutant form of KRAS and thus an activation of oncogenic KRAS-triggered pathways. In this model, we are able to examine the effects of KRAS signalling without compromising cell viability.

We treated type II pneumocyte cells *in vitro* with either 4-OHT or human recombinant IFNγ (or both) and examined transcriptional changes. We observed a downregulation of components of the IFN pathway upon $KRAS^{G12V}$ activation by 4-OHT, consistent with previous data (Figure 54). Additionally, treatment of the cells *in vitro* with human recombinant IFNγ was able to upregulate such genes, in a similar manner to the murine cell lines. Activation of oncogenic KRAS was able to at least partially reduce the transcriptional effects of IFNγ. Together, this data shows that there is a link between KRAS-driven pathways and the IFN pathway, and that the effects seen with the $KRAS^{G12C}$ inhibitor are not due to increased stress or effects on cell viability resulting from treatment with a targeted agent.

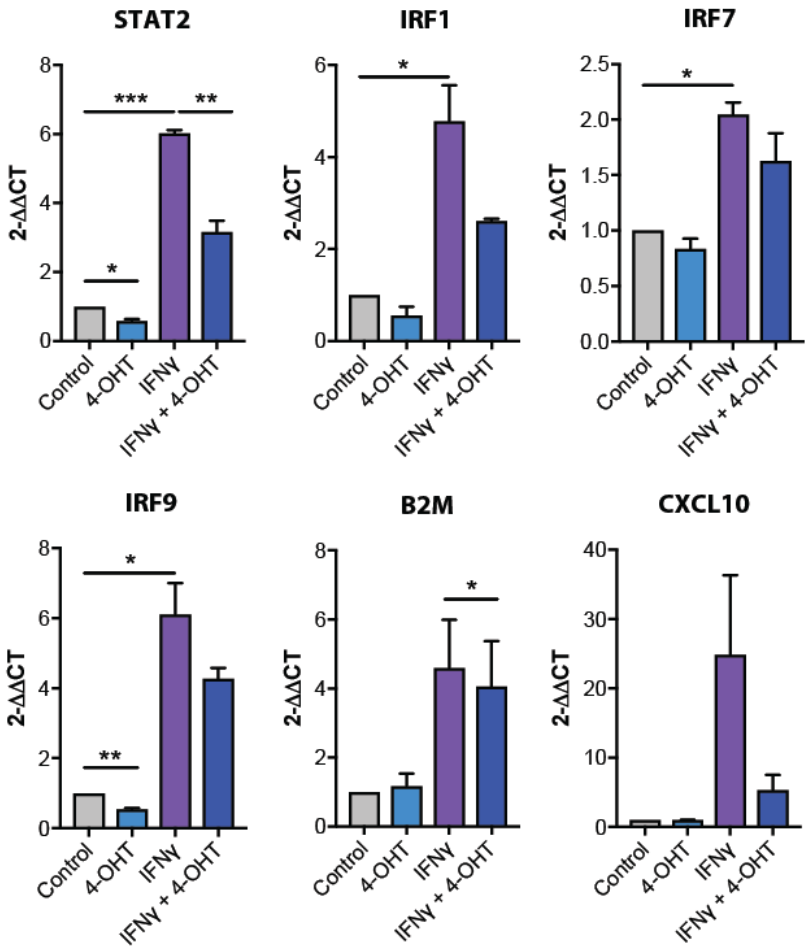

Figure 54. KRAS negatively regulates IFN response genes in a model of conditional KRAS^{G12V} activation.

qPCR data of IFN pathway genes upon 4-OHT (500nM, 24h) and/or human recombinant IFNγ (100ng/ml) treatment in human KRAS^{G12V}-ER pneumocytes. $2^{-\Delta\Delta CT}$ method was used for the analysis, using at least two different housekeeping genes (normalised to control for each gene, mean+SEM of 3 biological replicates, ratio paired T test).

5.4.1 KRAS-dependent regulation of IFNγ–related genes occurs independently of the JAK-STAT1 pathway, at least partially via MYC

We then sought to address the molecular mechanism underlying the crosstalk between oncogenic KRAS signalling and IFN responses. In order to examine this, we performed experiments where we perturbed IFN signalling and examined whether the effects of KRAS^{G12C} inhibition were altered.

Firstly, we treated 3LL ΔNRAS cells with the JAK inhibitor Ruxolitinib (Mesa et al., 2012) to block JAK-STAT mediated IFN signalling. As shown in Figure 55A, we were not able to detect phosphorylated STAT1 in the absence of IFNγ treatment suggesting that the JAK-STAT1 pathway is probably not activated in homeostatic conditions. IFNγ treatment increased the levels of pSTAT1, indicative of the activation of the IFNγ pathway. Interestingly, KRAS inhibition did not further enhance pSTAT1 levels, which suggested that the transcriptional effects of MRTX would not occur due to an increased JAK-STAT1 activation. In contrast, Ruxolitinib treatment was able to effectively suppress STAT1 phosphorylation, while not directly affecting total STAT1 protein levels, consistent with its role as a JAK1/2 inhibitor. We were also able to confirm the upregulation of STAT2 by MRTX by the protein level, which served as a further confirmation of our mRNA data.

Transcriptionally, we showed that treatment with Ruxolitinib did not alter the upregulation of IFN response genes by MRTX in 3LL ΔNRAS cells (Figure 55B). Figure 55C shows that the upregulation of genes by MRTX was not significantly changed by ruxolitinib treatment. When treating 3LL ΔNRAS cells with Ruxolitinib, we were able to abrogate the transcriptional effects of IFNγ (Figure 55D). However, the expression of IFN pathway genes (STATs, IRFs) was still equally increased in MRTX+IFN conditions compared to IFNγ alone, as summarised in Figure 55E (with the exception of Irf7, whose fold change induction was actually higher in Ruxolitinib-treated conditions). This data indicates that MRTX treatment still had an effect despite IFNγ was unable to adequately exert its function, suggesting a JAK-independent mechanism of KRAS-dependent regulation of IFN genes.

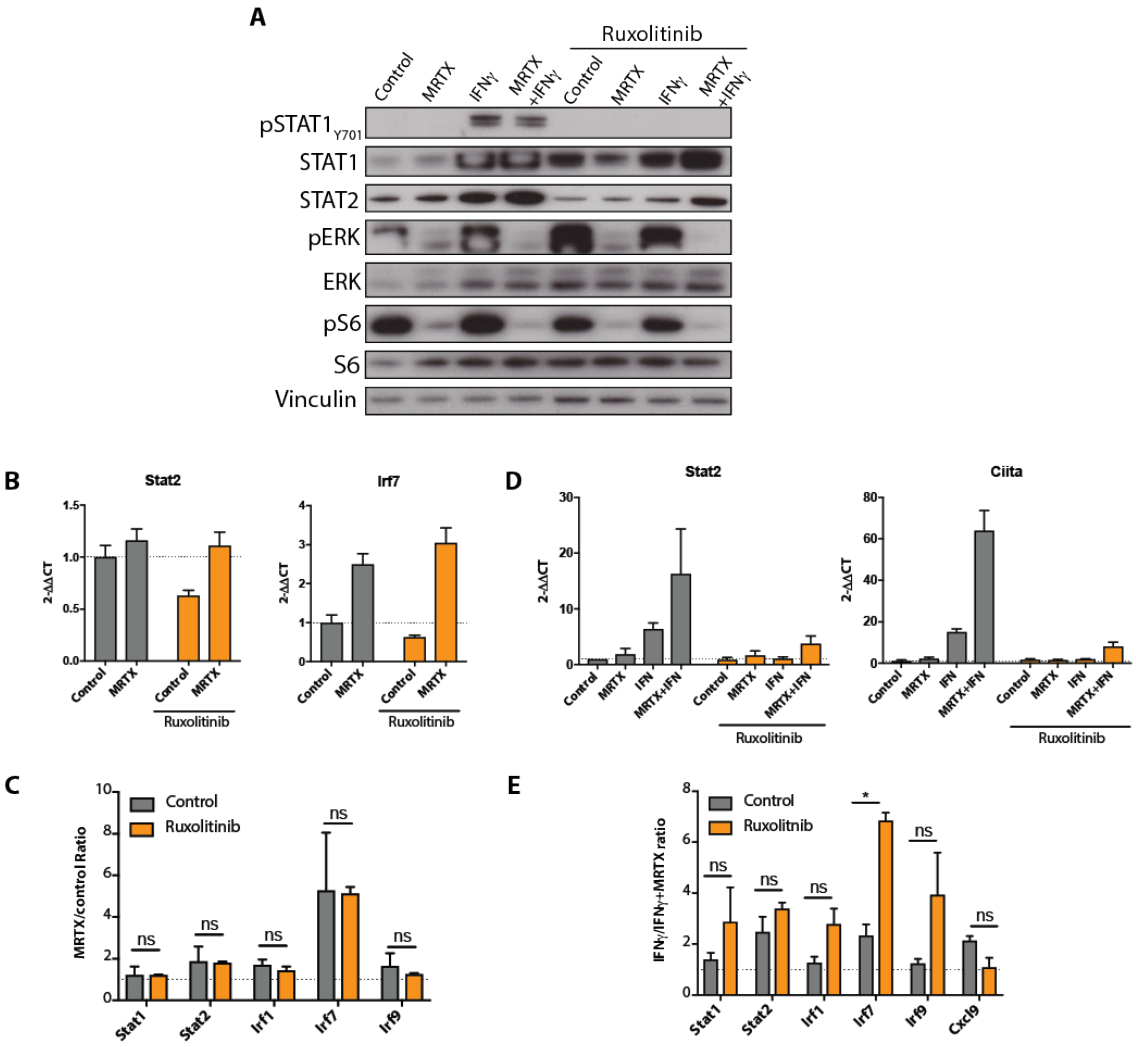

Figure 55. Pharmacological blockade of JAK does not alter KRAS-dependent regulation of IFN genes.

A) Western blot after treatment of 3LL ΔNRAS cells *in vitro* with MRTX (50nM), recombinant IFNγ (100ng/ml) and/or Ruxolitinib (500nM, 2h pre-incubation) for 24h. B) qPCR data of Stat2 and Irf7 upon MRTX (50nM, 24h) treatment in presence or absence of 500nM Ruxolitinib (2h pre-incubation) in 3LL ΔNRAS cells. $2^{-\Delta\Delta CT}$ method was used for the analysis, using at least two different housekeeping genes (normalised to control for each gene, Mean+SEM of 2 biological replicates). C) Summary of the ratio between MRTX and control conditions for different genes (normalised to control for each gene, Mean+SEM of 2 biological replicates, Student's T test). D) qPCR data of Stat2 and Ciita upon MRTX (50nM, 24h) and/or mouse recombinant IFNγ (100ng/ml) treatment, in presence or absence of 500nM Ruxolitinib (2h pre-incubation) in 3LL ΔNRAS cells. Data was analysed as in (B). E) Summary of the ratio between MRTX+IFNγ and MRTX conditions for different genes (normalised to control for each gene, Mean+SEM of 2 biological replicates, Student's T test).

As a validation of the data in Figure 55, we performed another set of experiments where we genetically abrogated the mRNA expression of Stat1 in 3LL ΔNRAS cells by treatment with a silencing RNA (siRNA) targeting murine Stat1 gene. After successful knockdown of Stat1 (Figure 56A), we confirmed that the presence of Stat1 is not required for the upregulation of IFN pathway genes by MRTX (Figure 56B). In addition, even though transcriptional responses to IFNγ treatment were dampened by siStat1 (Figure 56C), replicating the data with the JAK inhibitor shown in Figure 55C, concomitant MRTX treatment was still able to increase the expression of STAT and IRF genes.

Collectively, this data suggests that KRAS-dependent regulation of IFN pathway and IFN response genes occurs independently from the canonical JAK-STAT1 pathway. Despite the fact that the expression of these genes can be regulated by the IFNγ-JAK1-STAT1 pathway, KRAS inhibition is able to increase their expression even further, suggesting an alternative regulation mechanism that acts in a synergistic manner.

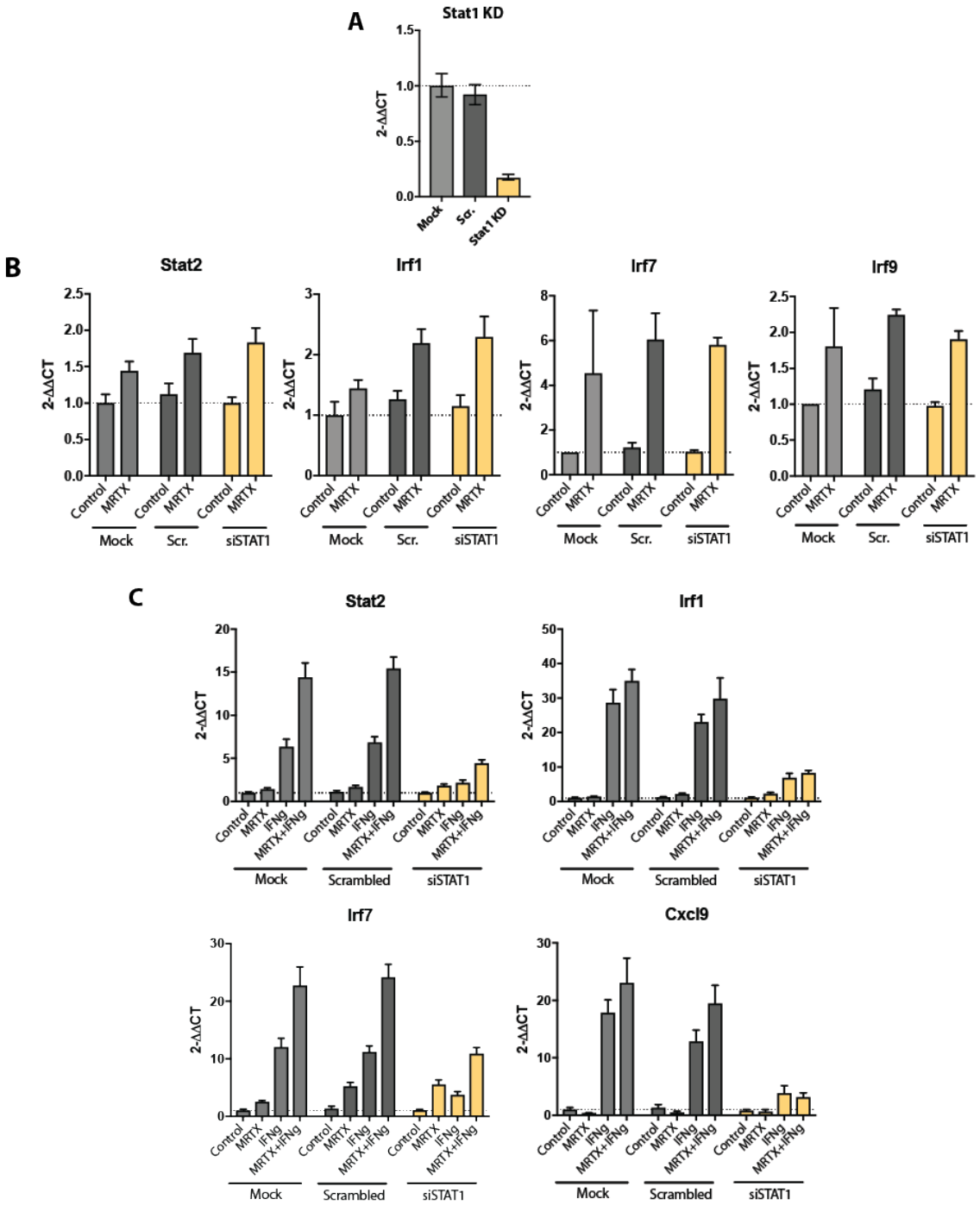

Figure 56. Silencing of Stat1 does not alter KRAS-dependent regulation of IFN genes.

A) qPCR analysis of Stat1 levels after 48h of Stat1 siRNA treatment. $2^{-\Delta\Delta CT}$ method was used for the analysis, using at least two different housekeeping genes (normalised to control, Mean+SEM of two technical replicates, one representative experiment out of 2 is shown). B) 3LL ΔNRAS cells were treated with siRNA against Stat1 for 48h before 24h treatment with MRTX (50nM, 24h). $2^{-\Delta\Delta CT}$ method was used for the analysis, using at least two different housekeeping genes

(normalised to control, Mean+SEM of two independent experiments) C) 3LL ΔNRAS cells were treated with siRNA against Stat1 for 48h before 24h treatment with MRTX (50nM) and/or IFNγ (100ng/ml) for 24h. Data was analysed as in (B).

As an alternative mechanism, we sought to examine whether known negative regulators of the IFN response could be regulated by KRAS. Suppressor of cytokine signalling 1 (SOCS1) is a JAK inhibitor (Liau et al., 2018) known to play a negative role in the regulation of IFN responses. We have observed that MRTX treatment of 3LL ΔNRAS cells reduces expression levels of the Socs1 gene (Figure 57A). Consistently, activation of oncogenic KRAS by 4-OHT administration in $KRAS^{G12V}$-ER-expressing human pneumocytes increased SOCS1 expression (Figure 57B). However, we have previously shown that inhibition of the JAK-STAT pathway does not affect the KRAS-dependent regulation of IFN responses. We therefore suggest that SOCS1, which acts by inhibiting the catalytic activity of JAK, is probably not the mediator between KRAS and IFN responses, but this hypothesis remains to be tested.

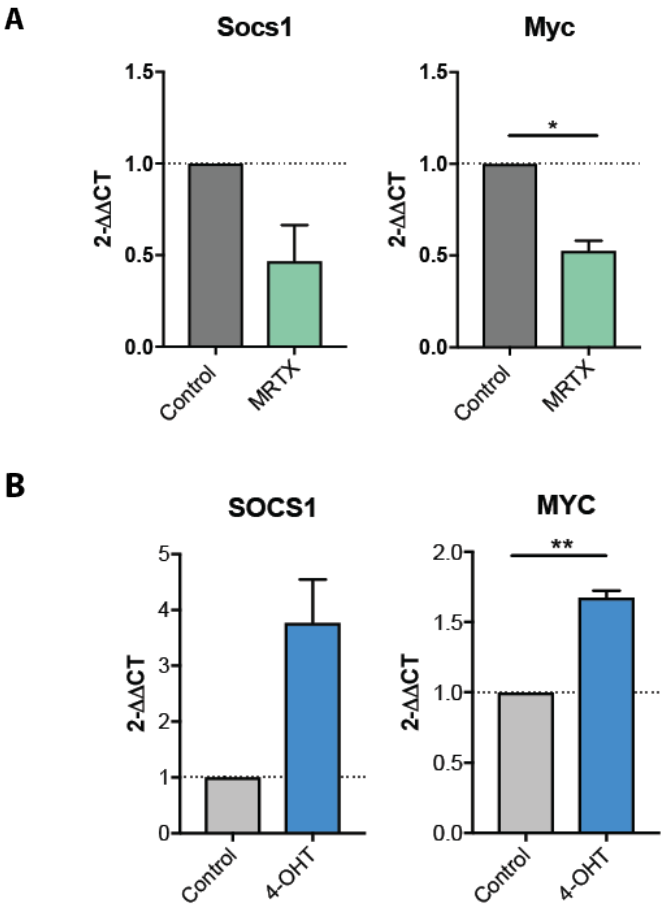

Figure 57. IFN negative regulators MYC and SOCS1 are regulated by KRAS.

A) 3LL ΔNRAS cells were treated with MRTX (50nM) for 24h *in vitro*. Graphs show qPCR data, analysed using the $2^{-\Delta\Delta CT}$ method with at least two housekeeping genes, relative to the control sample for each gene (Mean+SEM of 3 independent experiments, ratio paired Student's T test). B) Human $KRAS^{G12V}$-ER type II pneumocytes were treated with 500nM 4-OHT for 24h *in vitro*. Data was analysed as in (A).

The oncogene MYC has been previously suggested to inhibit IFN responses by direct transcriptional regulation of components of the IFN pathway (Muthalagu et al., 2020). We have observed that MYC can be transcriptionally regulated by KRAS in 3LL ΔNRAS cells and type II pneumocytes *in vitro* (Figure 57). We therefore postulate that KRAS-dependent regulation of MYC may be a possible mechanism of regulation of IFN response genes in KRAS-mutant cell lines.

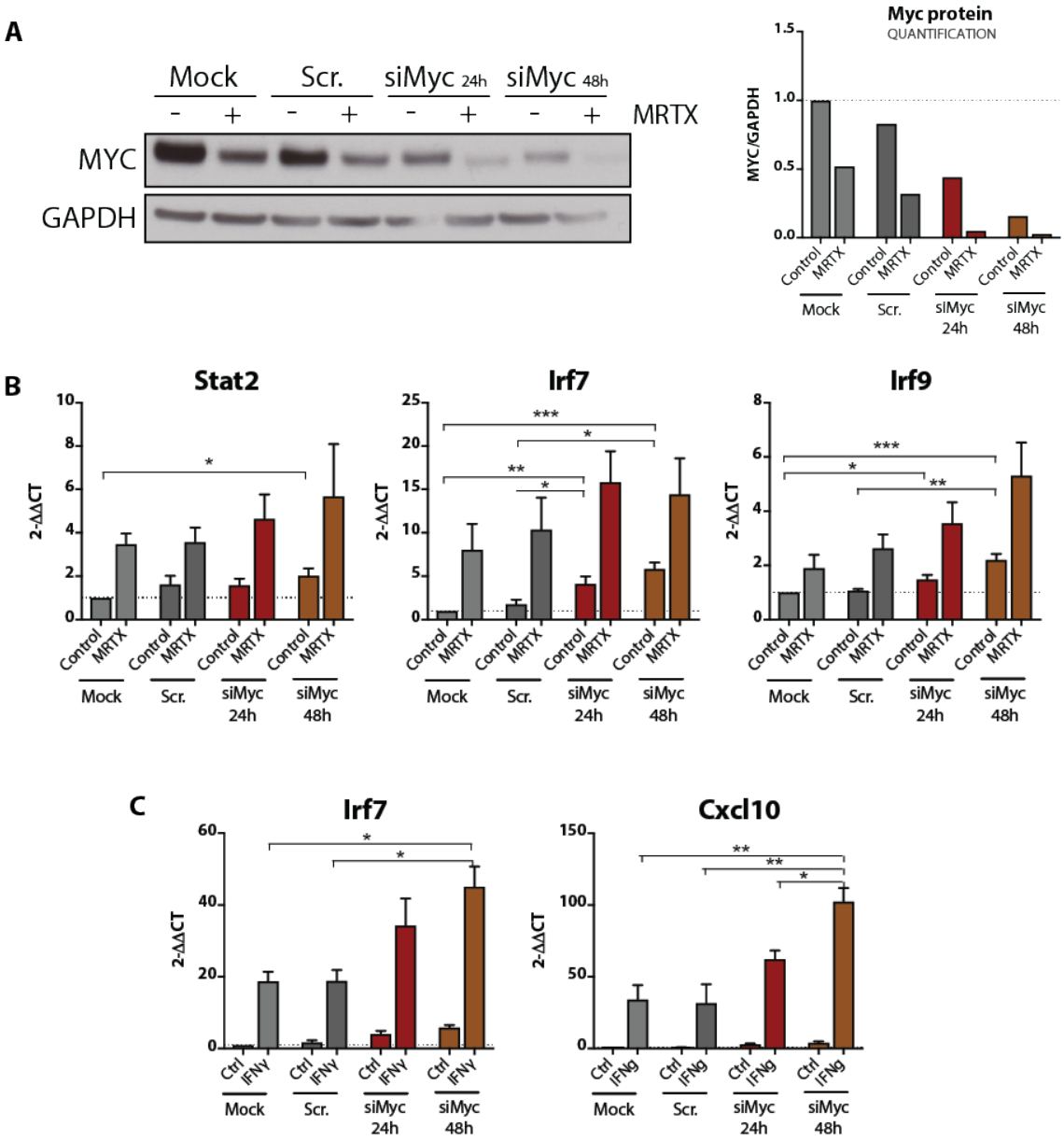

Figure 58. MYC-dependent regulation of IFN genes.

A) 3LL ΔNRAS cells were treated *in vitro* with siRNA against Myc for 24h or 48h prior to MRTX (50nM) treatment. Protein was extracted for western blot analysis 24h after MRTX treatment. One representative experiment out of two is shown, quantification of Myc (normalised to Gapdh) is displayed on the right. B) qPCR analysis. Cells were treated as in A. $2^{-\Delta\Delta CT}$ method was used for the analysis, using at least two different housekeeping genes (normalised to control, mean+SEM of three biological replicates, ANOVA multiple comparisons). C) qPCR analysis of 3LL ΔNRAS cells treated with siRNA against Myc for 24h or 48h prior to treatment with mouse IFNγ (100ng/ml). Data was analysed as in B.

In order to test this hypothesis, we silenced the expression of MYC in 3LL ΔNRAS cells by using an siRNA against the mouse Myc gene. As shown in Figure 58A (quantification on the right), we were able to reduce the protein expression of Myc about 50% after 24h of treatment with the siRNA, which was reduced even further (down to about 15%) after 48h of treatment. We then performed gene expression analyses to assess the effects of Myc knockdown on the expression of IFN pathway genes. Consistent with literature ((Muthalagu et al., 2020)), we observed an upregulation of genes such as Stat2, Irf7 and Irf9 after knockdown of Myc (Figure 58B). Nevertheless, the upregulation of these genes was stronger after KRAS inhibition (Figure 58B, grey bars), than after Myc knockdown. Importantly, the protein data shows that after MRTX treatment, MYC levels are very similar to those after 24h of MYC siRNA treatment. However, in all genes examined, the upregulation was more prominent after MRTX treatment than after 24h of MYC knockdown, suggesting Myc-independent mechanisms of regulation of these genes. This data suggests that in addition to KRAS-dependent MYC regulation, there may be further mechanisms in place that lead to the transcriptional regulation of components of the IFN pathway. Nonetheless, it is very challenging experimentally to discern the effects of MYC and KRAS, as KRAS regulates MYC expression. For example, the increase in the expression of IFN genes upon MRTX treatment after Myc knockdown may be due to an even further reduction in MYC levels (Figure 58A). As an alternative experimental approach, in the future we could make use of an inducible version of Myc (i.e. Myc-ER) to aim to rescue the effects of MRTX treatment.

Additionally, we performed an experiment where we treated 3LL ΔNRAS cells with recombinant IFNγ and/or Myc siRNA. We were able to observe that, in a similar manner to KRAS inhibition (Figure 52), Myc knockdown was able to enhance the effects of IFNγ (Figure 58C). This indicates that both oncogenes play a similar role in limiting the responsiveness of tumour cells to IFNγ. This plausibly reflects a pro-tumorigenic role of inhibition of IFN responses, likely contributing to immune evasion. The relevance of this phenomenon *in vivo* is yet to be established, and will be the subject of further investigation.

5.5 Conclusions

In this chapter, we have examined the effects of *in vivo* pharmacological KRAS^{G12C} inhibition on the tumour microenvironment of an immune evasive lung cancer model. We have described a profound remodelling of the TME and an increase in inflammatory gene expression profiles triggered by tumour-specific KRAS inhibition. These findings underscore the immunosuppressive role of oncogenic KRAS, which can be reverted by the newly developed KRAS^{G12C} inhibitors, which are currently undergoing clinical testing. Our findings are in line with the data from Amgen (Canon et al., 2019), but both have made use of transplantable murine KRAS-mutant models, which may not fully mimic human lung tumour growth. The effects of KRAS deletion on a slower growing, carcinogen-driven tumour model seem to differ and will be addressed in 6.4. We therefore need to use caution when interpreting data from transplantable models which may not reflect the tumour evolution of slower growing models and human cancer.

In this section, we have investigated the role for oncogenic KRAS signalling in dampening tumour cell-intrinsic interferon responses. This role of oncogenic KRAS potentially uncovers a new mechanism by which KRAS mutant tumours are able to evade anti-tumour immune responses, although this was not formally proven in this work and thus remains to be tested. Additionally, we have shown that treatment with KRAS^{G12C} inhibitors is able to overcome this phenomenon and enhances responses to IFNγ by tumour cells. This may possibly explain the increased immunogenicity and profound TME changes observed upon MRTX treatment *in vivo*. In addition, several reports have described a correlation between IFNγ responses and immune checkpoint blockade in cancer patients (Grasso et al., 2020), which conceivably explains the outstanding synergy observed between a KRAS^{G12C} inhibitor and anti-PD1 treatment reported in (Canon et al., 2019) using the immunogenic CT26 colon cancer model. It remains to be explored whether such a combination would also be effective in a highly aggressive and immune evasive tumour model, such as our 3LL ΔNRAS cell line. Preliminary work in the lab suggests that this combination may not be sufficient to trigger immunological rejection in this model, and therefore, future work will aim to unravel novel

combinatorial strategies to enhance immunological responses triggered by KRAS inhibitors in non-immunogenic KRAS-mutant lung cancer models.

Chapter 6. Results 4: Development and characterisation of novel spontaneous KRAS-mutant lung cancer models

6.1 Introduction

In previous chapters, we have shown the role of oncogenic KRAS signalling in shaping immune responses in KRAS-mutant lung cancer. The use of a $KRAS^{G12C}$ transplantable mouse lung cancer model has proven very useful to examine the molecular mechanisms responsible for shaping the TME and regulating the immune responses both *in vitro* and *in vivo*. Nevertheless, transplantable tumour models carry significant limitations. The rapid development of such tumours does not allow for the immune selection and tumour heterogeneity processes associated to a spontaneously developing tumour. In contrast, tumours that spontaneously arise in the lung in response to oncogenic insults more closely recapitulate the tumour evolution occurring in the clinical disease.

The most widely used mouse model of spontaneous KRAS-mutant lung cancer is the KP model developed in Tyler Jacks' lab. In this model, intratracheal adenoviral Cre recombinase delivery results in activation of oncogenic KRAS and a recombination event that leads to the loss of the Trp53 gene. These mice develop lung tumours that pathologically resemble human lung adenocarcinoma (DuPage et al., 2009). Nevertheless, research in our labhas shown that this model is not sensitive to immune therapies and shows no differential growth in immunocompetent mice and mice lacking an adaptive immune system ($Rag^{-/-}$) (de Carné Trécesson et al., 2020). We hypothesised that these tumours are not immunogenic due to a scarcity of somatic mutations, which do not result in a sufficient neoantigen burden to be recognised by the adaptive immunity.

Hence, we aimed to develop novel spontaneous mouse models of KRAS-mutant lung cancer that contain a sufficient somatic mutation burden to be likely to be recognised by the immune system. Such a model would constitute an excellent tool to examine tumour-immune system interactions in KRAS-mutant lung cancer, in a

manner that more closely recapitulates human disease than transplantable tumour models.

6.2 Widespread KRAS^{G12D} activation in lung cells leads to excessive inflammation

We commenced by developing a model that would serve as a modified version of the KP mouse, driven by oncogenic KRAS and deletion of p53. One of the drawbacks of the KP mouse model, as mentioned before, is the lack of mutation burden that likely leads to an insufficient number of neoantigens. In order to increase the likelihood of immune recognition, we added a gene encoding for the human APOBEC3B cytidine deaminase. APOBEC is a family of single-stranded DNA C-to-U editing enzymes that play a role in the defence against viral infections due to their DNA editing capabilities. In cancer, APOBEC family members are often dysregulated and lead to an increase in somatic mutations that have pro-tumorigenic effects (Wang et al., 2018). The APOBEC family member APOBEC3B is frequently upregulated and its target sequence is frequently found mutated in NSCLC patients (Burns et al., 2013). The increased mutation burden triggered by APOBEC3B has been associated with survival benefits in response to immunotherapy, suggesting that APOBEC3B induced mutations can increase the visibility of tumours to the immune system (Wang et al., 2018).

In replacement of intratracheal Adeno-Cre delivery, we developed our mouse model making use of the Sftpc-CreERT2 system. In this system, tamoxifen administration will induce stabilisation of the Cre recombinase specifically in surfactant protein C (SPC)-expressing alveolar type II epithelial cells (Gui et al., 2012), shown to be the cell of origin of lung adenocarcinoma (Pikor et al., 2013), leading to activation of an oncogenic KRAS and deletion of p53 as tumour initiating events and expression of the APOBEC transgene. In this manner, we sought to avoid unspecific recombination and transformation events in cells other than lung epithelial cells, such as immune cells in the lung. In order to visualise recombination events, we added a ubiquitously expressed membrane-targeted tdTomato - membrane-targeted GFP (mTmG) cassette, where activation of Cre results in GFP expression by the cell. A summary of the breeding strategy for this model (labelled as sKPAT) is displayed in Figure 59.

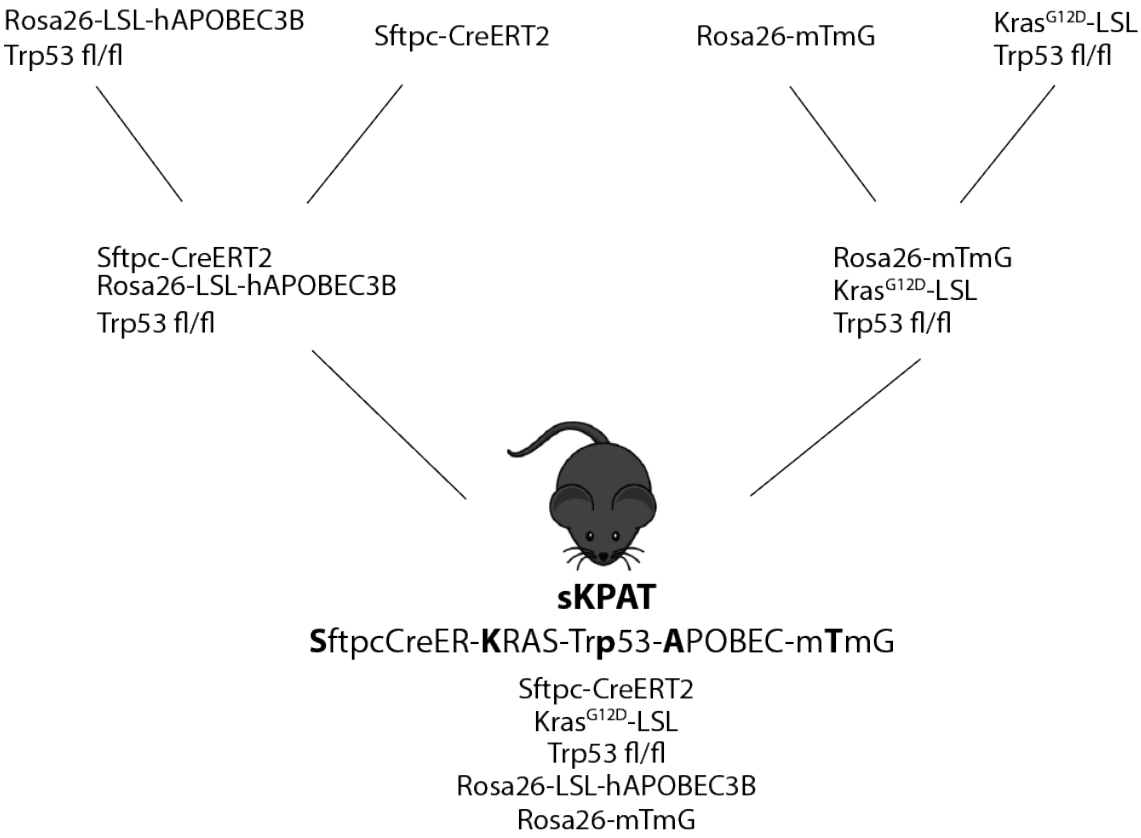

Figure 59. sKPAT model breeding strategy.

Once the sKPAT mouse model was bred, we administered three doses of tamoxifen to 8-10-week-old mice to initiate tumour growth. We expected tumours to require approximately 12-14 weeks to develop, following the growth kinetics of the KP mice (DuPage et al., 2009). Nevertheless, approximately two weeks after tamoxifen administration, mice started developing lung-related symptoms such as heavy breathing, leading to an abrupt end of the experiment. An extensive histopathological analysis of the lungs of these mice found the presence of bronchiolo-alveolar early stage carcinomas and hyperplasias expanding in the lung parenchyma, probably as a consequence of oncogenic processes activated in these cells (Figure 60A, left). This neoplastic process triggered an abnormal production of surfactant by the type II pneumocytes (Figure 60A, right). In adjacent lung parenchyma, predominantly at the periphery of the lobes, alveolar spaces were found to be filled with a large number of macrophages, which we were able to confirm by macrophage marker F4/80 staining (Figure 60A and B). This heavy cellular infiltration, probably in response to the high levels of surfactant and

inflammatory signals secreted by neoplastic cells, were attributed as the cause for the clinical signs displayed by the animals. We hypothesised that the Sftpc-CreERT2 system led to a widespread activation of oncogenic KRAS simultaneously, which initiated a strong inflammatory response that affected the respiratory health of these mice. We confirmed this by GFP staining of the lungs, where we indeed found GFP expression throughout the entirety of the lung (Figure 60C). It is noteworthy to mention that mice that had not been part of the experiment eventually began to exhibit similar symptoms, even in the absence of tamoxifen (Figure 60B and C), suggesting that the Sftpc-CreERT2 system can lead to leakiness. Taken together, these results show the inadequacy of this system to be used as a model KRAS-mutant lung cancer.

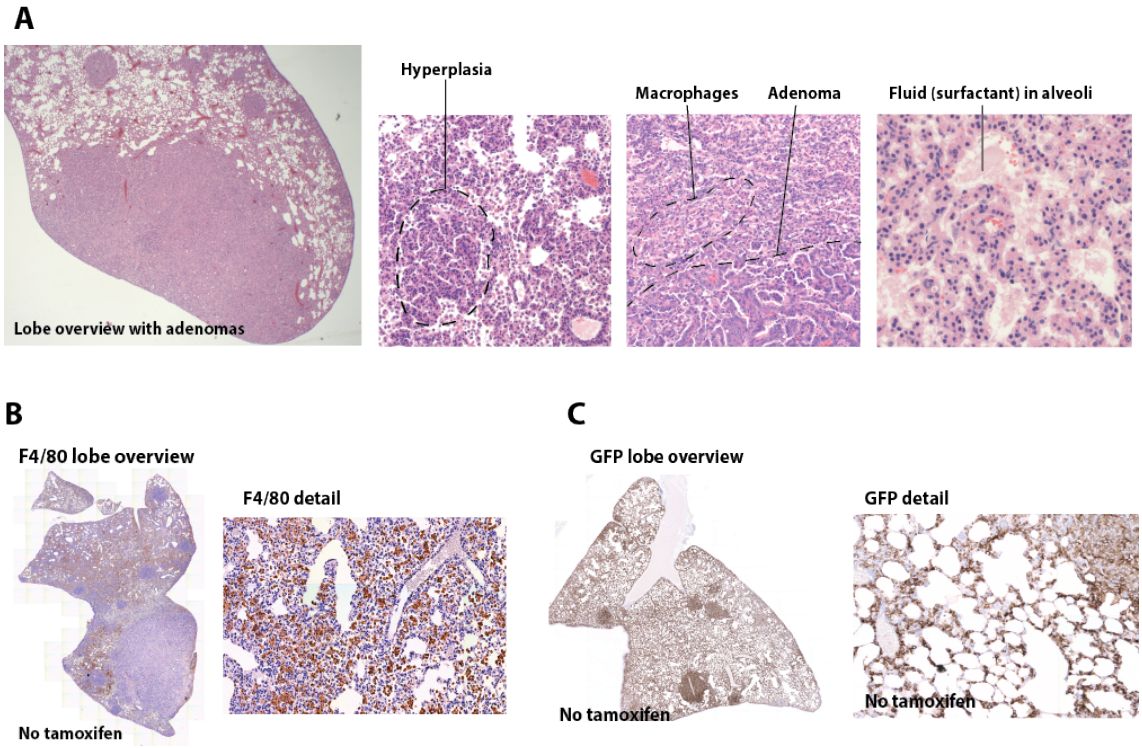

Figure 60. Histological analysis of the sKPAT mouse model.

A) H&E staining of lungs. An overview of a whole lung is displayed (left) and details of hyperplasia, macrophage infiltration and surfactant accumulation are shown on the right (10X and 20X magnification, respectively). B) Immunohistochemical analysis of F4/80 expression, a whole lobe and a more detailed picture are represented (10X and 20X magnification, respectively). C) Immunohistochemical analysis of GFP expression, a whole lobe and a more detailed picture are represented (10X and 20X magnification, respectively).

6.3 Development and characterisation of urethane-based mouse lung cancer models

6.3.1 Tumour growth kinetics of novel urethane-based models

The use of an inducible version of oncogenic KRAS under a lung cell specific promoter proved to not be suitable as a model for KRAS-mutant lung cancer. We therefore sought alternative manners to develop KRAS-mutant lung cancer models with a high mutation burden. One of the ways to achieve this is to induce lung tumour formation by carcinogen administration. Urethane is a carcinogen known to trigger the formation of lung tumours driven by a $KRAS^{Q61R}$ mutation that contain an average of 185 single-nucleotide variations (SNVs) in FVB mice (Westcott et al., 2015). However, we wanted to use the C57Bl/6 strain to be able to breed other genes onto our model and this strain is known to be less sensitive to urethane-induced tumour formation (Gurley et al., 2015).

To overcome this hurdle and accelerate tumour growth in C57Bl/6 mice, we firstly engineered our mouse model to contain a floxed allele for Trp53 under the previously described Sftpc-CreERT2 promoter (Figure 61A, model ur-sP – **ur**ethane-**S**ftpcCreER-Tr**p**53-). We hypothesised that the loss of the tumour suppressor p53 would increase the aggressiveness of the tumours, provided that the oncogenic transformation by urethane and the p53 loss would occur on the same cell. In addition, inactivation of p53 in other alveolar cells should not result in their oncogenic transformation, hence avoiding the concerns with the excessive inflammation described before.

As depicted in Figure 62 (blue bars in Figure 62A), the ur-sP model led to lung tumour growth after administration of three doses of urethane and subsequent three doses of tamoxifen in the course of two weeks. Tumour growth was monitored by regular CT scanning, with the first tumours arising 12 weeks post-urethane administration. However, to achieve a tumour burden high enough to be used in therapeutic experiments the model required a latency of about 35-40 weeks, which may be too long to feasibly work with.

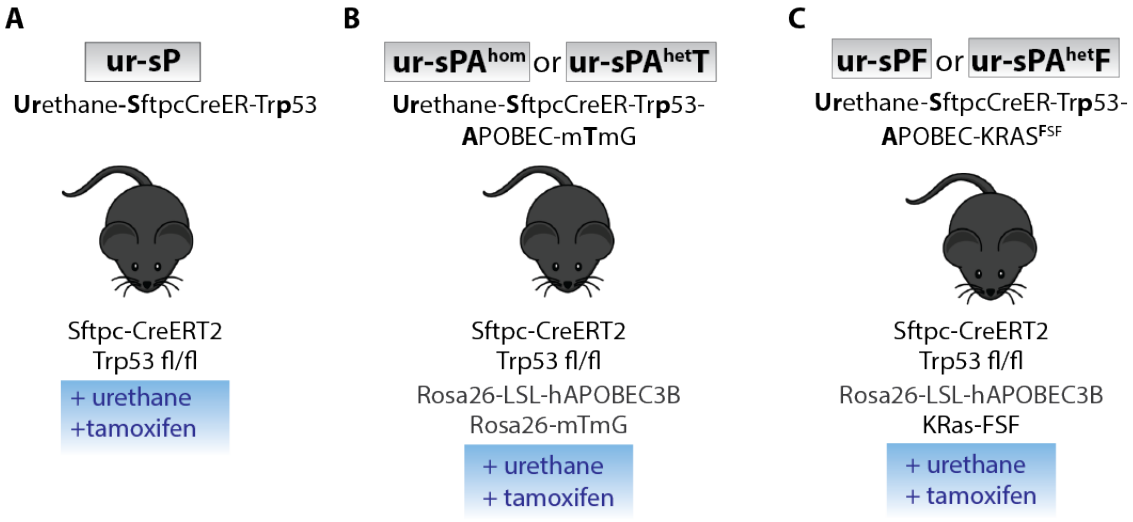

Figure 61. Schematics of urethane-based models.

We aimed to increase the mutational burden and potential aggressiveness of this model by adding the human APOBEC3B transgene mentioned in 6.2. In addition, we added the aforementioned mTmG cassette to be able to track recombination events (Figure 61B). In a technical note, it is important to note that both the mTmG and the APOBEC3B gene are expressed under the same ubiquitous (Rosa26) promoter, hence we could not obtain both genes expressed in homozygosity. Therefore, two versions of these models were assessed, one where both APOBEC and mTmG were expressed heterozygously (ur-sPA^{het}T, –**ur**ethane-**S**ftpcCreER-Tr**p**53-**A**POBEC^{het}-m**T**mG-), and one where APOBEC was expressed homozygously (but no mTmG reporter was introduced, ur-sPA^{hom}, –**ur**ethane-**S**ftpcCreER-Tr**p**53-**A**POBEC^{hom}). Both versions had a very different tumour growth kinetic (Figure 62A, purple and red bars). The ur-sPA^{het}T version (purple bars) had a very slow tumour growth up until 20 weeks post induction, and the growth thereafter was comparable to the previous ur-sP model. In contrast, the ur-sPA^{hom} model (Figure 62A, red bars) developed tumours more rapidly and in a larger number than the ur-sP and ur-sPA^{het}T models. A number of reasons could explain this variable growth. There could be a dose-dependent activity of APOBEC3B, where when expressed homozygously, it leads to an increase in mutation burden that increases the aggressiveness of the tumour, for which its heterozygous expression is not sufficient. Additionally, we cannot rule out the immunogenicity of the GFP protein expressed after the recombination of the mTmG cassette. An immune rejection of this antigen could explain the slower growth of this tumours,

compared with the previous model, in the onset. These tumours would then develop immune evasive properties and escape. Lastly, these experiments carry a lot of variability, so the experiment would have to be repeated in order to fully understand the mechanisms underlying differential tumour growth in these three models.

A

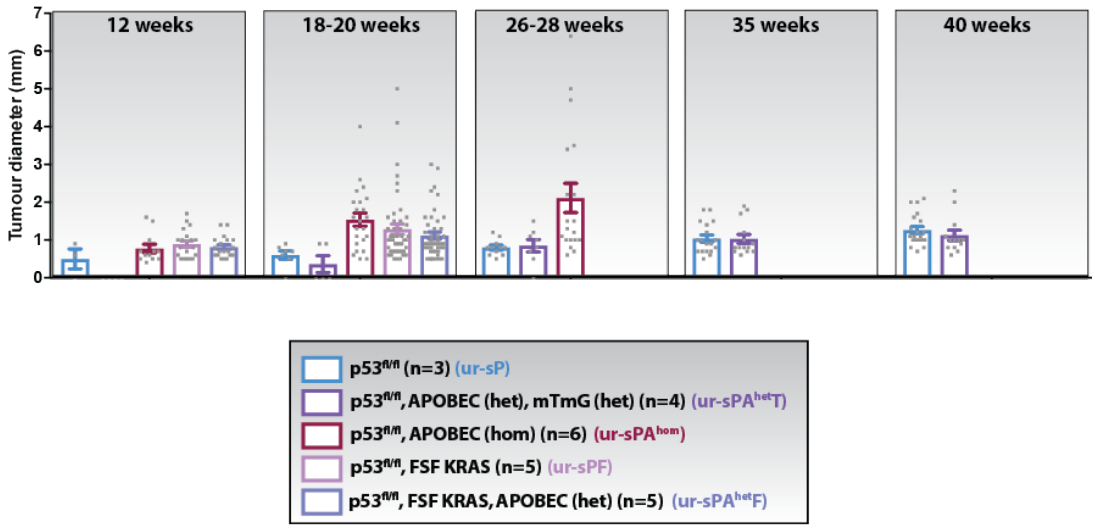

B

Average number of tumours per mouse

	12 weeks	18-20 weeks	26-28 weeks	35 weeks	40 weeks
ur-sP	1.0	2.3	3.7	6.0	6.7
ur-sPA^{het}T	0.0	0.5	2.0	3.5	3.3
ur-sPA^{hom}	2.0	3.8	3.2	NA	NA
ur-sPF	4.0	9.2	NA	NA	NA
ur-sPA^{het}F	3.8	9.0	NA	NA	NA

Figure 62. Tumour growth of urethane-based models.

A) Tumour diameter data per time point after urethane treatment as obtained by CT analysis (data obtained and analysed by Chris Moore). Each dot represents one tumour (mean±SEM). This graph shows pooled data from different experiments. B) Summary of average number of tumours found by CT imaging per mouse. NA=non-applicable (experiments had been terminated due to high lung tumour burden by these time points). het=heterozygous, hom=homozygous.

Finally, it has been reported that the wild-type allele accompanying a heterozygous KRAS mutation has tumour suppressive properties (Westcott et al., 2015) (Zhou et al., 2016). We hypothesised that losing this wild-type allele would increase the aggressiveness of the tumour and result in a more rapid tumour progression or a larger number of tumours. Hence, we bred in our model a Kras allele that is preceded by a FRT-STOP-FRT cassette. In the absence of FLP administration, this allele is effectively silenced, and hence, these mice would only express one (wild-type) allele of KRAS, which will become mutated in a subset of lung cells after urethane administration. In these transformed cells, there would be no wild-type KRAS allele to inhibit tumour growth (Figure 61C). For this model, we also developed two versions, one driven by urethane and loss of p53 only (ur-sPF, –**ur**ethane-**S**ftpcCreER-Tr**p**53-KRAS$^{\mathbf{F}SF}$-), and one with additional expression of APOBEC, ur-sPA^{het}F –**ur**ethane-**S**ftpcCreER-Tr**p**53-**A**POBEC$^{\mathbf{het}}$-KRAS$^{\mathbf{F}SF}$- (Figure 62A, pink and light purple bars). These two models developed tumours in a larger number (Figure 62B) than the previous models described, with mice having to be sacrificed due to high mutation burden 20 weeks post-urethane administration. Expression of the mutagen APOBEC in this setting did not make a clear difference in tumour growth. We hypothesised that this model may be too rapid to allow for the mutagenesis incurred by APOBEC to occur. The fact that APOBEC is expressed in a heterozygous manner could also explain its lack of effect on tumour growth, consistent with previous findings. It will be crucial in all these models to assess their somatic mutation burden by whole exome analysis to better understand the role of urethane- and APOBEC-driven mutagenesis.

6.3.2 Assessment of the immunogenicity of the new urethane-based models

To begin to address the immunogenicity of these tumours, we performed a FACS analysis of their TME using the antibody panel described in (Figure 27). We firstly assessed the immune infiltration of the ur-sPA^{hom} model (Figure 61B) approximately 30 weeks after tumour initiation by urethane and tamoxifen (Figure 63A). The overall amount of infiltrating immune cells in these tumours was not different compared to a healthy lung sample (Figure 63B, left). Within the immune compartment however, as expected, the composition of populations was profoundly

altered, with an overall exclusion of adaptive cells accompanied by an expansion of the myeloid compartment, as displayed Figure 63B (right). The only significant changes included an exclusion of NK cells, suggesting this model may be susceptible to NK cell cytotoxicity, and an expansion in the neutrophil compartment. This observation is in line with the role of oncogenic KRAS in promoting the expression of neutrophil chemoattractant molecules (see 4.6). There was a trend, albeit non-significant, towards T cell exclusion, suggestive of immune evasive properties acquired by the tumour. Regarding T cell phenotypes, as displayed in Figure 63C, we encountered a decrease in naïve T cells accompanied by an increase in antigen-experienced T cells (effector and memory). In line with this finding, particularly in the CD8 compartment, PD-1-expressing T cells were significantly increased (Figure 63D). These results suggest that the immune system has encountered foreign antigens, probably stemming from the tumour cells, and increases our confidence in the immunogenicity of this tumour model. We could also observe an increase in MHCII-expressing macrophages, potentially serving as a source for T cell priming (Figure 63E). We therefore hypothesised that this tumour model was likely able to be recognised by the immune system and comprised a suitable model to examine responses to immunotherapies such as immune checkpoint blockade. We believed that the rest of urethane-driven models described here, which are driven by the same oncogenic events, would display a comparable immune landscape.

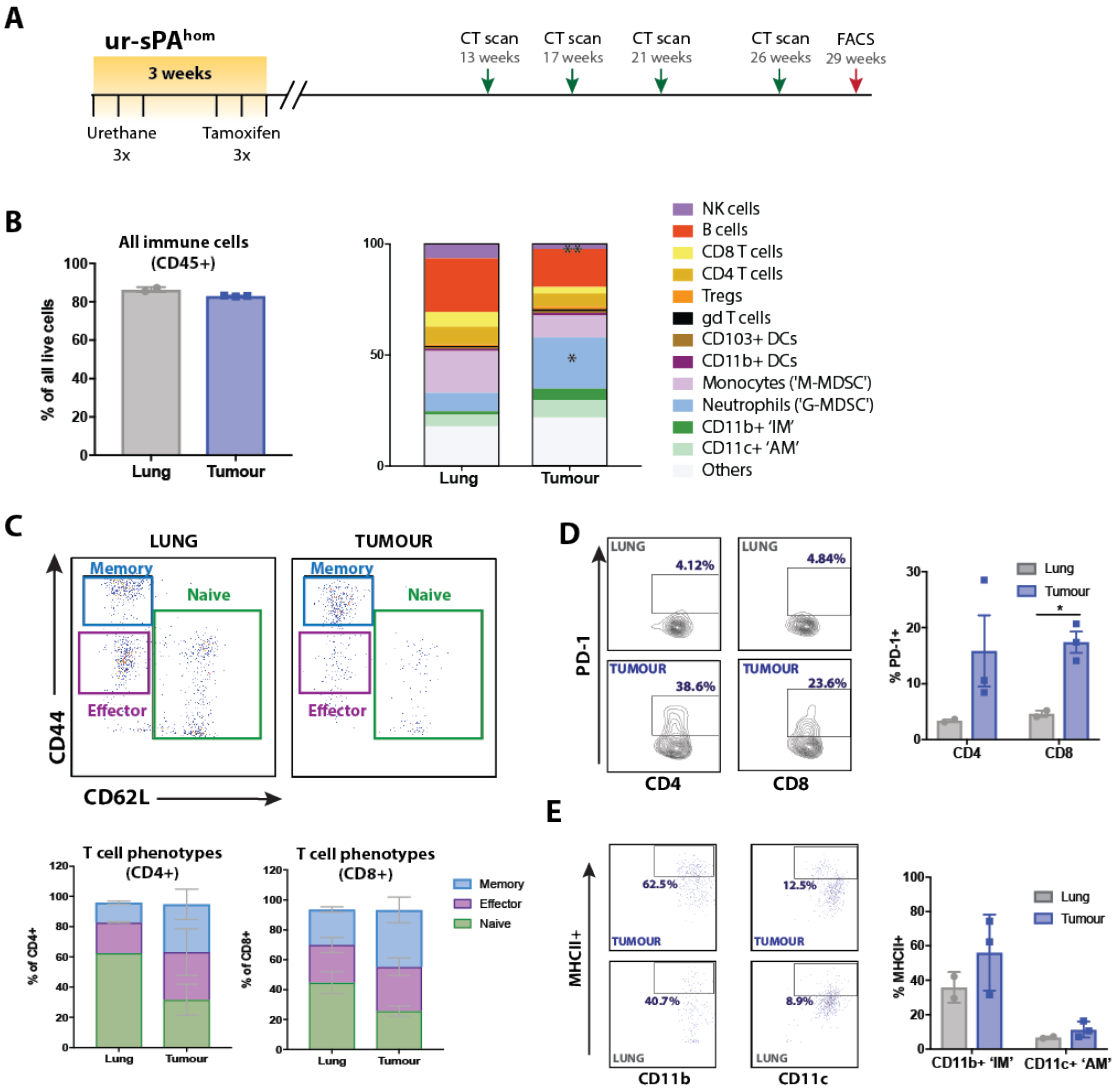

Figure 63. Immune phenotyping of ur-sPA^{hom} model.

A) Schematics of immunophenotyping experiment in the ur-sPA^{hom} model. B) Overall immune infiltration in the ur-sPA^{hom} model (left, n=3, each dot represents one mouse), compared to healthy lung (n=2, each dot represents one mouse, student's T test). Summary of all immune cell populations examined (right), gating strategy to identify populations is described in Figure 28. DC=dendritic cells, IM=interstitial macrophages, AM= alveolar macrophages. C) Assessment of T cell phenotypes based on the expression of CD44 and CD62L. (Mean±SD). D) PD-1+ T cells (Mean±SD, student's T test). E) MHCII expression on macrophages (pre-gated to obtain CD11b+ or CD11c+ macrophages as in Figure 28 (Mean±SD, student's T test).

We then assessed whether our models could be responsive to immunotherapy treatment strategies, by treating lung tumours with a combination of the checkpoint blockade (ICB) antibodies anti-PD-L1 and anti-CTLA-4 (Sharma and Allison, 2015).

A response to treatments aimed to boost anti-tumour immune responses would serve as evidence that this tumour model is indeed visible by the immune system. For this experiment, we made use of the ur-sPF and ur-sPA^{het}F models, as they were able to yield a larger number of tumours at an earlier time point as shown in Figure 62. Tumours were treated with ICB approximately 18 weeks post-urethane administration (Figure 64A). Since no growth differences were found between ur-sPA^{het}F (APOBEC+) and ur-sPF (APOBEC-) tumours (Figure 62A), both subsets were used, albeit evenly distributed across control and treatment groups to avoid any potential bias. In the results shown in Figure 64, mice of both genotypes were pooled, since when data was analysed separately for sPA^{het}F and ur-sPF tumours no significant changes were found. Figure 64B shows that there was no difference in pre-treatment tumour sizes in the randomised experimental groups, measured by microCT scan analysis. Mice were administered with either IgG isotype control (5 mice) or a combination of the anti-PD-L1 and anti-CTLA-4 monoclonal antibodies (4 mice) for a total of four doses during the course of two weeks. There was no significant difference in tumour volume change after treatment across experimental groups (Figure 64C), at any of the time points analysed (1, 2 or 4 weeks after treatment initiation), suggesting that the ICB treatment had no effect on tumour growth in this setting.

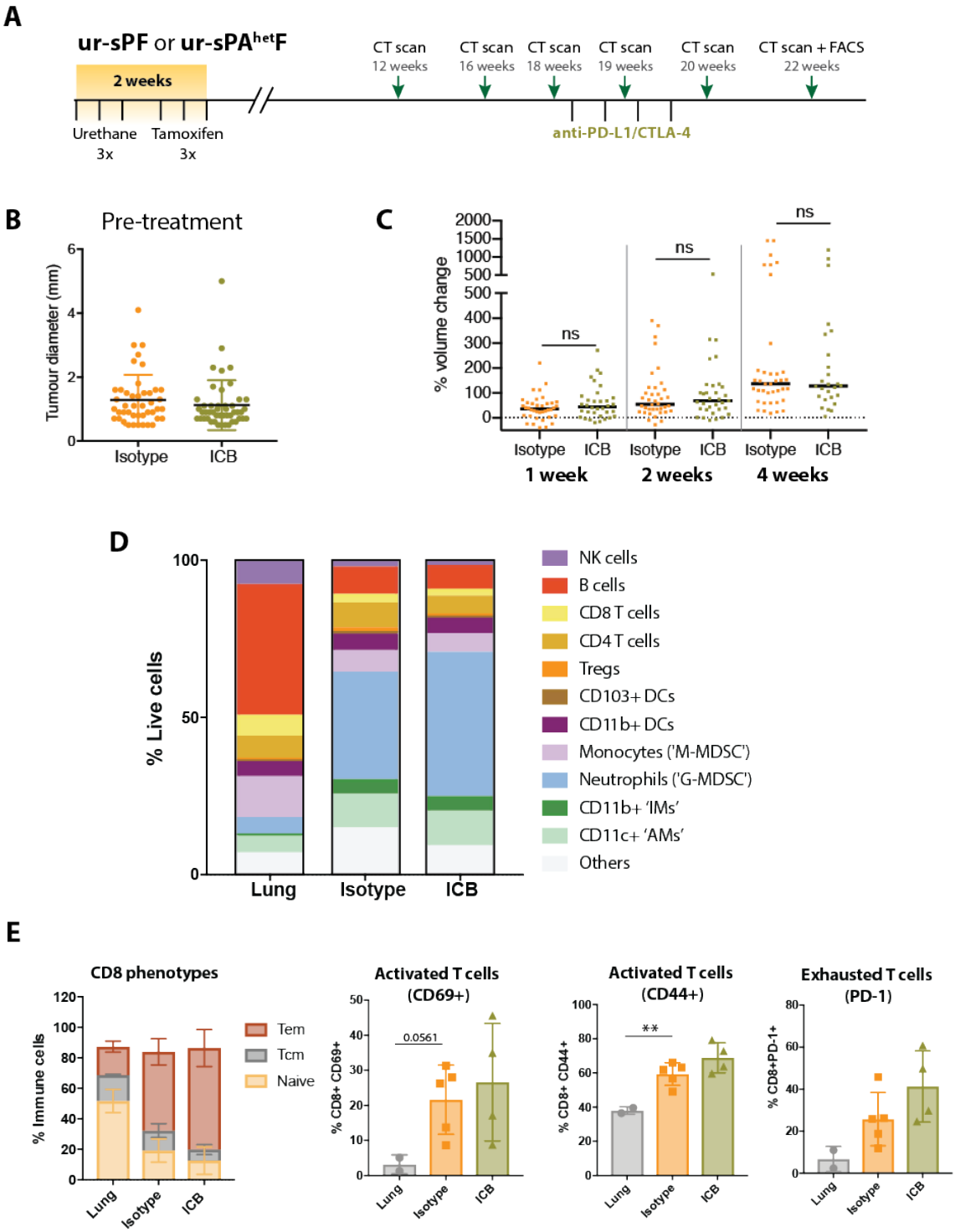

Figure 64. Immunotherapy response of ur-sPF and ur-sPA^{het}F models (pooled).

A) Schematics of ICB experiment. B) Tumour diameter measured by CT scan data obtained and analysed by Chris Moore. Animals were randomised into two experimental groups: IgG isotype control (n=5) and anti-PD-L1/CTLA-4 (ICB, n=4). Mean±SEM. C) Tumour volume changes relative to pre-treatment sizes for both experimental groups at different time points post-treatment. Tumour volume data based on CT scanning obtained by Chris Moore. Black line represents mean,

Mann-Whitney test. D) Summary of all immune populations analysed by FACS following the gating strategy described previously (Figure 28). Samples of healthy lung from two C57Bl/6 were taken as a reference. E) T cell phenotype analysis obtained by FACS (gated as in Figure 63C). Graphs show the mean±SEM, analysed by an unpaired Student's T test. Tem: T effector memory, Tcm: T central memory.

Four weeks after treatment initiation, mice were sacrificed to examine their TME by FACS analysis. Figure 64D shows a summary of the immune composition of these tumours compared to a healthy lung. As expected, control tumours displayed an exclusion of cytotoxic and adaptive cells, accompanied by an expansion of myeloid cells, consistent with the results from the previous model. Treatment with ICB did not seem to significantly alter the composition of the TME, consistent with the previous finding that no effects were observed on tumour growth. We observed an expansion of neutrophils in the ICB treatment group, which could potentially suggest an inflammatory response to tumour cell death, although this increase was not significant. We sought to find evidence of increased T cell activation by examining T cell phenotypes (Figure 64E). The naïve T cell compartment was decreased in control tumours compared to healthy lung, suggestive of a previous T cell activation. We found a further decrease in the naïve compartment, together with an increase in the Tem compartment after ICB treatment, though none of these observations were significant. Together with this finding, we observed a trend towards increased activated and exhausted cells after ICB treatment, although not significant. We therefore concluded that although we did find some slight evidence towards an increased activated T cell compartment, the effects were very mild and could possibly explain the lack of therapeutic efficacy of ICB in this model.

We cannot exclude the possibility that these models do not harbour a sufficient amount of mutation-derived neoantigens to elicit an anti-tumour immune response, even when they express the mutagen APOBEC. This could be due to the fact that in this model, in contrast to the previous one we immunophenotyped, APOBEC is expressed heterozygously. In the future, we will perform a whole exome sequencing analysis to elucidate the mutation burden of this and the rest of our mouse models to fully comprehend the immunogenicity of all the models and if possible, link them to their APOBEC status. Additionally, treatment with ICB alone

could be insufficient to boost the immune response in this setting. In fact, most therapeutic approaches for NSCLC in the clinic include a combination of chemotherapy regimens with ICB (according to NICE© guidelines). The use of chemotherapy in combination with ICB could be useful to trigger a degree of immunogenic cell death that will promote antigen release and T cell priming, potentially increasing ICB efficacy. It will be interesting to test such approaches in our mouse models as a manner to determine their immunogenicity.

6.4 Urethane-based models for genetic KRAS deletion

6.4.1 Long-term effects of KRAS deletion on spontaneous tumour growth

We have made use of urethane-based approaches to obtain potentially immunogenic mouse models of KRAS-mutant lung cancer. However, the main goal of this thesis is to elucidate mechanisms by which oncogenic KRAS mutations in lung tumours modulate their TME, and to assess how blocking such signals, either experimentally or therapeutically, affect the TME composition and anti-tumour immune responses. Thus far, we have made use of $KRAS^{G12C}$ inhibitors and transplantable KRAS-mutant mouse cell lines to answer these questions, but we are aware of the caveats of such systems, namely that they do not fully recapitulate the evolution of a spontaneously arising malignancy. Unfortunately, as far as we are aware, there are no spontaneous mouse models of $KRAS^{G12C}$ mutant lung cancer that have a large number of mutations, as the only spontaneous model available, to our knowledge, is the G12C version of the KP mouse (Li et al., 2018). Thus, we developed an alternative way in which we could inhibit oncogenic KRAS in urethane-based lung cancer models. We made use of the $K\text{-}Ras^{lox}$ allele described in (Puyol et al., 2010) as a tool to delete the KRAS gene in our models. In this system, the mouse Kras gene is flanked by lox sites, and administration of Cre recombinase leads to its deletion. When bred homozygously, it leads to the complete loss of the KRAS gene. Using this tool, we have generated a number of mouse models, summarised in Figure 65.

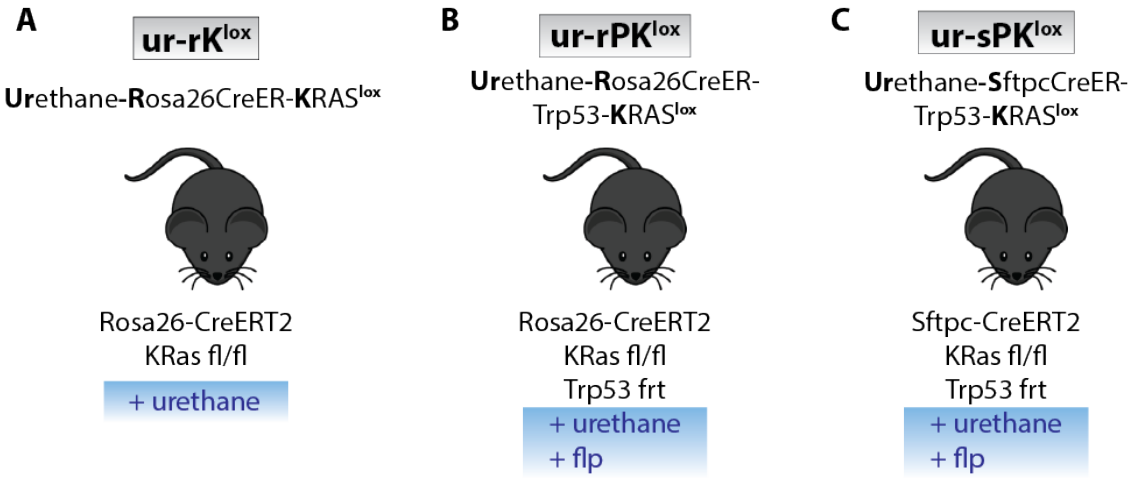

Figure 65. Urethane-based, inducible KRAS deletion models.

Firstly, we developed a mouse model harbouring the KRAS^{lox} allele and a ubiquitously-expressing (Rosa26) CreERT2 allele. In this system, administration of tamoxifen would lead to the loss of the KRAS gene in the whole organism (Figure 66A). We initiated tumours by administration of three doses of urethane, as described before. We monitored tumour growth by CT scanning and when tumours reached an adequate size, they were treated with tamoxifen for KRAS deletion. Tamoxifen treatment led to a halt in tumour growth, evidenced by the fact that by 44 weeks, all mice in the control group had been sacrificed due to a large tumour burden, while most of the mice in the tamoxifen-treated group were still alive, as displayed in Figure 66A (some mice did have to be sacrificed for reasons other than a large tumour burden). This finding gave us confidence that we could indeed successfully eliminate KRAS in this model, and that this led to a significant improvement in tumour progression.

Nevertheless, as mentioned before, C57Bl/6 mice are largely resistant to urethane treatment, explaining the long latency of this model. We therefore inserted a Trp53^{frt} allele, similarly to previously described models, to increase the aggressiveness of the tumours and lead to a more rapid tumour progression. We were also concerned that loss of KRAS in all cells by the use of a ubiquitous promoter for Cre could potentially carry toxicities. In order to avoid this, for one of the models we made use of the previously described lung-specific Sftpc-CreERT2 promoter (Gui et al., 2012) (Figure 65B and C, models ur-rPK^{lox} –**ur**ethane-**R**osa26CreER-Tr**p**53-**K**RAS$^{\mathbf{lox}}$- and ur-sPK^{lox} –**ur**ethane-**S**ftpcCreER-Tr**p**53-**K**RAS$^{\mathbf{lox}}$-).

As displayed in Figure 66B, we treated these mice with urethane for tumour initiation, followed by administration of Flp virus to delete p53. We then monitored tumour growth and at 26 weeks post-urethane, tumours reached a sufficient size to be readily detected and all mice were treated with tamoxifen to delete KRAS. We followed tumour growth of these models pre-treatment, as illustrated by the tumour diameter in Figure 66B (below, left), and found no significant differences in the basal tumour growth of these models. To determine the effects of tamoxifen treatment, we then measured reduction in tumour growth as a percentage of the

tumour volume of each tumour in the pre-treatment scan, so we could individually follow the growth of each tumour. In the ur-rPK^{lox} model, ubiquitous KRAS deletion by tamoxifen administration led to a dramatic reduction in tumour volume, which was sustained in time up to 16 weeks after treatment (Figure 66B, below right, green bars). In contrast, in the ur-sPK^{lox} model, despite showing significant early tumour shrinkage, approximately 1/10 of tumours relapsed late after tamoxifen administration (Figure 66B, below right, blue bars). This relapse was sustained despite a re-administration of tamoxifen 9 weeks after first tamoxifen dosing (Figure 66B, below right, red arrows), suggesting that this was not due to a lack of insufficient Cre exposure. Tumour relapse occurred in 4/5 mice, indicating that this phenomenon was widespread and not an isolated event in a reduced subset of mice. We hypothesised that some tumour cells could lose the expression of the Sftpc gene before the administration of tamoxifen, as a result of a potential de-differentiation process during tumour growth. Loss of the Sftpc gene would result in loss of expression of CreER in these cells, meaning that these cells would continue to express KRAS even after tamoxifen administration. We believe that tamoxifen is able to delete KRAS in a large number of cells, evidenced by the profound tumour regression that we observed. However, the cells where KRAS has not been deleted continue to grow and eventually lead to the relapse observed in a number of tumours. Further experiments examining KRAS recombination in this setting will be necessary to confirm our hypothesis.

We therefore concluded that biallelic loss of KRAS in urethane-based tumour models leads to a profound tumour regression. We also suggest that the ur-rPK^{lox} mouse is a suitable model to examine long-term mechanisms of resistance to KRAS inhibition, as tumours seemed to be beginning to relapse by the end of the experiment. In contrast, this could not be performed using the ur-sPK^{lox} model, as we believe that tumour relapse in this model reflects a technical caveat rather than a biological mechanism of resistance. However, we were primarily interested in examining short-term effects of oncogenic KRAS loss on anti-tumour immune responses, for which both models can be used as they both show strong evidence of KRAS loss at relatively short time points (up to 4 weeks post-KRAS deletion).

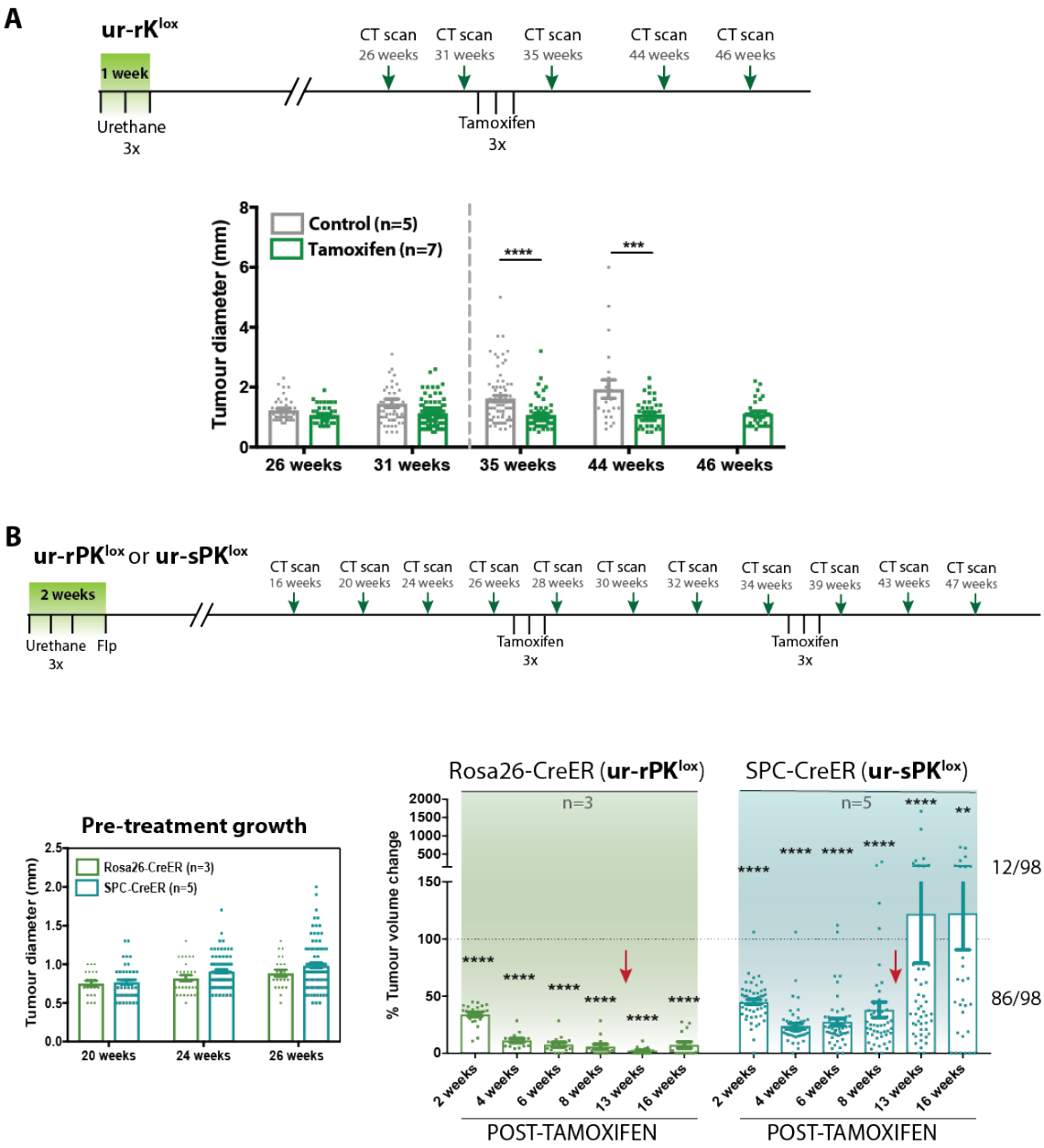

Figure 66. Effects of KRAS deletion on tumour growth.

A) Schematic of experiment with ur-rK^{lox} mice (above). CT scan data (below, obtained by Chris Moore) of tumour diameters before and after treatment (Mean±SEM, Mann Whitney test). Control n=5 mice, tamoxifen n=7 mice. Each dot represents one tumour. B) Schematic of experiment with ur-rPK^{lox} and ur-sPK^{lox} mice (above). Tumours grow in a similar kinetic (below, left, quantification of tumour diameter) before tamoxifen treatment (mean±SEM, ur-rPK^{lox} n=3 mice, ur-sPK^{lox} n=5 mice). Each dot represents one tumour. Data of tumour volume change, as a percentage of the tumour volume pre-treatment for each mouse (obtained by Chris Moore, mean±SEM, Mann-Whitney test). Each dot represents one tumour. Red arrows indicate time points of tamoxifen re-administration.

6.4.2 Short-term effects of KRAS loss in the TME in urethane-based models

We made use of our mouse models of genetic KRAS deletion to perform short-term experiments in order to be able to validate our previous findings using the therapeutic $KRAS^{G12C}$ inhibitor (Chapter 5) in a spontaneous tumour setting. Firstly, we used a cohort of ur-rPK^{lox} and ur-sPK^{lox} mice to assess changes in immune infiltration by flow cytometric analysis after genetic KRAS deletion (Figure 67A). For this experiment, only ur-sPK^{lox} mice received tamoxifen, whereas a mixture of both strains were included in the control group. The reason for this is that SPC-Cre mediated lung-specific KRAS loss is more specific than Rosa26 driven ubiquitous KRAS loss, and thus more comparable to tumour-specific pharmacological $KRAS^{G12C}$ inhibition. Pre- and post-treatment CT scan data showed that all tamoxifen-treated tumours were regressing at the time of tissue harvest (Figure 67B). This data confirmed that tamoxifen mediated KRAS deletion was successful in this experiment.

We then carried out flow cytometric analysis of control and tamoxifen-treated ur-sPK^{lox} tumours using our immune profiling FACS panel. Mice were treated with tamoxifen for a total of 6 days. As shown in Figure 67C, we did not detect any changes in infiltration of different populations of T cells after KRAS deletion. Additionally, infiltrating CD8+ T cells did not show any significant differences in their activation status after tamoxifen treatment (Figure 67D and E). This data is in stark contrast with our previous observations using the $KRAS^{G12C}$ inhibitor, which was able to induce significant T cell activation in the immune microenvironment of 3LL ΔNRAS tumours (5.2). In the myeloid compartment, monocyte influx was significantly increased after tamoxifen treatment, together with an increase in the interstitial macrophage population (Figure 67F). Even though there was a non-significant trend towards increased CD103+ cross-presenting DCs after KRAS deletion, we found no differences in the infiltration of MHCII+ macrophages, a finding that we had observed in our $KRAS^{G12C}$ inhibitor experiment (5.2).

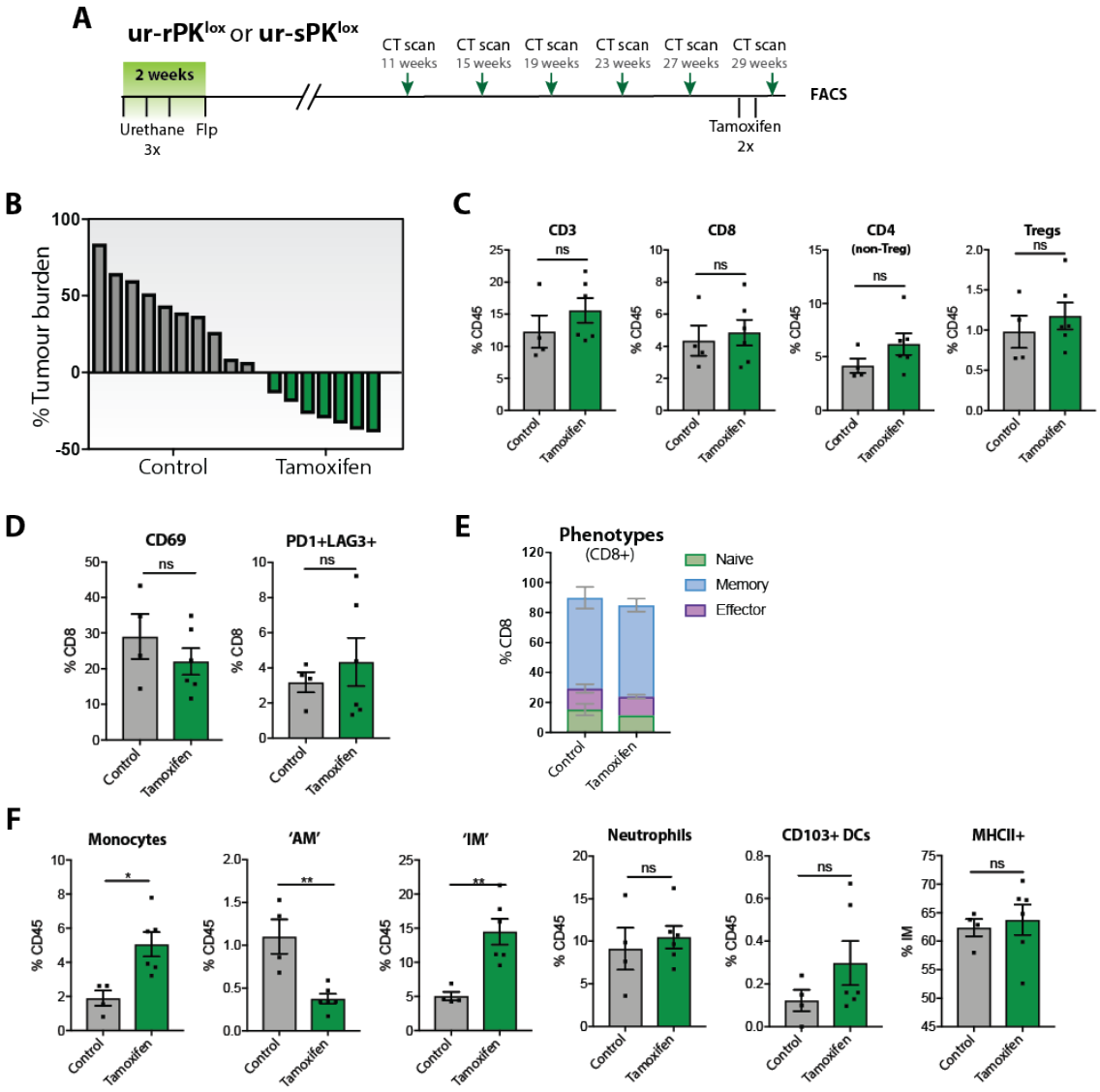

Figure 67. Short-term KRAS deletion FACS analysis.

A) Schematic of short-term KRAS deletion immunophenotyping experiment. B) CT analysis data of variation mouse tumour volumes (mm^3) in control and tamoxifen (150mg/kg) groups in pre- and post-treatment scans. C) FACS analysis data of T cell populations (gated as in Figure 28). Control n=4, tamoxifen n=6, each dot represents one mouse, Mean±SEM, Student's T test. D) Assessment of T cell phenotypes based on the expression of CD44 and CD62L E) Examination of T cell activation/exhaustion markers (statistical analysis as in C). F) Myeloid cell population data (analysis as in C).

We therefore were unable to successfully validate our findings of $KRAS^{G12C}$ inhibition on the remodelling of the TME in this spontaneous KRAS genetic loss model. On one hand, we believe that 6 days of treatment may not be enough to observe changes in the lymphocyte compartment. In addition, we hypothesise that,

in contrast to pharmacological inhibition in the 3LL ΔNRAS model, genetic KRAS deletion in this model leads to strong tumour regression, probably associated to a high degree of tumour cell death. We also believe that the increased influx of myeloid cells reflects an inflammatory response to signals from dying tumour cells rather than a direct consequence of the inhibition of oncogenic KRAS signalling. We therefore concluded that the strong effects of KRAS deletion on tumour cell viability make this model unsuitable to assess changes in immune infiltration upon loss of oncogenic KRAS signalling.

In another experiment, we treated urethane driven tumour-bearing KRAS^{lox} mice with tamoxifen for a total of 4 days, after which we assessed changes in gene expression between control and tamoxifen-treated groups (Figure 68A). We hypothesised that a shorter treatment time would at least partially prevent the large degree of tumour cell death observed in Figure 67.

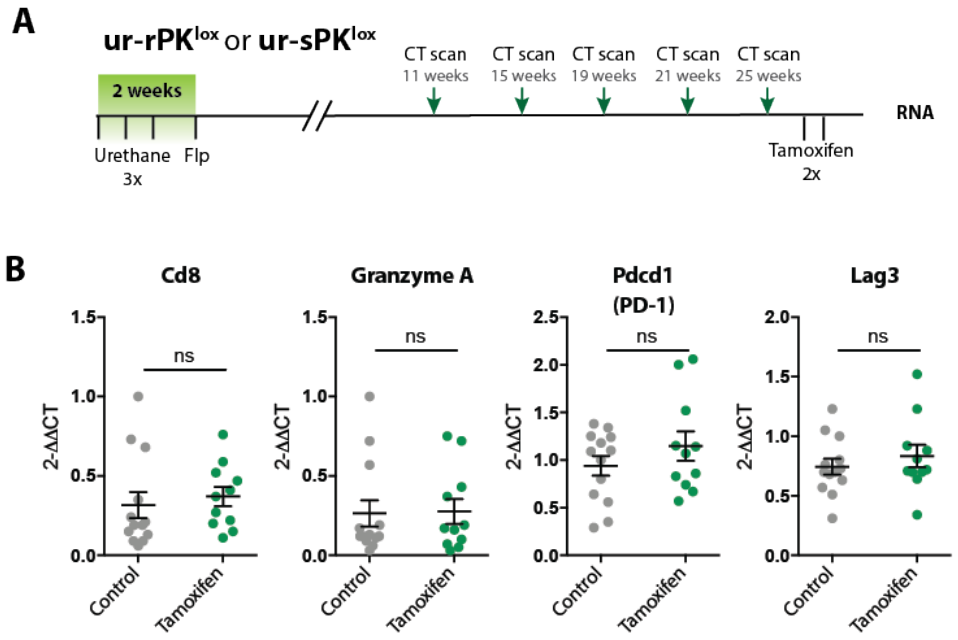

Figure 68. Short-term KRAS deletion RNA analysis (immune infiltrate).

A) Schematic of short-term KRAS deletion RNA experiment. B) Gene expression analysis was performed using the $2^{-\Delta\Delta CT}$ method, normalised to one control sample for each gene (control n=13, tamoxifen n=11 tumours). Mean±SEM, Student's T test.

In line with our previous findings, we encountered no changes in gene expression of CD8+ T cells, cytotoxic molecule Granzyme A and activation/exhaustion markers PD-1 and Lag3 (Figure 68B). This data recapitulates previous observations that genetic KRAS deletion in this model does not trigger a remodelling of the T cells in the TME of urethane-driven tumours. In addition, in this experiment mice were only treated with tamoxifen for 4 days, which may not be enough to trigger *de novo* T cell priming and exhaustion.

This experiment also allowed us to assess transcriptional effects after abrogation of KRAS signalling. As shown in Figure 69A, known KRAS-target genes Dusp6, Etv4 and Myc were significantly downregulated after tamoxifen treatment, confirming successful KRAS deletion. We then used this model to validate our findings on the crosstalk between KRAS signalling and the IFN response (see section 5.4). We found that KRAS deletion in this setting led to an upregulation of the IFN pathway genes Stat2 and Irf7, while JAK negative regulator Socs1 was significantly decreased (Figure 69B, top). Additionally, T cell chemoattractant molecules Cxcl9 and Cxcl10 were also significantly upregulated, together with the antigen presentation machinery component B2m (Figure 69B, bottom).

This data confirms our previous findings using a MRTX1257, where $KRAS^{G12C}$ inhibition was able to increase IFN response genes *in vivo* in a transplantable model of NSCLC. This data also highlights the suitability of this model to assess transcriptional effects of acute KRAS deletion *in vivo*, in a urethane-driven spontaneous model of lung cancer, as a strong KRAS inhibition is achieved after only 4 days of tamoxifen treatment.

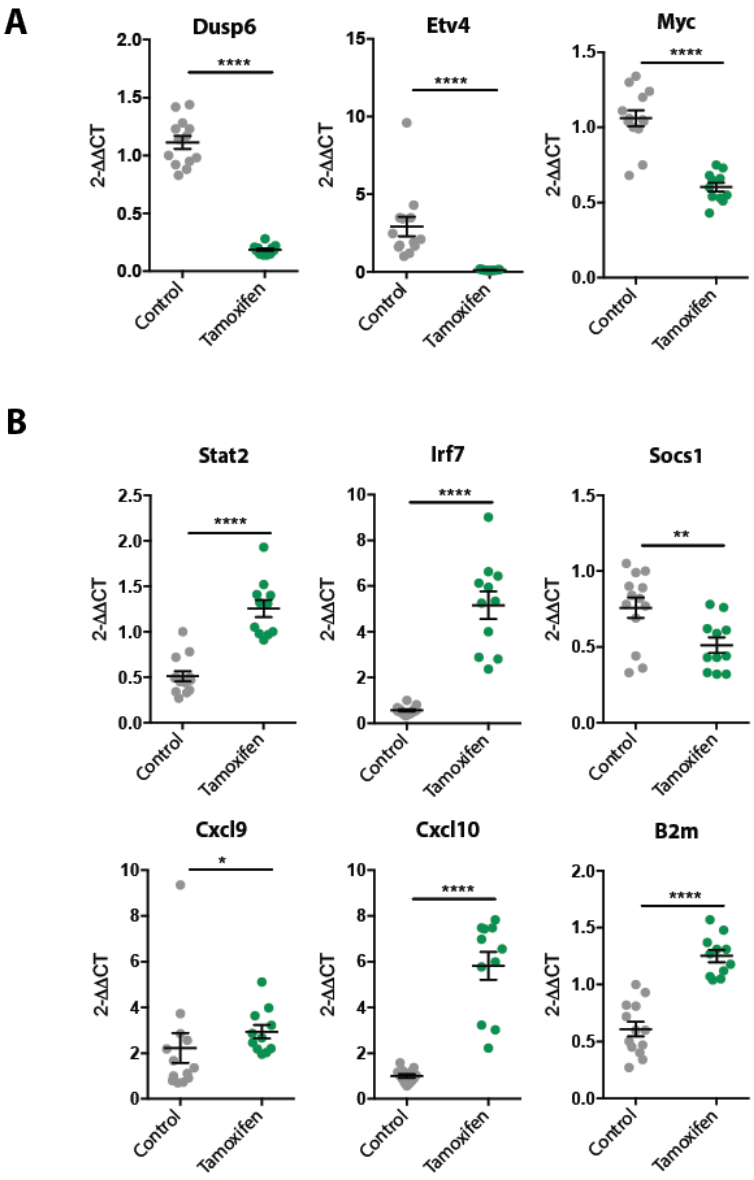

Figure 69. Short-term KRAS deletion RNA analysis (RAS pathway).

A) Gene expression analysis of KRAS target genes. Analysis was performed using the $2^{-\Delta\Delta CT}$ method, normalised to one control sample for each sample (control n=13, tamoxifen n=11 tumours). Mean±SEM, Student's T test. B) Gene expression analysis of IFN response genes. Analysis was performed as in (A).

6.5 Conclusions

In this chapter, we have shown the development of novel spontaneous mouse models of KRAS-mutant lung cancer. These models are based on administration of the carcinogen urethane to induce highly-mutated lung tumours which we hope to be visible to the immune system. Although we have not yet performed genomic analyses on these tumours to examine their mutational burden, we have shown some limited evidence of immune cell activation after tumour induction. Other APOBEC-expressing models in the lab have shown to harbour a larger number of mutations than non APOBEC-expressing tumours (de Carné Trécesson et al., 2020), but this remains to be tested in our models. Nevertheless, our models (and other urethane driven and APOBEC expressing models in the lab known to have higher mutation burden (de Carné Trécesson et al., 2020) do not seem to respond to immunotherapeutic approaches. The link between increased mutational burden and responses to immunotherapy is disputed, as it merely reflects a higher likelihood of immune recognition by the tumour and is likely just one of all the different processes occurring in tumours that may affect anti-tumour immunity (Chan et al., 2019). The slower growing nature of these types of tumours, however, render them more similar to clinical cancer than other transplantable models described elsewhere (Chapter 3), and thus may comprise models for non-ICB responsive NSCLC patients. It would have been interesting to harvest samples of these tumours at different stages of development to elucidate their mechanisms of immune evasion (by single cell RNA sequencing, for instance), which may shed light into processes occurring in human cancer. In retrospective, given the disputed nature of the predictive value of TMB on immunogenicity, it is unclear whether the addition of APOBEC to these models was an adequate approach and perhaps the focus should have been on examining the characteristics of these faster growing (p53 deleted and with one KRAS allele floxed) urethane-driven tumours in order to find novel therapeutic targets.

In addition, we have developed spontaneous urethane-based models of genetic KRAS deletion that can be used to investigate short-term and long-term effects of KRAS loss, including resistance mechanisms, which may be of general interest given the current clinical advent of novel KRAS inhibitors. Using these models,

KRAS inhibition appeared to have none of the consequences on the remodelling of the TME observed in Chapter 5. We suggest that the slower growth of this model allows for a complete regression of the tumours after KRAS inhibition, which is not observed in our transplantable models. This marked tumour regression could potentially mask all the effects on TME remodelling observed in other models, but this hypothesis remains to be tested. This model is in line with clinical data using $KRAS^{G12C}$ inhibitors, where a large number of patients show marked tumour regression (Hong et al., 2020), again underscoring the preponderance of spontaneous models in reflecting human tumours than transplantable models. Preliminary data presented here suggests long-term tumour relapse that could reflect resistance mechanisms that will be of future investigation and could shed light into potential resistance mechanisms arising in the clinic.

Chapter 7. Discussion

7.1 Introduction

The work in this thesis has aimed to elucidate mechanisms of immune evasion triggered by oncogenic KRAS in lung cancer. We have established that KRAS is able, via a myriad of manners, to establish an immunosuppressive microenvironment and evade anti-tumour immune responses.

In addition, with the advent of novel $KRAS^{G12C}$ inhibitors, we have assessed the effects of such drugs on the immune microenvironment. We have shown that, consistent with the immunosuppressive role of KRAS, inhibiting tumour cell intrinsic KRAS signalling results in profound changes in the TME to render tumours more inflammatory and less immunosuppressive.

For the purpose of this thesis, we have developed and characterised a number of murine models of NSCLC. We have made use of a derivative of a known murine $KRAS^{G12C}$-mutant transplantable cell line to explore KRAS-induced immune evasion mechanisms and assess the effects of newly developed $KRAS^{G12C}$ inhibitors on the TME. Furthermore, we have also developed new carcinogen-driven models as spontaneous models of lung cancer and aimed to rise their mutational burden to increase their visibility to the immune system.

7.2 Mouse models of KRAS-mutant lung cancer, beyond KP

Classic mouse tumour models to study KRAS-mutant lung cancer include genetically engineered mouse models (GEMM) and transplantable cell lines, both of human and murine origin. Each of these models has its advantages and caveats. The use of human cell lines, or patient derived xenografts (PDX), is extremely practical, as they can be cultured *in vitro* for mechanistic experiments and also grown *in vivo*. There is a wide range of such cell lines available, carrying different driver mutations and alterations, reflecting the molecular heterogeneity found in human cancer. Here, we have used human lung cancer cell lines to perform an initial characterisation of the transcriptional effects $KRAS^{G12C}$ inhibitors. Their human origin makes them suitable for mechanistic studies, but as tumour models, they need to be grown in immunodeficient mice to avoid immunological rejection. Hence, as *in vivo* models, they are not useful for studies of anti-tumour immunity. In addition, we have made use of murine cell lines, which can be transplanted into immunocompetent mice to perform *in vivo* studies. Unfortunately, murine cell lines are scarcer and are thus more limited in the variety of genomic alterations that they exhibit. Additionally, the tumour evolution of a transplanted cell line *in vivo* does not recapitulate the heterogeneity present in spontaneously arising tumours and human cancer.

Alternatively, GEMMs where lung tumours can be genetically induced (by expression of an oncogene often accompanied by loss of a tumour suppressor gene) in the lung may more closely recapitulate the tumour growth and evolution of a human cancer arising from oncogenic insults. Spontaneous models of KRAS-mutant lung cancer, such as KP, has been of great use to elucidate molecular mechanisms of tumour growth, but due to their scarcity of somatic mutations (Chung et al., 2017) they may not be ideal for studies of the adaptive immune system.

The advent of new models driven by the administration of carcinogens may yield a higher mutational burden and more closely recapitulate human disease evolution (Westcott et al., 2015). However, C57Bl/6 mice are known to be resistant to chemically-induced carcinogenesis (Tuveson and Jacks, 1999), so we aimed to

genetically engineer C57Bl/6 mice to make them susceptible to carcinogens. We found that removal of the tumour suppressor gene Trp53 and loss of the wild-type allele of Kras can increase the aggressiveness and hence reduce the latency of lung tumours after urethane administration in C57Bl/6 mice. The fact that the loss of the wild-type allele of KRAS was able to speed up tumour growth has been previously shown and is evidenced by the frequent loss of heterozygosity of RAS genes in murine carcinogenesis studies and human cancer (Westcott et al., 2015) (Mainardi et al., 2014). A number or potential molecular mechanisms having been reported to explain the tumour suppressor function of the wild type allele of RAS, which may well vary across models, tumour entities and the precise RAS isoform involved, as reviewed in (Zhou et al., 2016).

We propose that, thanks to the genetic alterations introduced, our new C57Bl/6 urethane-based lung cancer models are suitable for experimental studies due to their relatively short latency. In our systems, all mice exhibited tumours (1-3 tumours per mouse depending on the model) 18-20 weeks post administration of three doses of urethane. This was more efficient than an average of approximately one or two tumours per mouse found 24 weeks after ten doses of urethane reported in (Miller et al., 2003). The exact somatic mutation burden of our models remains to be characterised but, based on the literature, we expect it to be higher than classical models such as KP (Westcott et al., 2015). It will likewise be interesting to address whether, with our new C57Bl/6 models, we are able to recapitulate the mutational burden of urethane-induced of the known FVB and BALB/c-based models.

In addition, we have tried to combine urethane treatment with the expression of genes that increase mutagenesis, such as the cytidine deaminase APOBEC, to further increase the mutational load. Dysregulations in APOBEC family members occur frequently in cancer and they have been extensively associated with increased somatic mutation burden (Burns et al., 2013) and increased sensitivity to immunotherapy in mouse cancer models ((Driscoll et al., 2020)) and in the clinical setting (Wang et al., 2018). This data suggests that APOBEC-induced mutations can promote neoantigen-mediated immune recognition. As a preliminary result, we found that homozygous expression of APOBEC increases tumour growth, but we

failed to observe this in a heterozygous expression model. It will be crucial to determine the mutational burden of these tumours, to elucidate whether addition of APOBEC expression is able to increase the number of mutations in this model. Additionally, APOBEC-mediated mutagenesis is widely known to contribute to the rise of subclonal mutations that increase tumour heterogeneity and presence of subclonal neoantigens (Swanton et al., 2015). Mutation burden analysis of our tumours may shed light on the contribution of APOBEC to the emergence of subclonal mutations in our models. We aimed to increase the mutational load of our models to increase our chances for this model to be visible to the immune system. However, it is necessary to bear in mind the controversy of such a correlation and therefore, other means need to be undertaken in order to properly assess the immunogenicity of our models.

We aimed to examine the immunogenicity of such models by ICB treatment, but in our experiment, these mice failed to respond to anti-PD-L1/CTLA-4 treatment. We postulate that while treatment with immunotherapy alone may not be sufficient for tumour regression in this model, perhaps a rational treatment combination aimed at increasing immune visibility could render these tumours susceptible to immune rejection. In clinical settings, ICB treatments can be administered in combination with chemotherapy ((Saigi et al., 2019) and NICE© guidelines). The use of chemotherapy could trigger immunogenic cell death and promote antigen release and T cell priming. It will be interesting to assess whether this treatment combination has any efficacy in our tumour models. Nonetheless, responsiveness to immunotherapy is not the only manner to assess the immunogenicity of a tumour. Alternatively, it could be interesting to examine the growth of this tumour model in an immunodeficient background, or to deplete cytotoxic T cells (for instance by making use of CD8-neutralising antibodies) to examine the contributions of the adaptive immune system on the growth of this tumour model. Work remains to be done on these models, but we are confident that we have generated a short-latency urethane-based KRAS mutant lung cancer model that can be used to investigate aspects of the TME and other therapeutic treatments.

Urethane administration results in $KRAS^{Q61R}$ mutations that act as tumour drivers (Westcott et al., 2015). Thus, our urethane-based models cannot be used to

investigate the use of $KRAS^{G12C}$ inhibitors. Therefore, as an alternative, we have developed spontaneous models where KRAS can be deleted genetically during tumour development ($KRAS^{lox}$). Inducible deletion of genes involved in tumorigenesis, such as B-Raf and C-Raf, has been of utmost relevance to elucidate their role in tumour development and examine outcomes of targeted therapies (Blasco et al., 2011). In a similar manner, we have used our $KRAS^{lox}$ mice to assess the effects of KRAS loss on urethane-driven tumour growth and to validate our findings obtained with the use of $KRAS^{G12C}$ inhibitors. Our $KRAS^{lox}$ models can be useful to not only assess the effects of such inhibition on anti-tumour immunity, but also resistance mechanisms and rational combination strategies in a spontaneous immunocompetent setting that closely recapitulates the human disease.

7.3 KRAS signalling exerts immunosuppressive actions

The main goal of this project was to identify and characterise molecular mechanisms by which oncogenic KRAS signalling could promote immunosuppression. We have made use of an array of different models (human cell lines, murine cell lines and spontaneous mouse models) and taken advantage of the new $KRAS^{G12C}$ inhibitors as a tool to elucidate tumour cell-intrinsic KRAS-driven mechanisms. Our findings add to the growing evidence supporting non-tumour cell intrinsic, immunoregulatory functions of oncogenes, such as Myc (Rakhra et al., 2010) (Sodir et al., 2011) (Casey et al., 2016, Kortlever et al., 2017) and tumour suppressor genes, such as p53 (Spranger and Gajewski, 2018) (Wellenstein et al., 2019) in cancer. Such roles and mechanisms have also been described for oncogenic KRAS, in immunodeficient models of cancer (Sparmann and Bar-Sagi, 2004) (Ancrile et al., 2007) and in models of colorectal and pancreatic cancer (Pylayeva-Gupta et al., 2012) (Liao et al., 2019). Here, adding on to previous published research from our lab (Coelho et al., 2017), we have shown that oncogenic KRAS promotes immunosuppressive actions in immunocompetent models of lung cancer by driving a myriad of different mechanisms that affect different biological processes, summarised in Figure 70. The use of a large number of different systems has revealed that several mechanisms (i.e. particular cytokines secreted, specific genes regulated) largely vary across the models examined. However, the different mechanisms observed consistently lead to immunosuppressive actions and evasion of immune responses.

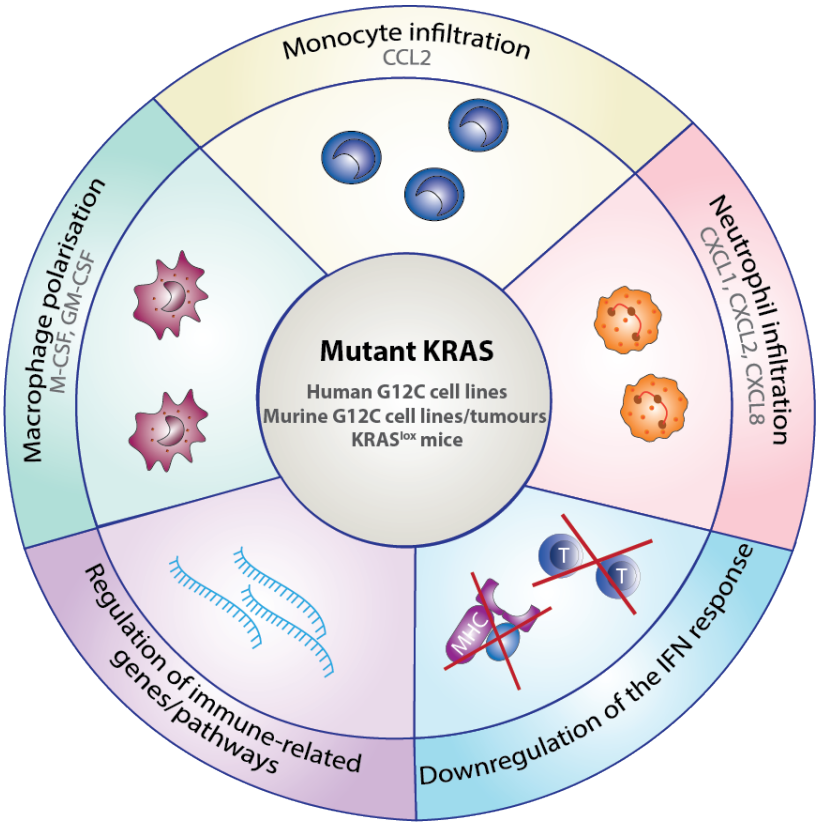

Figure 70. Summary of KRAS-mediated immune suppressive mechanisms

One mechanism that we have identified reveals a connection between oncogenic KRAS signalling and a downregulation of tumour cell-intrinsic IFN responses, a correlation which had previously been described in other contexts (Muthalagu et al., 2020) (Klampfer et al., 2003), albeit the specific molecular mechanisms underlying this phenomenon differed from the ones reported in this thesis. This again highlights the aforementioned diversity in model- or tumour type- specific molecular mechanisms driven by KRAS that ultimately converge in the same biological outcome, namely a downregulation of IFN responses in presence of oncogenic KRAS. The IFN pathway contributes to immune responses by affecting processes like antigen presentation and recruitment of effector cells. We have observed that KRAS signalling directly affects such responses in a wide range of models, hence providing a universal mechanism for immune evasion in KRAS-mutant NSCLC. It will be of outmost importance to deeply characterise the role of KRAS in shaping IFN responses, and how that leads to immune suppression in NSCLC. Classically, the presence of IFNγ signalling in tumours has been associated with the presence of anti-tumour, activated T cells (Kellar et al., 2015).

Similarly, defects in the IFN pathway have been associated with resistance to immunotherapy treatments (Zaretsky et al., 2016). Moreover, more recently it has been suggested that tumour cell-intrinsic IFN type I signalling plays an important role in tumour progression and anti-tumour immunity (Musella et al., 2017). In contrast, other reports have described a detrimental role for sustained IFN signalling in responses to immune checkpoint blockade (Benci et al., 2016) (Jacquelot et al., 2019). We propose that, while boosting IFN responses as a consequence of KRAS signalling inhibition may have a beneficial impact on anti-tumour immune responses, careful consideration will have to be taken when designing treatment regimens to avoid the undesired effects of an exacerbated IFN signalling.

We have also identified several mechanisms by which KRAS-driven oncogenic signalling contributes to the recruitment and/or polarisation of myeloid cells in the TME. Gene expression analysis of KRAS-inhibitor treated human cell lines and RNA and protein analysis of our 3LL ΔNRAS model *in vitro,* has revealed that a number of factors that play a role in macrophage polarisation, such as GM-CSF and M-CSF, are KRAS-dependent in a number of models. The role of KRAS in inducing GM-CSF production had already been described in a model of pancreatic cancer (Pylayeva-Gupta et al., 2012), but we suggest this mechanism may also play a role in KRAS-mutant lung cancer. M-CSF had not been described as a KRAS-dependent cytokine before, so it will be important to characterise this mechanism, especially considering that M-CSF levels have been correlated with poor survival in lung cancer (Baghdadi et al., 2018). Consistently, we have observed a repolarisation of macrophages to a more pro-inflammatory phenotype when treating tumours with $KRAS^{G12C}$ inhibitors. In addition, we have observed that KRAS is able to regulate a number of neutrophil chemoattractant molecules, namely CXCL1, CXCL2 and CXCL8. As with GM-CSF, the dependency of these factors on KRAS signalling has been previously described in the context of pancreatic cancer (Sparmann and Bar-Sagi, 2004). In concordance with this data, *in vivo* treatment of tumours with $KRAS^{G12C}$ inhibitors resulted in a significant decrease in neutrophil infiltration, consistent with a reduction in neutrophil chemoattractants released by the tumour. In line with these findings, we found that several of the KRAS-mutant mouse models that we examined bear a high

infiltration of neutrophils, known to exert pro-tumorigenic and immune suppressive actions also in lung cancer patients (Gabrilovich et al., 2012). The receptor for these chemokines, CXCR2, has been proposed as a therapeutic target to boost immune responses in pancreatic cancer (Chao et al., 2016) and we postulate that this therapeutic approach could potentially be used in KRAS-mutant lung cancer.

Finally, we have investigated the role of the monocyte chemoattractant CCL2 as a KRAS-dependent cytokine in our 3LL ΔNRAS murine model of lung cancer. The association between KRAS signalling and CCL2 has been described previously (Ji et al., 2006), (Yoshimura, 2018), but we have analysed the role of tumour-derived CCL2 in tumour progression and the shaping of the TME in orthotopic tumours. We have observed that tumour-specific CCL2 deletion leads to a substantial improvement in survival of tumour-bearing mice, confirming the pro-tumorigenic role of CCL2 and revealing that tumour cells themselves constitute an important source of CCL2 in the TME. We suggest that this constitutes a mechanism by which oncogenic KRAS is able to shape the immunosuppressive microenvironment in this model, evidenced by our observation that tumour-specific pharmacological KRAS inhibition reduces monocyte infiltration.

7.3.1 Targeting monocytes/macrophages as a therapeutic approach for KRAS-mutant NSCLC

We and others have unveiled an important role of KRAS signalling in the generation of an immunosuppressive microenvironment, consisting largely of tumour-promoting and immunosuppressive tumour-associated macrophages (TAMs). Consistently, it has been widely proposed that targeting myeloid cells constitutes a suitable therapeutic approach in cancer (Zhu et al., 2015). In work performed using the same model as this thesis, the 3LL murine transplantable cell line, other researchers have shown that broad depletion of macrophages (via a genetic mechanism) leads to abrogation of tumour growth and an increase in T cell infiltration, yet it warns of toxic effects of such pan-macrophage targeting treatments, namely their impairment of bone marrow erythropoiesis (Jing et al., 2018). Other mechanisms to block macrophage survival or infiltration to tumours,

such as CCR2 inhibitors (Schmall et al., 2015) and CSF1R targeted drugs (Cannarile et al., 2017) are also being tested as therapeutic approaches in cancer. In line with the finding in mouse models, broad monocyte/macrophage targeting by CCR2 inhibition has caused safety concerns in clinical trials (Noel et al., 2020). We therefore believe that targeting specific TAM subsets or tumour-specific factors would represent a more targeted therapeutic approach. In this line, we suggest that tumour-specific CCL2 deletion blocks the infiltration of a subset of TAMs, which results in a remodelling of the TME and an improvement in survival of tumour-bearing mice. We have yet to investigate the use of CCL2 neutralising antibodies (Teng et al., 2017), but we strongly believe that the inflammatory milieu of the tumour is one of the main sources of CCL2 in the mice, rendering this approach more tumour-specific than broad macrophage inhibition. However, we are aware that not all tumour models examined are able to secrete CCL2 and alternative mechanisms have been proposed for KRAS-induced macrophage infiltration (Liou et al., 2015) (Pylayeva-Gupta et al., 2012), yet significant TAM infiltration is a widespread phenomenon across KRAS-mutant lung cancer (Busch et al., 2016). This is in line with the previously mentioned notion that even though the specific molecular mechanisms may vary across tumour types, the final outcome, in this case a large infiltration of TAMs, remains consistent. To address this, future work will also aim to deeply characterise the specific populations of TAMs responsible for immune suppression and tumour growth across models, by making use of multicolour flow cytometry and imaging modalities such as imaging mass cytometry, in an attempt to find novel TAM markers that can be therapeutically targeted to reduce toxicities associated to pan-macrophage inhibition.

7.4 Pharmacological KRAS^{G12C} inhibition reverses immunosuppressive actions triggered by mutant KRAS

In recent years, the field of KRAS-related cancer research has been revolutionised by the advent of covalent KRAS^{G12C} inhibitors, which have been developed from basic drug discovery all the way to the clinical trial setting. Early clinical evidence suggests that this type of drugs can have significant therapeutic benefits, particularly in KRAS-mutant lung cancer patients (Canon et al., 2019) (Hallin et al., 2020) (Hong et al., 2020). However, most targeted therapies, despite being able to achieve early tumour regression, often inevitably lead to the emergence of resistance mechanisms that ultimately result in cancer progression. We believe that this is likely also going to be the case with KRAS^{G12C} inhibitors, as suggested by early pre-clinical data in our lab ((Molina-Arcas et al., 2019) and unpublished data). We therefore aim to investigate new rational treatment combinations that will result in durable clinical responses (Molina-Arcas et al., 2019). Examples of such treatment combinations include new Phase 1b clinical trials initiated by both Amgen and Mirati Therapeutics investigating the combination of KRAS^{G12C} inhibitors and SHP2 inhibitors to prevent adaptive resistance mechanisms that restore RAS signalling upon KRAS^{G12C} inhibition (NCT04185883 and NCT04330664). Such targeted therapy combinations targeting different nodes of the same pathway are already a part of clinical practice in diseases such as BRAF^{V600E}-mutant melanoma, where patients are administered a combination of BRAF and MEK inhibitors (following NICE© guidelines). However, a number of resistance mechanisms have been described for this treatment combination, which, together with data suggesting TME modulation by BRAF^{V600E} inhibitor (Kakadia et al., 2018) have led to the design of new clinical trials examining the administration of combined BRAF and MEK inhibition with immunotherapies (Ribas et al., 2019). Contrary to targeted therapies, successful immunotherapies are able to achieve long-term clinical responses driven by immune rejection of the tumours. We have demonstrated that similarly to BRAF^{V600E} targeting, tumour-specific KRAS^{G12C} targeting also results in profound remodelling of the TME.

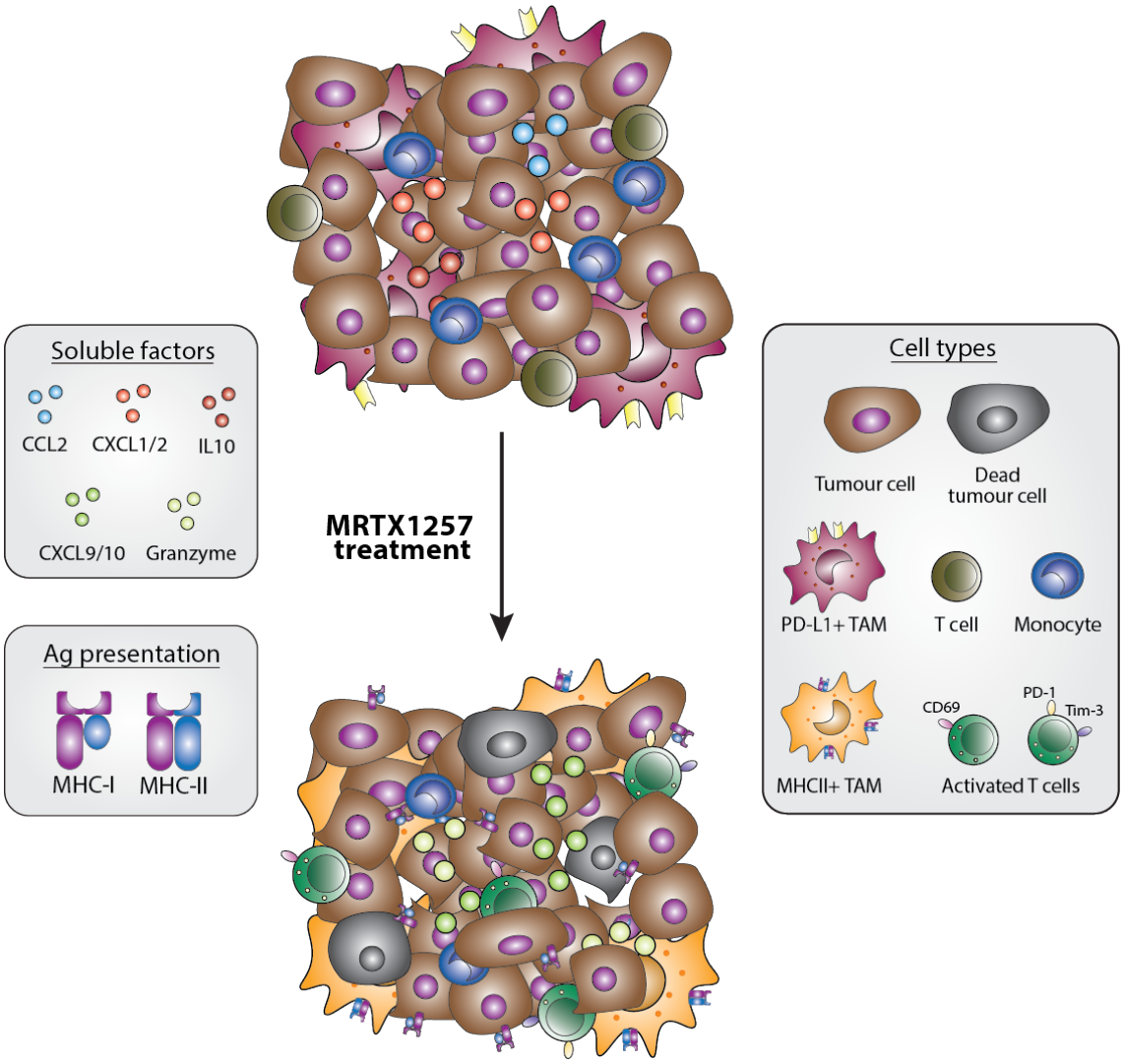

Figure 71. KRAS^{G12C} inhibition profoundly alters the TME.
TAM=tumour-associated macrophage.

To address changes in the tumour immune microenvironment occurring in consequence of KRAS^{G12C} inhibition, we have genetically modified the widely used murine transplantable lung 3LL cell line (3LL ΔNRAS) to make it sensitive to KRAS^{G12C} inhibitors.

Multicolour flow cytometry analysis of lung 3LL ΔNRAS tumours after KRAS^{G12C} inhibitor treatment showed an increase in activated T cells and a decrease in immunosuppressive cells as a consequence of the treatment. In line with this, gene expression analysis confirmed an upregulation of pro-inflammatory pathways after KRAS^{G12C} inhibition. A summary of the changes in the immune microenvironment

found after $KRAS^{G12C}$ is presented in Figure 71. These results are in line with the findings in (Canon et al., 2019), where they also observed a great impact on anti-tumour immunity in pre-clinical models of $KRAS^{G12C}$ inhibition. These reports, however, made use of an *in vivo* model based on a $KRAS^{G12C}$ derivative of the colon cancer cell line CT26. This cell line is known to be immunogenic due to the presence of a strong antigen, gp70423–431, that can elicit T cell responses (Huang et al., 1996) (Lechner et al., 2013). In contrast, in our work we have used the immune evasive 3LL ΔNRAS cell line and tumour model, which, despite harbouring a large number of somatic mutations, is refractory to immunotherapy approaches (Bullock et al., 2019) and observed similar findings in TME remodelling. We henceforth suggest that tumour cell-specific KRAS blockade can have profound effects on anti-tumour immunity, even in very immunosuppressive tumour models. This is a finding that may potentially be translatable to patients exhibiting immunosuppressive TMEs that are intrinsically resistant to immunotherapy (van Maldegem and Downward, 2020).

Our data suggests that $KRAS^{G12C}$ inhibition results in a prominent T cell activation, which leads to an increase in PD-1-expressing T cell number in the TME after MRTX treatment. This finding suggests that KRAS inhibition could be combined with checkpoint blockade approaches, such as anti-PD1 antibodies, a treatment regime investigated in (Canon et al., 2019) and now being investigated in clinical trials. In their report (Canon et al., 2019) they showed the efficacy of the combination of KRAS inhibition and immunotherapy in the $CT26^{KRASG12C}$ pre-clinical model. We would like to extend this finding to additional models of KRAS-mutant lung cancer. Preliminary data in the lab suggests that this combination may not be sufficient to render a deeply immunosuppressive model such as 3LL ΔNRAS responsive to immunotherapeutic approaches. Our finding is further strengthened by data reported in (Quintana et al., 2020), where they observe that combination of a SHP2 inhibitor, while proving synergistic with immunotherapies in immunogenic models such as CT26, does not confer sensitivity to anti-PD1 in refractory models such as 4T1 breast carcinoma and B16F10 melanoma. Therefore, it will be of outmost importance to examine additional rational therapeutic combinations beyond anti-PD1 that will trigger an immune rejection of these immunosuppressive tumours, leading to long-lasting tumour regression.

As far as we know, the 3LL ΔNRAS model is one of the first murine lung $KRAS^{G12C}$ transplantable cell lines developed that is susceptible to KRAS inhibitors and we have demonstrated that this cell line is highly sensitive to $KRAS^{G12C}$ inhibition. However, it remains to be addressed whether the same immunological effects would be achieved in models with a lower sensitivity. To this end, we have made use of a 3LL cell line where NRAS has not been deleted and is therefore less sensitive to $KRAS^{G12C}$ inhibition, and we have shown that at least in the repression of the IFN pathway, this cell line behaves in a similar manner to our 3LL ΔNRAS model, suggesting that this mechanism is not related to cell death induced by the drug. In addition, during the course of this work, other murine KRAS-mutant cell lines have been engineered by people in our lab to express $KRAS^{G12C}$. We have obtained a G12C-version of the KPB6 cell line, a derivative from KP tumours. We expect this cell line to be weakly immunogenic due to its scarcity of mutations, although this is yet to be demonstrated. Additionally, we have obtained a cell line from a KP mouse expressing APOBEC, grown in an immunodeficient setting (KPAR). Work from people in our lab has established that this model is immunogenic, and a G12C-version of the cell line has been generated (KPAR-G12C) (de Carné Trécesson et al., 2020). We therefore now have available a variety of $KRAS^{G12C}$ models with different degrees of immunogenicity and sensitivity to $KRAS^{G12C}$ inhibitors. In the future, we will make use of these new models to expand our investigation of the TME and immune responses in response to $KRAS^{G12C}$ inhibitors, but they can also be used to study other rational treatment combinations with $KRAS^{G12C}$ inhibitors and mechanisms of resistance to $KRAS^{G12C}$-targeting drugs.

7.5 Final conclusions

With this work, we show that, by triggering a number of different mechanisms, oncogenic KRAS signalling plays an important role in shaping the tumour immune microenvironment and evading anti-tumour immune responses in NSCLC. By making use of different models of KRAS-mutant lung cancer we have been able to identify universal mechanisms of TME regulation by KRAS that may constitute therapeutic vulnerabilities for KRAS-mutant (particularly non-G12C) patients.

On the other hand, the advent of novel $KRAS^{G12C}$ inhibitors has unveiled a new therapeutic avenue for $KRAS^{G12C}$ cancer patients. However, it is currently widely accepted that targeted therapies can lead to resistance mechanisms and that, in contrast, long lasting clinical responses can be obtained by an immune rejection of tumours. Examining the effects of $KRAS^{G12C}$ inhibitors on the tumour immune microenvironment and anti-tumour immune responses can help to identify new therapeutic targets that increase the immune visibility of the tumours. Such knowledge can be used to design rational treatment combinations that aim to achieve long lasting anti-tumour immune responses.

We believe that we have made a contribution to the field by providing new mouse models, insight into KRAS-driven molecular mechanisms and suggestions of new rational therapeutic targets and combinations for $KRAS^{G12C}$ and non-$KRAS^{G12C}$ NSCLC patients. This type of research is of utmost relevance, considering that current therapeutic options for these patients are scarce and there is a large need to develop new treatment strategies that will result in long-term responses.

Chapter 8. Appendix

Reference List

AGALIOTI, T., GIANNOU, A. D., KRONTIRA, A. C., KANELLAKIS, N. I., KATI, D., VREKA, M., PEPE, M., SPELLA, M., LILIS, I., ZAZARA, D. E., NIKOLOULI, E., SPIROPOULOU, N., PAPADAKIS, A., PAPADIA, K., VOULGARIDIS, A., HAROKOPOS, V., STAMOU, P., MEINERS, S., EICKELBERG, O., SNYDER, L. A., ANTIMISIARIS, S. G., KARDAMAKIS, D., PSALLIDAS, I., MARAZIOTI, A. & STATHOPOULOS, G. T. 2017. Mutant KRAS promotes malignant pleural effusion formation. *Nat Commun,* 8**,** 15205.

ALEXANDROV, L. B., NIK-ZAINAL, S., WEDGE, D. C., APARICIO, S. A., BEHJATI, S., BIANKIN, A. V., BIGNELL, G. R., BOLLI, N., BORG, A., BORRESEN-DALE, A. L., BOYAULT, S., BURKHARDT, B., BUTLER, A. P., CALDAS, C., DAVIES, H. R., DESMEDT, C., EILS, R., EYFJORD, J. E., FOEKENS, J. A., GREAVES, M., HOSODA, F., HUTTER, B., ILICIC, T., IMBEAUD, S., IMIELINSKI, M., JAGER, N., JONES, D. T., JONES, D., KNAPPSKOG, S., KOOL, M., LAKHANI, S. R., LOPEZ-OTIN, C., MARTIN, S., MUNSHI, N. C., NAKAMURA, H., NORTHCOTT, P. A., PAJIC, M., PAPAEMMANUIL, E., PARADISO, A., PEARSON, J. V., PUENTE, X. S., RAINE, K., RAMAKRISHNA, M., RICHARDSON, A. L., RICHTER, J., ROSENSTIEL, P., SCHLESNER, M., SCHUMACHER, T. N., SPAN, P. N., TEAGUE, J. W., TOTOKI, Y., TUTT, A. N., VALDES-MAS, R., VAN BUUREN, M. M., VAN 'T VEER, L., VINCENT-SALOMON, A., WADDELL, N., YATES, L. R., AUSTRALIAN PANCREATIC CANCER GENOME, I., CONSORTIUM, I. B. C., CONSORTIUM, I. M.-S., PEDBRAIN, I., ZUCMAN-ROSSI, J., FUTREAL, P. A., MCDERMOTT, U., LICHTER, P., MEYERSON, M., GRIMMOND, S. M., SIEBERT, R., CAMPO, E., SHIBATA, T., PFISTER, S. M., CAMPBELL, P. J. & STRATTON, M. R. 2013. Signatures of mutational processes in human cancer. *Nature,* 500**,** 415-21.

ALMOGUERA, C., SHIBATA, D., FORRESTER, K., MARTIN, J., ARNHEIM, N. & PERUCHO, M. 1988. Most human carcinomas of the exocrine pancreas contain mutant c-K-ras genes. *Cell,* 53**,** 549-54.

ANCRILE, B., LIM, K. H. & COUNTER, C. M. 2007. Oncogenic Ras-induced secretion of IL6 is required for tumorigenesis. *Genes Dev,* 21**,** 1714-9.

ANDER, S. E., DIAMOND, M. S. & COYNE, C. B. 2019. Immune responses at the maternal-fetal interface. *Sci Immunol,* 4.

ARCE VARGAS, F., FURNESS, A. J. S., LITCHFIELD, K., JOSHI, K., ROSENTHAL, R., GHORANI, E., SOLOMON, I., LESKO, M. H., RUEF, N., RODDIE, C., HENRY, J. Y., SPAIN, L., BEN AISSA, A., GEORGIOU, A., WONG, Y. N. S., SMITH, M., STRAUSS, D., HAYES, A., NICOL, D., O'BRIEN, T., MARTENSSON, L., LJUNGARS, A., TEIGE, I., FRENDEUS, B., MELANOMA, T. R., RENAL, T. R., CONSORTIA, T. R. L., PULE, M., MARAFIOTI, T., GORE, M., LARKIN, J., TURAJLIC, S., SWANTON, C., PEGGS, K. S. & QUEZADA, S. A. 2018. Fc Effector Function Contributes to the Activity of Human Anti-CTLA-4 Antibodies. *Cancer Cell,* 33**,** 649-663 e4.

BAGHDADI, M., ENDO, H., TAKANO, A., ISHIKAWA, K., KAMEDA, Y., WADA, H., MIYAGI, Y., YOKOSE, T., ITO, H., NAKAYAMA, H., DAIGO, Y., SUZUKI, N. & SEINO, K. I. 2018. High co-expression of IL-34 and M-CSF correlates with tumor progression and poor survival in lung cancers. *Sci Rep,* 8**,** 418.

BALLIN, M., GOMEZ, D. E., SINHA, C. C. & THORGEIRSSON, U. P. 1988. Ras oncogene mediated induction of a 92 kDa metalloproteinase; strong correlation with the malignant phenotype. *Biochem Biophys Res Commun,* 154**,** 832-8.

BENCI, J. L., XU, B., QIU, Y., WU, T. J., DADA, H., TWYMAN-SAINT VICTOR, C., CUCOLO, L., LEE, D. S. M., PAUKEN, K. E., HUANG, A. C., GANGADHAR, T. C., AMARAVADI, R. K., SCHUCHTER, L. M., FELDMAN, M. D., ISHWARAN, H., VONDERHEIDE, R. H., MAITY, A., WHERRY, E. J. & MINN, A. J. 2016. Tumor Interferon Signaling Regulates a Multigenic Resistance Program to Immune Checkpoint Blockade. *Cell,* 167**,** 1540-1554 e12.

BERGERS, G. & HANAHAN, D. 2008. Modes of resistance to anti-angiogenic therapy. *Nat Rev Cancer,* 8**,** 592-603.

BLASCO, R. B., FRANCOZ, S., SANTAMARIA, D., CANAMERO, M., DUBUS, P., CHARRON, J., BACCARINI, M. & BARBACID, M. 2011. c-Raf, but not B-Raf, is essential for development of K-Ras oncogene-driven non-small cell lung carcinoma. *Cancer Cell,* 19**,** 652-63.

BORDEN, E. C., SEN, G. C., UZE, G., SILVERMAN, R. H., RANSOHOFF, R. M., FOSTER, G. R. & STARK, G. R. 2007. Interferons at age 50: past, current and future impact on biomedicine. *Nat Rev Drug Discov,* 6**,** 975-90.

BORGHAEI, H., PAZ-ARES, L., HORN, L., SPIGEL, D. R., STEINS, M., READY, N. E., CHOW, L. Q., VOKES, E. E., FELIP, E., HOLGADO, E., BARLESI, F., KOHLHAUFL, M., ARRIETA, O., BURGIO, M. A., FAYETTE, J., LENA, H., PODDUBSKAYA, E., GERBER, D. E., GETTINGER, S. N., RUDIN, C. M., RIZVI, N., CRINO, L., BLUMENSCHEIN, G. R., JR., ANTONIA, S. J., DORANGE, C., HARBISON, C. T., GRAF FINCKENSTEIN, F. & BRAHMER, J. R. 2015. Nivolumab versus Docetaxel in Advanced Nonsquamous Non-Small-Cell Lung Cancer. *N Engl J Med,* 373**,** 1627-39.

BOS, J. L., FEARON, E. R., HAMILTON, S. R., VERLAAN-DE VRIES, M., VAN BOOM, J. H., VAN DER EB, A. J. & VOGELSTEIN, B. 1987. Prevalence of ras gene mutations in human colorectal cancers. *Nature,* 327**,** 293-7.

BOTTCHER, J. P. & REIS E SOUSA, C. 2018. The Role of Type 1 Conventional Dendritic Cells in Cancer Immunity. *Trends Cancer,* 4**,** 784-792.

BOWMAN, R. L., KLEMM, F., AKKARI, L., PYONTECK, S. M., SEVENICH, L., QUAIL, D. F., DHARA, S., SIMPSON, K., GARDNER, E. E., IACOBUZIO-DONAHUE, C. A., BRENNAN, C. W., TABAR, V., GUTIN, P. H. & JOYCE, J. A. 2016. Macrophage Ontogeny Underlies Differences in Tumor-Specific Education in Brain Malignancies. *Cell Rep,* 17**,** 2445-2459.

BULLOCK, B. L., KIMBALL, A. K., POCZOBUTT, J. M., NEUWELT, A. J., LI, H. Y., JOHNSON, A. M., KWAK, J. W., KLECZKO, E. K., KASPAR, R. E., WAGNER, E. K., HOPP, K., SCHENK, E. L., WEISER-EVANS, M. C., CLAMBEY, E. T. & NEMENOFF, R. A. 2019. Tumor-intrinsic response to IFNgamma shapes the tumor microenvironment and anti-PD-1 response in NSCLC. *Life Sci Alliance,* 2.

BURNET, M. 1957. Cancer: a biological approach. III. Viruses associated with neoplastic conditions. IV. Practical applications. *Br Med J,* 1**,** 841-7.

BURNS, M. B., TEMIZ, N. A. & HARRIS, R. S. 2013. Evidence for APOBEC3B mutagenesis in multiple human cancers. *Nat Genet,* 45**,** 977-83.

BUSCH, S. E., HANKE, M. L., KARGL, J., METZ, H. E., MACPHERSON, D. & HOUGHTON, A. M. 2016. Lung Cancer Subtypes Generate Unique Immune Responses. *J Immunol,* 197**,** 4493-4503.

CANCER GENOME ATLAS RESEARCH, N. 2012. Comprehensive genomic characterization of squamous cell lung cancers. *Nature,* 489**,** 519-25.

CANNARILE, M. A., WEISSER, M., JACOB, W., JEGG, A. M., RIES, C. H. & RUTTINGER, D. 2017. Colony-stimulating factor 1 receptor (CSF1R) inhibitors in cancer therapy. *J Immunother Cancer,* 5**,** 53.

CANON, J., REX, K., SAIKI, A. Y., MOHR, C., COOKE, K., BAGAL, D., GAIDA, K., HOLT, T., KNUTSON, C. G., KOPPADA, N., LANMAN, B. A., WERNER, J., RAPAPORT, A. S., SAN MIGUEL, T., ORTIZ, R., OSGOOD, T., SUN, J. R.,

ZHU, X., MCCARTER, J. D., VOLAK, L. P., HOUK, B. E., FAKIH, M. G., O'NEIL, B. H., PRICE, T. J., FALCHOOK, G. S., DESAI, J., KUO, J., GOVINDAN, R., HONG, D. S., OUYANG, W., HENARY, H., ARVEDSON, T., CEE, V. J. & LIPFORD, J. R. 2019. The clinical KRAS(G12C) inhibitor AMG 510 drives anti-tumour immunity. *Nature,* 575**,** 217-223.

CASEY, S. C., TONG, L., LI, Y., DO, R., WALZ, S., FITZGERALD, K. N., GOUW, A. M., BAYLOT, V., GUTGEMANN, I., EILERS, M. & FELSHER, D. W. 2016. MYC regulates the antitumor immune response through CD47 and PD-L1. *Science,* 352**,** 227-31.

CHAN, T. A., YARCHOAN, M., JAFFEE, E., SWANTON, C., QUEZADA, S. A., STENZINGER, A. & PETERS, S. 2019. Development of tumor mutation burden as an immunotherapy biomarker: utility for the oncology clinic. *Ann Oncol,* 30**,** 44-56.

CHAO, T., FURTH, E. E. & VONDERHEIDE, R. H. 2016. CXCR2-Dependent Accumulation of Tumor-Associated Neutrophils Regulates T-cell Immunity in Pancreatic Ductal Adenocarcinoma. *Cancer Immunol Res,* 4**,** 968-982.

CHEN, D. S. & MELLMAN, I. 2017. Elements of cancer immunity and the cancer-immune set point. *Nature,* 541**,** 321-330.

CHUNG, W. J., DAEMEN, A., CHENG, J. H., LONG, J. E., COOPER, J. E., WANG, B. E., TRAN, C., SINGH, M., GNAD, F., MODRUSAN, Z., FOREMAN, O. & JUNTTILA, M. R. 2017. Kras mutant genetically engineered mouse models of human cancers are genomically heterogeneous. *Proc Natl Acad Sci U S A,* 114**,** E10947-E10955.

CIRRI, P. & CHIARUGI, P. 2011. Cancer associated fibroblasts: the dark side of the coin. *Am J Cancer Res,* 1**,** 482-97.

COELHO, M. A., DE CARNE TRECESSON, S., RANA, S., ZECCHIN, D., MOORE, C., MOLINA-ARCAS, M., EAST, P., SPENCER-DENE, B., NYE, E., BARNOUIN, K., SNIJDERS, A. P., LAI, W. S., BLACKSHEAR, P. J. & DOWNWARD, J. 2017. Oncogenic RAS Signaling Promotes Tumor Immunoresistance by Stabilizing PD-L1 mRNA. *Immunity,* 47**,** 1083-1099 e6.

CORONELLA-WOOD, J. A. & HERSH, E. M. 2003. Naturally occurring B-cell responses to breast cancer. *Cancer Immunol Immunother,* 52**,** 715-38.

COX, A. D. & DER, C. J. 2010. Ras history: The saga continues. *Small GTPases,* 1**,** 2-27.

DANG, C. V. 2012. MYC on the path to cancer. *Cell,* 149**,** 22-35.

DE CARNÉ TRÉCESSON, S., BOUMELHA, J., LAW, E. K., ROMERO-CLAVIJO, P., MUGARZA, E., COELHO, M. A., MOORE, C., RANA, S., CASWELL, D. R., MURILLO, M., HANCOCK, D. C., ARGYRIS, P. P., BROWN, W. L., DURFEE, C., LARSON, L. K., VOGEL, R. I., SUÁREZ-BONNET, A., PRIESTNALL, S. L., EAST, P., ROSS, S. J., MOLINA-ARCAS, M., SWANTON, C., HARRIS, R. & DOWNWARD, J. 2020. APOBEC3B expression generates an immunogenic model of Kras mutant lung cancer. *bioRxiv***,** 2020.12.22.423126.

DE SANTO, C., SERAFINI, P., MARIGO, I., DOLCETTI, L., BOLLA, M., DEL SOLDATO, P., MELANI, C., GUIDUCCI, C., COLOMBO, M. P., IEZZI, M., MUSIANI, P., ZANOVELLO, P. & BRONTE, V. 2005. Nitroaspirin corrects immune dysfunction in tumor-bearing hosts and promotes tumor eradication by cancer vaccination. *Proc Natl Acad Sci U S A,* 102**,** 4185-90.

DELA CRUZ, C. S., TANOUE, L. T. & MATTHAY, R. A. 2011. Lung cancer: epidemiology, etiology, and prevention. *Clin Chest Med,* 32**,** 605-44.

DENARDO, D. G., BARRETO, J. B., ANDREU, P., VASQUEZ, L., TAWFIK, D., KOLHATKAR, N. & COUSSENS, L. M. 2009. CD4(+) T cells regulate pulmonary metastasis of mammary carcinomas by enhancing protumor properties of macrophages. *Cancer Cell,* 16**,** 91-102.

DER, C. J., KRONTIRIS, T. G. & COOPER, G. M. 1982. Transforming genes of human bladder and lung carcinoma cell lines are homologous to the ras genes of Harvey and Kirsten sarcoma viruses. *Proc Natl Acad Sci U S A,* 79**,** 3637-40.

DIAZ-MONTERO, C. M., SALEM, M. L., NISHIMURA, M. I., GARRETT-MAYER, E., COLE, D. J. & MONTERO, A. J. 2009. Increased circulating myeloid-derived suppressor cells correlate with clinical cancer stage, metastatic tumor burden, and doxorubicin-cyclophosphamide chemotherapy. *Cancer Immunol Immunother,* 58**,** 49-59.

DIGHE, A. S., RICHARDS, E., OLD, L. J. & SCHREIBER, R. D. 1994. Enhanced in vivo growth and resistance to rejection of tumor cells expressing dominant negative IFN gamma receptors. *Immunity,* 1**,** 447-56.

DOWNWARD, J., RIEHL, R., WU, L. & WEINBERG, R. A. 1990. Identification of a nucleotide exchange-promoting activity for p21ras. *Proc Natl Acad Sci U S A,* 87**,** 5998-6002.

DRISCOLL, C. B., SCHUELKE, M. R., KOTTKE, T., THOMPSON, J. M., WONGTHIDA, P., TONNE, J. M., HUFF, A. L., MILLER, A., SHIM, K. G., MOLAN, A., WETMORE, C., SELBY, P., SAMSON, A., HARRINGTON, K., PANDHA, H., MELCHER, A., PULIDO, J. S., HARRIS, R., EVGIN, L. & VILE, R. G. 2020. APOBEC3B-mediated corruption of the tumor cell immunopeptidome induces heteroclitic neoepitopes for cancer immunotherapy. *Nat Commun,* 11**,** 790.

DUPAGE, M., DOOLEY, A. L. & JACKS, T. 2009. Conditional mouse lung cancer models using adenoviral or lentiviral delivery of Cre recombinase. *Nat Protoc,* 4**,** 1064-72.

ELLIS, R. W., DEFEO, D., SHIH, T. Y., GONDA, M. A., YOUNG, H. A., TSUCHIDA, N., LOWY, D. R. & SCOLNICK, E. M. 1981. The p21 src genes of Harvey and Kirsten sarcoma viruses originate from divergent members of a family of normal vertebrate genes. *Nature,* 292**,** 506-11.

FOLKMAN, J. 1971. Tumor angiogenesis: therapeutic implications. *N Engl J Med,* 285**,** 1182-6.

FORRESTER, K., ALMOGUERA, C., HAN, K., GRIZZLE, W. E. & PERUCHO, M. 1987. Detection of high incidence of K-ras oncogenes during human colon tumorigenesis. *Nature,* 327**,** 298-303.

GABRILOVICH, D. 2004. Mechanisms and functional significance of tumour-induced dendritic-cell defects. *Nat Rev Immunol,* 4**,** 941-52.

GABRILOVICH, D. I., OSTRAND-ROSENBERG, S. & BRONTE, V. 2012. Coordinated regulation of myeloid cells by tumours. *Nat Rev Immunol,* 12**,** 253-68.

GARON, E. B., RIZVI, N. A., HUI, R., LEIGHL, N., BALMANOUKIAN, A. S., EDER, J. P., PATNAIK, A., AGGARWAL, C., GUBENS, M., HORN, L., CARCERENY, E., AHN, M. J., FELIP, E., LEE, J. S., HELLMANN, M. D., HAMID, O., GOLDMAN, J. W., SORIA, J. C., DOLLED-FILHART, M., RUTLEDGE, R. Z., ZHANG, J., LUNCEFORD, J. K., RANGWALA, R., LUBINIECKI, G. M., ROACH, C., EMANCIPATOR, K., GANDHI, L. & INVESTIGATORS, K.-. 2015. Pembrolizumab for the treatment of non-small-cell lung cancer. *N Engl J Med,* 372**,** 2018-28.

GEORGE, J., LIM, J. S., JANG, S. J., CUN, Y., OZRETIC, L., KONG, G., LEENDERS, F., LU, X., FERNANDEZ-CUESTA, L., BOSCO, G., MULLER, C., DAHMEN, I., JAHCHAN, N. S., PARK, K. S., YANG, D., KARNEZIS, A. N., VAKA, D., TORRES, A., WANG, M. S., KORBEL, J. O., MENON, R., CHUN, S. M., KIM, D., WILKERSON, M., HAYES, N., ENGELMANN, D., PUTZER, B., BOS, M., MICHELS, S., VLASIC, I., SEIDEL, D., PINTHER, B., SCHAUB, P., BECKER, C., ALTMULLER, J., YOKOTA, J., KOHNO, T., IWAKAWA, R., TSUTA, K., NOGUCHI, M., MULEY, T., HOFFMANN, H., SCHNABEL, P. A., PETERSEN,

I., CHEN, Y., SOLTERMANN, A., TISCHLER, V., CHOI, C. M., KIM, Y. H., MASSION, P. P., ZOU, Y., JOVANOVIC, D., KONTIC, M., WRIGHT, G. M., RUSSELL, P. A., SOLOMON, B., KOCH, I., LINDNER, M., MUSCARELLA, L. A., LA TORRE, A., FIELD, J. K., JAKOPOVIC, M., KNEZEVIC, J., CASTANOS-VELEZ, E., ROZ, L., PASTORINO, U., BRUSTUGUN, O. T., LUND-IVERSEN, M., THUNNISSEN, E., KOHLER, J., SCHULER, M., BOTLING, J., SANDELIN, M., SANCHEZ-CESPEDES, M., SALVESEN, H. B., ACHTER, V., LANG, U., BOGUS, M., SCHNEIDER, P. M., ZANDER, T., ANSEN, S., HALLEK, M., WOLF, J., VINGRON, M., YATABE, Y., TRAVIS, W. D., NURNBERG, P., REINHARDT, C., PERNER, S., HEUKAMP, L., BUTTNER, R., HAAS, S. A., BRAMBILLA, E., PEIFER, M., SAGE, J. & THOMAS, R. K. 2015. Comprehensive genomic profiles of small cell lung cancer. *Nature,* 524**,** 47-53.

GIANNOU, A. D., MARAZIOTI, A., KANELLAKIS, N. I., GIOPANOU, I., LILIS, I., ZAZARA, D. E., NTALIARDA, G., KATI, D., ARMENIS, V., GIOTOPOULOU, G. A., KRONTIRA, A. C., LIANOU, M., AGALIOTI, T., VREKA, M., PAPAGEORGOPOULOU, M., FOUZAS, S., KARDAMAKIS, D., PSALLIDAS, I., SPELLA, M. & STATHOPOULOS, G. T. 2017. NRAS destines tumor cells to the lungs. *EMBO Mol Med,* 9**,** 672-686.

GIBBS, J. B., SIGAL, I. S., POE, M. & SCOLNICK, E. M. 1984. Intrinsic GTPase activity distinguishes normal and oncogenic ras p21 molecules. *Proc Natl Acad Sci U S A,* 81**,** 5704-8.

GOVINDAN, R., DING, L., GRIFFITH, M., SUBRAMANIAN, J., DEES, N. D., KANCHI, K. L., MAHER, C. A., FULTON, R., FULTON, L., WALLIS, J., CHEN, K., WALKER, J., MCDONALD, S., BOSE, R., ORNITZ, D., XIONG, D., YOU, M., DOOLING, D. J., WATSON, M., MARDIS, E. R. & WILSON, R. K. 2012. Genomic landscape of non-small cell lung cancer in smokers and never-smokers. *Cell,* 150**,** 1121-34.

GRASSO, C. S., TSOI, J., ONYSHCHENKO, M., ABRIL-RODRIGUEZ, G., ROSS-MACDONALD, P., WIND-ROTOLO, M., CHAMPHEKAR, A., MEDINA, E., TORREJON, D. Y., SHIN, D. S., TRAN, P., KIM, Y. J., PUIG-SAUS, C., CAMPBELL, K., VEGA-CRESPO, A., QUIST, M., MARTIGNIER, C., LUKE, J. J., WOLCHOK, J. D., JOHNSON, D. B., CHMIELOWSKI, B., HODI, F. S., BHATIA, S., SHARFMAN, W., URBA, W. J., SLINGLUFF, C. L., JR., DIAB, A., HAANEN, J., ALGARRA, S. M., PARDOLL, D. M., ANAGNOSTOU, V., TOPALIAN, S. L., VELCULESCU, V. E., SPEISER, D. E., KALBASI, A. & RIBAS, A. 2020. Conserved Interferon-gamma Signaling Drives Clinical Response to Immune Checkpoint Blockade Therapy in Melanoma. *Cancer Cell*.

GUI, Y. S., WANG, L., TIAN, X., FENG, R., MA, A., CAI, B., ZHANG, H. & XU, K. F. 2012. SPC-Cre-ERT2 transgenic mouse for temporal gene deletion in alveolar epithelial cells. *PLoS One,* 7**,** e46076.

GUILLIAMS, M., DE KLEER, I., HENRI, S., POST, S., VANHOUTTE, L., DE PRIJCK, S., DESWARTE, K., MALISSEN, B., HAMMAD, H. & LAMBRECHT, B. N. 2013. Alveolar macrophages develop from fetal monocytes that differentiate into long-lived cells in the first week of life via GM-CSF. *J Exp Med,* 210**,** 1977-92.

GURLEY, K. E., MOSER, R. D. & KEMP, C. J. 2015. Induction of Lung Tumors in Mice with Urethane. *Cold Spring Harb Protoc,* 2015**,** pdb prot077446.

GYSIN, S., SALT, M., YOUNG, A. & MCCORMICK, F. 2011. Therapeutic strategies for targeting ras proteins. *Genes Cancer,* 2**,** 359-72.

HALL, A., MARSHALL, C. J., SPURR, N. K. & WEISS, R. A. 1983. Identification of transforming gene in two human sarcoma cell lines as a new member of the ras gene family located on chromosome 1. *Nature,* 303**,** 396-400.

HALLIN, J., ENGSTROM, L. D., HARGIS, L., CALINISAN, A., ARANDA, R., BRIERE, D. M., SUDHAKAR, N., BOWCUT, V., BAER, B. R., BALLARD, J. A.,

BURKARD, M. R., FELL, J. B., FISCHER, J. P., VIGERS, G. P., XUE, Y., GATTO, S., FERNANDEZ-BANET, J., PAVLICEK, A., VELASTAGUI, K., CHAO, R. C., BARTON, J., PIEROBON, M., BALDELLI, E., PATRICOIN, E. F., 3RD, CASSIDY, D. P., MARX, M. A., RYBKIN, II, JOHNSON, M. L., OU, S. I., LITO, P., PAPADOPOULOS, K. P., JANNE, P. A., OLSON, P. & CHRISTENSEN, J. G. 2020. The KRAS(G12C) Inhibitor MRTX849 Provides Insight toward Therapeutic Susceptibility of KRAS-Mutant Cancers in Mouse Models and Patients. *Cancer Discov,* 10**,** 54-71.

HANAHAN, D. & COUSSENS, L. M. 2012. Accessories to the crime: functions of cells recruited to the tumor microenvironment. *Cancer Cell,* 21**,** 309-22.

HANAHAN, D. & FOLKMAN, J. 1996. Patterns and emerging mechanisms of the angiogenic switch during tumorigenesis. *Cell,* 86**,** 353-64.

HANNA, R. N., CEKIC, C., SAG, D., TACKE, R., THOMAS, G. D., NOWYHED, H., HERRLEY, E., RASQUINHA, N., MCARDLE, S., WU, R., PELUSO, E., METZGER, D., ICHINOSE, H., SHAKED, I., CHODACZEK, G., BISWAS, S. K. & HEDRICK, C. C. 2015. Patrolling monocytes control tumor metastasis to the lung. *Science,* 350**,** 985-90.

HARVEY, J. J. 1964. An Unidentified Virus Which Causes the Rapid Production of Tumours in Mice. *Nature,* 204**,** 1104-5.

HASHIMOTO, D., CHOW, A., NOIZAT, C., TEO, P., BEASLEY, M. B., LEBOEUF, M., BECKER, C. D., SEE, P., PRICE, J., LUCAS, D., GRETER, M., MORTHA, A., BOYER, S. W., FORSBERG, E. C., TANAKA, M., VAN ROOIJEN, N., GARCIA-SASTRE, A., STANLEY, E. R., GINHOUX, F., FRENETTE, P. S. & MERAD, M. 2013. Tissue-resident macrophages self-maintain locally throughout adult life with minimal contribution from circulating monocytes. *Immunity,* 38**,** 792-804.

HECHT, S. S. 2003. Tobacco carcinogens, their biomarkers and tobacco-induced cancer. *Nat Rev Cancer,* 3**,** 733-44.

HEIST, R. S., SEQUIST, L. V. & ENGELMAN, J. A. 2012. Genetic changes in squamous cell lung cancer: a review. *J Thorac Oncol,* 7**,** 924-33.

HELLMANN, M. D., CALLAHAN, M. K., AWAD, M. M., CALVO, E., ASCIERTO, P. A., ATMACA, A., RIZVI, N. A., HIRSCH, F. R., SELVAGGI, G., SZUSTAKOWSKI, J. D., SASSON, A., GOLHAR, R., VITAZKA, P., CHANG, H., GEESE, W. J. & ANTONIA, S. J. 2018. Tumor Mutational Burden and Efficacy of Nivolumab Monotherapy and in Combination with Ipilimumab in Small-Cell Lung Cancer. *Cancer Cell,* 33**,** 853-861 e4.

HERBST, R. S., SORIA, J. C., KOWANETZ, M., FINE, G. D., HAMID, O., GORDON, M. S., SOSMAN, J. A., MCDERMOTT, D. F., POWDERLY, J. D., GETTINGER, S. N., KOHRT, H. E., HORN, L., LAWRENCE, D. P., ROST, S., LEABMAN, M., XIAO, Y., MOKATRIN, A., KOEPPEN, H., HEGDE, P. S., MELLMAN, I., CHEN, D. S. & HODI, F. S. 2014. Predictive correlates of response to the anti-PD-L1 antibody MPDL3280A in cancer patients. *Nature,* 515**,** 563-7.

HOBBS, G. A., DER, C. J. & ROSSMAN, K. L. 2016. RAS isoforms and mutations in cancer at a glance. *J Cell Sci,* 129**,** 1287-92.

HOFER, F., FIELDS, S., SCHNEIDER, C. & MARTIN, G. S. 1994. Activated Ras interacts with the Ral guanine nucleotide dissociation stimulator. *Proc Natl Acad Sci U S A,* 91**,** 11089-93.

HONG, D. S., FAKIH, M. G., STRICKLER, J. H., DESAI, J., DURM, G. A., SHAPIRO, G. I., FALCHOOK, G. S., PRICE, T. J., SACHER, A., DENLINGER, C. S., BANG, Y. J., DY, G. K., KRAUSS, J. C., KUBOKI, Y., KUO, J. C., COVELER, A. L., PARK, K., KIM, T. W., BARLESI, F., MUNSTER, P. N., RAMALINGAM, S. S., BURNS, T. F., MERIC-BERNSTAM, F., HENARY, H., NGANG, J., NGARMCHAMNANRITH, G., KIM, J., HOUK, B. E., CANON, J., LIPFORD, J. R., FRIBERG, G., LITO, P., GOVINDAN, R. & LI, B. T. 2020. KRAS(G12C)

Inhibition with Sotorasib in Advanced Solid Tumors. *N Engl J Med,* 383**,** 1207-1217.

HUANG, A. Y., GULDEN, P. H., WOODS, A. S., THOMAS, M. C., TONG, C. D., WANG, W., ENGELHARD, V. H., PASTERNACK, G., COTTER, R., HUNT, D., PARDOLL, D. M. & JAFFEE, E. M. 1996. The immunodominant major histocompatibility complex class I-restricted antigen of a murine colon tumor derives from an endogenous retroviral gene product. *Proc Natl Acad Sci U S A,* 93**,** 9730-5.

HUNTER, J. C., MANANDHAR, A., CARRASCO, M. A., GURBANI, D., GONDI, S. & WESTOVER, K. D. 2015. Biochemical and Structural Analysis of Common Cancer-Associated KRAS Mutations. *Mol Cancer Res,* 13**,** 1325-35.

HURLEY, J. B., SIMON, M. I., TEPLOW, D. B., ROBISHAW, J. D. & GILMAN, A. G. 1984. Homologies between signal transducing G proteins and ras gene products. *Science,* 226**,** 860-2.

JACQUELOT, N., YAMAZAKI, T., ROBERTI, M. P., DUONG, C. P. M., ANDREWS, M. C., VERLINGUE, L., FERRERE, G., BECHAREF, S., VETIZOU, M., DAILLERE, R., MESSAOUDENE, M., ENOT, D. P., STOLL, G., UGEL, S., MARIGO, I., FOONG NGIOW, S., MARABELLE, A., PREVOST-BLONDEL, A., GAUDREAU, P. O., GOPALAKRISHNAN, V., EGGERMONT, A. M., OPOLON, P., KLEIN, C., MADONNA, G., ASCIERTO, P. A., SUCKER, A., SCHADENDORF, D., SMYTH, M. J., SORIA, J. C., KROEMER, G., BRONTE, V., WARGO, J. & ZITVOGEL, L. 2019. Sustained Type I interferon signaling as a mechanism of resistance to PD-1 blockade. *Cell Res,* 29**,** 846-861.

JANES, M. R., ZHANG, J., LI, L. S., HANSEN, R., PETERS, U., GUO, X., CHEN, Y., BABBAR, A., FIRDAUS, S. J., DARJANIA, L., FENG, J., CHEN, J. H., LI, S., LI, S., LONG, Y. O., THACH, C., LIU, Y., ZARIEH, A., ELY, T., KUCHARSKI, J. M., KESSLER, L. V., WU, T., YU, K., WANG, Y., YAO, Y., DENG, X., ZARRINKAR, P. P., BREHMER, D., DHANAK, D., LORENZI, M. V., HU-LOWE, D., PATRICELLI, M. P., REN, P. & LIU, Y. 2018. Targeting KRAS Mutant Cancers with a Covalent G12C-Specific Inhibitor. *Cell,* 172**,** 578-589 e17.

JI, H., HOUGHTON, A. M., MARIANI, T. J., PERERA, S., KIM, C. B., PADERA, R., TONON, G., MCNAMARA, K., MARCONCINI, L. A., HEZEL, A., EL-BARDEESY, N., BRONSON, R. T., SUGARBAKER, D., MASER, R. S., SHAPIRO, S. D. & WONG, K. K. 2006. K-ras activation generates an inflammatory response in lung tumors. *Oncogene,* 25**,** 2105-12.

JI, H., RAMSEY, M. R., HAYES, D. N., FAN, C., MCNAMARA, K., KOZLOWSKI, P., TORRICE, C., WU, M. C., SHIMAMURA, T., PERERA, S. A., LIANG, M. C., CAI, D., NAUMOV, G. N., BAO, L., CONTRERAS, C. M., LI, D., CHEN, L., KRISHNAMURTHY, J., KOIVUNEN, J., CHIRIEAC, L. R., PADERA, R. F., BRONSON, R. T., LINDEMAN, N. I., CHRISTIANI, D. C., LIN, X., SHAPIRO, G. I., JANNE, P. A., JOHNSON, B. E., MEYERSON, M., KWIATKOWSKI, D. J., CASTRILLON, D. H., BARDEESY, N., SHARPLESS, N. E. & WONG, K. K. 2007. LKB1 modulates lung cancer differentiation and metastasis. *Nature,* 448**,** 807-10.

JING, W., ZHANG, L., QIN, F., LI, X., GUO, X., LI, Y., QIU, C. & ZHAO, Y. 2018. Targeting macrophages for cancer therapy disrupts bone homeostasis and impairs bone marrow erythropoiesis in mice bearing Lewis lung carcinoma tumors. *Cell Immunol,* 331**,** 168-177.

JOYCE, J. A. & FEARON, D. T. 2015. T cell exclusion, immune privilege, and the tumor microenvironment. *Science,* 348**,** 74-80.

KAKADIA, S., YARLAGADDA, N., AWAD, R., KUNDRANDA, M., NIU, J., NARAEV, B., MINA, L., DRAGOVICH, T., GIMBEL, M. & MAHMOUD, F. 2018. Mechanisms of resistance to BRAF and MEK inhibitors and clinical update of US Food and

Drug Administration-approved targeted therapy in advanced melanoma. *Onco Targets Ther,* 11**,** 7095-7107.

KAMATA, T. & FERAMISCO, J. R. 1984. Epidermal growth factor stimulates guanine nucleotide binding activity and phosphorylation of ras oncogene proteins. *Nature,* 310**,** 147-50.

KAPLAN, D. H., SHANKARAN, V., DIGHE, A. S., STOCKERT, E., AGUET, M., OLD, L. J. & SCHREIBER, R. D. 1998. Demonstration of an interferon gamma-dependent tumor surveillance system in immunocompetent mice. *Proc Natl Acad Sci U S A,* 95**,** 7556-61.

KEIR, M. E., LIANG, S. C., GULERIA, I., LATCHMAN, Y. E., QIPO, A., ALBACKER, L. A., KOULMANDA, M., FREEMAN, G. J., SAYEGH, M. H. & SHARPE, A. H. 2006. Tissue expression of PD-L1 mediates peripheral T cell tolerance. *J Exp Med,* 203**,** 883-95.

KELLAR, A., EGAN, C. & MORRIS, D. 2015. Preclinical Murine Models for Lung Cancer: Clinical Trial Applications. *Biomed Res Int,* 2015**,** 621324.

KEMP, S. J., THORLEY, A. J., GORELIK, J., SECKL, M. J., O'HARE, M. J., ARCARO, A., KORCHEV, Y., GOLDSTRAW, P. & TETLEY, T. D. 2008. Immortalization of human alveolar epithelial cells to investigate nanoparticle uptake. *Am J Respir Cell Mol Biol,* 39**,** 591-7.

KIRSTEN, W. H. & MAYER, L. A. 1967. Morphologic responses to a murine erythroblastosis virus. *J Natl Cancer Inst,* 39**,** 311-35.

KLAMPFER, L., HUANG, J., CORNER, G., MARIADASON, J., ARANGO, D., SASAZUKI, T., SHIRASAWA, S. & AUGENLICHT, L. 2003. Oncogenic Ki-ras inhibits the expression of interferon-responsive genes through inhibition of STAT1 and STAT2 expression. *J Biol Chem,* 278**,** 46278-87.

KORTLEVER, R. M., SODIR, N. M., WILSON, C. H., BURKHART, D. L., PELLEGRINET, L., BROWN SWIGART, L., LITTLEWOOD, T. D. & EVAN, G. I. 2017. Myc Cooperates with Ras by Programming Inflammation and Immune Suppression. *Cell,* 171**,** 1301-1315 e14.

KOYAMA, S., AKBAY, E. A., LI, Y. Y., AREF, A. R., SKOULIDIS, F., HERTER-SPRIE, G. S., BUCZKOWSKI, K. A., LIU, Y., AWAD, M. M., DENNING, W. L., DIAO, L., WANG, J., PARRA-CUENTAS, E. R., WISTUBA, II, SOUCHERAY, M., THAI, T., ASAHINA, H., KITAJIMA, S., ALTABEF, A., CAVANAUGH, J. D., RHEE, K., GAO, P., ZHANG, H., FECCI, P. E., SHIMAMURA, T., HELLMANN, M. D., HEYMACH, J. V., HODI, F. S., FREEMAN, G. J., BARBIE, D. A., DRANOFF, G., HAMMERMAN, P. S. & WONG, K. K. 2016. STK11/LKB1 Deficiency Promotes Neutrophil Recruitment and Proinflammatory Cytokine Production to Suppress T-cell Activity in the Lung Tumor Microenvironment. *Cancer Res,* 76**,** 999-1008.

KUCAN BRLIC, P., LENAC ROVIS, T., CINAMON, G., TSUKERMAN, P., MANDELBOIM, O. & JONJIC, S. 2019. Targeting PVR (CD155) and its receptors in anti-tumor therapy. *Cell Mol Immunol,* 16**,** 40-52.

LAND, H., PARADA, L. F. & WEINBERG, R. A. 1983. Tumorigenic conversion of primary embryo fibroblasts requires at least two cooperating oncogenes. *Nature,* 304**,** 596-602.

LANIER, L. L. 2008. Up on the tightrope: natural killer cell activation and inhibition. *Nat Immunol,* 9**,** 495-502.

LAVIN, Y., KOBAYASHI, S., LEADER, A., AMIR, E. D., ELEFANT, N., BIGENWALD, C., REMARK, R., SWEENEY, R., BECKER, C. D., LEVINE, J. H., MEINHOF, K., CHOW, A., KIM-SHULZE, S., WOLF, A., MEDAGLIA, C., LI, H., RYTLEWSKI, J. A., EMERSON, R. O., SOLOVYOV, A., GREENBAUM, B. D., SANDERS, C., VIGNALI, M., BEASLEY, M. B., FLORES, R., GNJATIC, S., PE'ER, D., RAHMAN, A., AMIT, I. & MERAD, M. 2017. Innate Immune

Landscape in Early Lung Adenocarcinoma by Paired Single-Cell Analyses. *Cell,* 169**,** 750-765 e17.

LAVIN, Y. & MERAD, M. 2013. Macrophages: gatekeepers of tissue integrity. *Cancer Immunol Res,* 1**,** 201-9.

LECHNER, M. G., KARIMI, S. S., BARRY-HOLSON, K., ANGELL, T. E., MURPHY, K. A., CHURCH, C. H., OHLFEST, J. R., HU, P. & EPSTEIN, A. L. 2013. Immunogenicity of murine solid tumor models as a defining feature of in vivo behavior and response to immunotherapy. *J Immunother,* 36**,** 477-89.

LEMJABBAR-ALAOUI, H., HASSAN, O. U., YANG, Y. W. & BUCHANAN, P. 2015. Lung cancer: Biology and treatment options. *Biochim Biophys Acta,* 1856**,** 189-210.

LI, H. Y., MCSHARRY, M., BULLOCK, B., NGUYEN, T. T., KWAK, J., POCZOBUTT, J. M., SIPPEL, T. R., HEASLEY, L. E., WEISER-EVANS, M. C., CLAMBEY, E. T. & NEMENOFF, R. A. 2017. The Tumor Microenvironment Regulates Sensitivity of Murine Lung Tumors to PD-1/PD-L1 Antibody Blockade. *Cancer Immunol Res,* 5**,** 767-777.

LI, S., LIU, S., DENG, J., AKBAY, E. A., HAI, J., AMBROGIO, C., ZHANG, L., ZHOU, F., JENKINS, R. W., ADEEGBE, D. O., GAO, P., WANG, X., PAWELETZ, C. P., HERTER-SPRIE, G. S., CHEN, T., GUTIERREZ-QUICENO, L., ZHANG, Y., MERLINO, A. A., QUINN, M. M., ZENG, Y., YU, X., LIU, Y., FAN, L., AGUIRRE, A. J., BARBIE, D. A., YI, X. & WONG, K. K. 2018. Assessing Therapeutic Efficacy of MEK Inhibition in a KRAS(G12C)-Driven Mouse Model of Lung Cancer. *Clin Cancer Res,* 24**,** 4854-4864.

LIAO, W., OVERMAN, M. J., BOUTIN, A. T., SHANG, X., ZHAO, D., DEY, P., LI, J., WANG, G., LAN, Z., LI, J., TANG, M., JIANG, S., MA, X., CHEN, P., KATKHUDA, R., KORPHAISARN, K., CHAKRAVARTI, D., CHANG, A., SPRING, D. J., CHANG, Q., ZHANG, J., MARU, D. M., MAEDA, D. Y., ZEBALA, J. A., KOPETZ, S., WANG, Y. A. & DEPINHO, R. A. 2019. KRAS-IRF2 Axis Drives Immune Suppression and Immune Therapy Resistance in Colorectal Cancer. *Cancer Cell,* 35**,** 559-572 e7.

LIAU, N. P. D., LAKTYUSHIN, A., LUCET, I. S., MURPHY, J. M., YAO, S., WHITLOCK, E., CALLAGHAN, K., NICOLA, N. A., KERSHAW, N. J. & BABON, J. J. 2018. The molecular basis of JAK/STAT inhibition by SOCS1. *Nat Commun,* 9**,** 1558.

LIN, A., SCHILDKNECHT, A., NGUYEN, L. T. & OHASHI, P. S. 2010. Dendritic cells integrate signals from the tumor microenvironment to modulate immunity and tumor growth. *Immunol Lett,* 127**,** 77-84.

LIN, E. Y., LI, J. F., GNATOVSKIY, L., DENG, Y., ZHU, L., GRZESIK, D. A., QIAN, H., XUE, X. N. & POLLARD, J. W. 2006. Macrophages regulate the angiogenic switch in a mouse model of breast cancer. *Cancer Res,* 66**,** 11238-46.

LIOU, G. Y., DOPPLER, H., NECELA, B., EDENFIELD, B., ZHANG, L., DAWSON, D. W. & STORZ, P. 2015. Mutant KRAS-induced expression of ICAM-1 in pancreatic acinar cells causes attraction of macrophages to expedite the formation of precancerous lesions. *Cancer Discov,* 5**,** 52-63.

LITO, P., SOLOMON, M., LI, L. S., HANSEN, R. & ROSEN, N. 2016. Allele-specific inhibitors inactivate mutant KRAS G12C by a trapping mechanism. *Science,* 351**,** 604-8.

LOYHER, P. L., HAMON, P., LAVIRON, M., MEGHRAOUI-KHEDDAR, A., GONCALVES, E., DENG, Z., TORSTENSSON, S., BERCOVICI, N., BAUDESSON DE CHANVILLE, C., COMBADIERE, B., GEISSMANN, F., SAVINA, A., COMBADIERE, C. & BOISSONNAS, A. 2018. Macrophages of distinct origins contribute to tumor development in the lung. *J Exp Med,* 215**,** 2536-2553.

LUND, F. E. 2008. Cytokine-producing B lymphocytes-key regulators of immunity. *Curr Opin Immunol,* 20**,** 332-8.

MAHALE, J., SMAGURAUSKAITE, G., BROWN, K., THOMAS, A. & HOWELLS, L. M. 2016. The role of stromal fibroblasts in lung carcinogenesis: A target for chemoprevention? *Int J Cancer,* 138**,** 30-44.

MAINARDI, S., MIJIMOLLE, N., FRANCOZ, S., VICENTE-DUENAS, C., SANCHEZ-GARCIA, I. & BARBACID, M. 2014. Identification of cancer initiating cells in K-Ras driven lung adenocarcinoma. *Proc Natl Acad Sci U S A,* 111**,** 255-60.

MALUMBRES, M. & BARBACID, M. 2003. RAS oncogenes: the first 30 years. *Nat Rev Cancer,* 3**,** 459-65.

MARAZIOTI, A., LILIS, I., VREKA, M., APOSTOLOPOULOU, H., KALOGEROPOULOU, A., GIOPANOU, I., GIOTOPOULOU, G. A., KRONTIRA, A. C., ILIOPOULOU, M., KANELLAKIS, N. I., AGALIOTI, T., GIANNOU, A. D., JONES-PARIS, C., IWAKURA, Y., KARDAMAKIS, D., BLACKWELL, T. S., TARAVIRAS, S., SPELLA, M. & STATHOPOULOS, G. T. 2018. Myeloid-derived interleukin-1beta drives oncogenic KRAS-NF-kappaBeta addiction in malignant pleural effusion. *Nat Commun,* 9**,** 672.

MAYO, J. G. 1972. Biologic characterization of the subcutaneously implanted Lewis lung tumor. *Cancer Chemother Rep 2,* 3**,** 325-30.

MCCORMICK, F. 1993. Signal transduction. How receptors turn Ras on. *Nature,* 363**,** 15-6.

MCDONALD, E. R., 3RD, DE WECK, A., SCHLABACH, M. R., BILLY, E., MAVRAKIS, K. J., HOFFMAN, G. R., BELUR, D., CASTELLETTI, D., FRIAS, E., GAMPA, K., GOLJI, J., KAO, I., LI, L., MEGEL, P., PERKINS, T. A., RAMADAN, N., RUDDY, D. A., SILVER, S. J., SOVATH, S., STUMP, M., WEBER, O., WIDMER, R., YU, J., YU, K., YUE, Y., ABRAMOWSKI, D., ACKLEY, E., BARRETT, R., BERGER, J., BERNARD, J. L., BILLIG, R., BRACHMANN, S. M., BUXTON, F., CAOTHIEN, R., CAUSHI, J. X., CHUNG, F. S., CORTES-CROS, M., DEBEAUMONT, R. S., DELAUNAY, C., DESPLAT, A., DUONG, W., DWOSKE, D. A., ELDRIDGE, R. S., FARSIDJANI, A., FENG, F., FENG, J., FLEMMING, D., FORRESTER, W., GALLI, G. G., GAO, Z., GAUTER, F., GIBAJA, V., HAAS, K., HATTENBERGER, M., HOOD, T., HUROV, K. E., JAGANI, Z., JENAL, M., JOHNSON, J. A., JONES, M. D., KAPOOR, A., KORN, J., LIU, J., LIU, Q., LIU, S., LIU, Y., LOO, A. T., MACCHI, K. J., MARTIN, T., MCALLISTER, G., MEYER, A., MOLLE, S., PAGLIARINI, R. A., PHADKE, T., REPKO, B., SCHOUWEY, T., SHANAHAN, F., SHEN, Q., STAMM, C., STEPHAN, C., STUCKE, V. M., TIEDT, R., VARADARAJAN, M., VENKATESAN, K., VITARI, A. C., WALLROTH, M., WEILER, J., ZHANG, J., MICKANIN, C., MYER, V. E., PORTER, J. A., LAI, A., BITTER, H., LEES, E., KEEN, N., KAUFFMANN, A., STEGMEIER, F., HOFMANN, F., SCHMELZLE, T. & SELLERS, W. R. 2017. Project DRIVE: A Compendium of Cancer Dependencies and Synthetic Lethal Relationships Uncovered by Large-Scale, Deep RNAi Screening. *Cell,* 170**,** 577-592 e10.

MCGRANAHAN, N., ROSENTHAL, R., HILEY, C. T., ROWAN, A. J., WATKINS, T. B. K., WILSON, G. A., BIRKBAK, N. J., VEERIAH, S., VAN LOO, P., HERRERO, J., SWANTON, C. & CONSORTIUM, T. R. 2017. Allele-Specific HLA Loss and Immune Escape in Lung Cancer Evolution. *Cell,* 171**,** 1259-1271 e11.

MCGRATH, J. P., CAPON, D. J., GOEDDEL, D. V. & LEVINSON, A. D. 1984. Comparative biochemical properties of normal and activated human ras p21 protein. *Nature,* 310**,** 644-9.

MEDLER, T. R., COTECHINI, T. & COUSSENS, L. M. 2015. Immune response to cancer therapy: mounting an effective antitumor response and mechanisms of resistance. *Trends Cancer,* 1**,** 66-75.

MESA, R. A., YASOTHAN, U. & KIRKPATRICK, P. 2012. Ruxolitinib. *Nat Rev Drug Discov,* 11**,** 103-4.

MILBURN, M. V., TONG, L., DEVOS, A. M., BRUNGER, A., YAMAIZUMI, Z., NISHIMURA, S. & KIM, S. H. 1990. Molecular switch for signal transduction: structural differences between active and inactive forms of protooncogenic ras proteins. *Science,* 247**,** 939-45.

MILLER, Y. E., DWYER-NIELD, L. D., KEITH, R. L., LE, M., FRANKLIN, W. A. & MALKINSON, A. M. 2003. Induction of a high incidence of lung tumors in C57BL/6 mice with multiple ethyl carbamate injections. *Cancer Lett,* 198**,** 139-44.

MISHARIN, A. V., MORALES-NEBREDA, L., MUTLU, G. M., BUDINGER, G. R. & PERLMAN, H. 2013. Flow cytometric analysis of macrophages and dendritic cell subsets in the mouse lung. *Am J Respir Cell Mol Biol,* 49**,** 503-10.

MOLINA-ARCAS, M., HANCOCK, D. C., SHERIDAN, C., KUMAR, M. S. & DOWNWARD, J. 2013. Coordinate direct input of both KRAS and IGF1 receptor to activation of PI3 kinase in KRAS-mutant lung cancer. *Cancer Discov,* 3**,** 548-63.

MOLINA-ARCAS, M., MOORE, C., RANA, S., VAN MALDEGEM, F., MUGARZA, E., ROMERO-CLAVIJO, P., HERBERT, E., HORSWELL, S., LI, L. S., JANES, M. R., HANCOCK, D. C. & DOWNWARD, J. 2019. Development of combination therapies to maximize the impact of KRAS-G12C inhibitors in lung cancer. *Sci Transl Med,* 11.

MOODIE, S. A., WILLUMSEN, B. M., WEBER, M. J. & WOLFMAN, A. 1993. Complexes of Ras.GTP with Raf-1 and mitogen-activated protein kinase kinase. *Science,* 260**,** 1658-61.

MORVAN, M. G. & LANIER, L. L. 2016. NK cells and cancer: you can teach innate cells new tricks. *Nat Rev Cancer,* 16**,** 7-19.

MULLARD, A. 2019. Cracking KRAS. *Nat Rev Drug Discov,* 18**,** 887-891.

MUSELLA, M., MANIC, G., DE MARIA, R., VITALE, I. & SISTIGU, A. 2017. Type-I-interferons in infection and cancer: Unanticipated dynamics with therapeutic implications. *Oncoimmunology,* 6**,** e1314424.

MUTHALAGU, N., MONTEVERDE, T., RAFFO-IRAOLAGOITIA, X., WIESHEU, R., WHYTE, D., HEDLEY, A., LAING, S., KRUSPIG, B., UPSTILL-GODDARD, R., SHAW, R., NEIDLER, S., RINK, C., KARIM, S. A., GYURASZOVA, K., NIXON, C., CLARK, W., BIANKIN, A. V., CARLIN, L. M., COFFELT, S. B., SANSOM, O. J., MORTON, J. P. & MURPHY, D. J. 2020. Repression of the Type I Interferon Pathway Underlies MYC- and KRAS-Dependent Evasion of NK and B Cells in Pancreatic Ductal Adenocarcinoma. *Cancer Discov,* 10**,** 872-887.

NOEL, M., O'REILLY, E. M., WOLPIN, B. M., RYAN, D. P., BULLOCK, A. J., BRITTEN, C. D., LINEHAN, D. C., BELT, B. A., GAMELIN, E. C., GANGULY, B., YIN, D., JOH, T., JACOBS, I. A., TAYLOR, C. T. & LOWERY, M. A. 2020. Phase 1b study of a small molecule antagonist of human chemokine (C-C motif) receptor 2 (PF-04136309) in combination with nab-paclitaxel/gemcitabine in first-line treatment of metastatic pancreatic ductal adenocarcinoma. *Invest New Drugs,* 38**,** 800-811.

OKADA, F., RAK, J. W., CROIX, B. S., LIEUBEAU, B., KAYA, M., RONCARI, L., SHIRASAWA, S., SASAZUKI, T. & KERBEL, R. S. 1998. Impact of oncogenes in tumor angiogenesis: mutant K-ras up-regulation of vascular endothelial growth factor/vascular permeability factor is necessary, but not sufficient for tumorigenicity of human colorectal carcinoma cells. *Proc Natl Acad Sci U S A,* 95**,** 3609-14.

OSTREM, J. M., PETERS, U., SOS, M. L., WELLS, J. A. & SHOKAT, K. M. 2013. K-Ras(G12C) inhibitors allosterically control GTP affinity and effector interactions. *Nature,* 503**,** 548-51.

PARADA, L. F., TABIN, C. J., SHIH, C. & WEINBERG, R. A. 1982. Human EJ bladder carcinoma oncogene is homologue of Harvey sarcoma virus ras gene. *Nature,* 297**,** 474-8.

PATRICELLI, M. P., JANES, M. R., LI, L. S., HANSEN, R., PETERS, U., KESSLER, L. V., CHEN, Y., KUCHARSKI, J. M., FENG, J., ELY, T., CHEN, J. H., FIRDAUS, S. J., BABBAR, A., REN, P. & LIU, Y. 2016. Selective Inhibition of Oncogenic KRAS Output with Small Molecules Targeting the Inactive State. *Cancer Discov,* 6**,** 316-29.

PENG, W., CHEN, J. Q., LIU, C., MALU, S., CREASY, C., TETZLAFF, M. T., XU, C., MCKENZIE, J. A., ZHANG, C., LIANG, X., WILLIAMS, L. J., DENG, W., CHEN, G., MBOFUNG, R., LAZAR, A. J., TORRES-CABALA, C. A., COOPER, Z. A., CHEN, P. L., TIEU, T. N., SPRANGER, S., YU, X., BERNATCHEZ, C., FORGET, M. A., HAYMAKER, C., AMARIA, R., MCQUADE, J. L., GLITZA, I. C., CASCONE, T., LI, H. S., KWONG, L. N., HEFFERNAN, T. P., HU, J., BASSETT, R. L., JR., BOSENBERG, M. W., WOODMAN, S. E., OVERWIJK, W. W., LIZEE, G., ROSZIK, J., GAJEWSKI, T. F., WARGO, J. A., GERSHENWALD, J. E., RADVANYI, L., DAVIES, M. A. & HWU, P. 2016. Loss of PTEN Promotes Resistance to T Cell-Mediated Immunotherapy. *Cancer Discov,* 6**,** 202-16.

PERROT, I., BLANCHARD, D., FREYMOND, N., ISAAC, S., GUIBERT, B., PACHECO, Y. & LEBECQUE, S. 2007. Dendritic cells infiltrating human non-small cell lung cancer are blocked at immature stage. *J Immunol,* 178**,** 2763-9.

PERUCHO, M., GOLDFARB, M., SHIMIZU, K., LAMA, C., FOGH, J. & WIGLER, M. 1981. Human-tumor-derived cell lines contain common and different transforming genes. *Cell,* 27**,** 467-76.

PIKOR, L. A., RAMNARINE, V. R., LAM, S. & LAM, W. L. 2013. Genetic alterations defining NSCLC subtypes and their therapeutic implications. *Lung Cancer,* 82**,** 179-89.

POSTOW, M. A., CALLAHAN, M. K. & WOLCHOK, J. D. 2015. Immune Checkpoint Blockade in Cancer Therapy. *J Clin Oncol,* 33**,** 1974-82.

PRIOR, I. A., LEWIS, P. D. & MATTOS, C. 2012. A comprehensive survey of Ras mutations in cancer. *Cancer Res,* 72**,** 2457-67.

PUYOL, M., MARTIN, A., DUBUS, P., MULERO, F., PIZCUETA, P., KHAN, G., GUERRA, C., SANTAMARIA, D. & BARBACID, M. 2010. A synthetic lethal interaction between K-Ras oncogenes and Cdk4 unveils a therapeutic strategy for non-small cell lung carcinoma. *Cancer Cell,* 18**,** 63-73.

PYLAYEVA-GUPTA, Y., LEE, K. E., HAJDU, C. H., MILLER, G. & BAR-SAGI, D. 2012. Oncogenic Kras-induced GM-CSF production promotes the development of pancreatic neoplasia. *Cancer Cell,* 21**,** 836-47.

QIAN, B. Z., LI, J., ZHANG, H., KITAMURA, T., ZHANG, J., CAMPION, L. R., KAISER, E. A., SNYDER, L. A. & POLLARD, J. W. 2011. CCL2 recruits inflammatory monocytes to facilitate breast-tumour metastasis. *Nature,* 475**,** 222-5.

QIAN, B. Z. & POLLARD, J. W. 2010. Macrophage diversity enhances tumor progression and metastasis. *Cell,* 141**,** 39-51.

QUEZADA, S. A., PEGGS, K. S., CURRAN, M. A. & ALLISON, J. P. 2006. CTLA4 blockade and GM-CSF combination immunotherapy alters the intratumor balance of effector and regulatory T cells. *J Clin Invest,* 116**,** 1935-45.

QUINTANA, E., SCHULZE, C. J., MYERS, D. R., CHOY, T. J., MORDEC, K., WILDES, D., TOBVIS SHIFRIN, N., BELWAFA, A., KOLTUN, E. S., GILL, A. L., SINGH, M., KELSEY, S., GOLDSMITH, M. A., NICHOLS, R. & SMITH, J. A. M. 2020.

Allosteric inhibition of SHP2 stimulates anti-tumor immunity by transforming the immunosuppressive environment. *Cancer Res*.

RAKHRA, K., BACHIREDDY, P., ZABUAWALA, T., ZEISER, R., XU, L., KOPELMAN, A., FAN, A. C., YANG, Q., BRAUNSTEIN, L., CROSBY, E., RYEOM, S. & FELSHER, D. W. 2010. CD4(+) T cells contribute to the remodeling of the microenvironment required for sustained tumor regression upon oncogene inactivation. *Cancer Cell,* 18**,** 485-98.

REDDY, E. P., REYNOLDS, R. K., SANTOS, E. & BARBACID, M. 1982. A point mutation is responsible for the acquisition of transforming properties by the T24 human bladder carcinoma oncogene. *Nature,* 300**,** 149-52.

RIBAS, A., LAWRENCE, D., ATKINSON, V., AGARWAL, S., MILLER, W. H., JR., CARLINO, M. S., FISHER, R., LONG, G. V., HODI, F. S., TSOI, J., GRASSO, C. S., MOOKERJEE, B., ZHAO, Q., GHORI, R., MORENO, B. H., IBRAHIM, N. & HAMID, O. 2019. Combined BRAF and MEK inhibition with PD-1 blockade immunotherapy in BRAF-mutant melanoma. *Nat Med,* 25**,** 936-940.

RIZVI, N. A., HELLMANN, M. D., SNYDER, A., KVISTBORG, P., MAKAROV, V., HAVEL, J. J., LEE, W., YUAN, J., WONG, P., HO, T. S., MILLER, M. L., REKHTMAN, N., MOREIRA, A. L., IBRAHIM, F., BRUGGEMAN, C., GASMI, B., ZAPPASODI, R., MAEDA, Y., SANDER, C., GARON, E. B., MERGHOUB, T., WOLCHOK, J. D., SCHUMACHER, T. N. & CHAN, T. A. 2015. Cancer immunology. Mutational landscape determines sensitivity to PD-1 blockade in non-small cell lung cancer. *Science,* 348**,** 124-8.

RODENHUIS, S., VAN DE WETERING, M. L., MOOI, W. J., EVERS, S. G., VAN ZANDWIJK, N. & BOS, J. L. 1987. Mutational activation of the K-ras oncogene. A possible pathogenetic factor in adenocarcinoma of the lung. *N Engl J Med,* 317**,** 929-35.

RODERO, M. P., POUPEL, L., LOYHER, P. L., HAMON, P., LICATA, F., PESSEL, C., HUME, D. A., COMBADIERE, C. & BOISSONNAS, A. 2015. Immune surveillance of the lung by migrating tissue monocytes. *Elife,* 4**,** e07847.

RODRIGUEZ-VICIANA, P., WARNE, P. H., DHAND, R., VANHAESEBROECK, B., GOUT, I., FRY, M. J., WATERFIELD, M. D. & DOWNWARD, J. 1994. Phosphatidylinositol-3-OH kinase as a direct target of Ras. *Nature,* 370**,** 527-32.

ROMAN, M., BARAIBAR, I., LOPEZ, I., NADAL, E., ROLFO, C., VICENT, S. & GIL-BAZO, I. 2018. KRAS oncogene in non-small cell lung cancer: clinical perspectives on the treatment of an old target. *Mol Cancer,* 17**,** 33.

ROONEY, M. S., SHUKLA, S. A., WU, C. J., GETZ, G. & HACOHEN, N. 2015. Molecular and genetic properties of tumors associated with local immune cytolytic activity. *Cell,* 160**,** 48-61.

ROSENTHAL, R., CADIEUX, E. L., SALGADO, R., BAKIR, M. A., MOORE, D. A., HILEY, C. T., LUND, T., TANIC, M., READING, J. L., JOSHI, K., HENRY, J. Y., GHORANI, E., WILSON, G. A., BIRKBAK, N. J., JAMAL-HANJANI, M., VEERIAH, S., SZALLASI, Z., LOI, S., HELLMANN, M. D., FEBER, A., CHAIN, B., HERRERO, J., QUEZADA, S. A., DEMEULEMEESTER, J., VAN LOO, P., BECK, S., MCGRANAHAN, N., SWANTON, C. & CONSORTIUM, T. R. 2019. Neoantigen-directed immune escape in lung cancer evolution. *Nature,* 567**,** 479-485.

RULEY, H. E. 1983. Adenovirus early region 1A enables viral and cellular transforming genes to transform primary cells in culture. *Nature,* 304**,** 602-6.

SAIGI, M., ALBURQUERQUE-BEJAR, J. J. & SANCHEZ-CESPEDES, M. 2019. Determinants of immunological evasion and immunocheckpoint inhibition response in non-small cell lung cancer: the genetic front. *Oncogene,* 38**,** 5921-5932.

SANTOS, E., MARTIN-ZANCA, D., REDDY, E. P., PIEROTTI, M. A., DELLA PORTA, G. & BARBACID, M. 1984. Malignant activation of a K-ras oncogene in lung carcinoma but not in normal tissue of the same patient. *Science,* 223**,** 661-4.

SANTOS, E., TRONICK, S. R., AARONSON, S. A., PULCIANI, S. & BARBACID, M. 1982. T24 human bladder carcinoma oncogene is an activated form of the normal human homologue of BALB- and Harvey-MSV transforming genes. *Nature,* 298**,** 343-7.

SCHEFFZEK, K., AHMADIAN, M. R., KABSCH, W., WIESMULLER, L., LAUTWEIN, A., SCHMITZ, F. & WITTINGHOFER, A. 1997. The Ras-RasGAP complex: structural basis for GTPase activation and its loss in oncogenic Ras mutants. *Science,* 277**,** 333-8.

SCHEFFZEK, K., LAUTWEIN, A., KABSCH, W., AHMADIAN, M. R. & WITTINGHOFER, A. 1996. Crystal structure of the GTPase-activating domain of human p120GAP and implications for the interaction with Ras. *Nature,* 384**,** 591-6.

SCHMALL, A., AL-TAMARI, H. M., HEROLD, S., KAMPSCHULTE, M., WEIGERT, A., WIETELMANN, A., VIPOTNIK, N., GRIMMINGER, F., SEEGER, W., PULLAMSETTI, S. S. & SAVAI, R. 2015. Macrophage and cancer cell cross-talk via CCR2 and CX3CR1 is a fundamental mechanism driving lung cancer. *Am J Respir Crit Care Med,* 191**,** 437-47.

SCHREIBER, R. D., OLD, L. J. & SMYTH, M. J. 2011. Cancer immunoediting: integrating immunity's roles in cancer suppression and promotion. *Science,* 331**,** 1565-70.

SCHUMACHER, T. N. & SCHREIBER, R. D. 2015. Neoantigens in cancer immunotherapy. *Science,* 348**,** 69-74.

SCOLNICK, E. M., PAPAGEORGE, A. G. & SHIH, T. Y. 1979. Guanine nucleotide-binding activity as an assay for src protein of rat-derived murine sarcoma viruses. *Proc Natl Acad Sci U S A,* 76**,** 5355-9.

SERBINA, N. V. & PAMER, E. G. 2006. Monocyte emigration from bone marrow during bacterial infection requires signals mediated by chemokine receptor CCR2. *Nat Immunol,* 7**,** 311-7.

SHANKARAN, V., IKEDA, H., BRUCE, A. T., WHITE, J. M., SWANSON, P. E., OLD, L. J. & SCHREIBER, R. D. 2001. IFNgamma and lymphocytes prevent primary tumour development and shape tumour immunogenicity. *Nature,* 410**,** 1107-11.

SHARMA, P. & ALLISON, J. P. 2015. Immune checkpoint targeting in cancer therapy: toward combination strategies with curative potential. *Cell,* 161**,** 205-14.

SHIH, T. Y., WEEKS, M. O., YOUNG, H. A. & SCOLNICK, E. M. 1979. p21 of Kirsten murine sarcoma virus is thermolabile in a viral mutant temperature sensitive for the maintenance of transformation. *J Virol,* 31**,** 546-6.

SKOULIDIS, F., GOLDBERG, M. E., GREENAWALT, D. M., HELLMANN, M. D., AWAD, M. M., GAINOR, J. F., SCHROCK, A. B., HARTMAIER, R. J., TRABUCCO, S. E., GAY, L., ALI, S. M., ELVIN, J. A., SINGAL, G., ROSS, J. S., FABRIZIO, D., SZABO, P. M., CHANG, H., SASSON, A., SRINIVASAN, S., KIROV, S., SZUSTAKOWSKI, J., VITAZKA, P., EDWARDS, R., BUFILL, J. A., SHARMA, N., OU, S. I., PELED, N., SPIGEL, D. R., RIZVI, H., AGUILAR, E. J., CARTER, B. W., ERASMUS, J., HALPENNY, D. F., PLODKOWSKI, A. J., LONG, N. M., NISHINO, M., DENNING, W. L., GALAN-COBO, A., HAMDI, H., HIRZ, T., TONG, P., WANG, J., RODRIGUEZ-CANALES, J., VILLALOBOS, P. A., PARRA, E. R., KALHOR, N., SHOLL, L. M., SAUTER, J. L., JUNGBLUTH, A. A., MINO-KENUDSON, M., AZIMI, R., ELAMIN, Y. Y., ZHANG, J., LEONARDI, G. C., JIANG, F., WONG, K. K., LEE, J. J., PAPADIMITRAKOPOULOU, V. A., WISTUBA, II, MILLER, V. A., FRAMPTON, G. M., WOLCHOK, J. D., SHAW, A. T., JANNE, P. A., STEPHENS, P. J.,

RUDIN, C. M., GEESE, W. J., ALBACKER, L. A. & HEYMACH, J. V. 2018. STK11/LKB1 Mutations and PD-1 Inhibitor Resistance in KRAS-Mutant Lung Adenocarcinoma. *Cancer Discov,* 8**,** 822-835.

SMITH, M. R., DEGUDICIBUS, S. J. & STACEY, D. W. 1986. Requirement for c-ras proteins during viral oncogene transformation. *Nature,* 320**,** 540-3.

SODIR, N. M., SWIGART, L. B., KARNEZIS, A. N., HANAHAN, D., EVAN, G. I. & SOUCEK, L. 2011. Endogenous Myc maintains the tumor microenvironment. *Genes Dev,* 25**,** 907-16.

SOUKUP, K. & JOYCE, J. A. 2018. A Long-Distance Relay-tionship between Tumor and Bone. *Immunity,* 48**,** 13-16.

SPARMANN, A. & BAR-SAGI, D. 2004. Ras-induced interleukin-8 expression plays a critical role in tumor growth and angiogenesis. *Cancer Cell,* 6**,** 447-58.

SPRANGER, S., BAO, R. & GAJEWSKI, T. F. 2015. Melanoma-intrinsic beta-catenin signalling prevents anti-tumour immunity. *Nature,* 523**,** 231-5.

SPRANGER, S. & GAJEWSKI, T. F. 2018. Impact of oncogenic pathways on evasion of antitumour immune responses. *Nat Rev Cancer,* 18**,** 139-147.

SUMMERS, C., RANKIN, S. M., CONDLIFFE, A. M., SINGH, N., PETERS, A. M. & CHILVERS, E. R. 2010. Neutrophil kinetics in health and disease. *Trends Immunol,* 31**,** 318-24.

SWANTON, C., MCGRANAHAN, N., STARRETT, G. J. & HARRIS, R. S. 2015. APOBEC Enzymes: Mutagenic Fuel for Cancer Evolution and Heterogeneity. *Cancer Discov,* 5**,** 704-12.

SWEET, R. W., YOKOYAMA, S., KAMATA, T., FERAMISCO, J. R., ROSENBERG, M. & GROSS, M. 1984. The product of ras is a GTPase and the T24 oncogenic mutant is deficient in this activity. *Nature,* 311**,** 273-5.

TABIN, C. J., BRADLEY, S. M., BARGMANN, C. I., WEINBERG, R. A., PAPAGEORGE, A. G., SCOLNICK, E. M., DHAR, R., LOWY, D. R. & CHANG, E. H. 1982. Mechanism of activation of a human oncogene. *Nature,* 300**,** 143-9.

TAPAROWSKY, E., SUARD, Y., FASANO, O., SHIMIZU, K., GOLDFARB, M. & WIGLER, M. 1982. Activation of the T24 bladder carcinoma transforming gene is linked to a single amino acid change. *Nature,* 300**,** 762-5.

TENG, K. Y., HAN, J., ZHANG, X., HSU, S. H., HE, S., WANI, N. A., BARAJAS, J. M., SNYDER, L. A., FRANKEL, W. L., CALIGIURI, M. A., JACOB, S. T., YU, J. & GHOSHAL, K. 2017. Blocking the CCL2-CCR2 Axis Using CCL2-Neutralizing Antibody Is an Effective Therapy for Hepatocellular Cancer in a Mouse Model. *Mol Cancer Ther,* 16**,** 312-322.

TONG, L., MILBURN, M. V., DE VOS, A. M. & KIM, S. H. 1989. Structure of ras proteins. *Science,* 245**,** 244.

TRAHEY, M. & MCCORMICK, F. 1987. A cytoplasmic protein stimulates normal N-ras p21 GTPase, but does not affect oncogenic mutants. *Science,* 238**,** 542-5.

TUVESON, D. A. & JACKS, T. 1999. Modeling human lung cancer in mice: similarities and shortcomings. *Oncogene,* 18**,** 5318-24.

VAN MALDEGEM, F. & DOWNWARD, J. 2020. Mutant KRAS at the Heart of Tumor Immune Evasion. *Immunity,* 52**,** 14-16.

VAN MALDEGEM, F., VALAND, K., COLE, M., PATEL, H., ANGELOVA, M., RANA, S., COLLIVER, E., ENFIELD, K., BAH, N., TSANG, V. S. K., MUGARZA, E., MOORE, C., HOBSON, P., LEVI, D., MOLINA-ARCAS, M., SWANTON, C. & DOWNWARD, J. 2021. Characterisation of tumour immune microenvironment remodelling following oncogene inhibition in preclinical studies using an optimised imaging mass cytometry workflow. *bioRxiv***,** 2021.02.02.429358.

WANG, S., JIA, M., HE, Z. & LIU, X. S. 2018. APOBEC3B and APOBEC mutational signature as potential predictive markers for immunotherapy response in non-small cell lung cancer. *Oncogene,* 37**,** 3924-3936.

WARNE, P. H., VICIANA, P. R. & DOWNWARD, J. 1993. Direct interaction of Ras and the amino-terminal region of Raf-1 in vitro. *Nature,* 364**,** 352-5.

WATNICK, R. S., CHENG, Y. N., RANGARAJAN, A., INCE, T. A. & WEINBERG, R. A. 2003. Ras modulates Myc activity to repress thrombospondin-1 expression and increase tumor angiogenesis. *Cancer Cell,* 3**,** 219-31.

WELLENSTEIN, M. D., COFFELT, S. B., DUITS, D. E. M., VAN MILTENBURG, M. H., SLAGTER, M., DE RINK, I., HENNEMAN, L., KAS, S. M., PREKOVIC, S., HAU, C. S., VRIJLAND, K., DRENTH, A. P., DE KORTE-GRIMMERINK, R., SCHUT, E., VAN DER HEIJDEN, I., ZWART, W., WESSELS, L. F. A., SCHUMACHER, T. N., JONKERS, J. & DE VISSER, K. E. 2019. Loss of p53 triggers WNT-dependent systemic inflammation to drive breast cancer metastasis. *Nature,* 572**,** 538-542.

WELLENSTEIN, M. D. & DE VISSER, K. E. 2018. Cancer-Cell-Intrinsic Mechanisms Shaping the Tumor Immune Landscape. *Immunity,* 48**,** 399-416.

WESTCOTT, P. M., HALLIWILL, K. D., TO, M. D., RASHID, M., RUST, A. G., KEANE, T. M., DELROSARIO, R., JEN, K. Y., GURLEY, K. E., KEMP, C. J., FREDLUND, E., QUIGLEY, D. A., ADAMS, D. J. & BALMAIN, A. 2015. The mutational landscapes of genetic and chemical models of Kras-driven lung cancer. *Nature,* 517**,** 489-92.

WILLINGHAM, M. C., PASTAN, I., SHIH, T. Y. & SCOLNICK, E. M. 1980. Localization of the src gene product of the Harvey strain of MSV to plasma membrane of transformed cells by electron microscopic immunocytochemistry. *Cell,* 19**,** 1005-14.

WOLFMAN, A. & MACARA, I. G. 1990. A cytosolic protein catalyzes the release of GDP from p21ras. *Science,* 248**,** 67-9.

WU, Y. L., TSUBOI, M., HE, J., JOHN, T., GROHE, C., MAJEM, M., GOLDMAN, J. W., LAKTIONOV, K., KIM, S. W., KATO, T., VU, H. V., LU, S., LEE, K. Y., AKEWANLOP, C., YU, C. J., DE MARINIS, F., BONANNO, L., DOMINE, M., SHEPHERD, F. A., ZENG, L., HODGE, R., ATASOY, A., RUKAZENKOV, Y., HERBST, R. S. & INVESTIGATORS, A. 2020. Osimertinib in Resected EGFR-Mutated Non-Small-Cell Lung Cancer. *N Engl J Med,* 383**,** 1711-1723.

XU, X., ROCK, J. R., LU, Y., FUTTNER, C., SCHWAB, B., GUINNEY, J., HOGAN, B. L. & ONAITIS, M. W. 2012. Evidence for type II cells as cells of origin of K-Ras-induced distal lung adenocarcinoma. *Proc Natl Acad Sci U S A,* 109**,** 4910-5.

YANG, L., HUANG, J., REN, X., GORSKA, A. E., CHYTIL, A., AAKRE, M., CARBONE, D. P., MATRISIAN, L. M., RICHMOND, A., LIN, P. C. & MOSES, H. L. 2008. Abrogation of TGF beta signaling in mammary carcinomas recruits Gr-1+CD11b+ myeloid cells that promote metastasis. *Cancer Cell,* 13**,** 23-35.

YOKOSUKA, T., TAKAMATSU, M., KOBAYASHI-IMANISHI, W., HASHIMOTO-TANE, A., AZUMA, M. & SAITO, T. 2012. Programmed cell death 1 forms negative costimulatory microclusters that directly inhibit T cell receptor signaling by recruiting phosphatase SHP2. *J Exp Med,* 209**,** 1201-17.

YOSHIMURA, T. 2018. The chemokine MCP-1 (CCL2) in the host interaction with cancer: a foe or ally? *Cell Mol Immunol,* 15**,** 335-345.

YOUN, J. I., NAGARAJ, S., COLLAZO, M. & GABRILOVICH, D. I. 2008. Subsets of myeloid-derived suppressor cells in tumor-bearing mice. *J Immunol,* 181**,** 5791-802.

ZARETSKY, J. M., GARCIA-DIAZ, A., SHIN, D. S., ESCUIN-ORDINAS, H., HUGO, W., HU-LIESKOVAN, S., TORREJON, D. Y., ABRIL-RODRIGUEZ, G., SANDOVAL, S., BARTHLY, L., SACO, J., HOMET MORENO, B., MEZZADRA, R., CHMIELOWSKI, B., RUCHALSKI, K., SHINTAKU, I. P., SANCHEZ, P. J., PUIG-SAUS, C., CHERRY, G., SEJA, E., KONG, X., PANG, J., BERENT-MAOZ, B., COMIN-ANDUIX, B., GRAEBER, T. G., TUMEH, P. C.,

SCHUMACHER, T. N., LO, R. S. & RIBAS, A. 2016. Mutations Associated with Acquired Resistance to PD-1 Blockade in Melanoma. *N Engl J Med,* 375**,** 819-29.

ZHAO, Y., LIU, P., XIN, Z., SHI, C., BAI, Y., SUN, X., ZHAO, Y., WANG, X., LIU, L., ZHAO, X., CHEN, Z. & ZHANG, H. 2019. Biological Characteristics of Severe Combined Immunodeficient Mice Produced by CRISPR/Cas9-Mediated Rag2 and IL2rg Mutation. *Front Genet,* 10**,** 401.

ZHOU, B., DER, C. J. & COX, A. D. 2016. The role of wild type RAS isoforms in cancer. *Semin Cell Dev Biol,* 58**,** 60-9.

ZHOU, F. 2009. Molecular mechanisms of IFN-gamma to up-regulate MHC class I antigen processing and presentation. *Int Rev Immunol,* 28**,** 239-60.

ZHU, Y., HAWKINS, W. G. & DENARDO, D. G. 2015. Regramming myeloid responses to improve cancer immunotherapy. *Oncoimmunology,* 4**,** e974399.

ZHU, Y., HERNDON, J. M., SOJKA, D. K., KIM, K. W., KNOLHOFF, B. L., ZUO, C., CULLINAN, D. R., LUO, J., BEARDEN, A. R., LAVINE, K. J., YOKOYAMA, W. M., HAWKINS, W. G., FIELDS, R. C., RANDOLPH, G. J. & DENARDO, D. G. 2017. Tissue-Resident Macrophages in Pancreatic Ductal Adenocarcinoma Originate from Embryonic Hematopoiesis and Promote Tumor Progression. *Immunity,* 47**,** 597.